2011 Volume 1

The Journal on Advanced Studies in Theoretical and Experimental Physics, including Related Themes from Mathematics

PROGRESS IN PHYSICS

"All scientists shall have the right to present their scientific research results, in whole or in part, at relevant scientific conferences, and to publish the same in printed scientific journals, electronic archives, and any other media."
— Declaration of Academic Freedom, Article 8

ISSN 1555-5534

The Journal on Advanced Studies in Theoretical and Experimental Physics, including Related Themes from Mathematics

PROGRESS IN PHYSICS

A quarterly issue scientific journal, registered with the Library of Congress (DC, USA). This journal is peer reviewed and included in the abstracting and indexing coverage of: Mathematical Reviews and MathSciNet (AMS, USA), DOAJ of Lund University (Sweden), Zentralblatt MATH (Germany), Scientific Commons of the University of St. Gallen (Switzerland), Open-J-Gate (India), Referativnyi Zhurnal VINITI (Russia), etc.

Electronic version of this journal:
http://www.ptep-online.com

Postal Address

Department of Mathematics and Science,
University of New Mexico,
200 College Road, Gallup, NM 87301, USA

ISSN: 1555-5534 (print)
ISSN: 1555-5615 (online)

Standard Address Number: 297-5092
Printed in the United States of America

JANUARY 2011 **VOLUME 1**

CONTENTS

Adekugbe A. O. J. Re-Identification of the Many-World Background of Special Relativity as Four-World Background. Part I . . . 3

Adekugbe A. O. J. Re-Identification of the Many-World Background of Special Relativity as Four-World Background. Part II . . . 25

Benish R. J. Missing Measurements of Weak-Field Gravity . . . 40

Cahill R. T. and Brotherton D. Experimental Investigation of the Fresnel Drag Effect in RF Coaxial Cables . . . 43

May R. D. and Cahill R. T. Dynamical 3-Space Gravity Theory: Effects on Polytropic Solar Models . . . 49

Daywitt W. C. Particles and Antiparticles in the Planck Vacuum Theory . . . 55

Drezet A. Wave Particle Duality and the Afshar Experiment . . . 57

Zein W. A., Ibrahim N. A., and Phillips A. H. Noise and Fano-factor Control in AC-Driven Aharonov-Casher Ring . . . 65

Barbu C. Smarandache's Minimum Theorem in the Einstein Relativistic Velocity Model of Hyperbolic Geometry . . . 68

Smarandache F. S-Denying a Theory . . . 71

Comay E. On the Quantum Mechanical State of the Δ^{++} Baryon . . . 75

Minasyan V. and Samoilov V. Sound-Particles and Phonons with Spin 1 . . . 81

Khazan A. Applying Adjacent Hyperbolas to Calculation of the Upper Limit of the Periodic Table of Elements, with Use of Rhodium . . . 87

Weller D. L. How Black Holes Violate the Conservation of Energy . . . 89

Weller D. L. Five Fallacies Used to Link Black Holes to Einstein's Relativistic Space-Time . . . 93

Quznetsov G. Lee Smolin Five Great Problems and Their Solution without Ontological Hypotheses . . . 98

Messina J. F. On the Failure of Particle Dark Matter Experiments to Yield Positive Results . . . 101

Ries A. and Fook M.V. L. Application of the Model of Oscillations in a Chain System to the Solar System . . . 103

Mina A. N. and Phillips A. H. Photon-Assisted Resonant Chiral Tunneling Through a Bilayer Graphene Barrier . . . 112

Information for Authors and Subscribers

Progress in Physics has been created for publications on advanced studies in theoretical and experimental physics, including related themes from mathematics and astronomy. All submitted papers should be professional, in good English, containing a brief review of a problem and obtained results.

All submissions should be designed in LaTeX format using *Progress in Physics* template. This template can be downloaded from *Progress in Physics* home page http://www.ptep-online.com. Abstract and the necessary information about author(s) should be included into the papers. To submit a paper, mail the file(s) to the Editor-in-Chief.

All submitted papers should be as brief as possible. We accept brief papers, no larger than 8 typeset journal pages. Short articles are preferable. Large papers can be considered in exceptional cases to the section *Special Reports* intended for such publications in the journal. Letters related to the publications in the journal or to the events among the science community can be applied to the section *Letters to Progress in Physics*.

All that has been accepted for the online issue of *Progress in Physics* is printed in the paper version of the journal. To order printed issues, contact the Editors.

This journal is non-commercial, academic edition. It is printed from private donations. (Look for the current author fee in the online version of the journal.)

SPECIAL REPORT

Re-Identification of the Many-World Background of Special Relativity as Four-World Background. Part I.

Akindele O. Joseph Adekugbe

Center for The Fundamental Theory, P. O. Box 2575, Akure, Ondo State 340001, Nigeria.
E-mail: adekugbe@alum.mit.edu

The pair of co-existing symmetrical universes, referred to as our (or positive) universe and negative universe, isolated and shown to constitute a two-world background for the special theory of relativity (SR) in previous papers, encompasses another pair of symmetrical universes, referred to as positive time-universe and negative time-universe. The Euclidean 3-spaces (in the context of SR) of the positive time-universe and the negative time-universe constitute the time dimensions of our (or positive) universe and the negative universe respectively, relative to observers in the Euclidean 3-spaces of our universe and the negative universe and the Euclidean 3-spaces of our universe and the negative universe constitute the time dimensions of the positive time-universe and the negative time-universe respectively, relative to observers in the Euclidean 3-spaces of the positive time-universe and the negative time-universe. Thus time is a secondary concept derived from the concept of space according to this paper. The one-dimensional particle or object in time dimension to every three-dimensional particle or object in 3-space in our universe is a three-dimensional particle or object in 3-space in the positive time-universe. Perfect symmetry of natural laws is established among the resulting four universes and two outstanding issues about the new spacetime/intrinsic spacetime geometrical representation of Lorentz transformation/intrinsic Lorentz transformation in the two-world picture, developed in the previous papers, are resolved within the larger four-world picture in this first part of this paper.

1 Origin of time and intrinsic time dimensions

1.1 Orthogonal Euclidean 3-spaces

Let us start with an operational definition of orthogonal Euclidean 3-spaces. Given a three-dimensional Euclidean space (or a Euclidean 3-space) $\boldsymbol{E}^3$ with mutually orthogonal straight line dimensions x^1, x^2 and x^3 and another Euclidean 3-space $\boldsymbol{E}^{03}$ with mutually orthogonal straight line dimensions x^{01}, x^{02} and x^{03}, the Euclidean 3-space $\boldsymbol{E}^{03}$ shall be said to be orthogonal to the Euclidean 3-space $\boldsymbol{E}^3$ if, and only if, each dimension x^{0j} of $\boldsymbol{E}^{03}$; $j = 1, 2, 3$, is orthogonal to every dimension x^i; $i = 1, 2, 3$ of $\boldsymbol{E}^3$. In other words, $\boldsymbol{E}^{03}$ shall be said to be orthogonal to $\boldsymbol{E}^3$ if, and only if, $x^{0j} \perp x^i$; $i, j = 1, 2, 3$, at every point of the Euclidean 6-space generated by the orthogonal Euclidean 3-spaces.

We shall take the Euclidean 3-spaces $\boldsymbol{E}^3$ and $\boldsymbol{E}^{03}$ to be the proper (or classical) Euclidean 3-spaces of classical mechanics (including classical gravity), to be re-denoted by Σ' and $\Sigma^{0\prime}$ respectively for convenience in this paper. The reason for restricting to the proper (or classical) Euclidean 3-spaces is that we shall assume the absence of relativistic gravity while considering the special theory of relativity (SR) on flat spacetime, as shall be discussed further at the end of this paper.

Graphically, let us consider the Euclidean 3-space Σ' with mutually orthogonal straight line dimensions $x^{1\prime}$, $x^{2\prime}$ and $x^{3\prime}$ as a hyper-surface to be represented by a horizontal plane surface and the Euclidean 3-space $\Sigma^{0\prime}$ with mutually orthogonal straight line dimensions $x^{01\prime}$, $x^{02\prime}$ and $x^{03\prime}$ as a hyper-surface to be represented by a vertical plane surface. The union of the two orthogonal proper (or classical) Euclidean 3-spaces yields a compound six-dimensional proper (or classical) Euclidean space with mutually orthogonal dimensions $x^{1\prime}$, $x^{2\prime}$, $x^{3\prime}$, $x^{01\prime}$, $x^{02\prime}$ and $x^{03\prime}$ illustrated in Fig. 1.

As introduced (as *ansatz*) in [1] and as shall be derived formally in the two parts of this paper, the hyper-surface (or proper Euclidean 3-space) Σ' along the horizontal is underlied by an isotropic one-dimensional proper intrinsic space denoted by $\phi\rho'$ (that has no unique orientation in the Euclidean 3-space Σ'). The vertical proper Euclidean 3-space $\Sigma^{0\prime}$ is likewise underlied by an isotropic one-dimensional proper intrinsic space $\phi\rho^{0\prime}$ (that has no unique orientation in the Euclidean 3-space $\Sigma^{0\prime}$). The underlying intrinsic spaces $\phi\rho'$ and $\phi\rho^{0\prime}$ are also shown in Fig. 1.

Inclusion of the proper time dimension ct' along the vertical, normal to the horizontal hyper-surface (or horizontal Euclidean 3-space) Σ' in Fig. 1, yields the flat four-dimensional proper spacetime (Σ', ct') of classical mechanics (CM), (including classical gravitation), of the positive (or our) universe and inclusion of the proper intrinsic time dimension $\phi c\phi t'$ along the vertical, normal to the proper intrinsic space $\phi\rho'$ along the horizontal, yields the flat 2-dimensional proper intrinsic spacetime $(\phi\rho', \phi c\phi t')$ of intrinsic classical mechanics

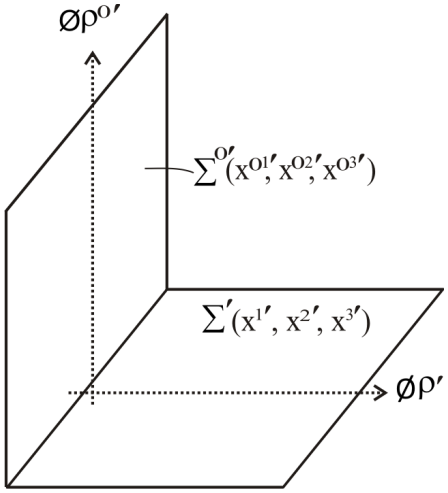

Fig. 1: Co-existing two orthogonal proper Euclidean 3-spaces (considered as hyper-surfaces) and their underlying isotropic one-dimensional proper intrinsic spaces.

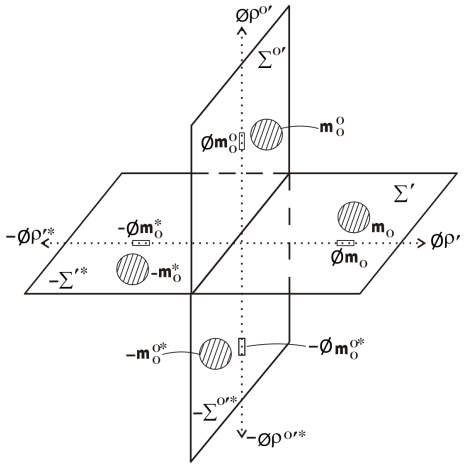

Fig. 2: Co-existing four mutually orthogonal proper Euclidean 3-spaces and their underlying isotropic one-dimensional proper intrinsic spaces, where the rest masses in the proper Euclidean 3-spaces and the one-dimensional intrinsic rest masses in the intrinsic spaces of a quartet of symmetry-partner particles or object are shown.

(ϕCM), (including intrinsic classical gravitation), of our universe. The proper Euclidean 3-space Σ' and its underlying one-dimensional proper intrinsic space $\phi\rho'$ shall sometimes be referred to as our proper (or classical) Euclidean 3-space and our proper (or classical) intrinsic space for brevity.

The vertical proper Euclidean 3-space $\Sigma^{0\prime}$ and its underlying one-dimensional proper intrinsic space $\phi\rho^{0\prime}$ in Fig. 1 are new. They are different from the proper Euclidean 3-space $-\Sigma'^*$ and its underlying proper intrinsic space $-\phi\rho'^*$ of the negative universe isolated in [1] and [2]. The Euclidean 3-space $-\Sigma'^*$ and its underlying proper intrinsic space $-\phi\rho'^*$ of the negative universe are "anti-parallel" to the Euclidean 3-space Σ' and its underlying intrinsic space $\phi\rho'$ of the positive universe, which means that the dimensions $-x^{1\prime*}$, $-x^{2\prime*}$ and $-x^{3\prime*}$ of $-\Sigma'^*$ are inversions in the origin of the dimensions $x^{1\prime}$, $x^{2\prime}$ and $x^{3\prime}$ of Σ'.

There are likewise the proper Euclidean 3-space $-\Sigma^{0\prime*}$ and its underlying proper intrinsic space $-\phi\rho^{0\prime*}$, which are "anti-parallel" to the new proper Euclidean 3-space $\Sigma^{0\prime}$ and its underlying proper intrinsic space $\phi\rho^{0\prime}$ in Fig. 1. Fig. 1 shall be made more complete by adding the negative proper Euclidean 3-spaces $-\Sigma'^*$ and $-\Sigma^{0\prime*}$ and their underlying one-dimensional intrinsic spaces $-\phi\rho'^*$ and $-\phi\rho^{0\prime*}$ to it, yielding Fig. 2.

The proper Euclidean 3-space Σ' with dimensions $x^{1\prime}$, $x^{2\prime}$ and $x^{3\prime}$ and the proper Euclidean 3-space $\Sigma^{0\prime}$ with dimensions $x^{01\prime}$, $x^{02\prime}$ and $x^{03\prime}$ in Fig. 2 are orthogonal Euclidean 3-spaces, which means that $x^{0j\prime} \perp x^{i\prime}$; $i, j = 1, 2, 3$, as defined earlier. The proper Euclidean 3-space $-\Sigma'^*$ with dimensions $-x^{1\prime*}$, $-x^{2\prime*}$ and $-x^{3\prime*}$ and the proper Euclidean 3-space $-\Sigma^{0\prime*}$ with dimensions $-x^{01\prime*}$, $-x^{02\prime*}$ and $-x^{03\prime*}$ are likewise orthogonal Euclidean 3-spaces.

Should the vertical Euclidean 3-spaces $\Sigma^{0\prime}$ and $-\Sigma^{0\prime*}$ and their underlying isotropic intrinsic spaces $\phi\rho^{0\prime}$ and $-\phi\rho^{0\prime*}$ exist naturally, then they should belong to a new pair of worlds (or universes), just as the horizontal proper Euclidean 3-space Σ' and $-\Sigma'^*$ and their underlying one-dimensional isotropic proper intrinsic spaces $\phi\rho'$ and $-\phi\rho'^*$ exist naturally and belong to the positive (or our) universe and the negative universe respectively, as found in [1] and [2]. The appropriate names for the new pair of universes with flat four-dimensional proper spacetimes ($\Sigma^{0\prime}$, $ct^{0\prime}$) and ($-\Sigma^{0\prime*}$, $-ct^{0\prime*}$) of classical mechanics (CM) and their underlying flat two-dimensional proper intrinsic spacetimes ($\phi\rho^{0\prime}$, $\phi c\phi t^{0\prime}$) and ($-\phi\rho^{0\prime*}$, $-\phi c\phi t^{0\prime*}$) of intrinsic classical mechanics (ϕCM), where the time dimensions and intrinsic time dimensions have not yet appeared in Fig. 2, shall be derived later in this paper.

As the next step, an assumption shall be made, which shall be justified with further development of this paper, that the four universes encompassed by Fig. 2, with flat four- dimensional proper spacetimes (Σ', ct'), ($-\Sigma'^*, -ct'^*$), ($\Sigma^{0\prime}, ct^{0\prime}$) and ($-\Sigma^{0\prime*}, -ct^{0\prime*}$) and their underlying flat proper intrinsic spacetimes ($\phi\rho', \phi c\phi t'$), ($-\phi\rho'^*, -\phi c\phi t'^*$), ($\phi\rho^{0\prime}, \phi c\phi t^{0\prime}$) and ($-\phi\rho^{0\prime*}, -\phi c\phi t^{0\prime*}$) respectively, where the proper time and proper intrinsic time dimensions have not yet appeared in Fig. 2, exist naturally and exhibit perfect symmetry of state and perfect symmetry of natural laws. Implied by this assumption are the following facts:

1. Corresponding to every given point P in our proper Euclidean 3-space Σ', there are unique symmetry- partner point P^0, P^* and P^{0*} in the proper Euclidean 3-spaces $\Sigma^{0\prime}$, $-\Sigma'^*$ and $-\Sigma^{0\prime*}$ respectively;
2. Corresponding to every particle or object of rest mass m_0 located at a point in our proper Euclidean 3-space Σ', there are identical symmetry-partner particles or ob-

jects of rest masses to be denoted by m_0^0, $-m_0^*$ and $-m_0^{0*}$ located at the symmetry-partner points in $\Sigma^{0\prime}$, $-\Sigma^{\prime *}$ and $-\Sigma^{0\prime *}$ respectively, as illustrated in Fig. 2 already and

3. Corresponding to motion at a speed v of the rest mass m_0 of a particle or object through a point along a direction in our proper Euclidean space $\Sigma^{\prime}$, relative to an observer in $\Sigma^{\prime}$, there are identical symmetry- partner particles or objects of rest masses m_0^0, $-m_0^*$ and $-m_0^{0*}$ in simultaneous motions at equal speed v along identical directions through the symmetry-partner points in the proper Euclidean 3-spaces $\Sigma^{0\prime}$, $-\Sigma^{\prime *}$ and $-\Sigma^{0\prime *}$ respectively, relative to identical symmetry-partner observers in the respective Euclidean 3-spaces.

4. A further requirement of the symmetry of state among the four universes encompassed by Fig. 2 is that the motion at a speed v of a particle along the $X-$ axis, say, of its frame in any one of the four proper Euclidean 3-spaces, (in $\Sigma^{0\prime}$, say), relative to an observer (or frame of reference) in that proper Euclidean 3-space (or universe), is equally valid relative to the symmetry-partner observers in the three other proper Euclidean 3-spaces (or universes). Consequently the simultaneous rotations by equal intrinsic angle $\phi\psi$ of the intrinsic affine space coordinates of the symmetry-partner particles' frames $\phi\tilde{x}^{\prime}$, $\phi\tilde{x}^{0\prime}$, $-\phi\tilde{x}^{\prime *}$ and $-\phi\tilde{x}^{0\prime *}$ relative to the intrinsic affine space coordinates of the symmetry-partner observers' frames $\phi\tilde{x}$, $\phi\tilde{x}^0$, $-\phi\tilde{x}^*$ and $-\phi\tilde{x}^{0*}$ respectively in the context of the intrinsic special theory of relativity (ϕSR), as developed in [1], implied by item 3, are valid relative to every one of the four symmetry-partner observers in the four proper Euclidean 3-spaces (or universes). Thus every one of the four symmetry-partner observers can validly draw the identical relative rotations of affine intrinsic spacetime coordinates of symmetry-partner frames of reference in the four universes encompassed by Fig. 2 with respect to himself and construct ϕSR and consequently SR in his universe with the diagram encompassing the four universes he obtains.

Inherent in item 4 above is the fact that the four universes with flat four-dimensional proper physical (or metric) spacetimes $(\Sigma^{\prime}, ct^{\prime})$, $(\Sigma^{0\prime}, ct^{0\prime})$, $(-\Sigma^{\prime *}, -ct^{\prime *})$ and $(-\Sigma^{0\prime *}, -ct^{0\prime *})$ of classical mechanics (CM) in the universes encompassed by Fig. 2, (where the proper time dimensions have not yet appeared), are stationary dynamically relative to one another at all times. Otherwise the speed v of a particle in a universe (or in a Euclidean 3-space in Fig. 2) relative to an observer in that universe (or in that Euclidean 3-space), will be different relative to the symmetry-partner observer in another universe (or in another Euclidean 3-space), who must obtain the speed of the particle relative to himself as the resultant of the particle's speed v relative to the observer in the particle's universe and the speed V_0 of the particle's universe (or particle's Euclidean 3-space) relative to his universe (or his Euclidean 3-space). The simultaneous identical relative rotations by equal intrinsic angle of intrinsic affine spacetime coordinates of symmetry-partner frames of reference in the four universes, which symmetry of state requires to be valid with respect to every one of the four symmetry-partner observers in the four universes, will therefore be impossible in the situation where some or all the four universes (or Euclidean 3-spaces in Fig. 2) are naturally in motion relative to one another.

Now the proper intrinsic metric space $\phi\rho^{0\prime}$ along the vertical in the first quadrant is naturally rotated at an intrinsic angle $\phi\psi_0 = \frac{\pi}{2}$ relative to the proper intrinsic metric space $\phi\rho^{\prime}$ of the positive (or our) universe along the horizontal in the first quadrant in Fig. 2. The proper intrinsic metric space $-\phi\rho^{\prime *}$ of the negative universe is naturally rotated at intrinsic angle $\phi\psi_0 = \pi$ relative to our proper intrinsic metric space $\phi\rho^{\prime}$ and the proper intrinsic metric space $-\phi\rho^{0\prime *}$ along the vertical in the third quadrant is naturally rotated at intrinsic angle $\phi\psi_0 = \frac{3\pi}{2}$ relative to our proper intrinsic metric space $\phi\rho^{\prime}$ in Fig. 2. The intrinsic angle of natural rotations of the intrinsic metric spaces $\phi\rho^{0\prime}$, $-\phi\rho^{\prime *}$ and $-\phi\rho^{0\prime *}$ relative to $\phi\rho^{\prime}$ has been denoted by $\phi\psi_0$ in order differentiate it from the intrinsic angle of relative rotation of intrinsic affine spacetime coordinates in the context of ϕSR denoted by $\phi\psi$ in [1].

The natural rotations of the one-dimensional proper intrinsic metric spaces $\phi\rho^{0\prime}$, $-\phi\rho^{\prime *}$ and $-\phi\rho^{0\prime *}$ relative to our proper intrinsic metric space $\phi\rho^{\prime}$ at different intrinsic angles $\phi\psi_0$ discussed in the foregoing paragraph, implies that the intrinsic metric spaces $\phi\rho^{0\prime}$, $-\phi\rho^{\prime *}$ and $-\phi\rho^{0\prime *}$ possess different intrinsic speeds, to be denoted by ϕV_0, relative to our intrinsic metric space $\phi\rho^{\prime}$. This is deduced in analogy to the fact that the intrinsic speed ϕv of the intrinsic rest mass ϕm_0 of a particle relative to an observer causes the rotations of the intrinsic affine spacetime coordinates $\phi\tilde{x}^{\prime}$ and $\phi c\phi\tilde{t}^{\prime}$ of the particle's intrinsic frame at equal intrinsic angle $\phi\psi$ relative to the intrinsic affine spacetime coordinates $\phi\tilde{x}$ and $\phi c\phi\tilde{t}$ respectively of the observe's intrinsic frame in the context of intrinsic special relativity (ϕSR), as developed in [1] and presented graphically in Fig. 8a of that paper.

Indeed the derived relation, $\sin\phi\psi = \phi v/\phi c$, between the intrinsic angle $\phi\psi$ of inclination of the intrinsic affine space coordinate $\phi\tilde{x}^{\prime}$ of the particle's intrinsic frame relative to the intrinsic affine space coordinate $\phi\tilde{x}$ of the observer's intrinsic frame in the context of ϕSR, presented as Eq. (18) of [1], is equally valid between the intrinsic angle $\phi\psi_0$ of natural rotation of a proper intrinsic metric space $\phi\rho^{0\prime}$, say, relative to our proper intrinsic metric space $\phi\rho^{\prime}$ in Fig. 2 and the implied natural intrinsic speed ϕV_0 of $\phi\rho^{0\prime}$ relative to $\phi\rho^{\prime}$. In other words, the following relation obtains between $\phi\psi_0$ and ϕV_0:

$$\sin\phi\psi_0 = \phi V_0/\phi c \tag{1}$$

It follows from (1) that the intrinsic metric space $\phi\rho^{0\prime}$ naturally possesses intrinsic speed $\phi V_0 = \phi c$ relative to our in-

trinsic metric space $\phi\rho'$, which is so since $\phi\rho^{0\prime}$ is naturally inclined at intrinsic angle $\phi\psi_0 = \frac{\pi}{2}$ relative to $\phi\rho'$; the proper intrinsic metric space $-\phi\rho'^*$ of the negative universe naturally possesses zero intrinsic speed ($\phi V_0 = 0$) relative to our proper intrinsic metric space $\phi\rho'$, since $-\phi\rho'^*$ is naturally inclined at intrinsic angle $\phi\psi_0 = \pi$ relative to $\phi\rho'$ and the intrinsic metric space $-\phi\rho^{0\prime*}$ naturally possesses intrinsic speed $\phi V_0 = -\phi c$ relative to our intrinsic metric space $\phi\rho'$, since $-\phi\rho^{0\prime*}$ is naturally inclined at $\phi\psi_0 = \frac{3\pi}{2}$ relative to $\phi\rho'$ in Fig. 2.

On the other hand, $-\phi\rho^{0\prime*}$ possesses positive intrinsic speed $\phi V_0 = \phi c$ relative to $-\phi\rho'^*$, since $-\phi\rho^{0\prime*}$ is naturally inclined at intrinsic angle $\phi\psi_0 = \frac{\pi}{2}$ relative to $-\phi\rho'^*$ and $\phi\rho^{0\prime}$ naturally possesses negative intrinsic speed $\phi V_0 = -\phi c$ relative to $-\phi\rho'^*$, since $\phi\rho^{0\prime}$ is naturally inclined at $\phi\psi_0 = \frac{3\pi}{2}$ relative to $-\phi\rho'^*$ in Fig 2. These facts have been illustrated in Figs. 10a and 10b of [1] for the concurrent open intervals $(-\frac{\pi}{2}, \frac{\pi}{2})$ and $(\frac{\pi}{2}, \frac{3\pi}{2})$ within which the intrinsic angle $\phi\psi$ could take on values with respect to 3-observers in the Euclidean 3-spaces Σ' of the positive universe and $-\Sigma'^*$ of the negative universe.

The natural intrinsic speed $\phi V_0 = \phi c$ of $\phi\rho^{0\prime}$ relative to $\phi\rho'$ will be made manifest in speed $V_0 = c$ of the Euclidean 3-space $\Sigma^{0\prime}$ relative to our Euclidean 3-space Σ'; the natural zero intrinsic speed ($\phi V_0 = 0$) of the intrinsic space $-\phi\rho'^*$ of the negative universe relative to $\phi\rho'$ will be made manifest in natural zero speed ($V_0 = 0$) of the Euclidean 3-space $-\Sigma'^*$ of the negative universe relative to our Euclidean 3-space Σ' and the natural intrinsic speed $\phi V_0 = -\phi c$ of $-\phi\rho^{0\prime*}$ relative to $\phi\rho'$ will be made manifest in natural speed $V_0 = -c$ of the Euclidean 3-space $-\Sigma^{0\prime*}$ relative to our Euclidean 3-space Σ' in Fig. 2. By incorporating the additional information in this and the foregoing two paragraphs into Fig. 2 we have Fig. 3, which is valid with respect to 3-observers in our proper Euclidean 3-spaces Σ', as indicated.

There are important differences between the speeds V_0 of the Euclidean 3-spaces that appear in Fig. 3 and speed v of relative motion of particles and objects that appear in the special theory of relativity (SR). First of all, the speed v of relative motion is a property of the particle or object in relative motion, which exists nowhere in the vast space outside the particle at any given instant. This is so because there is nothing (no action-at-a-distance) in relative motion to transmit the velocity of a particle to positions outside the particle. On the other hand, the natural speed V_0 of a Euclidean 3-space is a property of that Euclidean 3-space, which has the same magnitude at every point of the Euclidean 3-space with or without the presence of a particle or object of any rest mass.

The natural speed V_0 of a Euclidean 3-space is isotropic. This means that it has the same magnitude along every direction of the Euclidean 3-space. This is so because each dimension $x^{0j\prime}$; $j = 1, 2, 3$, of $\Sigma^{0\prime}$ is rotated at equal angle $\psi_0 = \frac{\pi}{2}$ relative to every dimension $x^{i\prime}$; $i = 1, 2, 3$, of Σ', (which implies that each dimension $x^{0j\prime}$ of $\Sigma^{0\prime}$ possesses speed $V_0 = c$ naturally relative to every dimension $x^{i\prime}$ of Σ'), thereby making $\Sigma^{0\prime}$ an orthogonal Euclidean 3-space to Σ'. What should be the natural velocity $\vec{V}_0$ of a Euclidean 3-space has components of equal magnitude V_0 along every direction and at every point in that Euclidean 3-space. On the other hand, the speed v of relative motion of a particle or object is not isotropic because the velocity $\vec{v}$ of relative motion along a direction in a Euclidean 3-space has components of different magnitudes along different directions of that Euclidean 3-space. Only the speed $v = c$ of translation of light (or photon) in space is known to be isotropic.

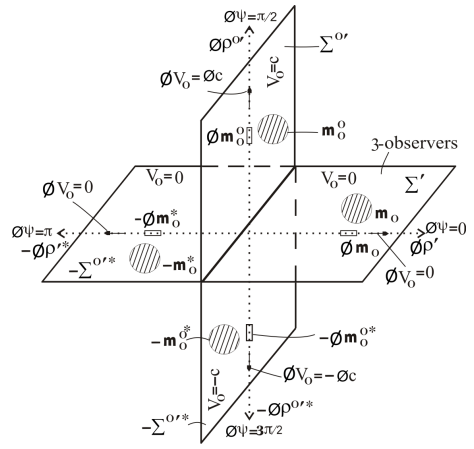

Fig. 3: Co-existing four mutually orthogonal proper Euclidean 3-spaces and their underlying isotropic one-dimensional proper intrinsic spaces, where the speeds V_0 of the Euclidean 3-spaces and the intrinsic speeds ϕV_0 of the intrinsic spaces, relative to 3-observers in our proper Euclidean 3-space (considered as a hyper-surface along the horizontal) in the first quadrant are shown.

Now a material particle or object of any magnitude of rest mass that is located at any point in a Euclidean 3-space acquires the natural speed V_0 of that Euclidean 3-space. Thus the rest mass m_0 of the particle or object located in our proper Euclidean 3-space Σ' possesses the spatially uniform natural zero speed ($V_0 = 0$) of Σ' relative to every particle, object or observer in Σ' in Fig. 3. Likewise the rest mass m_0^0 of a particle or object located at any point in the proper Euclidean 3-space $\Sigma^{0\prime}$ acquires the isotropic and spatially uniform natural speed $V_0 = c$ of $\Sigma^{0\prime}$ relative to every particle, object or observer in our Euclidean 3-space Σ'.

The rest mass $-m_0^*$ located at any point in the proper Euclidean 3-space $-\Sigma'^*$ of the negative universe acquires the spatially uniform natural zero speed ($V_0 = 0$) of $-\Sigma'^*$ relative to all particles, objects and observers in our Euclidean 3-space Σ' and the rest mass $-m_0^{0*}$ of a particle or object located at any point in the proper Euclidean 3-space $-\Sigma^{0\prime*}$ acquires the isotropic and spatially uniform natural speed $V_0 = -c$ of $-\Sigma^{0\prime*}$ relative to all particles, objects and observers in our Euclidean 3-space Σ' in Fig. 3.

However, as deduced earlier, symmetry of state among the four universes whose proper (or classical) Euclidean 3-

spaces appear in Fig. 2 or 3 requires that the four universes must be stationary relative to one another always. Then in order to resolve the paradox ensuing from this and the foregoing two paragraphs namely, all the four universes (or their proper Euclidean 3-spaces in Fig. 2 or 3) are stationary relative to one another always (as required by symmetry of state among the four universes), yet the two universes with flat proper spacetimes $(\Sigma^{0\prime}, ct^{0\prime})$ and $(-\Sigma^{0\prime *}, -ct^{0\prime *})$ naturally possess constant speeds $V_0 = c$ and $V_0 = -c$ respectively relative to the flat spacetime (Σ', ct') of our universe, we must consider the constant speeds $V_0 = c$ and $V_0 = -c$ of the universes with the flat spacetimes $(\Sigma^{0\prime}, ct^{0\prime})$ and $(-\Sigma^{0\prime *}, -ct^{0\prime *})$ respectively relative to our universe (or speeds $V_0 = c$ and $V_0 = -c$ of the Euclidean 3-spaces $\Sigma^{0\prime}$ and $-\Sigma^{0\prime *}$ respectively relative to our Euclidean 3-space Σ' in Fig. 3) as absolute speeds of non-detectable absolute motion. This way, although the two proper Euclidean 3-spaces $\Sigma^{0\prime}$ and $-\Sigma^{0\prime *}$ naturally possess speeds $V_0 = c$ and $V_0 = -c$ respectively relative to our proper Euclidean 3-space Σ', the four proper Euclidean 3-spaces encompassed by Fig. 2 or 3 are stationary dynamically (or translation-wise) relative to one another, as required by symmetry of state among the four universes with the four proper Euclidean 3-spaces in Fig. 2 or Fig. 3.

The fact that the natural speed $V_0 = c$ of the proper Euclidean 3-space $\Sigma^{0\prime}$ relative to our proper Euclidean 3-space Σ' or of the rest mass m_0^0 in $\Sigma^{0\prime}$ relative to the symmetry-partner rest mass m_0 in Σ' is an absolute speed of non-detectable absolute motion is certain. This is so since there is no relative motion involving large speed $V_0 = c$ between the rest mass of a particle in the particle's frame and the rest mass of the particle in the observer's frame, (where m_0^0 is the rest mass of the particle and $\Sigma^{0\prime}$ in which m_0^0 is in motion at speed $V_0 = c$ is the particle's frame, while m_0 is the rest mass of the particle located in the observer's frame Σ' in this analogy, knowing that m_0 and m_0^0 are equal in magnitude).

The observer's frame always contains special-relativistic (or Lorentz transformed) coordinates and parameters in special relativity. On the other hand, non-detectable absolute motion does not alter the proper (or classical) coordinates and parameters, as in the case of the non-detectable natural absolute motion at absolute speed $V_0 = c$ of m_0^0 in $\Sigma^{0\prime}$ relative to m_0 that possesses zero absolute speed ($V_0 = 0$) in Σ' in Fig. 3.

We have derived another important difference between the natural speeds V_0 of the Euclidean 3-spaces that appear in Fig. 3 and the speeds v of relative motions of material particles and objects that appear in SR. This is the fact that the isotropic and spatially uniform speed V_0 of a Euclidean 3-space is an absolute speed of non-detectable absolute motion, while speed v of particles and objects is a speed of detectable relative motion.

Thus the isotropic speed $V_0 = c$ acquired by the rest mass m_0^0 located in the proper Euclidean 3-space $\Sigma^{0\prime}$ relative to its symmetry-partner m_0 and all other particles, objects and observers in our proper Euclidean 3-space Σ' in Fig. 3 is a non-detectable absolute speed. Consequently m_0^0 in $\Sigma^{0\prime}$ does not propagate away at speed $V_0 = c$ in $\Sigma^{0\prime}$ from m_0 in Σ' but remains tied to m_0 in Σ' always, despite its isotropic absolute speed c in $\Sigma^{0\prime}$ relative to m_0 in Σ'. The speed $V_0 = -c$ acquired by the rest mass $-m_0^{0*}$ in the proper Euclidean 3-space $-\Sigma^{0\prime *}$ relative to its symmetry-partner rest mass m_0 and all other particles, objects and observers in our Euclidean 3-space Σ' in Fig. 3 is likewise an absolute speed of non-detectable absolute motion. Consequently $-m_0^{0*}$ in $-\Sigma^{0\prime *}$ does not propagate away at speed $V_0 = -c$ in $-\Sigma^{0\prime *}$ from m_0 in Σ' but remains tied to m_0 in Σ' always, despite the absolute speed $V_0 = -c$ of $-m_0^{0*}$ in $-\Sigma^{0\prime *}$ relative to m_0 in Σ'.

On the other hand, the rest mass $-m_0^{0*}$ in $-\Sigma^{0\prime *}$ possesses positive absolute speed $V_0 = c$ and rest mass m_0^0 in $\Sigma^{0\prime}$ possesses negative absolute speed $V_0 = -c$ with respect to the symmetry-partner rest mass $-m_0^*$ and all other particles, objects and observers in $-\Sigma'^*$. This is so since the proper intrinsic space $-\phi\rho^{0\prime *}$ underlying $-\Sigma^{0\prime *}$ is naturally rotated by intrinsic angle $\phi\psi_0 = \frac{\pi}{2}$ relative to the proper intrinsic space $-\phi\rho'^*$ underlying $-\Sigma'^*$ and $\phi\rho^{0\prime}$ underlying $\Sigma^{0\prime}$ is naturally rotated by intrinsic angle $\phi\psi_0 = \frac{3\pi}{2}$ relative to $-\phi\rho'^*$, as mentioned earlier. Consequently $-\phi\rho^{0\prime *}$ naturally possesses absolute intrinsic speed $\phi V_0 = \phi c$ relative to $-\phi\rho'^*$ and $\phi\rho^{0\prime}$ naturally possesses absolute intrinsic speed $\phi V_0 = -\phi c$ relative to $-\phi\rho'^*$. These are then made manifest outwardly as the absolute speed $V_0 = c$ of the Euclidean 3-space $-\Sigma^{0\prime *}$ and absolute speed $V_0 = -c$ of the Euclidean 3-space $\Sigma^{0\prime}$ respectively relative to the Euclidean 3-space $-\Sigma'^*$ of the negative universe.

Let the quartet of symmetry-partner particles or objects of rest masses m_0 in Σ', m_0^0 in $\Sigma^{0\prime}$, $-m_0^*$ in $-\Sigma'^*$ and $-m_0^{0*}$ in $-\Sigma^{0\prime *}$ be located at initial symmetry-partner positions P_i, P_i^0, P_i^* and P_i^{0*} respectively in their respective Euclidean 3-spaces. Then let the particle or object of rest mass m_0 in Σ' be in motion at constant speed v along the $\tilde{x}'-$axis of its frame in our proper Euclidean 3-space Σ' relative to a 3-observer in Σ'. The symmetry-partner particle or object of rest mass m_0^0 in $\Sigma^{0\prime}$ will be in simultaneous motion at equal speed v along the $\tilde{x}^{0\prime}-$axis of its frame in $\Sigma^{0\prime}$ relative to the symmetry-partner observer in $\Sigma^{0\prime}$; the symmetry-partner particle or object of rest mass $-m_0^*$ in $-\Sigma'^*$ will be in simultaneous motion at equal speed v along the $-\tilde{x}'^*-$axis of its frame in $-\Sigma'^*$ relative to the symmetry-partner 3-observer in $-\Sigma'^*$ and the symmetry-partner particle or object of rest mass $-m_0^{0*}$ in $-\Sigma^{0\prime *}$ will be in simultaneous motion at equal speed v along the $-\tilde{x}^{0\prime *}-$axis of its frame in $-\Sigma^{0\prime *}$ relative to the symmetry-partner 3-observer in $-\Sigma^{0\prime *}$.

Thus after a period of time of commencement of motion, the quartet of symmetry-partner particles or objects have covered equal distances along the identical directions of motion in their respective proper Euclidean 3-spaces to arrive at new symmetry-partner positions P, P^0, P^* and P^{0*} in their respective proper Euclidean 3-spaces. This is possible because the four Euclidean 3-spaces are stationary relative to one an-

other always. The quartet of symmetry-partner particles or objects are consequently located at symmetry-partner positions in their respective proper Euclidean 3-spaces always, even when they are in motion relative to symmetry-partner frames of reference in their respective proper Euclidean 3-spaces.

The speed $V_0 = c$ of the proper Euclidean 3-space $\Sigma^{0\prime}$ relative to our proper Euclidean 3-space Σ' is the outward manifestation of the intrinsic speed $\phi V_0 = \phi c$ of the intrinsic metric space $\phi\rho^{0\prime}$ underlying $\Sigma^{0\prime}$ relative to our intrinsic metric space $\phi\rho'$ and relative to our Euclidean 3-space Σ' in Fig. 3. Then since $V_0 = c$ is absolute and is the same at every point of the Euclidean 3-space $\Sigma^{0\prime}$, the intrinsic speed $\phi V_0 = \phi c$ of $\phi\rho^{0\prime}$ relative to $\phi\rho'$ and Σ' is absolute and is the same at every point along the length of $\phi\rho^{0\prime}$. The intrinsic speed $\phi V_0 = -\phi c$ of the intrinsic metric space $-\phi\rho^{0\prime *}$ relative to our intrinsic metric space $\phi\rho'$ and relative to our Euclidean 3-space Σ' is likewise an absolute intrinsic speed and is the same at every point along the length of $-\phi\rho^{0\prime *}$. The zero intrinsic speed ($\phi V_0 = 0$) of the intrinsic metric space $-\phi\rho'^*$ of the negative universe relative to our intrinsic metric space $\phi\rho'$ and relative to our Euclidean 3-space Σ' is the same along the length of $-\phi\rho'^*$.

It follows from the foregoing paragraph that although the proper intrinsic metric spaces $\phi\rho^{0\prime}$ and $-\phi\rho^{0\prime *}$ along the vertical possess intrinsic speeds $\phi V_0 = \phi c$ and $\phi V_0 = -\phi c$ respectively, relative to our proper intrinsic metric space $\phi\rho'$ and relative to our Euclidean 3-space Σ', the four intrinsic metric spaces $\phi\rho'$, $\phi\rho^{0\prime}$, $-\phi\rho'^*$ and $-\phi\rho^{0\prime *}$ in Fig. 3 are stationery relative to one another always, since the intrinsic speeds $\phi V_0 = \phi c$ of $\phi\rho^{0\prime}$ and $\phi V_0 = -\phi c$ of $-\phi\rho'^*$ relative to our intrinsic metric space $\phi\rho'$ and our Euclidean 3-space Σ' are absolute intrinsic speeds, which are not made manifest in actual intrinsic motion.

Likewise, although the intrinsic rest mass ϕm_0^0 in $\phi\rho^{0\prime}$ acquires the intrinsic speed $\phi V_0 = \phi c$ of $\phi\rho^{0\prime}$, it is not in intrinsic motion at the intrinsic speed ϕc along $\phi\rho^{0\prime}$, since the intrinsic speed ϕc it acquires is an absolute intrinsic speed. The absolute intrinsic speed $\phi V_0 = -\phi c$ acquired by the intrinsic rest mass $-\phi m_0^{0*}$ in $-\phi\rho^{0\prime *}$ is likewise not made manifest in actual intrinsic motion of $-\phi m_0^{0*}$ along $-\phi\rho^{0\prime *}$. Consequently the quartet of intrinsic rest masses $\phi m_0, \phi m_0^0, -\phi m_0^*$ and $-\phi m_0^{0*}$ of symmetry-partner particles or objects in the quartet of intrinsic metric spaces $\phi\rho'$, $\phi\rho^{0\prime}$, $-\phi\rho'^*$ and $-\phi\rho^{0\prime *}$, are located at symmetry-partner points in their respective intrinsic spaces always, even when they are in intrinsic motions relative to symmetry-partner frames of reference in their respective Euclidean 3-spaces.

There is a complementary diagram to Fig. 3, which is valid with respect to 3-observers in the proper Euclidean 3-space $\Sigma^{0\prime}$ along the vertical, which must also be drawn along with Fig. 3. Now given the quartet of the proper physical (or metric) Euclidean 3-spaces and their underlying one-dimensional intrinsic metric spaces in Fig. 2, then Fig. 3 with the absolute speeds V_0 of the proper Euclidean 3-spaces and absolute intrinsic speed ϕV_0 of the proper intrinsic spaces assigned with respect to 3-observers in the proper Euclidean 3-space Σ' of the positive (or our) universe, ensues automatically.

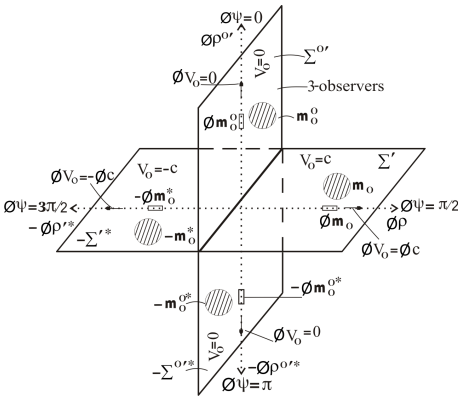

Fig. 4: Co-existing four mutually orthogonal proper Euclidean 3-spaces and their underlying isotropic one-dimensional proper intrinsic metric spaces, where the speeds V_0 of the Euclidean 3-spaces and the intrinsic speeds ϕV_0 of the intrinsic spaces, relative to 3-observers in the proper Euclidean 3-space $\Sigma^{0\prime}$ (considered as a hyper-surface) along the vertical in the first quadrant are shown.

On the other hand, the proper physical Euclidean 3-space $\Sigma^{0\prime}$ along the vertical in Fig. 2 possesses zero absolute speed ($V_0 = 0$) at every point of it and its underlying one- dimensional intrinsic space $\phi\rho^{0\prime}$ possesses zero absolute intrinsic speed ($\phi V_0 = 0$) at every point along its length with respect to 3-observers in $\Sigma^{0\prime}$. This is so since $\phi\rho^{0\prime}$ must be considered as rotated by zero intrinsic angle ($\phi\psi_0 = 0$) relative to itself (or relative to the vertical) when the observers of interest are the 3-observers in $\Sigma^{0\prime}$. Then letting $\phi\psi_0 = 0$ in (1) gives zero absolute intrinsic speed ($\phi V_0 = 0$) at every point along $\phi\rho^{0\prime}$ with respect to 3-observers in $\Sigma^{0\prime}$. The physical Euclidean 3-space $\Sigma^{0\prime}$ then possesses zero absolute speed ($V_0 = 0$) at every point of it as the outward manifestation of $\phi V_0 = 0$ at every point along $\phi\rho^{0\prime}$, with respect to 3-observers in $\Sigma^{0\prime}$. It then follows that Fig. 3 with respect to 3-observers in our Euclidean 3-space Σ' corresponds to Fig. 4 with respect to 3-observers in the Euclidean 3-space $\Sigma^{0\prime}$.

It is mandatory to consider the intrinsic metric space $\phi\rho'$ of the positive (or our) universe along the horizontal in the first quadrant as naturally rotated clockwise by a positive intrinsic angle $\phi\psi_0 = \frac{\pi}{2}$; the intrinsic metric space $-\phi\rho^{0\prime *}$ along the vertical in the fourth quadrant as naturally rotated clockwise by a positive intrinsic angle $\phi\psi_0 = \pi$ and the intrinsic metric space $-\phi\rho'^*$ of the negative universe along the horizontal in the third quadrant as naturally rotated clockwise by a positive intrinsic angle $\phi\psi_0 = \frac{3\pi}{2}$ relative to $\phi\rho^{0\prime}$ along the vertical in the first quadrant or with respect to 3-observers in the Euclidean 3-space $\Sigma^{0\prime}$, as indicated in Fig. 4. This way, the positive signs of our proper intrinsic space $\phi\rho'$ and of the

dimensions $x^{1\prime}$, $x^{2\prime}$ and $x^{3\prime}$ of our proper Euclidean 3-space Σ', as well as the positive signs of parameters in Σ' in our (or positive) universe in Fig. 3 are preserved in Fig. 4. The negative signs of $-\phi\rho'^{*}$, $-\Sigma'^{*}$ and of parameters in $-\Sigma'^{*}$ in the negative universe in Fig. 3 are also preserved in Fig. 4, by virtue of the clockwise sense of rotation by positive intrinsic angle $\phi\psi_0$ of $-\phi\rho^{0\prime *}$ and $-\phi\rho'^{*}$ relative to $\phi\rho^{0\prime}$ or with respect to 3-observers in $\Sigma^{0\prime}$ in Fig. 4.

If the clockwise rotations of $\phi\rho'$, $-\phi\rho^{0\prime *}$ and $-\phi\rho'^{*}$ relative to $\phi\rho^{0\prime}$ or with respect to 3-observers in $\Sigma^{0\prime}$ in Fig. 4, have been considered as rotation by negative intrinsic angles $\phi\psi_0 = -\frac{\pi}{2}, \phi\psi_0 = -\pi$ and $\phi\psi_0 = -\frac{3\pi}{2}$ respectively, then the positive sign of $\phi\rho', \Sigma'$ and of parameters in Σ' of the positive (or our) universe in Fig. 3 would have become negative sign in Fig. 4 and the negative sign of $-\phi\rho'^{*}$ and $-\Sigma'^{*}$ and of parameters in $-\Sigma'^{*}$ of the negative universe in Fig. 3 would have become positive sign in Fig. 4. That is, the positions of the positive and negative universes in Fig. 3 would have been interchanged in Fig. 4, which must not be.

We have thus been led to an important conclusion that natural rotations of intrinsic metric spaces by positive absolute intrinsic angle $\phi\psi_0$ (and consequently the relative rotations of intrinsic affine space coordinates in the context of intrinsic special relativity (ϕSR) by positive relative intrinsic angles, $\phi\psi$), are clockwise rotations with respect to 3-observers in the proper Euclidean 3-spaces $\Sigma^{0\prime}$ and $-\Sigma^{0\prime *}$ along the vertical (in Fig. 4). Whereas rotation of intrinsic metric spaces (and intrinsic affine space coordinates in the context of ϕSR) by positive intrinsic angles are anti-clockwise rotations with respect to 3-observers in the proper Euclidean 3-spaces Σ' and $-\Sigma'^{*}$ of the positive and negative universes along the horizontal in Fig. 3.

The origin of the natural isotropic absolute speeds V_0 of every point of the proper Euclidean 3-spaces and of the natural absolute intrinsic speeds ϕV_0 of every point along the lengths of the one-dimensional proper intrinsic spaces with respect to the indicated observers in Fig. 3 and Fig. 4, cannot be exposed in this paper. It must be regarded as an outstanding issue to be resolved elsewhere with further development. Nevertheless, a preemptive statement about their origin is appropriate at this point: They are the outward manifestations in the proper physical Euclidean 3-spaces and proper intrinsic spaces of the absolute speeds with respect to the indicated observers, of homogeneous and isotropic absolute spaces (distinguished co-moving coordinate systems) that underlie the proper physical Euclidean 3-spaces and their underlying proper intrinsic spaces in nature, which have not yet appeared in Figs. 3 and Fig. 4.

Leibnitz pointed out that Newtonian mechanics prescribes a distinguished coordinate system (the Newtonian absolute space) in which it is valid [3, see p. 2]. Albert Einstein said, "Newton might no less well have called his absolute space ether..." [4] and argued that the proper (or classical) physical Euclidean 3-space (of Newtonian mechanics) will be impossible without such ether. He also pointed out the existence of ether of general relativity as a necessary requirement for the possibility of that theory, just as the existence of luminiferous ether was postulated to support the propagation of electromagnetic waves. Every dynamical or gravitational law (including Newtonian mechanics) requires (or has) an ether. It is the non-detectable absolute speeds of the ethers of classical mechanics (known to Newton as absolute spaces), which underlie the proper physical Euclidean 3-spaces with respect to the indicated observers in Fig. 3 and 4, that are made manifest in the non-detectable absolute speeds V_0 of the proper Euclidean 3-spaces with respect to the indicated observers in those figures. However this a matter to be formally derived elsewhere, as mentioned above.

1.2 Geometrical contraction of the vertical Euclidean 3-spaces to one-dimensional spaces relative to 3-observers in the horizontal Euclidean 3-spaces and conversely

Let us consider the $x'y'-$plane of our proper Euclidean 3-space Σ' in Fig. 3: Corresponding to the $x'y'-$plane of Σ' is the $x^{0\prime}y^{0\prime}-$plane of the Euclidean 3-space $\Sigma^{0\prime}$. However since Σ' and $\Sigma^{0\prime}$ are orthogonal Euclidean 3-spaces, following the operational definition of orthogonal Euclidean 3-spaces at the beginning of the preceding sub-section, the dimensions $x^{0\prime}$ and $y^{0\prime}$ of the $x^{0\prime}y^{0\prime}-$plane of $\Sigma^{0\prime}$ are both perpendicular to each of the dimensions x' and y' of Σ'. Hence $x^{0\prime}$ and $y^{0\prime}$ are effectively parallel dimensions normal to the $x'y'-$ plane of Σ' with respect to 3-observers in Σ'. Symbolically:

$$x^{0\prime} \perp x' \text{ and } y^{0\prime} \perp x';\ x^{0\prime} \perp y' \text{ and } y^{0\prime} \perp y' \Rightarrow x^{0\prime} \| y^{0\prime} \quad (*)$$

Likewise, corresponding to the $x'z'-$plane of Σ' is the $x^{0\prime}z^{0\prime}-$plane of $\Sigma^{0\prime}$. Again the dimensions $x^{0\prime}$ and $z^{0\prime}$ of the $x^{0\prime}z^{0\prime}-$plane of $\Sigma^{0\prime}$ are both perpendicular to each of the dimensions x' and z' of the $x'z'-$ plane of Σ'. Hence $x^{0\prime}$ and $y^{0\prime}$ are effectively parallel dimensions normal to the $x'z'-$plane of Σ' with respect to 3-observers in Σ'. Symbolically:

$$x^{0\prime} \perp x' \text{ and } z^{0\prime} \perp x';\ x^{0\prime} \perp z' \text{ and } z^{0\prime} \perp z' \Rightarrow x^{0\prime} \| z^{0\prime} \quad (**)$$

Finally, corresponding to the $y'z'-$plane of Σ' is the $y^{0\prime}z^{0\prime}-$plane of $\Sigma^{0\prime}$. Again the dimensions $y^{0\prime}$ and $z^{0\prime}$ of the $y^{0\prime}z^{0\prime}-$plane of $\Sigma^{0\prime}$ are both perpendicular to each of the dimensions y' and z' of the $y'z'-$ plane of Σ'. Hence $y^{0\prime}$ and $z^{0\prime}$ are effectively parallel dimensions normal to the $y'z'-$plane of Σ' with respect to 3-observers in Σ'. Symbolically:

$$y^{0\prime} \perp y' \text{ and } z^{0\prime} \perp y';\ y^{0\prime} \perp z' \text{ and } z^{0\prime} \perp z' \Rightarrow y^{0\prime} \| z^{0\prime} \quad (***)$$

Indeed $x^{0\prime} \| y^{0\prime}$ and $x^{0\prime} \| z^{0\prime}$ in $(*)$ and $(**)$ already implies $y^{0\prime} \| z^{0\prime}$ in $(***)$.

The combination of $(*)$, $(**)$ and $(***)$ give $x^{0\prime} \| y^{0\prime} \| z^{0\prime}$ with respect to 3-observers in Σ', which says that the mutually perpendicular dimensions $x^{0\prime}$, $y^{0\prime}$ and $z^{0\prime}$ of $\Sigma^{0\prime}$ with

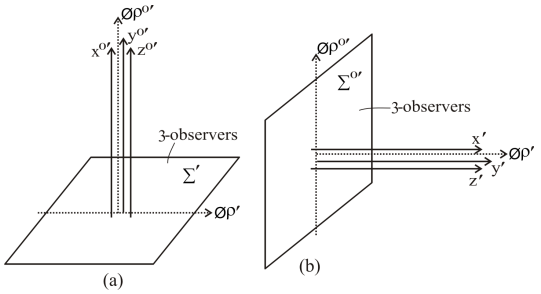

Fig. 5: Given the two orthogonal proper Euclidean 3-spaces $\Sigma^{0\prime}$ and Σ' of Fig. 1 then, (a) the mutually perpendicular dimensions of the proper Euclidean 3-space $\Sigma^{0\prime}$ with respect to 3-observers in it, are naturally "bundle" into parallel dimensions relative to 3-observers in our proper Euclidean 3-space Σ' and (b) the mutually perpendicular dimensions of our proper Euclidean 3-space Σ' with respect to 3-observer in it are naturally "bundled" into parallel dimensions relative to 3-observers in the proper Euclidean 3-space $\Sigma^{0\prime}$.

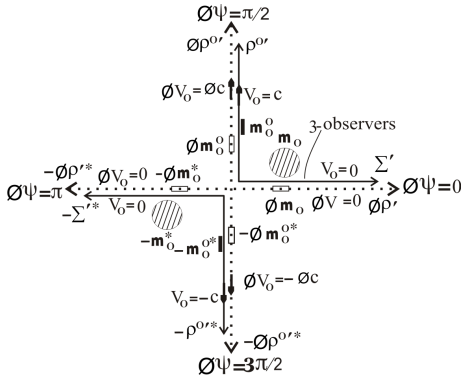

Fig. 6: (a) The proper Euclidean 3-spaces $\Sigma^{0\prime}$ and $-\Sigma^{0\prime *}$ along the vertical in Fig. 3, are naturally contracted to one-dimensional proper spaces $\rho^{0\prime}$ and $-\rho^{0\prime *}$ respectively relative to 3-observers in the proper Euclidean 3-spaces Σ' and $-\Sigma'^{*}$ along the horizontal.

respect to 3-observers in $\Sigma^{0\prime}$ are effectively parallel dimensions with respect to 3-observers in our Euclidean 3-space Σ'. In other words, the dimensions $x^{0\prime}$, $y^{0\prime}$ and $z^{0\prime}$ of $\Sigma^{0\prime}$ effectively form a "bundle", which is perpendicular to each of the dimensions x', y' and z' of Σ' with respect to 3-observers in Σ' in Fig. 3. The "bundle" must lie along a fourth dimension with respect to 3-observers in Σ' consequently, as illustrated in Fig. 5a, where the proper Euclidean 3-space Σ' is considered as a hyper-surface represented by a horizontal plane surface.

Conversely, the mutually perpendicular dimensions x', y' and z' of our Euclidean 3-space Σ' with respect to 3-observers in Σ' are effectively parallel dimensions with respect to 3-observers in the Euclidean 3-space $\Sigma^{0\prime}$ in Fig. 4. In other words, the dimensions x', y' and z' of Σ' effectively form a "bundle", which is perpendicular to each of the dimensions $x^{0\prime}$, $y^{0\prime}$ and $z^{0\prime}$ of $\Sigma^{0\prime}$ with respect to 3-observers in $\Sigma^{0\prime}$ in Fig. 4. The "bundle" of x', y' and z' must lie along a fourth dimension with respect to 3-observers in $\Sigma^{0\prime}$ consequently, as illustrated in Fig. 5b, where the proper Euclidean 3-space $\Sigma^{0\prime}$ is considered as a hyper-surface represented by a vertical plane surface.

The three dimensions $x^{0\prime}$, $y^{0\prime}$ and $z^{0\prime}$ that are shown as separated parallel dimensions, thereby constituting a "bundle" along the vertical with respect to 3-observers in Σ' in Fig. 5a, are not actually separated. Rather they lie along the singular fourth dimension, thereby constituting a one-dimensional space to be denoted by $\rho^{0\prime}$ with respect to 3-observers in Σ' in Fig. 5a. Likewise the "bundle" of parallel dimensions x', y' and z' effectively constitutes a one-dimensional space to be denoted by ρ' with respect to 3-observers in $\Sigma^{0\prime}$ in Fig. 5b. Thus Fig. 5a shall be replaced with the fuller diagram of Fig. 6a, which is valid with respect to 3-observers in the Euclidean 3-space Σ', while Fig. 5b shall be replaced with the fuller diagram of Fig. 6b, which is valid with respect to 3-observers in the proper Euclidean 3-space $\Sigma^{0\prime}$.

Representation of the Euclidean spaces Σ', $-\Sigma'^{*}$, $\Sigma^{0\prime}$ and $-\Sigma^{0\prime *}$ by plane surfaces in the previous diagrams in this paper has temporarily been changed to lines in Figs. 6a and 6b for convenience. The three-dimensional rest masses m_0 and $-m_0^*$ in the Euclidean 3-spaces Σ' and $-\Sigma'^{*}$ and m_0^0 and $-m_0^{0*}$ in $\Sigma^{0\prime}$and $-\Sigma^{0\prime *}$ have been represented by circles to remind us of their three-dimensionality, while the one-dimensional intrinsic rest masses in the one-dimensional intrinsic spaces $\phi\rho^{0\prime}$, $-\phi\rho^{0\prime *}$, $\phi\rho'$ and $-\phi\rho'^{*}$ and the one-dimensional rest masses in the one-dimensional spaces $\rho^{0\prime}$, $-\rho^{0\prime *}$, ρ' and $-\rho'^{*}$ have been represented by short line segments in Figs. 6a and 6b.

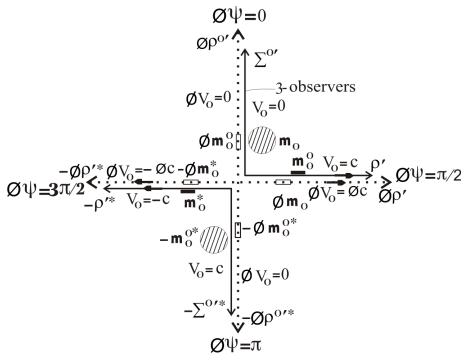

Fig. 6: (b) The proper Euclidean 3-spaces Σ' and $-\Sigma'^{*}$ along the horizontal in Fig. 4, are naturally contracted to one-dimensional proper spaces ρ' and $-\rho'^{*}$ respectively relative to 3-observers in the proper Euclidean 3-spaces $\Sigma^{0\prime}$ and $-\Sigma^{0\prime *}$ along the vertical.

Fig. 3 naturally simplifies as Fig. 6a with respect to 3-observers in the proper Euclidean 3-space Σ' of the positive (or our) universe, while Fig. 4 naturally simplifies as Fig. 6b with respect to 3-observers in the proper Euclidean 3-space $\Sigma^{0\prime}$ along the vertical. The vertical Euclidean 3-spaces $\Sigma^{0\prime}$ and $-\Sigma^{0\prime *}$ in Fig. 3 have been geometrically contracted to one-dimensional proper spaces $\rho^{0\prime}$ and $-\rho^{0\prime *}$ respectively with respect to 3-observers in the proper Euclidean 3-spaces Σ' and $-\Sigma'^{*}$ of the positive and negative universes and the proper Euclidean 3-spaces Σ' and $-\Sigma'^{*}$ of the positive and negative universes along the horizontal in Fig. 4, have been geometrically contracted to one-dimensional proper spaces ρ' and $-\rho'^{*}$ respectively with respect to 3-observers in the vertical proper Euclidean 3-spaces $\Sigma^{0\prime}$ and $-\Sigma^{0\prime *}$ in Fig. 6b, as actualization of the topic of this sub-section.

The isotropic absolute speed $V_0 = c$ of every point of the Euclidean 3-space $\Sigma^{0\prime}$ with respect to 3-observers in the Euclidean 3-space Σ' in Fig. 3 is now absolute speed $V_0 = c$ of every point along the one-dimensional space $\rho^{0\prime}$ with respect to 3-observers in Σ' in Fig. 6a. The isotropic absolute speed $V_0 = -c$ of every point of the Euclidean 3-space $-\Sigma^{0\prime *}$ with respect to 3-observers in Σ' in Fig. 3 is likewise absolute speed $V_0 = -c$ of every point along the one-dimensional space $-\rho^{0\prime *}$ with respect to 3-observers in Σ' in Fig. 6a.

Just as the absolute speed $V_0 = c$ of every point along $\rho^{0\prime}$ and the absolute intrinsic speed $\phi V_0 = \phi c$ of every point along the intrinsic space $\phi\rho^{0\prime}$ with respect to 3-observers in Σ' in Fig. 6a are isotropic, that is, without unique orientation in the Euclidean 3-space $\Sigma^{0\prime}$ that contracts to $\rho^{0\prime}$, with respect to 3-observers in Σ' and $-\Sigma'^{*}$, so are the one-dimensional space $\rho^{0\prime}$ and the one-dimensional intrinsic space $\phi\rho^{0\prime}$ isotropic dimension and isotropic intrinsic dimension respectively with no unique orientation in the Euclidean 3-space $\Sigma^{0\prime}$, with respect to 3-observers in the Euclidean 3-spaces Σ' and $-\Sigma'^{*}$. The one-dimensional space $-\rho^{0\prime *}$ and one-dimensional intrinsic space $-\phi\rho^{0\prime *}$ are likewise isotropic dimension and isotropic intrinsic dimension respectively with no unique orientation in the Euclidean 3-space $-\Sigma^{0\prime *}$ with respect to 3-observers in the Euclidean 3-spaces Σ' and $-\Sigma'^{*}$ in Fig. 6a.

The isotropic absolute speed $V_0 = c$ of every point of the Euclidean 3-space Σ' and the isotropic absolute speed $V_0 = -c$ of every point of the Euclidean 3-space $-\Sigma'^{*}$ with respect to 3-observers in $\Sigma^{0\prime}$ in Fig. 4 are now absolute speed $V_0 = c$ of every point along the one-dimensional space ρ' and absolute speed $V_0 = -c$ of every point along the one-dimensional space $-\rho'^{*}$ with respect to 3-observers in $\Sigma^{0\prime}$ Fig. 6b. Again the one-dimensional metric spaces ρ' and $-\rho'^{*}$ and the one-dimensional intrinsic metric spaces $\phi\rho'$ and $-\phi\rho'^{*}$ are isotropic dimensions and isotropic intrinsic dimensions respectively with no unique orientations in the Euclidean 3-spaces Σ' and $-\Sigma'^{*}$ that contract to ρ' and $-\rho'^{*}$ respectively, with respect to 3-observers in the vertical Euclidean 3-spaces $\Sigma^{0\prime}$ and $-\Sigma^{0\prime *}$ in Fig. 6b.

1.3 The vertical proper Euclidean 3-spaces as proper time dimensions relative to 3-observers in the horizontal proper Euclidean 3-spaces and conversely

Figs. 6a and 6b are intermediate diagrams. It shall be shown finally in this section that the one-dimensional proper spaces $\rho^{0\prime}$ and $-\rho^{0\prime *}$ in Fig. 6a naturally transform into the proper time dimensions ct' and $-ct'^{*}$ respectively and their underlying one-dimensional proper intrinsic spaces $\phi\rho^{0\prime}$ and $-\phi\rho^{0\prime *}$ naturally transform into the proper intrinsic time dimensions $\phi c\phi t'$ and $-\phi c\phi t'^{*}$ respectively with respect to 3-observers in the proper Euclidean 3-spaces Σ' and $-\Sigma'^{*}$ in that figure. It shall also be shown that the one-dimensional proper spaces ρ' and $-\rho'^{*}$ in Fig. 6b naturally transform into the proper time dimensions $ct^{0\prime}$ and $-ct^{0\prime *}$ respectively and their underlying proper intrinsic spaces $\phi\rho'$ and $-\phi\rho'^{*}$ naturally transform into proper intrinsic time dimensions $\phi c\phi t^{0\prime}$ and $-\phi c\phi t^{0\prime *}$ respectively with respect to 3-observers in the proper Euclidean 3-spaces $\Sigma^{0\prime}$ and $-\Sigma^{0\prime *}$ in that figure.

Now let us re-present the generalized forms of the intrinsic Lorentz transformations and its inverse derived and presented as systems (44) and (45) of [1] respectively as follows

$$\left.\begin{aligned} \phi c\,\phi\tilde{t}' &= \sec\phi\psi(\phi c\phi\tilde{t} - \phi\tilde{x}\sin\phi\psi);\\ &\quad (\text{w.r.t. } 1-\text{observer in } c\tilde{t});\\ \phi\tilde{x}' &= \sec\phi\psi(\phi\tilde{x} - \phi c\phi\tilde{t}\sin\phi\psi);\\ &\quad (\text{w.r.t. } 3-\text{observer in } \tilde{\Sigma}) \end{aligned}\right\} \tag{2}$$

and

$$\left.\begin{aligned} \phi c\phi\tilde{t} &= \sec\phi\psi(\phi c\phi\tilde{t}' + \phi\tilde{x}'\sin\phi\psi);\\ &\quad (\text{w.r.t. } 3-\text{observer in } \tilde{\Sigma}');\\ \phi\tilde{x} &= \sec\phi\psi(\phi\tilde{x}' + \phi c\phi\tilde{t}'\sin\phi\psi);\\ &\quad (\text{w.r.t. } 1-\text{observer in } c\tilde{t}') \end{aligned}\right\}. \tag{3}$$

As explained in [1], systems (2) and (3) can be applied for all values of the intrinsic angle $\phi\psi$ in the first cycle, $0 \le \phi\psi \le 2\pi$, except that $\phi\psi = \frac{\pi}{2}$ and $\phi\psi = \frac{3\pi}{2}$ must be avoided.

One observes from system (2) that the pure intrinsic affine time coordinate $\phi c\phi\tilde{t}'$ of the primed (or particle's) intrinsic frame with respect to an observer at rest relative to the particle's frame, transforms into an admixture of intrinsic affine time and intrinsic affine space coordinates of the unprimed (or observer's) intrinsic frame. The pure intrinsic affine space coordinate $\phi\tilde{x}'$ of the primed (or particle's) frame likewise transforms into an admixture of intrinsic affine space and intrinsic affine time coordinates of the unprimed (or particle's) intrinsic frame, when the particle's frame is in motion relative to the observer's frame. The inverses of these observations obtain from system (3), which is the inverse to system (2).

The observations made from system (2) and system (3) described in the foregoing paragraph make the concept of intrinsic affine spacetime induction relevant in relative intrinsic motion of two intrinsic spacetime frames of reference. In order to make this more explicit, let us re-write systems (2) and

(3) respectively as follows

$$\left.\begin{array}{rcl} \phi c\phi\tilde{t}' & = & \sec\phi\psi(\phi c\phi\tilde{t}+\phi c\phi\tilde{t}_i); \\ & & (\text{w.r.t. } 1-\text{observer in } c\tilde{t}); \\ \phi\tilde{x}' & = & \sec\phi\psi(\phi\tilde{x}+\phi\tilde{x}_i); \\ & & (\text{w.r.t. } 3-\text{observer in } \tilde{\Sigma}) \end{array}\right\} \quad (4)$$

and

$$\left.\begin{array}{rcl} \phi c\phi\tilde{t} & = & \sec\phi\psi(\phi c\phi\tilde{t}'+\phi c\phi\tilde{t}'_i); \\ & & (\text{w.r.t. } 3-\text{observer in } \tilde{\Sigma}'); \\ \phi\tilde{x} & = & \sec\phi\psi(\phi\tilde{x}'+\phi\tilde{x}'_i); \\ & & (\text{w.r.t. } 1-\text{observer in } c\tilde{t}') \end{array}\right\}. \quad (5)$$

A comparison of systems (4) and (2) gives the relations for the induced unprimed intrinsic affine spacetime coordinates $\phi c\phi\tilde{t}_i$ and $\phi\tilde{x}_i$ as follows

$$\phi c\phi\tilde{t}_i = \phi\tilde{x}\sin(-\phi\psi) = -\phi\tilde{x}\sin\phi\psi = -\frac{\phi v}{\phi c}\phi\tilde{x}; \quad (6)$$

w.r.t. $1-$ observer in $c\tilde{t}$ and

$$\phi\tilde{x}_i = \phi c\phi\tilde{t}\sin(-\phi\psi) = -\phi c\phi\tilde{t}\sin\phi\psi = -\frac{\phi v}{\phi c}\phi c\phi\tilde{t} = -\phi v\phi\tilde{t}; \quad (7)$$

w.r.t $3-$ observer in $\tilde{\Sigma}$.

Diagrammatically, the induced unprimed intrinsic affine time coordinate, $\phi c\phi\tilde{t}_i = \phi\tilde{x}\sin(-\phi\psi)$ in (6), appears in the fourth quadrant in Fig. 9a of [1] as $\phi\tilde{x}^*\sin(-\phi\psi)$ and the induced unprimed intrinsic affine space coordinate, $\phi\tilde{x}_i = \phi c\phi\tilde{t}\sin(-\phi\psi)$ in (7), appears in the second quadrant in Fig. 9b of [1] as $\phi c\phi\tilde{t}^*\sin(-\phi\psi)$.

And a comparison of systems (5) and (3) gives the relations for the induced primed intrinsic affine spacetime coordinates $\phi c\phi\tilde{t}'_i$ and $\phi\tilde{x}'_i$ as follows

$$\phi c\phi\tilde{t}'_i = \phi\tilde{x}'\sin\phi\psi = \frac{\phi v}{\phi c}\phi\tilde{x}'; \quad (8)$$

w.r.t. $3-$ observer in $\tilde{\Sigma}'$ and

$$\phi\tilde{x}'_i = \phi c\phi\tilde{t}'\sin\phi\psi = \frac{\phi v}{\phi c}\phi c\phi\tilde{t}' = \phi v\phi\tilde{t}'; \quad (9)$$

w.r.t. $1-$ observer in $c\tilde{t}'$.

Diagrammatically, the induced primed intrinsic affine time coordinate, $\phi c\phi\tilde{t}'_i = \phi\tilde{x}'\sin\phi\psi$ in Eq. (8), appears in the fourth quadrant in Fig. 8b of [1], where it is written as $\phi\tilde{x}'^*\sin\phi\psi$ and the induced primed intrinsic affine space coordinate, $\phi\tilde{x}'_i = \phi c\phi\tilde{t}'\sin\phi\psi$ in (9), appears in the second quadrant in Fig. 8a of [1], where it is written as $\phi c\phi\tilde{t}'^*\sin\phi\psi$.

The intrinsic affine time induction relation (6) states that an intrinsic affine space coordinate $\phi\tilde{x}$ of the unprimed intrinsic frame, which is inclined at negative intrinsic angle $-\phi\psi$ relative to the intrinsic affine space coordinate $\phi\tilde{x}'$ of the primed intrinsic frame, due to the negative intrinsic speed $-\phi v$ of the unprimed intrinsic frame relative to the primed intrinsic frame, projects (or induces) a negative unprimed intrinsic affine time coordinate, $\phi c\phi\tilde{t}_i = \phi\tilde{x}\sin(-\phi\psi) = -\phi\tilde{x}\sin\phi\psi$, along the vertical relative to the 1-observer in $c\tilde{t}$.

The intrinsic affine space induction relation (7) states that an intrinsic affine time coordinate $\phi c\phi\tilde{t}$ of the observer's (or unprimed) intrinsic frame, which is inclined at negative intrinsic angle $-\phi\psi$ relative to the intrinsic affine time coordinate $\phi c\phi\tilde{t}'$ of the particle's (or primed) intrinsic frame along the vertical, due to the negative intrinsic speed $-\phi v$ of the intrinsic observer's frame relative to the intrinsic particle's frame, induces a negative unprimed intrinsic affine space coordinate, $\phi\tilde{x}_i = \phi c\phi\tilde{t}\sin(-\phi\psi) = -\phi c\phi\tilde{t}\sin\phi\psi$, along the horizontal relative to 3-observer in $\tilde{\Sigma}$.

The intrinsic affine time induction relation (8) states that an intrinsic affine space coordinate $\phi\tilde{x}'$ of the particle's (or primed) intrinsic frame, which is inclined relative to the intrinsic affine space coordinate $\phi\tilde{x}$ of the observer's (or unprimed) intrinsic frame at a positive intrinsic angle $\phi\psi$, due to the intrinsic motion of the particle's (or primed) intrinsic frame at positive intrinsic speed ϕv relative to the observer's (or unprimed) intrinsic frame, induces positive primed intrinsic affine time coordinate, $\phi c\phi\tilde{t}'_i = \phi\tilde{x}'\sin\phi\psi$, along the vertical relative to the 3-observer in $\tilde{\Sigma}'$.

Finally the intrinsic affine space induction relation (9) states that an intrinsic affine time coordinate $\phi c\phi\tilde{t}'$ of the primed intrinsic frame, which is inclined at positive intrinsic angle $\phi\psi$ relative to the intrinsic affine time coordinate $\phi c\phi\tilde{t}$ along the vertical of the primed intrinsic frame, due to the intrinsic motion of the primed intrinsic frame at positive intrinsic speed ϕv relative to the unprimed intrinsic frame, induces positive primed intrinsic affine space coordinate, $\phi\tilde{x}'_i = \phi c\phi\tilde{t}'\sin\phi\psi$, along the horizontal relative to the 1-observer in $c\tilde{t}'$.

The outward manifestations on flat four-dimensional affine spacetime of the intrinsic affine spacetime induction relations (6)–(9) are given by simply removing the symbol ϕ from those relations respectively as follows

$$c\tilde{t}_i = \tilde{x}\sin(-\psi) = -\tilde{x}\sin\psi = -\frac{v}{c}\tilde{x}; \quad (10)$$

w.r.t. $1-$ observer in $c\tilde{t}$;

$$\tilde{x}_i = c\tilde{t}\sin(-\psi) = -c\tilde{t}\sin\psi = -\frac{v}{c}c\tilde{t} = -v\tilde{t}; \quad (11)$$

w.r.t. $3-$ observer in $\tilde{\Sigma}$;

$$c\tilde{t}'_i = \tilde{x}'\sin\psi = \frac{v}{c}\tilde{x}'; \quad (12)$$

w.r.t. $3-$ observer in $\tilde{\Sigma}'$ and

$$\tilde{x}'_i = c\tilde{t}'\sin\psi = \frac{v}{c}c\tilde{t}' = v\tilde{t}'; \quad (13)$$

w.r.t. $1-$ observer in $c\tilde{t}'$.

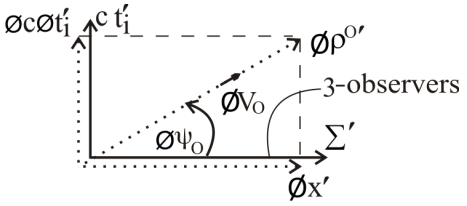

Fig. 7: Proper intrinsic metric time dimension and proper metric time dimension are induced along the vertical with respect to 3-observers in the proper Euclidean 3-space Σ' (as a hyper-surface represented by a line) along the horizontal, by a proper intrinsic metric space that is inclined to the horizontal.

However the derivation of the intrinsic affine spacetime induction relations (6)–(9) in the context of ϕSR and their outward manifestations namely, the affine spacetime induction relations (10)–(13) in the context of SR, are merely to demonstrate explicitly the concept of intrinsic affine spacetime induction that is implicit in intrinsic Lorentz transformation (ϕLT) and its inverse in the context of ϕSR and affine spacetime induction that is implicit in Lorentz transformation (LT) and its inverse in the context of SR.

On the other hand, our interest in this sub-section is in intrinsic metric time induction that arises by virtue of possession of absolute intrinsic speed ϕV_0 naturally at every point along the length of a proper intrinsic metric space, $\phi\rho^{0\prime}$, say, relative to another proper intrinsic metric space, $\phi\rho'$, say, in Fig. 3. Let us assume, for the purpose of illustration, that a proper intrinsic metric space $\phi\rho^{0\prime}$ possesses an absolute intrinsic speed $\phi V_0 < \phi c$ naturally at every point along its length relative to our proper intrinsic metric space $\phi\rho'$ along the horizontal, instead of the absolute intrinsic speed $\phi V_0 = \phi c$ of every point along the length of $\phi\rho^{0\prime}$ relative to $\phi\rho'$ in Fig. 3. Then $\phi\rho^{0\prime}$ will be inclined at an absolute intrinsic angle $\phi\psi_0 < \frac{\pi}{2}$ relative to $\phi\rho'$ along the horizontal, as illustrated in Fig. 7, instead of inclination of $\phi\rho^{0\prime}$ to the horizontal by absolute intrinsic angle $\phi\psi_0 = \frac{\pi}{2}$ in Fig. 3.

As shown in Fig. 7, the inclined proper intrinsic metric space $\phi\rho^{0\prime}$ induces proper intrinsic metric time dimension $\phi c\phi t'_i$ along the vertical with respect to 3-observers in our proper Euclidean 3-space Σ' along the horizontal. The intrinsic metric time induction relation with respect to 3-observers in Σ' in Fig. 7, takes the form of the primed intrinsic affine time induction relation (8) with respect to 3-observer in $\tilde{\Sigma}'$ in the context of ϕSR. We must simply replace the primed intrinsic affine spacetime coordinates $\phi c\phi\tilde{t}'_i$ and $\phi\tilde{x}'$ by proper intrinsic metric spacetime dimensions $\phi c\phi t'_i$ and $\phi\rho^{0\prime}$ respectively and the relative intrinsic angle $\phi\psi$ and relative intrinsic speed ϕv by absolute intrinsic angle $\phi\psi_0$ and absolute intrinsic speed ϕV_0 in (8) to have as follows

$$\phi c\phi t'_i = \phi\rho^{0\prime}\sin\phi\psi_0 = \frac{\phi V_0}{\phi c}\phi\rho^{0\prime}; \qquad (14)$$

w.r.t. all 3 − observers in Σ'. And the outward manifestation of (14) is

$$ct'_i = \rho^{0\prime}\sin\psi_0 = \frac{V_0}{c}\rho^{0\prime}; \qquad (15)$$

w.r.t. all 3 − observers in Σ'.

The induced proper intrinsic metric time dimension $\phi c\phi t'_i$ along the vertical in (14) is made manifest in induced proper metric time dimension ct'_i in (15) along the vertical, as shown in Fig. 7. As indicated, relations (14) and (15) are valid with respect to all 3-observers in our proper Euclidean 3-space Σ' overlying our proper intrinsic metric space $\phi\rho'$ along the horizontal in Fig. 7.

As abundantly stated in [1] and under systems (2) and (3) earlier in this paper, the relative intrinsic angle $\phi\psi = \frac{\pi}{2}$ corresponding to relative intrinsic speed $\phi v = \phi c$, is prohibited by the intrinsic Lorentz transformation (2) and its inverse (3) in ϕSR and consequently $\phi\psi = \frac{\pi}{2}$ or $\phi v = \phi c$ is prohibited in the intrinsic affine time and intrinsic affine space induction relations (6) and (7) and their inverses (8) and (9) in ϕSR. Correspondingly, the angle $\psi = \frac{\pi}{2}$ or speed $v = c$ is prohibited in the affine time and affine space induction relations (10) and (11) and their inverses (12) and (13) in SR.

On the other hand, the absolute intrinsic speed ϕV_0 can be set equal to ϕc and hence the absolute intrinsic angle $\phi\psi_0$ can be set equal to $\frac{\pi}{2}$ in (14). This is so since, as prescribed earlier in this paper, the proper intrinsic metric space $\phi\rho^{0\prime}$ exists naturally along the vertical as in Fig. 3, corresponding to $\phi V_0 = \phi c$ and $\phi\psi_0 = \frac{\pi}{2}$ naturally in (14) with respect to 3-observers in Σ'. More over, as mentioned at the end of subsection 1.1 and as shall be developed fully elsewhere, the absolute intrinsic speed ϕV_0 of every point of the inclined $\phi\rho^{0\prime}$ with respect to all 3-observers in Σ' in Fig. 7, being the outward manifestation in $\phi\rho^{0\prime}$ of the absolute speed of the Newtonian absolute space (the ether of classical mechanics), it can take on values in the range $0 \leq \phi V_0 \leq \infty$, since the maximum speed of objects in classical mechanics is infinite speed. Thus by letting $\phi V_0 = \phi c$ and $\phi\psi_0 = \frac{\pi}{2}$ in (14) we have

$$\phi c\phi t'_i \equiv \phi c\phi t' = \phi\rho^{0\prime}; \quad \text{for } \phi V_0 = \phi c \text{ or } \phi\psi_0 = \frac{\pi}{2} \text{ in Fig. 7;} \qquad (16)$$

w.r.t. all 3 − observers in Σ'.

While relation (14) states that a proper intrinsic metric space $\phi\rho^{0\prime}$, which is inclined to $\phi\rho'$ along the horizontal at absolute intrinsic angle $\phi\psi_0 < \frac{\pi}{2}$, induces proper intrinsic metric time dimension $\phi c\phi t'_i$ along the vertical, whose length is a fraction $\phi V_0/\phi c$ or $\sin\phi\psi_0$ times the length of $\phi\rho^{0\prime}$, with respect to all 3-observers in our proper Euclidean 3-space Σ' along the horizontal, relation (16) states that a proper intrinsic metric space $\phi\rho^{0\prime}$, which is naturally inclined at intrinsic angle $\phi\psi_0 = \frac{\pi}{2}$ relative to $\phi\rho'$ along the horizontal, thereby lying along the vertical, induces proper intrinsic metric time dimension $\phi c\phi t'_i \equiv \phi c\phi t'$ along the vertical, whose length is the

length of $\phi\rho^{0\prime}$, with respect to all 3-observers in our proper Euclidean 3-space Σ' along the horizontal.

The preceding paragraph implies that a proper intrinsic metric space $\phi\rho^{0\prime}$ that is naturally rotated along the vertical is wholly converted (or wholly transformed) into proper intrinsic metric time dimension $\phi c\phi t'$ relative to all observers in our Euclidean 3-space Σ' (along the horizontal). Eq. (16) can therefore be re-written as the transformation of proper intrinsic metric space into proper intrinsic metric time dimension:

$$\phi\rho^{0\prime} \rightarrow \phi c\phi t'; \quad \text{for } \phi V_0 = \phi c \text{ or } \phi\psi_0 = \pi/2 \text{ in Fig. 7;} \quad (17)$$

w.r.t. all 3 − observers in Σ' and the outward manifestation of Eq. (17) is the transformation of the one-dimensional proper metric space $\rho^{0\prime}$ into proper metric time dimension ct':

$$\rho^{0\prime} \rightarrow ct'; \quad \text{for } V_0 = c \text{ or } \psi_0 = \pi/2 \text{ in Eq.(15);} \quad (18)$$

w.r.t. all 3 − observers in Σ'.

The condition required for the transformations (17) and (18) to obtain are naturally met by $\phi\rho^{0\prime}$ and $\rho^{0\prime}$ in Fig. 6a. This is the fact that they are naturally inclined at absolute intrinsic angle $\phi\psi_0 = \frac{\pi}{2}$ and absolute angle $\psi_0 = \frac{\pi}{2}$ respectively relative to our proper intrinsic space $\phi\rho'$ along the horizontal and consequently they naturally possess absolute intrinsic speed $\phi V_0 = \phi c$ and absolute speed $V_0 = c$ respectively at every point along their lengths with respect to all 3-observers in our proper Euclidean 3-space Σ' in that diagram.

The transformations (17) and (18) with respect to 3-observers in our proper Euclidean 3-space Σ' correspond to the following with respect to 3-observers in the proper Euclidean 3-space $-\Sigma'^{*}$ of the negative universe in Fig. 6a:

$$-\phi\rho^{0\prime *} \rightarrow -\phi c\phi t'^{*}; \quad \text{for } \phi V_0 = \phi c \text{ or } \phi\psi_0 = \pi/2; \quad (19)$$

w.r.t. all 3 − observers in $-\Sigma'^{*}$ and

$$-\rho^{0\prime *} \rightarrow -ct'^{*}; \quad \text{for } V_0 = c \text{ or } \psi_0 = \pi/2; \quad (20)$$

w.r.t. all 3 − observers in $-\Sigma'^{*}$.

The counterparts of transformations (17) and (18), which are valid with respect to 3-observers in the proper Euclidean 3-space $\Sigma^{0\prime}$ in Fig. 6b are the following

$$\phi\rho' \rightarrow \phi c\phi t^{0\prime}; \quad \text{for } \phi V_0 = \phi c \text{ or } \phi\psi_0 = \pi/2; \quad (21)$$

w.r.t. all 3 − observers in $\Sigma^{0\prime}$ and

$$\rho' \rightarrow ct^{0\prime}; \quad \text{for } V_0 = c \text{ or } \psi_0 = \pi/2; \quad (22)$$

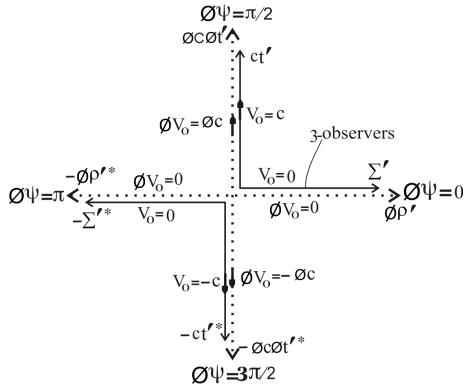

Fig. 8: a) The one-dimensional proper spaces $\rho^{0\prime}$ and $-\rho^{0\prime *}$ in Fig. 6a transform into proper time dimensions ct' and $-ct'^{*}$ respectively and the proper intrinsic spaces $\phi\rho^{0\prime}$ and $-\phi\rho^{0\prime *}$ in Fig. 6a transform into proper intrinsic time dimensions $\phi c\phi t'$ and $-\phi c\phi t'^{*}$ respectively, relative to 3-observers in the proper Euclidean 3-spaces Σ' and $-\Sigma'^{*}$ (represented by lines) along the horizontal.

w.r.t. all 3 − observers in $\Sigma^{0\prime}$ and the counterparts of transformations (19) and (20), which are valid with respect to 3-observers in the proper Euclidean 3-space $-\Sigma^{0\prime *}$ in Fig. 6b are the following

$$-\phi\rho'^{*} \rightarrow -\phi c\phi t^{0\prime *}; \quad \text{for } V_0 = c \text{ or } \psi_0 = \pi/2; \quad (23)$$

w.r.t. all 3 − observers in $-\Sigma^{0\prime *}$ and

$$-\rho'^{*} \rightarrow -ct^{0\prime *}; \quad \text{for } V_0 = c \text{ or } \psi_0 = \pi/2; \quad (24)$$

w.r.t. all 3 − observers in $-\Sigma^{0\prime *}$.

Application of transformations (17)–(20) on Fig. 6a gives Fig. 8a and application of transformation (21)–(24) on Fig. 6b gives Fig. 8b. Again representation of Euclidean 3-spaces by plane surfaces in the previous diagrams in this paper has temporarily been changed to lines in Figs. 8a and 8b, as done in Figs. 6a and 6b, for convenience.

The three-dimensional rest masses of the symmetry-partner particles or objects in the proper Euclidean 3-spaces and the one-dimensional rest masses in the proper time dimensions, as well as their underlying one-dimensional intrinsic rest masses in the proper intrinsic spaces and proper intrinsic time dimensions have been deliberately left out in Figs. 8a and 8b, unlike in Figs. 6a and 6b where they are shown. This is necessary because of further discussion required in locating the one-dimensional particles or objects in the time dimensions, which shall be done later in this paper. As indicated in Figs. 8a and 8b, the proper time dimensions ct' and $ct^{0\prime}$ possess absolute speed $V_0 = c$ at every point along their lengths, relative to 3-observers in the proper Euclidean 3-spaces Σ' and $\Sigma^{0\prime}$ respectively, like the one-dimensional

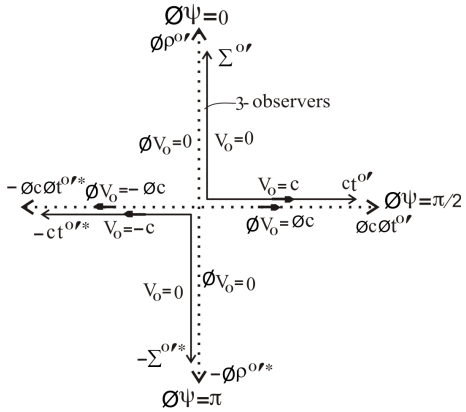

Fig. 8: b) The one-dimensional proper spaces ρ' and $-\rho'^*$ in Fig. 6b transform into proper time dimensions $ct^{0\prime}$ and $-ct^{0\prime *}$ respectively and the proper intrinsic spaces $\phi\rho'$ and $-\phi\rho'^*$ in Fig. 6b transform into proper intrinsic time dimensions $\phi c\phi t^{0\prime}$ and $-\phi c\phi t^{0\prime *}$ respectively relative to 3-observers in the proper Euclidean 3-spaces $\Sigma^{0\prime}$ and $-\Sigma^{0\prime *}$ (represented by lines) along the vertical.

spaces $\rho^{0\prime}$ and ρ' in Figs. 6a and 6b that transform into ct' and $ct^{0\prime}$ respectively in Figs. 8a and 8b. As also indicated in Figs. 8a and 8b, the proper intrinsic time dimensions $\phi c\phi t'$ and $\phi c\phi t^{0\prime}$ possess absolute intrinsic speed $\phi V_0 = \phi c$ at every point along their lengths relative to 3-observers in the proper Euclidean 3-spaces Σ' and $\Sigma^{0\prime}$ respectively, like the intrinsic spaces $\phi\rho^{0\prime}$ and $\phi\rho'$ in Figs. 6a and 6b that transform into $\phi c\phi t'$ and $\phi c\phi t^{0\prime}$ respectively in Figs. 8a and 8b. The time dimensions ct' and $ct^{0\prime}$ and the intrinsic time dimensions $\phi c\phi t'$ and $\phi c\phi t^{0\prime}$ are isotropic dimensions (with no unique orientations in the proper Euclidean 3-spaces $\Sigma^{0\prime}$ and Σ' that transform into ct' and $ct^{0\prime}$ respectively). These follow from the isotropy of the one-dimensional spaces $\rho^{0\prime}$ and ρ' in the Euclidean 3-spaces $\Sigma^{0\prime}$ and Σ' respectively in Figs. 6a and 6b that transform into ct' and $ct^{0\prime}$ respectively in Figs. 8a and 8b and from the isotropy of the one-dimensional intrinsic spaces $\phi\rho^{0\prime}$ and $\phi\rho'$ in the Euclidean 3-spaces $\Sigma^{0\prime}$ and Σ' respectively in Figs. 6a and 6b that transform into $\phi c\phi t'$ and $\phi c\phi t^{0\prime}$ respectively in Figs. 8a and 8b.

Fig. 8a is the final form to which the quartet of mutually orthogonal proper Euclidean 3-spaces and underlying one-dimensional proper intrinsic spaces in Fig. 2 naturally simplify with respect to 3-observers in the proper Euclidean 3-spaces Σ' and $-\Sigma'^*$ of the positive (or our) universe and the negative universe and Fig. 8b is the final form to which the quartet of proper Euclidean 3-spaces and underlying one-dimensional proper intrinsic spaces in Fig. 2 naturally simplify with respect to 3-observers in the proper Euclidean 3-spaces $\Sigma^{0\prime}$ and $-\Sigma^{0\prime *}$ of the positive and negative time-universes.

It follows from the natural simplification of Fig. 2 to Figs. 8a and 8b that the concept of time is secondary to the concept of space. Indeed the concept of time had evolved from the concept of space and the concept of intrinsic time had evolved from the concept of intrinsic space. This is so since given the quartet of mutually orthogonal proper metric Euclidean 3-spaces/underlying one-dimensional proper intrinsic metric spaces in Fig. 2, then the straight line one-dimensional proper metric time manifolds (or proper metric time dimensions) evolve automatically relative to 3-observers in the proper Euclidean 3-spaces, as illustrated in Figs. 8a and 8b. Thus one could ask for the origin of space without at the same time asking for the origin of time in the present picture. The origin of time and intrinsic time dimensions, which we seek in this section, has been achieved.

2 Perfect symmetry of natural laws among the isolated four universes

The four universes encompassed by Figs. 8a and 8b are the positive (or our) universe with flat proper spacetime (Σ', ct') of SR and its underlying flat two-dimensional proper intrinsic spacetime $(\phi\rho', \phi c\phi t')$ of ϕSR in Fig. 8a and the negative universe with flat proper spacetime $(-\Sigma'^*, -ct'^*)$ of SR and its underlying two-dimensional flat proper intrinsic spacetime $(-\phi\rho'^*, -\phi c\phi t'^*)$ of ϕSR in Fig. 8a.

The third universe is the one with flat proper spacetime $(\Sigma^{0\prime}, ct^{0\prime})$ of SR and its underlying flat proper intrinsic spacetime $(\phi\rho^{0\prime}, \phi c\phi t^{0\prime})$ of ϕSR in Fig. 8b. This third universe shall be referred to as the positive time-universe, since its proper Euclidean 3-space $\Sigma^{0\prime}$ and its proper intrinsic space $\phi\rho^{0\prime}$ are the proper time dimension ct' and proper intrinsic time dimension $\phi c\phi t'$ respectively of the positive (or our) universe.

The fourth universe is the one with flat proper spacetime $(-\Sigma^{0\prime *}, -ct^{0\prime *})$ of SR and its underlying flat proper intrinsic spacetime $(-\phi\rho^{0\prime *}, -\phi c\phi t^{0\prime *})$ of ϕSR in Fig. 8b. This fourth universe shall be referred to as the negative time-universe, since its proper Euclidean 3-space $-\Sigma^{0\prime *}$ and its proper intrinsic space $-\phi\rho^{0\prime *}$ are the proper time dimension $-ct'^*$ and proper intrinsic time dimension $-\phi c\phi t'^*$ respectively of the negative universe.

As prescribed earlier in this paper, the four worlds (or universes) encompassed by Figs. 8a and 8b, listed above, coexist in nature and exhibit perfect symmetry of natural laws and perfect symmetry of state among themselves. Perfect symmetry of laws among the four universes shall be demonstrated hereunder, while perfect symmetry of state among the universes shall be be demonstrated in the second part of this paper.

Demonstration of perfect symmetry of natural laws between the positive (or our) universe and the negative universe in [1] and [2] involves three steps. In the first step, the affine spacetime/intrinsic affine spacetime diagrams of Figs. 8a and 8b and Figs. 9a and 9b of [1] are derived upon the metric spacetimes/intrinsic metric spacetimes of the positive (or our) universe and the negative universe of Fig. 8a above, (which was prescribed to exist in nature and constitute a two-world background of SR in [1]).

Physical quantity or constant	Symbol	Intrinsic quantity or constant	Sign	
			positive time-universe	negative time-universe
Distance (or dimension) of space	dx^0 or x^0	$d\phi x^0$ or ϕx^0	+	−
Interval (or dimension) of time	dt^0 or t^0	$d\phi t^0$ or ϕt^0	+	−
Mass	m^0	ϕm^0	+	−
Electric charge	q	q	+ or −	− or +
Absolute entropy	S^0	ϕS^0	+	−
Absolute temperature	T	T	+	+
Energy (total, kinetic)	E^0	ϕE^0	+	−
Potential energy	U^0	ϕU^0	+ or −	− or +
Radiation energy	$h\nu^0$	$h\phi\nu^0$	+	−
Electrostatic potential	Φ_E^0	$\phi\Phi_E^0$	+ or −	+ or −
Gravitational potential	Φ^0	$\phi\Phi^0$	−	−
Electric field	$\vec{E}^0$	ϕE^0	+ or −	− or +
Magnetic field	$\vec{B}^0$	ϕB^0	+ or −	− or +
Planck constant	h	h	+	+
Boltzmann constant	k	ϕk	+	−
Thermal conductivity	k	ϕk	+	−
Specific heat capacity	c_p	ϕc_p	+	+
velocity	$\vec{v}$	ϕv	+ or −	+ or −
speeds of particles	v	ϕv	+	+
Speed of light	c	ϕc	+	+
Electric permittivity	ϵ_o^o	$\phi\epsilon_o^o$	+	+
Magnetic permeability	μ_o^o	$\phi\mu_o^o$	+	+
Angular measure	θ, φ	$\phi\theta, \phi\varphi$	+ or −	+ or −
Parity	Π	$\phi\Pi$	+ or −	− or +
⋮	⋮	⋮	⋮	⋮

Table 1. Signs of spacetime/intrinsic spacetime dimensions, some physical parameters/intrinsic parameters and some physical constants/intrinsic constants in the positive time-universe and negative time-universe.

The intrinsic Lorentz transformation/Lorentz transformation (ϕLT/LT) was then derived from those diagrams in the positive and negative universes, thereby establishing intrinsic Lorentz invariance (ϕLI) on flat two-dimensional intrinsic spacetimes and Lorentz invariance (LI) on flat four-dimensional spacetimes in the two universes in [1].

The first step in demonstrating perfect symmetry of laws between the positive (or our) universe and the negative universe in Fig. 8a of this paper described above, applies directly between the positive time-universe and the negative time-universe. The counterparts of Figs. 8a, 8b, 9a and 9b of [1], drawn upon the metric spacetimes/intrinsic metric spacetimes of the positive and negative universes of Fig. 8a of this paper in that paper, can be drawn upon the metric spacetimes/intrinsic spacetimes of the positive time-universe and negative time-universe in Figs. 8b of this paper and intrinsic Lorentz transformations/Lorentz transformation (ϕLT/LT) derived from them in the positive time-universe and the negative time-universe, as shall not be done here in order to conserve space. Intrinsic Lorentz invariance (ϕLI) on flat two-dimensional intrinsic spacetimes and Lorentz invariance (LI) on flat four-dimensional spacetimes in the positive and negative time-universes then follow with respect to observers in those universes.

The second step in demonstrating the symmetry of laws between the positive (or our) universe and the negative universe in [1] and [2], involves the derivation of the relative signs of physical parameters and physical constants and of intrinsic parameters and intrinsic constants between the positive and negative universes in [2], summarized in Table 1 of that paper. Again this second step applies directly between the positive time-universe and the negative time-universe. The relative signs of physical parameters and physical constants and of intrinsic parameters and intrinsic constants derivable between the positive time-universe and the negative time-universe, summarized in Table 1 here, follow directly from the derived signs of physical parameters and physical constants and of intrinsic parameters and intrinsic constants in the pos-

itive and negative universes, summarized in Table 1 of [2].

Table 1 here is the same as Table 1 in [2]. The superscript "0" that appears on dimensions/intrinsic dimensions and some parameters/intrinsic parameters and constants/intrinsic constants in Table 1 here is used to differentiate the dimensions/intrinsic dimensions, parameters/intrinsic parameters and constants/intrinsic constants of the positive time-universe and negative time-universe from those of the positive (or our) universe and the negative universe in Table 1 of [2].

The third and final step in demonstrating the symmetry of natural laws between the positive (or our) universe and the negative universe in [1] and [2], consists in replacing the positive spacetime dimensions and the physical parameters and physical constants that appear in (the instantaneous differential) natural laws in the positive universe by the negative spacetime dimensions and physical parameters and physical constants of the negative universe (with the appropriate signs in Table 1 of [2]), and showing that these operations leave all natural laws unchanged in the negative universe, as done in section 5 of [2].

The third step in the demonstration of the perfect symmetry of natural laws between the positive and negative universes described in the foregoing paragraph, applies directly between the positive time-universe and the negative time-universe as well. Having established Lorentz invariance between the positive time-universe and negative time-universe at the first step, it is straight forward to use Table 1 above and follow the procedure in section 5 of [2] to demonstrate the invariance of natural laws between the positive time-universe and negative time-universe.

Symmetry of natural laws must be considered to have been established between the positive time-universe and the negative time-universe. A more detailed presentation than done above will amount to a repetition of the demonstration of symmetry of natural laws between the positive and negative universes in [1] and [2].

Finally the established validity of Lorentz invariance in the four universes encompassed by Figs. 8a and 8b, coupled with the identical signs of spacetime dimensions, physical parameters and physical constants in the positive (or our) universe and the positive time-universe and the identical signs of spacetime dimensions, physical parameters, physical constants in the negative universe and negative time-universe in Table 1 of [2] and Table 1 above, guarantee the invariance of natural laws between the positive (or our) universe and the positive time-universe and between the negative universe and the negative time-universe. This along with the established invariance of natural laws between the positive (or our) universe and the negative universe and between the positive time-universe and the negative time-universe, guarantees invariance of natural laws among the four universes.

Symmetry of natural laws among the four universes encompassed by Figs. 8a and 8b of this paper namely, the positive (or our) universe and the negative universe (in Fig. 8a), the positive time-universe and the negative time-universe (in Fig. 8b), has thus been shown. Perfect symmetry of state among the universes shall be demonstrated in the second part of this paper, as mentioned earlier.

3 Origin of one-dimensional particles, objects and observers in the time dimension and (3+1)-dimensionality of particles, objects and observers in special relativity

An implication of the geometrical contraction of the three dimensions $x^{01\prime}$, $x^{02\prime}$ and $x^{03\prime}$ of the proper Euclidean 3-space $\Sigma^{0\prime}$ of the positive time-universe in Fig. 2 or Fig. 3 into a one-dimensional space $\rho^{0\prime}$ relative to 3-observers in our proper Euclidean 3-space Σ' in Fig. 6a, which ultimately transforms into the proper time dimension ct' relative to 3-observers in Σ' in Fig. 8a, is that the dimensions of a particle or object, such as a box of rest mass m_0^0 and proper (or classical) dimensions $\Delta x^{0\prime}$, $\Delta y^{0\prime}$ and $\Delta z^{0\prime}$ in $\Sigma^{0\prime}$ with respect to 3-observers in $\Sigma^{0\prime}$, are geometrically "bundled" parallel to one another, thereby effectively becoming a one-dimensional box of equal rest mass m_0^0 and proper (or classical) length $\Delta\rho^{0\prime}$ along $\rho^{0\prime}$ in Fig. 6a, which transforms into an interval $c\Delta t'$ containing rest mass m_0^0 along the proper time dimension ct' in Fig. 8a, relative to 3-observers in our Euclidean 3-space Σ', where $c\Delta t' = \Delta\rho^{0\prime} = \sqrt{(\Delta x^{0\prime})^2 + (\Delta y^{0\prime})^2 + (\Delta z^{0\prime})^2}$.

Likewise all radial directions of a spherical particle or object of rest mass m_0^0 and proper (or classical) radius $r^{0\prime}$ in the proper Euclidean 3-space $\Sigma^{0\prime}$ of the positive time-universe, with respect to 3-observers in $\Sigma^{0\prime}$, are "bundled" parallel to one another, thereby becoming a one-dimensional particle or object of proper (or classical) length, $\Delta\rho^{0\prime} = r^{0\prime}$, along $\rho^{0\prime}$ in Fig. 6a, which ultimately transforms into interval $c\Delta t'$ $(= r^{0\prime})$ containing rest mass m_0^0 along the proper time dimension ct' in Fig. 8a, with respect to 3-observers in our proper Euclidean 3-space Σ'.

A particle or object of rest mass m_0^0 with arbitrary shape located in the proper Euclidean 3-space $\Sigma^{0\prime}$ of the positive time-universe with respect to 3-observers in $\Sigma^{0\prime}$, will have the lengths (or dimensions) from its centroid to its boundary along all directions geometrically "bundled" parallel to one another, thereby effectively becoming a one-dimensional particle or object of equal rest mass m_0^0 along the proper time dimension ct' with respect to 3-observers in Σ' in Fig. 8a.

The one-dimensional rest mass m_0^0 of proper length $c\Delta t'$ of a particle, object or observer in our proper time dimension ct' with respect to 3-observers in our Euclidean 3-space Σ' in Fig. 8a, will acquire the absolute speed $V_0 = c$, which the proper time dimension possesses at every point along its length with respect to 3-observers in Σ'. Consequently it will possess energy $m_0^0 V_0^2 = m_0^0 c^2 = E'$ in ct' with respect to 3-observers in Σ'. Indeed the one-dimensional rest mass m_0^0 in ct' will be made manifest in the state of energy $E' = m_0^0 c^2$ by virtue of its absolute speed c in ct' and not in the state

of rest mass m_0^0. In other words, instead of locating one-dimensional rest mass m_0^0 along the proper time dimension ct' in Fig. 8a, as done along the one-dimensional space $\rho^{0\prime}$ in Fig. 6a, we must locate one-dimensional equivalent rest mass E'/c^2 (= m_0) along ct' with respect to 3-observers in Σ', as the symmetry-partner in ct' to the three-dimensional rest mass m_0 in Σ'.

It follows from the foregoing that as the proper Euclidean 3-space $\Sigma^{0\prime}$ of the positive time-universe in Fig. 2 or 3 is geometrically contracted to one-dimensional space $\rho^{0\prime}$ with respect to 3-observers in our proper Euclidean 3-space Σ' in Fig. 6a, the three-dimensional rest mass m_0^0 in $\Sigma^{0\prime}$ with respect to 3-observers in $\Sigma^{0\prime}$ in Fig. 2 or Fig. 3, contracts to one-dimensional rest mass m_0^0 located in the one-dimensional space $\rho^{0\prime}$ with respect to 3-observers in our proper Euclidean 3-space Σ' in Fig. 6a. And as the one-dimensional proper space $\rho^{0\prime}$ in Fig. 6a ultimately transforms into the proper time dimension ct' with respect to 3-observers in our Euclidean 3-space Σ', the one-dimensional rest mass m_0^0 in $\rho^{0\prime}$ transforms into one-dimensional equivalent rest mass E'/c^2, (i.e. $m_0^0 \rightarrow E'/c^2$), located in the proper time dimension ct' in Fig. 8a with respect to 3-observers in our Euclidean 3-space Σ', (although E'/c^2 has not been shown in ct' in Fig. 8a).

It must be noted however that since the speed $V_0 = c$ acquired by the rest mass m_0^0 in the proper time dimension ct' is an absolute speed, which is not made manifest in actual motion (or translation) of m_0^0 along ct', the energy $m_0^0c^2 = E'$ possessed by m_0^0 in ct' is a non-detectable energy in the proper time dimension. Important to note also is the fact that the equivalent rest mass E'/c^2 of a particle or object in the proper time dimension ct' is not an immaterial equivalent rest mass. Rather it is a quantity of matter that possesses inertia (like the rest mass m_0^0) along the proper time dimension. This is so because the speed c in $m_0^0c^2 = E'$, being an absolute speed, is not made manifest in motion of m_0^0 along ct', as mentioned above. On the other hand, the equivalent mass, $m_{0\gamma} = E'_\gamma/c^2 = h\nu_0/c^2$, of a photon is purely immaterial, since the speed c in $m_{0\gamma}c^2 = h\nu_0$ is the speed of actual translation through space of photons and only a purely immaterial particle can attain speed c of actual translation in space or along the time dimension. While the material equivalent rest mass $E'/c^2(\equiv m_0^0)$ in ct' can appear as rest mass in SR, the immaterial equivalent mass $E'_{0\gamma}/c^2$ ($\equiv m_{0\gamma}$) of photon cannot appear in SR.

Illustrated in Fig. 9a are the three-dimensional rest mass m_0 of a particle or object at a point of distance d' from a point of reference or origin in our proper Euclidean 3-space Σ' and the symmetry-partner one-dimensional equivalent rest mass E'/c^2 at the symmetry-partner point of distance $d^{0\prime}$ along the proper time dimension ct' from the point of reference or origin, where the distances d' and $d^{0\prime}$ are equal. The three-dimensional rest mass m_0 in Σ' is underlied by its one-dimensional intrinsic rest mass ϕm_0 in the one-dimensional proper intrinsic space $\phi\rho'$ and the one-dimensional equivalent rest mass E'/c^2 in ct' is underlied by its one-dimensional equivalent intrinsic rest mass $\phi E'/\phi c^2$ in the proper intrinsic time dimension $\phi c\phi t'$ in Fig. 9a.

Fig. 9a pertains to a situation where the three-dimensional rest mass m_0 of the particle or object is at rest relative to the 3-observer in the proper Euclidean 3-space Σ' and consequently its one-dimensional equivalent rest mass E'/c^2 is at rest in the proper time dimension ct' relative to the 3-observer in Σ'. On the other hand, Fig. 9b pertains to a situation where the three-dimensional rest mass m_0 of the particle or object is in motion at a velocity $\vec{v}$ relative to the 3-observer in Σ', thereby becoming the special-relativistic mass, $m = \gamma m_0$ in Σ', relative to the 3-observer in Σ' and consequently the one-dimensional equivalent rest mass E'/c^2 of the particle or object is in motion at speed $v = |\vec{v}|$ in the proper time dimension ct' relative to the 3-observer in Σ', thereby becoming the special-relativistic equivalent mass $E/c^2 = \gamma E'/c^2$ in ct' relative to the 3-observer in Σ'.

The one-dimensional equivalent rest mass E'/c^2 of proper (or classical) length $c\Delta t' = d^{0\prime}$ located at a point in the proper time dimension ct' with respect to 3-observers in the proper Euclidean 3-space Σ' in Fig. 9a, acquires the absolute speed $V_0 = c$ of ct'. However, since the absolute speed $V_0 = c$ of ct' is not made manifest in the flow of ct' with respect to 3-observers in Σ', it is not made manifest in translation of E'/c^2 along ct' with respect to the 3-observers in Σ'. Moreover the equivalent rest mass E'/c^2 possesses zero speed ($v = 0$) of motion in ct' relative to the 3-observer in Σ', just as the rest mass m_0 possesses zero speed of motion in the Euclidean 3-space Σ' relative to the 3-observer in Σ'. Consequently m_0 and E'/c^2 remain stationary at their symmetry-partner locations in Σ' and ct' respectively relative to the 3-observer in Σ' in Fig. 9a.

Likewise the equivalent intrinsic rest mass $\phi E'/\phi c^2$ of proper intrinsic length $\phi c\Delta\phi t' = \phi d^{0\prime}$ located at a point in the proper intrinsic time dimension $\phi c\phi t'$ with respect to 3-observers in the proper Euclidean 3-space Σ' in Fig. 9a, acquires the absolute intrinsic speed $\phi V_0 = \phi c$ of $\phi c\phi t'$. However, since the absolute intrinsic speed ϕc of $\phi c\phi t'$ is not made manifest in the intrinsic flow of $\phi c\phi t'$ with respect to 3-observers in Σ', it is not made manifest in intrinsic translation of $\phi E'/\phi c^2$ along $\phi c\phi t'$ with respect to the 3-observers in Σ'. Moreover the equivalent intrinsic rest mass $\phi E'/\phi c^2$ possesses zero intrinsic speed ($\phi v = 0$) of intrinsic translation in $\phi c\phi t'$ relative to the 3-observer in Σ', just as the intrinsic rest mass ϕm_0 possesses zero intrinsic speed of intrinsic translation in the proper intrinsic space $\phi\rho'$ underlying Σ' relative to the 3-observer in Σ'. Consequently ϕm_0 and $\phi E'/\phi c^2$ remain stationary at their symmetry-partner locations in $\phi\rho'$ and $\phi c\phi t'$ respectively relative to the 3-observer in Σ' in Fig. 9a.

In a situation where the rest mass m_0 of the particle or object is in motion at a velocity $\vec{v}$ in the proper Euclidean 3-space Σ' and the one-dimensional equivalent rest mass E'/c^2

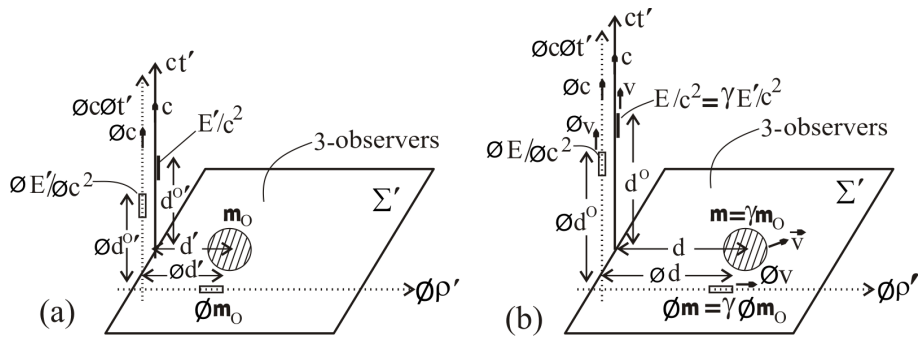

Fig. 9: The three-dimensional mass of an object at a position in the Euclidean 3-space and its one-dimensional equivalent mass at the symmetry-partner position in the time dimension, along with the underlying one-dimensional intrinsic mass of the object in intrinsic space and its equivalent intrinsic mass in the intrinsic time dimension, in the situations where (a) the object is stationary relative to the observer and (b) the object is in motion relative to the observer.

is in motion at speed $v = |\vec{v}|$ in the proper time dimension ct' relative to the 3-observer in Σ' in Fig. 9b, on the other hand, the special-relativistic equivalent mass $E/c^2 = \gamma E'/c^2$, acquires the absolute speed $V_0 = c$ of the proper time dimension ct', which is not made manifest in motion of $\gamma E'/c^2$ along ct' and as well possesses speed v of translation along ct' relative to the 3-observer in Σ'.

During a given period of time, the relativistic equivalent mass $\gamma E'/c^2$ has translated at constant speed v from an initial position P_1^0 to another position P_2^0 along the proper time dimension ct', while covering an interval $P_1^0P_2^0$ of ct'. During the same period of time, the special-relativistic mass $m = \gamma m_0$, has translated at equal constant speed $v = |\vec{v}|$ from an initial position P_1 to another position P_2 in the proper Euclidean 3-space Σ', while covering a distance P_1P_2 in Σ', where the interval $P_1^0P_2^0$ covered along ct' by $\gamma E'/c^2$ is equal to the distance P_1P_2 covered in Σ' by γm_0 and positions P_1 and P_2 in Σ' are symmetry-partner positions to positions P_1^0 and P_2^0 respectively in ct'. Consequently γm_0 and $\gamma E'/c^2$ are always located at symmetry-partner positions in Σ' and ct' respectively in the situation where they are in motion at any speed v in their respective domains relative to the 3-observer in Σ' in Fig. 9b.

It shall be reiterated for emphasis that the equivalent mass E'/c^2 or $\gamma E'/c^2$ in our proper metric time dimension ct' with respect to 3-observers in our proper Euclidean 3-space Σ', of a particle, object or observer in Figs. 9a and 9b, is actually the three-dimensional mass m_0^0 or γm_0^0 of the symmetry-partner particle, object or observer in the proper Euclidean 3-space $\Sigma^{0\prime}$ of the positive time-universe with respect to 3-observers in $\Sigma^{0\prime}$. This is the origin of the the one-dimensional particle, object or observer (or 1-particle, 1-object or 1-observer) in the time dimension to every 3-dimensional particle, object or observers (or 3-particle, 3-object or 3-observer) in 3-space in our universe.

Just as the proper time dimension $ct'(\equiv x^{0\prime})$ is added to the three dimensions $x^{1\prime}$, $x^{2\prime}$ and $x^{3\prime}$ of the proper Euclidean 3-space Σ' to have the four dimensions $x^{0\prime}$, $x^{1\prime}$, $x^{2\prime}$ and $x^{3\prime}$ of the flat four-dimensional proper metric spacetime, the one-dimensional equivalent rest mass E'/c^2 of a particle, object or observer in the proper time dimension ct' must be added to the three-dimensional rest mass m_0 of its symmetry-partner particle, object or observer in the proper Euclidean 3-space Σ' to have a 4-dimensional particle, object or observer of rest mass $(m_0, E'/c^2)$ on the flat four-dimensional proper spacetime (Σ', ct') in our notation.

However it is more appropriate to refer to 4-dimensional particles, objects and observers on flat 4-dimensional spacetime as (3+1)-dimensional particles, objects and observers, because the one-dimensional particles, objects and observers (or 1-particles, 1-objects and 1-observers) in the time dimension ct' are themselves distinct particles, objects and observers, (which are geometrically contracted from three-dimensional particles, objects and observers in the Euclidean 3-space $\Sigma^{0\prime}$ of the positive time-universe), which are separated in the time dimension ct' from their symmetry-partner three-dimensional continuum particles, objects and observers (or 3-particles, 3-objects and 3-observers) in the continuum Euclidean 3-space Σ'.

The 1-particle, 1-object or 1-observer in the time dimension can be thought of as weakly bonded to the 3-particle, 3-object or 3-observer in the Euclidean 3-space to form a (3+1)-dimensional particle, object or observer in spacetime and a (3+1)-dimensional particle, object or observer can be decomposed into its component 1-particle, 1-object or 1-observer in the time dimension and 3-particle, 3-object or 3-observer in the Euclidean 3-space. On the other hand, what should be referred to as a continuum 4-dimensional particle, object or observer (or 4-particle, 4-object or 4-observer) on four-dimensional spacetime continuum should be non-decomposable into its component dimensions, just as a continuum 3-dimensional particle, object or observer in the Euclidean 3-space continuum cannot be decomposed into its component dimensions.

There are no continuum non-decomposable four-dimensional particles, objects and observers on four-dimensional spacetime in the context of the present theory. Rather there are (3+1)-dimensional particles, objects and observers that can be decomposed into one-dimensional particles, objects and observers in the time dimension and three-dimensional particles, objects and observers in the Euclidean 3-space. Relativistic physics must be formulated partially with respect to 1-observers in the time dimension as distinct from relativistic physics formulated partially with respect to 3-observers in the Euclidean 3-space. The partial physics formulated with respect to 1-observer in the time dimension and 3-observer in the Euclidean 3-space must then be composed into the full relativistic physics on four-dimensional spacetime.

It is also important to note that it is the partial physics formulated with respect to 1-observers in the time dimension, which, of course, contains component of physics projected from the Euclidean 3-space in relativistic physics, is what the 1-observers in the time dimension could observe. It is likewise the partial physics formulated with respect to 3-observers in the Euclidean 3-space, which, of course, contains component of physics projected from the time dimension in relativistic physics, that the 3-observers in the Euclidean 3-space could observe.

The foregoing paragraph has been well illustrated with the derivation of the intrinsic Lorentz transformation of system (13) of [1] as combination of partial intrinsic Lorentz transformation (11) derived from Fig. 8a with respect to the 3-observer (Peter) in the Euclidean 3-space $\tilde{\Sigma}$ and partial intrinsic Lorentz transformation (12) derived from Fig. 8b with respect to the 1-observer ($\tilde{\text{P}}$eter) in the time dimension $c\tilde{t}$ in that paper. The Lorentz transformation of system (28) of [1], as the outward manifestation on flat four-dimensional spacetime of the intrinsic Lorentz transformation (11) in that paper, has likewise been composed from partial Lorentz transformation with respect to the 3-observer in $\tilde{\Sigma}$ and partial Lorentz transformation with respect to the 1-observer in the time dimension $c\tilde{t}$.

Let us collect the partial Lorentz transformations derived with respect to the 1-observer in $c\tilde{t}$ in the LT and its inverse of systems (28) and (29) of [1] to have as follows

$$\left.\begin{array}{rcl} c\tilde{t}' & = & c\tilde{t}\sec\psi - \tilde{x}\tan\psi; \\ \tilde{x} & = & \tilde{x}'\sec\psi + c\tilde{t}\tan\psi;\ \tilde{y} = \tilde{y}';\ \tilde{z} = \tilde{z}'; \\ & & (\text{w.r.t. } 1-\text{observer in } c\tilde{t}) \end{array}\right\}. \qquad (25)$$

These coordinate transformations simplify as follows from the point of view of what can be measured with laboratory rod and clock discussed in detail in sub-section 4.5 of [1]:

$$\tilde{t} = \tilde{t}'\cos\psi;\ \tilde{x} = \tilde{x}'\sec\psi;\ \tilde{y} = \tilde{y}';\ \tilde{z} = \tilde{z}' \qquad (26)$$

w.r.t. $1-$ observer in $c\tilde{t}$.

System (26) derived with respect to the 1-observer in $c\tilde{t}$, corresponds to system (42) of [1], derived with respect to 3-observer in $\tilde{\Sigma}$ in that paper, which shall be re-presented here as follows

$$\tilde{t} = \tilde{t}'\sec\psi;\ \tilde{x} = \tilde{x}'\cos\psi;\ \tilde{y} = \tilde{y}';\ \tilde{z} = \tilde{z}' \qquad (27)$$

w.r.t. $3-$ observer in $\tilde{\Sigma}$.

We find from systems (26) and (27) that while 3-observers in the Euclidean 3-space observe length contraction and time dilation of relativistic events, their symmetry-partner 1-observers in the time dimension observe length dilation and time contraction of relativistic events.

It is clear from all the foregoing that a 3-observer in the Euclidean 3-space and his symmetry-partner 1-observer in the time dimension are distinct observers who can be composed (or "weakly bonded") into a (3+1)-dimensional observer that can be decomposed back into its component 3-observer and 1-observer for the purpose of formulating relativistic physics, which is composed from partial relativistic physics formulated separately with respect to 3-observers in the Euclidean 3-space and 1-observers in the time dimension.

Every parameter in the Euclidean 3-space has its counterpart (or symmetry-partner) in the time dimension. We have seen the case of rest mass m_0 in the proper Euclidean 3-space Σ' and its symmetry-partner one-dimensional equivalent rest mass E'/c^2 in the proper time dimension ct', as illustrated in Figs. 9a and 9b. A classical three-vector quantity $\vec{q}\,'$ in the proper Euclidean 3-space Σ' has its symmetry-partner classical scalar quantity $q^{0\prime}$ in the proper time dimension ct'. The composition of the two yields what is usually referred to as four-vector quantity denoted by $q'_\lambda = (q^{0\prime}, \vec{q}\,')$ or $q'_\lambda = (q^{0\prime}, q^{1\prime}, q^{2\prime}, q^{3\prime})$. We now know that the scalar components $q^{0\prime}$ in the time dimension ct' of four-vector quantities in the positive (or our) universe are themselves three-vector quantities $\vec{q}^{\,0\prime}$ in the Euclidean 3-space $\Sigma^{0\prime}$ of the positive time-universe with respect to 3-observers in $\Sigma^{0\prime}$. The three-vector quantities $\vec{q}^{\,0\prime}$ in $\Sigma^{0\prime}$, (which are identical symmetry-partners to the three-vector quantities $\vec{q}\,'$ in our Euclidean 3-space Σ'), become contracted to one-dimensional scalar quantities $q^{0\prime} = |\vec{q}^{\,0\prime}|$ in the time dimension ct' relative to 3-observers in Σ', even as the proper Euclidean 3-space $\Sigma^{0\prime}$ containing $\vec{q}^{\,0\prime}$ becomes contracted to the proper time dimension ct' relative to 3-observers in Σ'.

4 Final justification for the new spacetime/intrinsic spacetime diagrams for Lorentz transformation/intrinsic Lorentz transformation in the four-world picture

New geometrical representations of Lorentz transformation and intrinsic Lorentz transformation (LT/ϕLT) and their inverses were derived and presented as Figs. 8a and 8b and Figs. 9a and 9b within the two-world picture isolated in [1]. However at least two outstanding issues about those diagrams remain to be resolved in order to finally justify them. The first issue is the unexplained origin of Fig. 8b that must necessarily be drawn to complement Fig. 8a of [1] in deriving ϕLT/LT.

The second issue is the unspecified reason why anticlockwise relative rotations of intrinsic affine spacetime coordinates are positive rotations (involving positive intrinsic angles $\phi\psi$) with respect to 3-observers in the Euclidean 3-spaces Σ' and $-\Sigma'^{*}$ in Fig. 8a of [1], while, at the same time, clockwise relative rotations of intrinsic affine spacetime coordinates are positive rotations (involving positive intrinsic angles $\phi\psi$) with respect to 1-observers in the time dimensions ct' and $-ct'^{*}$ in Fig. 8b of [1]. These two issues shall be resolved within the four-world picture encompassed by Figs. 8a and 8b of this paper in this section.

Let us as done in deriving Figs. 8a and 8b and their inverses Figs. 9a and 9b of [1] towards the derivation of intrinsic Lorentz transformation/Lorentz transformation (ϕLT/LT) and their inverses in the positive and negative universes in [1], prescribe particle's (or primed) frame and observer's (or unprimed) frame in terms of extended affine spacetime coordinates in the positive (or our) universe as $(\tilde{x}', \tilde{y}', \tilde{z}', c\tilde{t}')$ and $(\tilde{x}, \tilde{y}, \tilde{z}, c\tilde{t})$ respectively. They are underlied by intrinsic particle's frame and intrinsic observer's frame in terms of extended intrinsic affine coordinates $(\phi\tilde{x}', \phi c\phi\tilde{t}')$ and $(\phi\tilde{x}, \phi c\phi\tilde{t})$ respectively.

The prescribed perfect symmetry of state between the positive and negative universes in [1] implies that there are identical symmetry-partner particle's frame and observer's frame $(-\tilde{x}'^{*}, -\tilde{y}'^{*}, -\tilde{z}'^{*}, -c\tilde{t}'^{*})$ and $(-\tilde{x}^{*}, -\tilde{y}^{*}, -\tilde{z}^{*}, -c\tilde{t}^{*})$ respectively, as well as their underlying identical symmetry-partner intrinsic particle's frame and symmetry-partner intrinsic observer's frame $(-\phi\tilde{x}'^{*}, -\phi c\phi\tilde{t}'^{*})$ and $(-\phi\tilde{x}^{*}, -\phi c\phi\tilde{t}^{*})$ respectively in the negative universe.

Let us consider the motion at a constant speed v of the rest mass m_0 of the particle along the $\tilde{x}'-$axis of its frame and the underlying intrinsic motion at constant intrinsic speed ϕv of the intrinsic rest mass ϕm_0 of the particle along the intrinsic space coordinate $\phi\tilde{x}'$ of its frame relative to a 3-observer in the positive universe. Again the prescribed perfect symmetry of state between the positive and negative universes implies that the rest mass $-m_0^{*}$ of the symmetry-partner particle is in simultaneous motion at equal constant speed v along the $-\tilde{x}'^{*}-$axis of its frame of reference and its intrinsic rest mass $-\phi m_0^{*}$ is in simultaneous intrinsic motion at equal intrinsic speed ϕv along the intrinsic space coordinate $-\phi\tilde{x}'^{*}-$axis of its frame relative to the symmetry-partner 3-observer in the negative universe.

As developed in sub-section 4.4 of [1], the simultaneous identical motions of the symmetry-partner particles' frames relative to the symmetry-partner observers' frames in the positive and negative universes, described in the foregoing paragraph, give rise to Fig. 8a of [1] with respect to 3-observers in the Euclidean 3-spaces Σ' and $-\Sigma'^{*}$, which shall be reproduced here as Fig. 10a.

The diagram of Fig. 10a involving relative rotations of extended intrinsic affine spacetime coordinates, has been drawn upon the flat four-dimensional proper metric spacetime of classical mechanics (CM) and its underlying flat two-dimensional proper intrinsic metric spacetime of intrinsic classical mechanics (ϕCM) of the positive (or our) universe and the negative universe contained in Fig. 8a of this paper. The prescribed symmetry of state among the four universes encompassed by Figs. 8a and 8b of this paper, implies that identical symmetry-partner particles undergo identical motions simultaneously relative to identical symmetry-partner observers (or frames of reference) in the four universes. It follows from this that Fig. 10b drawn upon the flat four-dimensional proper metric spacetime of CM and its underlying flat two-dimensional proper intrinsic metric spacetime of ϕCM of the positive time-universe and the negative time-universe contained in Fig. 8b of this paper, co-exists with Fig. 10a in nature.

Fig. 10b is valid with respect to 3-observers in the Euclidean 3-spaces $\Sigma^{0\prime}$ of the positive time-universe and $-\Sigma^{0\prime *}$ of the negative time-universe as indicated. It must be noted that the anti-clockwise rotations of primed intrinsic coordinates $\phi\tilde{x}'$ and $\phi c\phi\tilde{t}'$ relative to the unprimed intrinsic coordinates $\phi\tilde{x}$ and $\phi c\phi\tilde{t}$ respectively by positive intrinsic angle $\phi\psi$ with respect to 3-observers in the Euclidean 3-space Σ' and $-\Sigma'^{*}$ in Fig. 10a, correspond to clockwise rotations of the primed intrinsic coordinates $\phi\tilde{x}^{0\prime}$ and $\phi c\phi\tilde{t}^{0\prime}$ relative to the unprimed intrinsic coordinates $\phi\tilde{x}^{0}$ and $\phi c\phi\tilde{t}^{0}$ respectively by positive intrinsic angle $\phi\psi$ with respect to 3-observers in $\Sigma^{0\prime}$ and $-\Sigma^{0\prime *}$ in Fig. 10b.

Fig. 10b co-exists with Fig. 10a in nature and must complement Fig. 10a towards deriving intrinsic Lorentz transformation/Lorentz transformation (ϕLT/LT) graphically in the positive (or our) universe and the negative universe by physicists in our universe and the negative universe. However Fig. 10b in its present form cannot serve a complementary role to Fig. 10a, because it contains the spacetime and intrinsic spacetime coordinates of the positive time-universe and the negative time-universe, which are elusive to observers in our (or positive) universe and the negative universe, or which cannot appear in physics in the positive and negative universes.

In order for Fig. 10b to be able to serve a complementary role to Fig. 10a towards deriving the ϕLT/LT in the positive and negative universes, it must be appropriately modified. As found earlier in this paper, the proper Euclidean 3-spaces $\Sigma^{0\prime}$ and $-\Sigma^{0\prime *}$ of the positive and negative time-universes with respect to 3-observers in them, are proper time dimensions ct' and $-ct'^{*}$ respectively with respect to 3-observers in the proper Euclidean 3-spaces Σ' and $-\Sigma'^{*}$ of our universe and the negative universe and the proper time dimensions $ct^{0\prime}$ and $-ct^{0\prime *}$ of the positive and negative time-universes with respect to 3-observers in the proper Euclidean 3-spaces $\Sigma^{0\prime}$ and $-\Sigma^{0\prime *}$ of the positive and negative time-universes, are the proper Euclidean 3-spaces Σ' and $-\Sigma'^{*}$ of our universe and the negative universes respectively with respect to 3-observers in Σ' and $-\Sigma'^{*}$.

As follows from the foregoing paragraph, Fig. 10b will contain the spacetime and intrinsic spacetime coordinates of

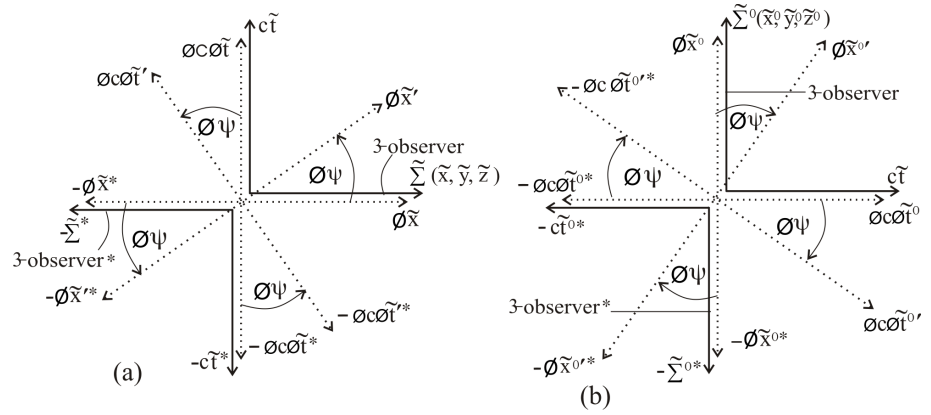

Fig. 10: a) Relative rotations of intrinsic affine spacetime coordinates of a pair of frames in the positive (or our) universe and of the symmetry-partner pair of frames in the negative universe, which are valid relative to symmetry-partner 3-observers in the Euclidean 3-spaces in the positive and negative universes. b) Relative rotations of intrinsic affine spacetime coordinates of a pair of frames in the positive time-universe and of the symmetry-partner pair of frames in the negative time-universe, which are valid relative to symmetry-partner 3-observers in the Euclidean 3-spaces in the positive and negative time-universes.

our (or positive) universe and the negative universe solely by performing the following transformations of spacetime and intrinsic spacetime coordinates on it with respect to 3-observers in the Euclidean 3-spaces Σ' and $-\Sigma'^{*}$ of our universe and the negative universe:

$$\left.\begin{array}{lcl} \tilde{\Sigma}^0 & \rightarrow & c\tilde{t};\ c\tilde{t}^0 \rightarrow \tilde{\Sigma};\ -\tilde{\Sigma}^{0*} \rightarrow -c\tilde{t}^{*};\\ & & -c\tilde{t}^{0*} \rightarrow -\tilde{\Sigma}^{*}. \\ \phi\tilde{x}^0 & \rightarrow & \phi c\phi\tilde{t};\ \phi c\phi\tilde{t}^0 \rightarrow \phi\tilde{x};\\ & & -\phi\tilde{x}^{0*} \rightarrow -\phi c\phi\tilde{t}^{*};\\ & & -\phi c\phi\tilde{t}^{0*} \rightarrow -\phi\tilde{x}^{*}. \\ \phi\tilde{x}^{0\prime} & \rightarrow & \phi c\phi\tilde{t}';\ \phi c\phi\tilde{t}^{0\prime} \rightarrow \phi\tilde{x}';\\ & & -\phi\tilde{x}^{0\prime *} \rightarrow -\phi c\phi\tilde{t}'^{*};\\ & & -\phi c\phi\tilde{t}^{0\prime *} \rightarrow -\phi\tilde{x}'^{*}. \end{array}\right\} \quad (28)$$

By implementing the coordinate/intrinsic coordinate transformations of systems (28) on Fig. 10b we have Fig. 11a.

Fig. 11a is valid with respect to 1-observers in the proper time dimensions ct' and $-ct'^{*}$ of the positive and negative universes as indicated, where these 1-observers are the 3-observers in the Euclidean 3-spaces $\Sigma^{0\prime}$ and $-\Sigma^{0\prime *}$ in Fig. 10b. Since Fig. 11a contains the spacetime/intrinsic spacetime coordinates of the positive (or our) universe and the negative universe solely, it can serve as a complementary diagram to Fig. 10a towards the deriving ϕLT/LT in the positive (or our) universe and the negative universe. Indeed Fig. 10a and Fig. 11a are the same as Figs. 8a and 8b of [1], with which the ϕLT/LT were derived in the positive (or our) universe and the negative universe in that paper, except for intrinsic spacetime projections in Figs. 8a and 8b of [1], which are not shown in Figs. 10a and Fig. 11a here.

On the other hand, Fig. 10a will contain the spacetime/intrinsic spacetime coordinates of the positive time-universe and the negative time-universe solely, as shown in Fig. 11b, by performing the inverses of the transformations of spacetime and intrinsic spacetime coordinates of system (28), (that is, by reversing the directions of the arrows in system (28)) on Fig. 10a. Just as Fig. 11a must complement Fig. 10a for the purpose of deriving the ϕLT/LT in the positive (or our) universe and the negative universe, as presented in sub-section 4.4 of [1], Fig. 11b must complement Fig. 10b for the purpose of deriving the ϕLT/LT in the positive time-universe and the negative time-universe.

The clockwise sense of relative rotations of intrinsic affine spacetime coordinates by positive intrinsic angles $\phi\psi$ with respect to 1-observers in the time dimension $c\tilde{t}$ and $-c\tilde{t}^{*}$ in Fig. 11a follows from the validity of the clockwise sense of relative rotations of intrinsic affine spacetime coordinates by positive intrinsic angle $\phi\psi$ with respect to 3-observers in the Euclidean 3-spaces $\Sigma^{0\prime}$ and $-\Sigma^{0\prime *}$ in Fig. 10b. The 1-observers in $c\tilde{t}$ and $-c\tilde{t}^{*}$ in Fig. 11a are what the 3-observers in $\tilde{\Sigma}^0$ and $-\tilde{\Sigma}^{0*}$ in Fig. 10b transform into, as noted above.

Thus the second outstanding issue about the diagrams of Figs. 8a and 8b of [1], mentioned at the beginning of this section namely, the unexplained reason why anti-clockwise relative rotations of intrinsic affine spacetime coordinates with respect to 3-observers in the Euclidean 3-spaces Σ' and $-\Sigma'^{*}$ are positive rotations involving positive intrinsic angles $\phi\psi$ in Fig. 8a of [1], while, at the same time, clockwise relative rotations of intrinsic affine spacetime coordinates with respect to 1-observers in the time dimensions ct' and $-ct'^{*}$ are positive rotations involving positive intrinsic angles $\phi\psi$ in Fig. 8b of [1], has now been resolved.

Since Fig. 8b of [1] or Fig. 11a of this paper has been shown to originate from Fig. 10b of this paper, which is valid with respect to 3-observers in the Euclidean 3-spaces $\Sigma^{0\prime}$ and $-\Sigma^{0\prime *}$ of the positive and negative time-universes, the origin

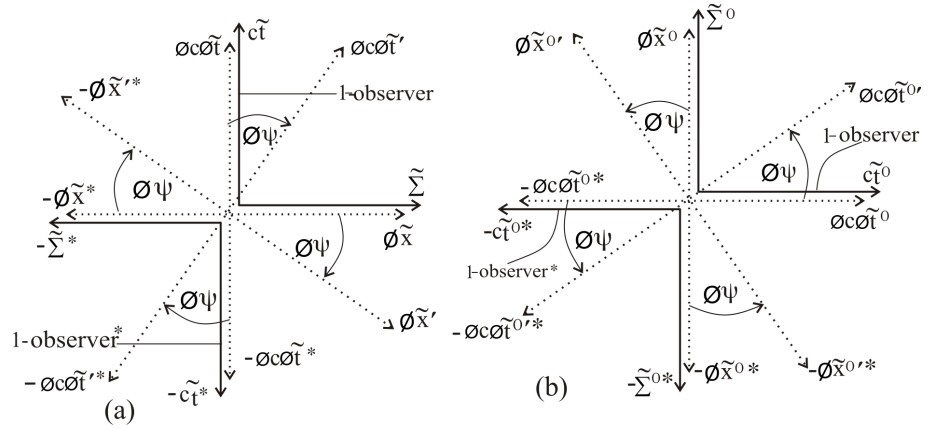

Fig. 11: a) Complementary diagram to Fig. 10a obtained by transforming the spacetime/intrinsic spacetime coordinates of the positive time-universe and the negative time-universe in Fig. 10b into the spacetime/intrinsic spacetime coordinates of the positive (or our) universe and the negative universe; is valid with respect to 1-observers in the time dimensions of our universe and the negative universe. b) Complementary diagram to Fig. 10b obtained by transforming the spacetime/intrinsic spacetime coordinates of the positive (or our) universe and the negative universe in Fig. 10a into the spacetime/intrinsic spacetime coordinates of the positive time-universe and the negative time-universe; is valid with respect to 1-observers in the time dimensions of the positive time-universe and the negative time-universe.

from the positive time-universe and negative time-universe of Fig. 8b of [1] (or Fig. 11a of this paper), which must necessarily be drawn to complement Fig. 8a of [1] (or Fig. 10a of this paper) in deriving the ϕLT/LT in our (or positive) universe and the negative universe, has been shown. Thus the first outstanding issue about Figs. 8a and 8b of [1], which was unresolved in [1], mentioned at the beginning of this section, namely the unexplained origin of Fig. 8b that must always be drawn to complement Fig. 8a in [1] in deriving the ϕLT/LT, has now been resolved. The four-world background of Figs. 8a and its complementary diagram of Fig. 8b in [1] (or Fig. 10a and Fig. 11a of this paper), has thus been demonstrated.

The new geometrical representation of the intrinsic Lorentz transformation/Lorentz transformation (ϕLT/LT) of Figs. 8a and 8b in [1] (or Fig. 10a and Fig. 11a of this paper), which was said to rest on a two-world background in [1] and [2], because those diagrams contain the spacetime/intrinsic spacetime coordinates of the positive (or our) universe and the negative universe solely and the origin of Fig. 8b in [1] (or Fig. 11a of this paper) from the diagram of Fig. 10b of this paper in the positive time-universe and the negative time-universe was unknown in [1]. The ϕLT/LT and consequently the intrinsic special theory of relativity/special theory of relativity (ϕSR/SR) shall be said to rest on a four-world background henceforth.

5 Invariance of the flat four-dimensional proper (or classical) metric spacetime in the context of special relativity

The flat four-dimensional proper physical (or metric) spacetime, which is composed of the proper Euclidean 3-space Σ' and the proper time dimension ct' in the first quadrant in Fig. 8a of this paper, is the flat four-dimensional proper metric spacetime of classical mechanics (including classical gravitation), of the positive (or our) universe, usually denoted by $(x^{0\prime}, x^{1\prime}, x^{2\prime}, x^{3\prime})$, where the dimension $x^{0\prime}$ is along the one-dimensional proper space $\rho^{0\prime}$ in Fig. 6a, which transforms into the proper time dimension ct' in Fig. 8a; hence $x^{0\prime} = ct'$ and $x^{1\prime}$, $x^{2\prime}$ and $x^{3\prime}$ are the dimensions of the proper Euclidean 3-space Σ'. The notation (Σ', ct') for the flat four-dimensional proper physical (or metric) spacetime adopted in [1] and [2], (although the prime label on Σ' and ct' did not appear in those papers), is being adhered to in this paper for convenience.

When the special theory of relativity operates on the flat four-dimensional proper metric spacetime $(x^{0\prime}, x^{1\prime}, x^{2\prime}, x^{3\prime})$; $x^{0\prime} = ct'$ (or (Σ', ct') in our notation), it is the extended intrinsic affine spacetime coordinates $\phi\tilde{x}'$ and $\phi c\phi\tilde{t}'$ of the primed (or particle's) frame that are rotated relative to their projective extended affine intrinsic spacetime coordinates $\phi\tilde{x}$ and $\phi c\phi\tilde{t}$ of the unprimed (or observer's) frame. It is consequently the primed intrinsic affine coordinates $\phi\tilde{x}'$ and $\phi c\phi\tilde{t}'$ that transform into the unprimed intrinsic affine coordinates $\phi\tilde{x}$ and $\phi c\phi\tilde{t}$ in intrinsic Lorentz transformation (ϕLT) in the context of intrinsic special theory of relativity (ϕSR).

It is the extended affine spacetime coordinates $c\tilde{t}'$, $\tilde{x}'$, $\tilde{y}'$ and $\tilde{z}'$ of the primed frame on the flat four-dimensional proper physical (or metric) spacetime $(x^{0\prime}, x^{1\prime}, x^{2\prime}, x^{3\prime})$ (or (Σ', ct') in our notation) that transform into the extended affine spacetime coordinates $c\tilde{t}$, $\tilde{x}$, $\tilde{y}$ and $\tilde{z}$ of the unprimed frame, also on the flat four-dimensional proper physical (or metric) spacetime $(x^{0\prime}, x^{1\prime}, x^{2\prime}, x^{3\prime})$ (or (Σ', ct') in our notation) in Lorentz transformation (LT) in the context of the special theory of

relativity (SR).

The special theory of relativity, as an isolated phenomenon, cannot transform the extended flat proper metric spacetime ($x^{0\prime}$, $x^{1\prime}$, $x^{2\prime}$, $x^{3\prime}$) (or (Σ', ct') in our notation) on which it operates, to an extended flat relativistic metric spacetime (x^0, x^1, x^2, x^3) (or (Σ, ct) in our notation), because SR involves the transformation of extended affine spacetime coordinates with no physical (or metric) quality. Or because the spacetime geometry associated with SR is affine spacetime geometry. A re-visit to the discussion of affine and metric spacetimes in sub-section 4.4 of [1] may be useful here. The primed coordinates $\tilde{x}'$, $\tilde{y}'$, $\tilde{z}'$ and $c\tilde{t}'$ of the particle's frame and the unprimed coordinates $\tilde{x}$, $\tilde{y}$, $\tilde{z}$ and $c\tilde{t}$ of the observer's frame in the context of SR are affine coordinates with no metric quality, both of which exist on the flat proper (or classical) metric spacetime ($x^{0\prime}$, $x^{1\prime}$, $x^{2\prime}$, $x^{3\prime}$) (or (Σ', ct') in our notation).

It is gravity (a metric phenomenon) that can transform extended flat four-dimensional proper (or classical) metric spacetime (with prime label) ($x^{0\prime}$, $x^{1\prime}$, $x^{2\prime}$, $x^{3\prime}$) (or (Σ', ct') in our notation) into extended four-dimensional "relativistic" spacetime (x^0, x^1, x^2, x^3) (or (Σ, ct)), (without prime label), where (x^0, x^1, x^2, x^3) (or (Σ, ct)) is known to be curved in all finite neighborhood of a gravitation field source in the context of the general theory of relativity (GR). The rest mass m_0 of a test particle on the flat proper (or classical) metric spacetime ($x^{0\prime}$, $x^{1\prime}$, $x^{2\prime}$, $x^{3\prime}$) (or (Σ', ct')) is also known to transform into the inertial mass m on the curved "relativistic" physical (or metric) spacetime (x^0, x^1, x^2, x^3) (or (Σ, ct)) in the context of GR, where m is known to be trivially related to m_0 as $m = m_0$, by virtue of the principle of equivalence of Albert Einstein [5].

However our interest in [1] and [2] and in the two parts of this paper is not in the metric phenomenon of gravity, but in the special theory of relativity (with affine spacetime geometry), as an isolated subject from gravity. We have inherently assumed the absence of gravity by restricting to the extended flat four-dimensional proper (or classical) metric spacetime ($x^{0\prime}$, $x^{1\prime}$, $x^{2\prime}$, $x^{3\prime}$) (or (Σ', ct') in our notation), as the metric spacetime that supports SR in the absence of relativistic gravity in [1] and [2] and up to this point in this paper. The transformation of the flat proper (or classical) metric spacetime ($x^{0\prime}$, $x^{1\prime}$, $x^{2\prime}$, $x^{3\prime}$) (or (Σ', ct')) into "relativistic" metric spacetime (x^0, x^1, x^2, x^3) (or (Σ, ct)) in the context of a theory of gravity, shall be investigated with further development within the present four-world picture, in which four-dimensional spacetime is underlined by two-dimensional intrinsic spacetime in each of the four symmetrical worlds (or universes).

This first part of this paper shall be ended at this point, while justifications for the co-existence in nature of the four symmetrical worlds (or universes) in Figs. 8a and 8b of this paper, as the actual background of the special theory of relativity in each universe, shall be concluded in the second part.

Submitted on January 26, 2010 / Accepted on March 01, 2010

References

1. Adekugbe A. O. J. Two-world background of special relativity. Part I. *Progress in Physics*, 2010, v. 1, 30–48.
2. Adekugbe A. O. J. Two-world background of special relativity. Part II. *Progress in Physics*, 2010, v. 1, 49–61.
3. Adler R., Bazin M., Schiffer M. Introduction to general relativity. Second Edition. McGraw-Hill Book Company, New York, 1975.
4. Einstein A. Sidelights on relativity. Methuen, 1922.
5. Bonnor W. B. Negative mass in general relativity. *Gen. Relat. Grav.*, 1989, v. 21, 1143–1157.

SPECIAL REPORT

Re-Identification of the Many-World Background of Special Relativity as Four-World Background. Part II.

Akindele O. J. Adekugbe

Center for The Fundamental Theory, P. O. Box 2575, Akure, Ondo State 340001, Nigeria.
E-mail: adekugbe@alum.mit.edu

The re-identification of the many-world background of the special theory of relativity (SR) as four-world background in the first part of this paper (instead of two-wold background isolated in the initial papers), is concluded in this second part. The flat two-dimensional intrinsic spacetime, which underlies the flat four-dimensional spacetime in each universe, introduced as *ansatz* in the initial paper, is derived formally within the four-world picture. The identical magnitudes of masses, identical sizes and identical shapes of the four members of every quartet of symmetry-partner particles or objects in the four universes are shown. The immutability of Lorentz invariance on flat spacetime of SR in each of the four universes is shown to arise as a consequence of the perfect symmetry of relative motion at all times among the four members of every quartet of symmetry-partner particles and objects in the four universes. The perfect symmetry of relative motions at all times, coupled with the identical magnitudes of masses, identical sizes and identical shapes, of the members of every quartet of symmetry-partner particles and objects in the four universes, guarantee perfect symmetry of state among the universes.

1 Isolating the two-dimensional intrinsic spacetime that underlies four-dimensional spacetime

1.1 Indispensability of the flat 2-dimensional intrinsic spacetime underlying flat 4-dimensional spacetime

The flat two-dimensional proper intrinsic metric spacetimes denoted by $(\phi\rho', \phi c\phi t')$ and $(-\phi\rho'^{*}, -\phi c\phi t'^{*})$, which underlies the flat four-dimensional proper metric spacetimes (Σ', ct') and $(-\Sigma'^{*}, -ct'^{*})$ of the positive and negative universes respectively, were introduced as *ansatz* in sub-section 4.4 of [1]. They have proved very useful and indispensable since their introduction. For instance, the new spacetime/intrinsic spacetime diagrams for the derivation of Lorentz transformation/intrinsic Lorentz transformation and their inverses in the four-world picture, (referred to as two-world picture in [1]), derived and presented as Figs. 8a and 8b of [1] (or Figs. 10a and 11a of part one of this paper [3]) and their inverses namely, Figs. 9a and 9b of [1], involve relative rotations of intrinsic affine spacetime coordinates, without any need for relative rotations of affine spacetime coordinates.

Once the intrinsic Lorentz transformation (ϕLT) and its inverse have been derived graphically as transformation of the primed intrinsic affine spacetime coordinates $\phi\tilde{x}'$ and $\phi c\phi\tilde{t}'$ of the intrinsic particle's frame into the unprimed intrinsic affine spacetime coordinates $\phi\tilde{x}$ and $\phi c\phi\tilde{t}$ of the intrinsic observer's frame and its inverse, then Lorentz transformation (LT) and its inverse in terms of primed affine spacetime coordinates $\tilde{x}', \tilde{y}', \tilde{z}'$ and $c\tilde{t}'$ of the particle's frame and the unprimed affine spacetime coordinates $\tilde{x}, \tilde{y}, \tilde{z}$ and $c\tilde{t}$ of the observer's frame can be written straight away, as the outward manifestations on flat four-dimensional spacetime of the intrinsic Lorentz transformation (ϕLT) and its inverse on flat two-dimensional intrinsic spacetime, as demonstrated in sub-section 4.4 of [1].

The indispensability of the flat two-dimensional proper intrinsic metric spacetime $(\phi\rho', \phi c\phi t')$ underlying flat four-dimensional proper metric spacetime (Σ', ct'), arises from the fact that it is possible for the intrinsic affine spacetime coordinates $\phi\tilde{x}'$ and $\phi c\phi\tilde{t}'$ of the intrinsic particle's frame $(\phi\tilde{x}', \phi c\phi\tilde{t}')$ that contains the one-dimensional intrinsic rest mass ϕm_0 of the particle in the intrinsic affine space coordinate $\phi\tilde{x}'$, to rotate anti-clockwise by an intrinsic angle $\phi\psi$ relative to the horizontal and vertical respectively and thereby project the intrinsic affine spacetime coordinates $\phi\tilde{x}$ and $\phi c\phi\tilde{t}$ of the intrinsic observer's frame $(\phi\tilde{x}, \phi c\phi\tilde{t})$ along the horizontal and vertical respectively, where the projective intrinsic affine space coordinate $\phi\tilde{x}$ of the observer's frame along the horizontal contains the one-dimensional intrinsic relativistic mass, $\phi m = \gamma\phi m_0$, of the particle, as happens in the first and second quadrants in Fig. 8a of [1], although the intrinsic rest mass ϕm_0 in the inclined $\phi\tilde{x}'$ and intrinsic relativistic mass ϕm in the projective $\phi\tilde{x}$ along the horizontal are not shown in that diagram.

The projective unprimed intrinsic affine coordinates $\phi\tilde{x}$ and $\phi c\phi\tilde{t}$ that constitute the observer's intrinsic frame, containing one-dimensional intrinsic relativistic mass ϕm of the particle in $\phi\tilde{x}$, are then made manifest outwardly in the unprimed affine spacetime coordinates $\tilde{x}$, $\tilde{y}$, $\tilde{z}$ and $c\tilde{t}$ of the observer's fame on flat four-dimensional spacetime, containing the three-dimensional relativistic mass, $m = \gamma m_0$, of the particle in affine 3-space $\tilde{\Sigma}(\tilde{x}, \tilde{y}, \tilde{z})$ of the observer's frame.

On the other hand, diagrams obtained by replacing the

inclined primed intrinsic affine coordinates $\phi\tilde{x}', \phi c\phi\tilde{t}', -\phi\tilde{x}'^*$ and $-\phi c\phi\tilde{t}'^*$ of the symmetry-partner intrinsic particles' frames $(\phi\tilde{x}', \phi c\phi\tilde{t}')$ and $(-\phi\tilde{x}'^*, -\phi c\phi\tilde{t}'^*)$ by inclined primed affine spacetime coordinates $\tilde{x}', c\tilde{t}', -\tilde{x}'^*$ and $-c\tilde{t}'^*$ respectively of the symmetry-partner particles' frames $(\tilde{x}', \tilde{y}', \tilde{z}', c\tilde{t}')$ and $(-\tilde{x}'^*, -\tilde{y}'^*, -\tilde{z}'^*, -c\tilde{t}'^*)$ in the positive and negative universes in Figs. 8a and 8b of [1], that is, by letting $\phi\tilde{x}' \to \tilde{x}'$; $\phi c\phi\tilde{t}' \to c\tilde{t}'$; $-\phi\tilde{x}'^* \to -\tilde{x}'^*$; $-\phi c\phi\tilde{t}'^* \to -c\tilde{t}'^*$; $\phi\tilde{x} \to \tilde{x}$; $\phi c\phi\tilde{t} \to c\tilde{t}$; $-\phi\tilde{x}^* \to -\tilde{x}^*$ and $-\phi c\phi\tilde{t}^* \to -c\tilde{t}^*$ in those diagrams, as would be done in the four-world picture in the absence of the intrinsic spacetime coordinates, are invalid or will not work.

The end of the foregoing paragraph is so since the affine space coordinates $\tilde{y}'$ and $\tilde{z}'$ of the particle's frame are not rotated along with the affine space coordinate $\tilde{x}'$ from affine 3-space $\tilde{\Sigma}'(\tilde{x}', \tilde{y}', \tilde{z}')$ of the particle's frame (as a hyper-surface) along the horizontal towards the time dimension $c\tilde{t}$ along the vertical. And the only rotated coordinate $\tilde{x}'$, which is inclined at angle ψ to the horizontal, cannot contain the three-dimensional rest mass m_0 of the particle, which can then be "projected" as three-dimensional relativistic mass, $m = \gamma m_0$, into the projective affine 3-space $\tilde{\Sigma}(\tilde{x}, \tilde{y}, \tilde{z})$ of the observer's frame (as a hyper-surface) along the horizontal. It then follows that the observational fact of the evolution of the rest mass m_0 of the particle into relativistic mass, $m = \gamma m_0$, in SR, is impossible in the context of diagrams involving rotations of the affine spacetime coordinates $\tilde{x}'$ and $c\tilde{t}'$ of the particle's frame relative to the affine spacetime coordinates $\tilde{x}$ and $c\tilde{t}$ of the observer's frame, which are in relative motion along their collinear $\tilde{x}'-$ and $\tilde{x}-$axes in the four-world picture. This rules out the possibility (or validity) of such diagrams in the four-world picture. As noted in [1], if such diagrams are drawn, it must be understood that they are hypothetical or intrinsic (i.e. non-observable).

Further more, it is possible for the intrinsic affine spacetime coordinates $\phi\tilde{x}'$ and $\phi c\phi\tilde{t}'$ of the particle's intrinsic frame $(\phi\tilde{x}', \phi c\phi\tilde{t}')$, containing the one-dimensional intrinsic rest mass ϕm_0 of the particle in the intrinsic affine space coordinate $\phi\tilde{x}'$, to rotate relative to their projective affine intrinsic spacetime coordinates $\phi\tilde{x}$ and $\phi c\phi\tilde{t}$ of the observer's intrinsic frame $(\phi\tilde{x}, \phi c\phi\tilde{t})$, that contains the 'projective' one-dimensional intrinsic relativistic mass, $\phi m = \gamma\phi m_0$, of the particle in the projective intrinsic affine space coordinate $\phi\tilde{x}$, by intrinsic angles $\phi\psi$ larger that $\frac{\pi}{2}$, that is, in the range $\frac{\pi}{2} < \phi\psi \leq \pi$, (assuming rotation by $\phi\psi = \frac{\pi}{2}$ can be avoided), in Fig. 8a of [1]. This will make the particle's intrinsic frame $(\phi\tilde{x}', \phi c\phi\tilde{t}')$ containing the positive intrinsic rest mass ϕm_0 of the particle in the inclined affine intrinsic coordinate $\phi\tilde{x}'$ in the positive universe to make transition into the negative universe through the second quadrant to become particle's intrinsic frame $(-\phi\tilde{x}'^*, -\phi c\phi\tilde{t}'^*)$ containing negative intrinsic rest mass $-\phi m_0^*$ of the particle in the negative intrinsic affine space coordinate $-\phi\tilde{x}'^*$, as explained in section 2 of [2].

The negative intrinsic affine spacetime coordinates $-\phi\tilde{x}'^*$ and $-\phi c\phi\tilde{t}'^*$ of the intrinsic particle's frame, into which the positive intrinsic affine coordinates $\phi\tilde{x}'$ and $\phi c\phi\tilde{t}'$ of the particle's intrinsic frame in the positive universe transform upon making transition into the negative universe through the second quadrant, will be inclined intrinsic affine coordinates in the second quadrant and the third quadrant respectively. They will project intrinsic affine coordinates $-\phi\tilde{x}^*$ and $-\phi c\phi\tilde{t}^*$ of the observer's intrinsic frame along the horizontal and vertical respectively in the third quadrant. Thus the observer's intrinsic frame $(-\phi\tilde{x}^*, -\phi c\phi\tilde{t}^*)$ containing negative intrinsic relativistic mass, $-\phi m^* = -\gamma\phi m_0^*$, in the intrinsic affine space coordinate $-\phi\tilde{x}^*$, will automatically appear in the negative universe, upon the particle's intrinsic frame $(\phi\tilde{x}', \phi c\phi\tilde{t}')$ containing positive intrinsic rest mass ϕm_0 of the particle in the first quadrant making transition into the second quadrant. The observer's intrinsic frame $(-\phi\tilde{x}^*, -\phi c\phi\tilde{t}^*)$ containing relativistic intrinsic mass $-\phi m^* = -\gamma\phi m_0^*$ in $-\phi x^*$ will then be made manifest in observer's frame $(-\tilde{x}^*, -\tilde{y}^*, -\tilde{z}^*, -c\tilde{t}^*)$ on flat spacetime of the negative universe, containing negative three-dimensional relativistic mass, $-m^* = -\gamma m_0^*$, of the particle.

It is therefore possible for a particle in relative motion in the positive universe to make transition into the negative universe in the context of the geometrical representation of ϕLT/LT in the two-world picture (now re-identified as four-world picture) in Figs. 8a and 8b of [1], assuming rotation of intrinsic affine spacetime coordinates $\phi\tilde{x}'$ and $\phi c\phi\tilde{t}'$ of the particle's intrinsic frame relative to the intrinsic affine spacetime coordinates $\phi\tilde{x}$ and $\phi c\phi\tilde{t}$ of the observer's intrinsic frame by intrinsic angle $\phi\psi = \frac{\pi}{2}$, corresponding to intrinsic speed $\phi v = \phi c$ of relative intrinsic motion, can be avoided in the process of rotation by $\phi\psi > \frac{\pi}{2}$.

On the other hand, letting the affine spacetime coordinates $\tilde{x}'$ and $c\tilde{t}'$ of the particle's frame $(\tilde{x}', \tilde{y}', \tilde{z}', c\tilde{t}')$ to rotate relative to the affine spacetime coordinates $\tilde{x}$ and $c\tilde{t}$ respectively of the observer's frame $(\tilde{x}, \tilde{y}, \tilde{z}, c\tilde{t})$ in the positive universe by angle ψ larger than $\frac{\pi}{2}$, that is in the range $\frac{\pi}{2} < \psi \leq \pi$, (assuming $\psi = \frac{\pi}{2}$ can be avoided), will cause the affine spacetime coordinates $\tilde{x}'$ and $c\tilde{t}'$ to make transition into the negative universe through the second quadrant to become inclined affine coordinates $-\tilde{x}'^*$ and $-c\tilde{t}'^*$ in the second and third quadrants respectively. However the non-rotated affine space coordinates $\tilde{y}'$ and $\tilde{z}'$ of the particle's frame will remain along the horizontal in the first quadrant in the positive universe. This situation in which only two of four coordinates of a frame make transition from the positive universe into the negative universe is impossible.

Moreover since the three-dimensional rest mass m_0 of the particle cannot be contained in the only rotated affine space coordinate $\tilde{x}'$, the rest mass of the particle will be unable to make transition into the negative universe with the rotated coordinates $\tilde{x}'$ and $c\tilde{t}'$. It is therefore impossible for a particle in relative motion in the positive universe to make transition into the negative universe in the context of diagrams involving rotation of affine spacetime coordinates $\tilde{x}'$ and $c\tilde{t}'$ of the particle's frame relative to affine spacetime coordinates $\tilde{x}$ and

$c\tilde{t}$ of the observer's frame, where the two frames are in motion along their collinear $\tilde{x}'-$ and $\tilde{x}-$axes, in the two-world picture (now re-identified as four-world picture). This further renders such diagrams ineffective and impossible.

Relative rotations of intrinsic affine spacetime coordinates in the spacetime/intrinsic spacetime diagrams for deriving intrinsic Lorentz transformation/Lorentz transformation are unavoidable in the present many-world picture. This makes the flat two-dimensional intrinsic metric spacetime underlying flat four-dimensional metric spacetime indispensable in the context of the present theory.

1.2 Origin of the intrinsic space and intrinsic time dimensions

It has been shown that the quartet of Euclidean 3-spaces and underlying one-dimensional intrinsic spaces in Fig. 2 of part one of this paper [3], simplifies naturally as Figs. 6a and 6b of that paper, where Fig. 6a is valid with respect to 3-observers in our proper Euclidean 3-space Σ' and 3-observer* in the proper Euclidean 3-space $-\Sigma'^{*}$ of the negative universe and Fig. 6b is valid with respect to 3-observers in the proper Euclidean 3-space $\Sigma^{0\prime}$ of the positive time-universe and 3-observer* in the proper Euclidean 3-space $-\Sigma^{0\prime *}$ of the negative time-universe, as indicated in those diagrams. Figs. 6a and 6b of [3] ultimately transform into Figs. 8a and 8b respectively of that paper naturally with respect to the same 3-observers in the proper Euclidean 3-spaces with respect to whom Figs. 6a and 6b are valid.

The one-dimensional proper intrinsic spaces underlying the proper Euclidean 3-spaces have been introduced without deriving them in the first part of this paper [3]. Now let us assume that the underlying one-dimensional proper intrinsic spaces have not been known in Figs. 6a and 6b of [3]. Then let us reproduce the first quadrant of those figures without the intrinsic spaces as Figs. 1a and 1b respectively here.

The one-dimensional proper (or classical) space $\rho^{0\prime}$ along the vertical in Fig. 1a (to which the proper Euclidean 3-space $\Sigma^{0\prime}$ of the positive time-universe naturally contracts with respect to 3-observers in our proper Euclidean 3-space Σ'), projects a component to be denoted by ρ' into our proper Euclidean 3-space Σ' (considered as a hyper-surface along the horizontal), which is given as follows:

$$\rho' = \rho^{0\prime} \cos\psi_0 = \rho^{0\prime} \cos\frac{\pi}{2} = 0 \qquad (1)$$

where the fact that $\rho^{0\prime}$ is naturally inclined at absolute angle $\psi_0 = \frac{\pi}{2}$ to the horizontal, corresponding to absolute speed $V_0 = c$ of every point along $\rho^{0\prime}$ relative to 3-observers in Σ' (discussed extensively in sub-section 1.1 of [3]) has been used in (1).

Equation (1) states that the one-dimensional space $\rho^{0\prime}$ along the vertical projects zero component (or nothing) into the Euclidean 3-space Σ' (as a hyper-surface) along the horizontal. However we shall not ascribe absolute nothingness

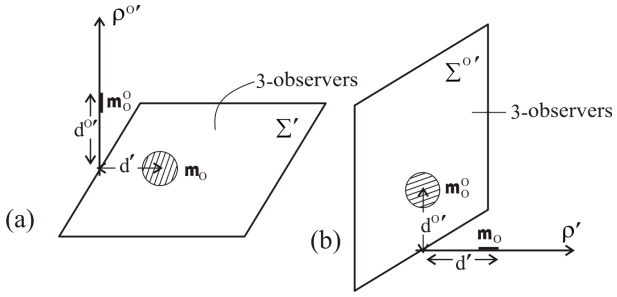

Fig. 1: (a) The proper Euclidean 3-space of our universe Σ' (as a hyper-surface along the horizontal), containing the rest mass m_0 of an object and the one-dimensional proper space $\rho^{0\prime}$ containing the one-dimensional rest mass m_0^0 of the symmetry-partner object in the positive time-universe relative to 3-observers in Σ'; $\rho^{0\prime}$ containing one-dimensional m_0^0 being the proper Euclidean 3-space $\Sigma^{0\prime}$ of the positive time-universe containing three-dimensional rest mass m_0^0 with respect to 3-observers in $\Sigma^{0\prime}$. (b) The proper Euclidean 3-space of the positive time-universe $\Sigma^{0\prime}$ (as a hyper-surface along the vertical), containing the rest mass m_0^0 of an object and the one-dimensional proper space ρ' containing the one-dimensional rest mass m_0 of the symmetry-partner object in our universe relative to 3-observers in $\Sigma^{0\prime}$; ρ' containing one-dimensional m_0 being the proper Euclidean 3-space Σ' of the positive (or our) universe containing three-dimensional rest mass m_0 with respect to 3-observers in Σ'.

to the projection of the physical one-dimensional space $\rho^{0\prime}$ along the vertical into the Euclidean 3-space Σ' along the horizontal in Fig. 1a. The one-dimensional space $\rho^{0\prime}$ certainly "casts a shadow" into Σ'.

Actually, it is the factor $\cos\frac{\pi}{2}$ that vanishes in (1) and not $\rho^{0\prime}$ multiplying it. Thus let us re-write (1) as follows:

$$\rho' = \rho^{0\prime} \cos\frac{\pi}{2} = 0 \times \rho^{0\prime} \equiv \phi\rho' \qquad (2)$$

where $\phi\rho'$ is without the superscript "0" label because it lies in (or underneath) our Euclidean 3-space Σ' (without superscript "0" label) along the horizontal.

Thus instead of associating absolute nothingness to the projection of $\rho^{0\prime}$ along the vertical into the Euclidean 3-space Σ' along the horizontal, as done in (1), a dimension $\phi\rho'$ of intrinsic (that is, non-observable and non-detectable) quality, has been attributed to it in (2). Hence $\phi\rho'$ shall be referred to as intrinsic space. It is proper (or classical) intrinsic space by virtue of its prime label.

Any interval of the one-dimensional intrinsic space (or intrinsic space dimension) $\phi\rho'$ is equivalent to zero interval of the one-dimensional physical space $\rho^{0\prime}$, (as follows from $\phi\rho' \equiv 0 \times \rho^{0\prime}$ in (2)). It then follows that any interval of the proper intrinsic space $\phi\rho'$ is equivalent to zero distance of the physical proper Euclidean 3-space Σ'. Or any interval of $\phi\rho'$ is no interval of space. The name nospace shall be coined for $\phi\rho'$ from the last statement, as an alternative to intrinsic space, where $\phi\rho'$ is proper (or classical) nospace by virtue of

the prime label on it.

As derived in sub-section 1.2 of the first part of this paper [3], the Euclidean 3-space $\Sigma^{0\prime}$ of the positive time-universe is geometrically contracted to the one-dimensional space $\rho^{0\prime}$ with respect to 3-observers in our Euclidean 3-space Σ' between Fig. 3 and Fig. 6a of [3], where $\rho^{0\prime}$ can be considered to be along any direction of the Euclidean 3-space $\Sigma^{0\prime}$ that contracts to it, with respect to 3-observers in Σ'. Thus $\rho^{0\prime}$ is an isotropic one-dimensional space with no unique orientation in the Euclidean 3-space $\Sigma^{0\prime}$ that contracts to it with respect to 3-observers in Σ'. The one-dimensional intrinsic space (or one-dimensional nospace) $\phi\rho'$, which $\rho^{0\prime}$ projects into the Euclidean 3-space Σ', is consequently an isotropic intrinsic space dimension with no unique orientation in Σ' with respect to 3-observers in Σ'.

The one-dimensional proper (or classical) space ρ' along the horizontal in Fig. 1b, to which our proper Euclidean 3-space Σ' geometrically contracts with respect to 3-observers in the proper Euclidean 3-space $\Sigma^{0\prime}$ of the positive time-universe, as explained between Fig. 4 and Fig. 6b in sub-section 1.2 of [3], likewise projects one-dimensional proper intrinsic space (or proper nospace) $\phi\rho^{0\prime}$ into the proper Euclidean 3-space $\Sigma^{0\prime}$ of the positive time-universe along the vertical in Fig. 1b (not yet shown in Fig. 1b), where $\phi\rho^{0\prime}$ is an isotropic one-dimensional intrinsic space dimension (with no unique orientation) in $\Sigma^{0\prime}$ with respect to 3-observers in $\Sigma^{0\prime}$.

As follows from all the foregoing, Fig. 1a must be replaced with Fig. 2a, where the one-dimensional proper intrinsic space $\phi\rho'$ projected into the proper Euclidean 3-space Σ' by the one-dimensional proper space $\rho^{0\prime}$ with respect to 3-observers in Σ' has been shown. Fig. 1b must likewise be replaced with Fig 2b, where the one-dimensional proper intrinsic space (or proper nospace) $\phi\rho^{0\prime}$ projected into the proper Euclidean 3-space $\Sigma^{0\prime}$ by the one-dimensional proper space ρ' with respect to 3-observers in $\Sigma^{0\prime}$ has been shown.

The one-dimensional isotropic proper (or classical) intrinsic space $\phi\rho'$ underlying the proper (or classical) Euclidean 3-space Σ' of the positive (or our) universe with respect to 3-observers in Σ' and the one-dimensional isotropic proper (or classical) intrinsic space $\phi\rho^{0\prime}$ underlying the proper (or classical) Euclidean 3-space $\Sigma^{0\prime}$ of the positive time-universe with respect to 3-observers in $\Sigma^{0\prime}$, have thus been derived. The derivations of the proper intrinsic space $-\phi\rho'^{*}$ underlying the proper Euclidean 3-space $-\Sigma'^{*}$ of the negative universe with respect to 3-observers in $-\Sigma'^{*}$ and of $-\phi\rho^{0\prime *}$ underlying the proper Euclidean 3-space $-\Sigma^{0\prime *}$ of the negative time-universe with respect to 3-observers* in $-\Sigma'^{0*}$, follow directly from the derivations of $\phi\rho'$ underlying Σ' and $\phi\rho^{0\prime}$ underlying $\Sigma^{0\prime}$ above.

Following the introduction of the flat 2-dimensional proper intrinsic spacetimes $(\phi\rho', \phi c\phi t')$ and $(-\phi\rho'^{*}, -\phi c\phi t'^{*})$ that underlie the flat four-dimensional proper spacetimes (Σ', ct') and $(-\Sigma'^{*}, -ct'^{*})$ of the positive (or our) universe and the negative universe respectively as *ansatz* in sub-section 4.4 of [1],

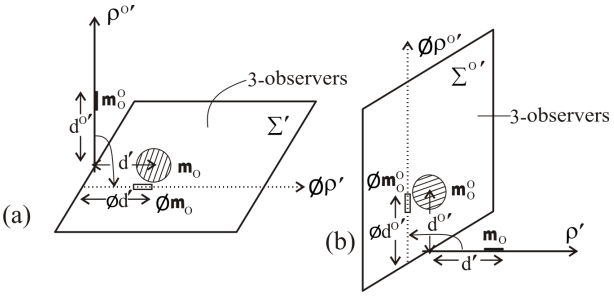

Fig. 2: (a) The one-dimensional proper space $\rho^{0\prime}$ containing one-dimensional rest mass m_0^0 along the vertical, projects one-dimensional proper intrinsic space $\phi\rho'$ containing one-dimensional intrinsic rest mass ϕm_0 into the proper Euclidean 3-space Σ' (as a hyper-surface) containing the rest mass m_0 along the horizontal, with respect to 3-observers in Σ'. (b) The one-dimensional proper space ρ' containing one-dimensional rest mass m_0 along the horizontal, projects one-dimensional proper intrinsic space $\phi\rho^{0\prime}$ containing one-dimensional intrinsic rest mass ϕm_0^0 into the proper Euclidean 3-space $\Sigma^{0\prime}$ (as a hyper-surface) containing rest mass m_0^0 along the vertical, with respect to 3-observers in $\Sigma^{0\prime}$

the one-dimensional proper intrinsic spaces $\phi\rho'$ and $-\phi\rho'^{*}$ underlying the proper Euclidean 3-spaces Σ' and $-\Sigma'^{*}$ of the positive and negative universes and the proper intrinsic spaces $\phi\rho^{0\prime}$ and $-\phi\rho^{0\prime *}$ underlying the proper Euclidean 3-spaces $\Sigma^{0\prime}$ and $-\Sigma^{0\prime *}$ of the positive and negative time-universes were introduced without deriving them in Figs. 2, 3 and 4 and Figs. 6a and 6b of the first part of this paper [3]. The existence in nature of the one-dimensional isotropic intrinsic spaces underlying the physical Euclidean 3-spaces has now been validated.

1.3 Origin of one-dimensional intrinsic rest mass in one-dimensional proper intrinsic space underlying rest mass in proper Euclidean 3-space

The one-dimensional proper space $\rho^{0\prime}$, being orthogonal to the proper Euclidean 3-space Σ' (as a hyper-surface) along the horizontal, possesses absolute speed $V_0 = c$ at every point along its length with respect to 3-observers in Σ', as has been well discussed in sub-section 1.1 of [3]. Consequently, the one-dimensional rest mass m_0^0 of a particle or object in $\rho^{0\prime}$ acquires the absolute speed $V_0 = c$ of $\rho^{0\prime}$ with respect to 3-observers in Σ' in Figs. 1a and 2a.

On the other hand, the Euclidean 3-space Σ' being along the horizontal (as a hyper-surface), possesses zero absolute speed ($V_0 = 0$) at every point of it with respect to 3-observers in Σ'. The projective intrinsic space (or nospace) $\phi\rho'$, being along the horizontal, likewise possesses zero absolute intrinsic speed ($\phi V_0 = 0$) at every point along its length with respect to 3-observers in Σ' in Fig. 2a.

The one-dimensional rest mass m_0^0 in the one-dimensional proper space $\rho^{0\prime}$ along the vertical in Figs. 1a or 2a, can be said to be in non-detectable absolute motion at constant

absolute speed $V_0 = c$ along $\rho^{0\prime}$ with respect to 3-observers in the proper Euclidean 3-space Σ' in that figure. There is a mass relation in the context of absolute motion that can be applied for the non-detectable absolute motion at absolute speed $V_0 = c$ of m_0^0 along $\rho^{0\prime}$, which shall be derived elsewhere in the systematic development of the present theory. It shall be temporarily written hereunder because of the need to use it at this point.

Let us revisit Fig. 7 of part one of this paper [3], drawn to illustrate the concept of time and intrinsic time induction only. It is assumed that the proper intrinsic metric space $\phi\rho^{0\prime}$ possesses absolute intrinsic speed $\phi V_0 < \phi c$ at every point along its length, thereby causing $\phi\rho^{0\prime}$ to be inclined at a constant absolute intrinsic angle, $\phi\psi_0 < \frac{\pi}{2}$, relative to its projection $\phi\rho'$ along the horizontal in that figure. This is so since the uniform absolute intrinsic speed ϕV_0 along the length of $\phi\rho^{0\prime}$ is related to the constant absolute intrinsic angle $\phi\psi_0$ of inclination to the horizontal of $\phi\rho^{0\prime}$ as, $\sin\phi\psi_0 = \phi V_0/\phi c$, (see Eq. (1) of [3]). It follows from this relation that when the inclined $\phi\rho^{0\prime}$ lies along the horizontal, thereby being the same as its projection $\phi\rho'$ along the horizontal, it possesses constant zero absolute intrinsic speed ($\phi V_0 = 0$) at every point along its length along the horizontal with respect to the 3-observer in Σ' in that figure, just as it has been said that the projective $\phi\rho'$ along the horizontal possesses absolute intrinsic speed $V_0 = 0$ at every point along its length with respect to 3-observers Σ' in Fig. 2a earlier. And for $\phi\rho^{0\prime}$ to lie along the vertical in Fig. 7 of [3], it possesses constant absolute intrinsic speed $\phi V_0 = \phi c$ at every point along its length with respect to the 3-observer in Σ'.

Now let a one-dimensional intrinsic rest mass ϕm_0^0 be located at any point along the inclined proper intrinsic metric space $\phi\rho^{0\prime}$ in Fig. 7 of [3]. Then ϕm_0^0 will acquire absolute intrinsic speed $\phi V_0 < \phi c$ along the inclined $\phi\rho^{0\prime}$. It will project another intrinsic rest mass ϕm_0 (since it is not in relative motion) into the proper intrinsic space $\phi\rho'$, which the inclined $\phi\rho^{0\prime}$ projects along the horizontal. The relation between the 'projective' intrinsic rest mass ϕm_0 in the projective proper intrinsic space $\phi\rho'$ along the horizontal and the intrinsic rest mass ϕm_0^0 along the inclined proper intrinsic space $\phi\rho^{0\prime}$ (not shown in Fig. 7 of [3]), is the intrinsic mass relation in the context of absolute intrinsic motion to be derived formally elsewhere. It is given as follows:

$$\phi m_0 = \phi m_0^0 \cos^2\phi\psi_0 = \phi m_0^0\left(1 - \frac{\phi V_0^2}{\phi c^2}\right) \tag{3}$$

The outward manifestation in the proper 3-dimensional Euclidean space Σ' (in Fig. 7 of [3]) of Eq. (3), obtained by simply removing the symbol ϕ, is the following

$$m_0 = m_0^0 \cos^2\psi_0 = m_0^0\left(1 - \frac{V_0^2}{c^2}\right) \tag{4}$$

Corresponding to relations (3) and (4) in the contexts of absolute intrinsic motion and absolute motion, there are the intrinsic mass relation in the context of relative intrinsic motion (or in the context of intrinsic special theory of relativity (ϕSR)) and mass relation in the context of relative motion (or in the context of SR). The generalized forms involving intrinsic angle $\phi\psi$ and angle ψ of intrinsic mass relation in the context of ϕSR and mass relation in the context of SR, derived and presented as Eqs. (15) and (16) in section 3 of [2] are the following

$$\phi m = \phi m_0 \sec\phi\psi = \phi m_0\left(1 - \frac{\phi v^2}{\phi c^2}\right)^{-1/2} \tag{5}$$

and

$$m = m_0 \sec\psi = m_0\left(1 - \frac{v^2}{c^2}\right)^{-1/2} \tag{6}$$

One finds that relations (3) and (4) in the context of absolute intrinsic motion and absolute motion differ grossly from the corresponding relations (5) and (6) in relative intrinsic motion (or in the context of ϕSR) and in relative motion (or in the context of SR).

Since the one-dimensional rest mass m_0^0 possesses absolute speed $V_0 = c$ of non-detectable absolute motion along $\rho^{0\prime}$ with respect to 3-observers in Σ' in Fig. 2a, relation (4) can be applied for the "projection" of m_0^0 into the Euclidean 3-space Σ' with respect to 3-observers in Σ' in that figure. We must simply let $\psi_0 = \frac{\pi}{2}$ and $V_0 = c$ in Eq. (4) to have

$$m_0 = m_0^0 \cos^2\frac{\pi}{2} = m_0^0\left(1 - \frac{c^2}{c^2}\right) = 0 \tag{7}$$

Equation (7) states that the one-dimensional rest mass m_0^0 in the one-dimensional space $\rho^{0\prime}$ along the vertical in Fig. 2a, (to which the three-dimensional rest mass m_0^0 in the proper Euclidean 3-space $\Sigma^{0\prime}$ of the positive time-universe with respect to 3-observers in $\Sigma^{0\prime}$ contracts relative to 3-observers in our Euclidean 3-space Σ'), projects zero rest mass (or nothing) into our Euclidean 3-space Σ' along the horizontal. However the one-dimensional rest mass m_0^0 in $\rho^{0\prime}$ along the vertical certainly 'casts a shadow' into the Euclidean 3-space Σ' considered as a hyper-surface along the horizontal in Fig. 2a.

It is the factor $\cos^2\frac{\pi}{2}$ or $(1 - c^2/c^2)$ that vanishes and not the rest mass m_0^0 multiplying it in Eq. (7). Thus let us re-write Eq. (7) as follows:

$$m_0 = m_0^0 \cos^2\frac{\pi}{2} = 0 \times m_0^0 \equiv \phi m_0 \tag{8}$$

Instead of ascribing absolute nothingness to the "projection" of the one-dimensional rest mass m_0^0 in the one-dimensional space $\rho^{0\prime}$ along the vertical into our proper Euclidean 3-space as a hyper-surface Σ' along the horizontal in Fig. 2a in Eq. (7), a one-dimensional quantity ϕm_0 of intrinsic (that is, nonobservable and non-detectable) quality has been ascribed to it in Eq. (8). Hence ϕm_0 shall be referred to as intrinsic rest mass.

Any quantity of the one-dimensional intrinsic rest mass ϕm_0 is equivalent to zero quantity of the one-dimensional rest

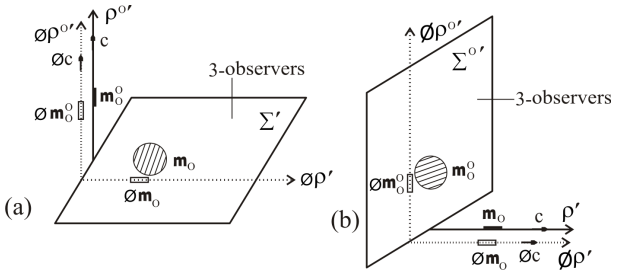

Fig. 3: (a) The proper intrinsic space $\phi\rho^{0\prime}$ containing intrinsic rest mass ϕm_0^0, projected into the proper Euclidean 3-space $\Sigma^{0\prime}$ along the vertical by one-dimensional proper space ρ' containing one-dimensional rest mass m_0 along the horizontal in Fig. 2b, is added to Fig. 2a, where it lies parallel to $\rho^{0\prime}$ along the vertical, giving rise to a flat four-dimensional proper space $(\Sigma', \rho^{0\prime})$ underlied by flat two-dimensional proper intrinsic space $(\phi\rho', \phi\rho^{0\prime})$ with respect to 3-observers in Σ'. (b) The proper intrinsic space $\phi\rho'$ containing intrinsic rest mass ϕm_0, projected into the proper Euclidean 3-space Σ' along the horizontal by one-dimensional proper space $\rho^{0\prime}$ containing one-dimensional rest mass m_0^0 along the vertical in Fig. 2a, is added to Fig. 2b, where it lies parallel to ρ' along the horizontal, giving rise to a flat four-dimensional proper space $(\Sigma^{0\prime}, \rho')$ underlied by flat two-dimensional proper intrinsic space $(\phi\rho^{0\prime}, \phi\rho')$ with respect to 3-observers in $\Sigma^{0\prime}$.

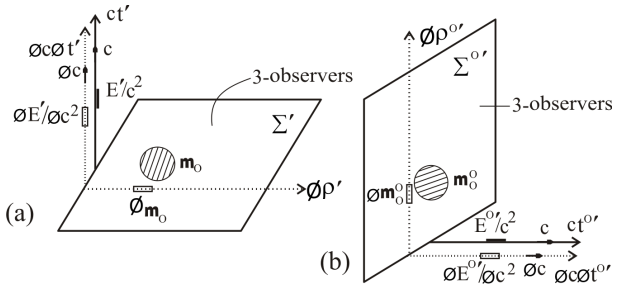

Fig. 4: (a) The one-dimensional proper space $\rho^{0\prime}$ and the proper intrinsic space $\phi\rho^{0\prime}$ along the vertical with respect to 3-observers in Σ' in Fig. 3a, transform into the proper time dimension ct' and proper intrinsic time dimension $\phi c\phi t'$ respectively, giving rise to a flat four-dimensional proper spacetime (Σ', ct') underlied by flat two-dimensional proper intrinsic spacetime $(\phi\rho', \phi c\phi t')$ with respect to 3-observers in Σ'. (b) The one-dimensional proper space ρ' and the proper intrinsic space $\phi\rho'$ along the horizontal with respect to 3-observers in $\Sigma^{0\prime}$ in Fig. 3b, transform into the proper time dimension $ct^{0\prime}$ and proper intrinsic time dimension $\phi c\phi t^{0\prime}$ respectively, giving rise to a flat four-dimensional proper spacetime $(\Sigma^{0\prime}, ct^{0\prime})$ underlied by flat two-dimensional proper intrinsic spacetime $(\phi\rho^{0\prime}, \phi c\phi t^{0\prime})$ with respect to 3-observers in $\Sigma^{0\prime}$.

mass m_0^0 in the one-dimensional space $\rho^{0\prime}$, as follows from $\phi m_0 \equiv 0 \times m_0^0$ in Eq. (8). It then follows that any quantity of the intrinsic rest mass ϕm_0 is equivalent to zero quantity of three-dimensional rest mass m_0 in Σ'. Or any quantity of intrinsic rest mass is no rest mass. An alternative name coined from the preceding statement namely, nomass, shall be given to the intrinsic rest mass ϕm_0. The intrinsic rest mass ϕm_0 in the proper (or classical) intrinsic space is the proper (or classical) nomass.

The 'projective' intrinsic rest mass (or proper nomass) ϕm_0 in the projective proper intrinsic space $\phi\rho'$, lies directly underneath the rest mass m_0 in the proper Euclidean 3-space Σ', as already shown in Fig. 2a. The one-dimensional rest mass m_0 in the one-dimensional proper (or classical) space ρ' along the horizontal in Fig. 2b, likewise "projects" intrinsic rest mass (or proper nomass) ϕm_0^0 into the projective proper (or classical) intrinsic space $\phi\rho^{0\prime}$, which lies directly underneath the rest mass m_0^0 in the proper Euclidean 3-space $\Sigma^{0\prime}$ of the positive time-universe with respect to 3-observers in $\Sigma^{0\prime}$, as already shown in Fig. 2b.

Now the proper Euclidean 3-space $\Sigma^{0\prime}$ of the positive time-universe with respect to 3-observers in it in Fig. 2b, is what appears as one-dimensional proper space $\rho^{0\prime}$ along the vertical with respect to 3-observers in our proper Euclidean 3-space Σ' in Fig. 2a. The one-dimensional proper intrinsic space $\phi\rho^{0\prime}$ projected into (or underneath) $\Sigma^{0\prime}$ by ρ' along the horizontal in Fig. 2b, must be added to Fig. 2a, where it must lie parallel to $\rho^{0\prime}$ along the vertical, thereby converting Fig. 2a to Fig. 3a with respect to 3-observers in Σ'. The one-dimensional proper intrinsic space $\phi\rho'$ projected into (or underneath) our proper Euclidean 3-space Σ' by $\rho^{0\prime}$ along the vertical in Fig. 2a, must likewise be added to Fig. 2b, where it must lie parallel to ρ' along the horizontal, thereby converting Fig. 2b to Fig. 3b with respect to 3-observers in $\Sigma^{0\prime}$.

Finally, as explained for the transformations of Figs. 6a and 6b into Figs. 8a and 8b respectively in sub-section 1.3 of part one of this paper [3], the one-dimensional proper (or classical) space $\rho^{0\prime}$ and the one-dimensional proper (or classical) intrinsic space $\phi\rho^{0\prime}$ lying parallel to it along the vertical in Fig. 3a, transform into the proper time dimension ct' and the proper intrinsic time dimension $\phi c\phi t'$ of the positive (or our) universe with respect to 3-observers in our proper Euclidean 3-space Σ', thereby converting Fig. 3a to the final Fig. 4a.

The one-dimensional proper (or classical) space ρ' and the one-dimensional proper (or classical) intrinsic space $\phi\rho'$ lying parallel to it along the horizontal in Fig. 3b, likewise transform into the proper time dimension $ct^{0\prime}$ and the proper intrinsic time dimension $\phi c\phi t^{0\prime}$ of the positive time-universe with respect to 3-observers in the proper Euclidean 3-space $\Sigma^{0\prime}$ of the positive time-universe, thereby converting Fig. 3b to the final Fig. 4b.

As also explained in drawing Figs. 9a and 9b of [3], the one-dimensional rest mass m_0^0 in the one-dimensional proper (or classical) space $\rho^{0\prime}$ and the one-dimensional intrinsic rest mass ϕm_0^0 in the proper (or classical) intrinsic space $\phi\rho^{0\prime}$ in Fig. 3a must be replaced by one-dimensional equivalent rest mass E'/c^2, where $E' = m_0^0 c^2$, in the proper time-dimension ct' and one-dimensional equivalent intrinsic rest mass $\phi E'/\phi c^2$, where $\phi E' = \phi m_0^0 \phi c^2$, in the proper intrinsic time

dimension $\phi c\phi t'$ respectively, as done in Fig. 4a. The one-dimensional rest mass m_0 in ρ' and the intrinsic rest mass ϕm_0 in $\phi\rho'$ along the horizontal in Fig. 3b must likewise be replaced by $E^{0\prime}/c^2$; $E^{0\prime} = m_0c^2$, in $ct^{0\prime}$ and $\phi E^{0\prime}/\phi c^2$; $\phi E^{0\prime} = \phi m_0\phi c^2$, in $\phi c\phi t^{0\prime}$ respectively, as done in Fig. 4b.

Fig. 4a now has flat two-dimensional proper intrinsic spacetime (or proper nospace-notime) $(\phi\rho', \phi c\phi t')$, containing intrinsic rest mass (or proper nomass) ϕm_0 (in $\phi\rho'$) and equivalent intrinsic rest mass $\phi E'/\phi c^2$ (in $\phi c\phi t'$), underlying flat four-dimensional proper spacetime (Σ', ct'), containing rest mass m_0 (in Σ') and equivalent rest mass E'/c^2 (in ct'), of the positive (or our) universe. Fig. 4b likewise now has flat two-dimensional proper intrinsic spacetime $(\phi\rho^{0\prime}, \phi c\phi t^{0\prime})$, containing intrinsic rest mass ϕm_0^0 (in $\phi\rho^{0\prime}$) and equivalent intrinsic rest mass $\phi E^{0\prime}/\phi c^2$ (in $\phi c\phi t^{0\prime}$), underlying flat proper spacetime $(\Sigma^{0\prime}, ct^{0\prime})$, containing rest mass m_0^0 (in $\Sigma^{0\prime}$) and equivalent rest mass $E^{0\prime}/c^2$ (in $ct^{0\prime}$), of the positive time-universe.

In tracing the origin of the proper intrinsic space $\phi\rho'$ and the intrinsic rest mass ϕm_0 contained in it in Fig. 4a, we find that the one-dimensional proper space $\rho^{0\prime}$ containing one-dimensional rest mass m_0^0 along the vertical with respect to 3-observers in the proper Euclidean 3-space Σ' of the positive (or our) universe in Fig. 2a or 3a, projects proper intrinsic space $\phi\rho'$ containing intrinsic rest mass ϕm_0 into the proper Euclidean 3-space Σ'. Then as $\rho^{0\prime}$ containing m_0^0 along the vertical in Fig. 2a or 3a (being along the vertical) naturally transforms into proper time dimension ct' containing equivalent rest mass E'/c^2 with respect to 3-observers in Σ' in Fig. 4a, its projection $\phi\rho'$ containing ϕm_0 into Σ' along the horizontal (being along the horizontal) remains unchanged with respect to 3-observers in Σ'.

The conclusion then is that the proper Euclidean 3-space $\Sigma^{0\prime}$ of the positive time-universe with respect to 3-observers in $\Sigma^{0\prime}$, (which is one-dimensional space $\rho^{0\prime}$ with respect to 3-observers in our proper Euclidean 3-space Σ'), is ultimately the origin of the one-dimensional proper intrinsic space $\phi\rho'$ underlying the proper Euclidean 3-space Σ' of our universe and the three-dimensional rest mass m_0^0 of a particle of object in the proper Euclidean 3-space $\Sigma^{0\prime}$ of the positive time-universe with respect to 3-observers in $\Sigma^{0\prime}$ is the origin of the one-dimensional intrinsic rest mass ϕm_0 in the proper intrinsic space $\phi\rho'$ lying directly underneath the rest mass m_0 of the symmetry-partner particle or object in the proper Euclidean 3-space Σ' of our universe. In other words, the proper Euclidean 3-space $\Sigma^{0\prime}$ containing the three-dimensional rest mass m_0^0 of a particle or object in the positive time-universe, "casts a shadow" of one-dimensional isotropic proper intrinsic space $\phi\rho'$ containing one-dimensional intrinsic rest mass ϕm_0 into the proper Euclidean 3-space Σ' containing the rest mass m_0 of the symmetry-partner particle or object in our universe, where ϕm_0 in $\phi\rho'$ lies directly underneath m_0 in Σ'.

And in tracing the origin of the proper intrinsic time dimension $\phi c\phi t'$ that contains the equivalent intrinsic rest mass $\phi E'/\phi c^2$, lying parallel to the proper time dimension ct' containing the equivalent rest mass E'/c^2 in Fig. 4a, we find that the one-dimensional proper space ρ' containing one-dimensional rest mass m_0 along the horizontal with respect to 3-observers in the proper Euclidean 3-space $\Sigma^{0\prime}$ of the positive time-universe in Fig. 2b or 3b, where ρ' is the Euclidean 3-space Σ' of our universe with respect to 3-observers in Σ', as derived between Fig. 4 and Fig. 6b in sub-section 1.2 of [3], projects one-dimensional proper intrinsic space $\phi\rho^{0\prime}$ containing intrinsic rest mass ϕm_0^0 underneath the proper Euclidean 3-space $\Sigma^{0\prime}$ containing rest mass m_0^0 of the positive time-universe with respect to 3-observers in $\Sigma^{0\prime}$ in Fig. 2b or 3b. The proper Euclidean 3-space $\Sigma^{0\prime}$ containing the rest mass m_0^0 and its underlying proper intrinsic space $\phi\rho^{0\prime}$ containing intrinsic rest mass ϕm_0^0 with respect to 3-observers in the proper Euclidean 3-space $\Sigma^{0\prime}$ of the positive time-universe in Fig. 3b, are the proper time dimension ct' of our universe containing equivalent rest mass E'/c^2 and its underlying proper intrinsic time dimension $\phi c\phi t'$ of our universe containing equivalent intrinsic rest mass $\phi E'/\phi c^2$ with respect to 3-observers in Σ' in Fig. 4a.

The conclusion then is that the proper Euclidean 3-space Σ' of the positive (or our) universe is the origin of the proper intrinsic time dimension $\phi c\phi t'$ that lies parallel to the proper time dimension ct' of the positive (or our) universe in Fig. 4a. The three-dimensional rest mass m_0 of a particle or object in the proper Euclidean 3-space Σ' of our universe is the origin of the one-dimensional equivalent intrinsic rest mass $\phi E'/\phi c^2$ in the proper intrinsic time dimension $\phi c\phi t'$ that lies besides the one-dimensional equivalent rest mass E'/c^2 in the proper time dimension ct' of our universe in Fig. 4a.

The two-dimensional proper intrinsic metric spacetime (or proper metric nospace-notime) $(\phi\rho', \phi c\phi t')$, containing intrinsic rest mass ϕm_0 in $\phi\rho'$ and equivalent intrinsic rest mass $\phi E/\phi c^2$ in $\phi c\phi t'$, which underlies the flat proper metric spacetime (Σ', ct'), containing rest mass m_0 in Σ' and equivalent rest mass E'/c^2 in ct', has thus been derived within the four-world picture. The intrinsic special theory of relativity (ϕSR) operates on the flat proper intrinsic metric spacetime $(\phi\rho', \phi c\phi t')$ and the special theory of relativity (SR) operates on the flat proper metric spacetime (Σ', ct') in the absence of relativistic gravitational field. The flat two-dimensional proper intrinsic spacetime was introduced as *ansatz* in section 4.4 of [1] and it has proved indispensable in the present theory since then, as discussed fully earlier in sub-section 1.1 of this paper.

The derivations of the flat two-dimensional proper intrinsic spacetime $(\phi\rho', \phi c\phi t')$ containing intrinsic rest masses $(\phi m_0, \phi E'/\phi c^2)$ of particles and bodies, which underlies the flat four-dimensional proper spacetime (Σ', ct') containing the rest masses $(m_0, E'/c^2)$ of particles and bodies in our universe and in the other three universes, as presented in this sub-section, is the best that can be done at the present level of the present evolving theory. The derivations certainly demystify the concepts of intrinsic spacetime and intrinsic mass

introduced as *ansatz* in section 4 of [1]. There are, however, more formal and more complete derivations of these concepts along with the concepts of absolute intrinsic spacetime containing absolute intrinsic rest mass, which underlies absolute spacetime containing absolute rest mass and relativistic intrinsic spacetime containing relativistic intrinsic mass, which underlies relativistic spacetime containing relativistic mass, to be presented elsewhere with further development.

2 Validating perfect symmetry of state among the four universes isolated

Perfect symmetry of natural laws among the four universes namely, the positive universe, the negative universe, the positive time-universe and the negative time-universe, whose metric spacetimes and underlying intrinsic metric spacetimes are depicted in Figs. 8a and 8b of the first part of this paper [3], has been demonstrated in section 2 of that paper. Perfect symmetry of state among the universes shall now be demonstrated in this section. Perfect symmetry of state exists among the four universes if the masses of the four members of every quartet of symmetry-partner particles or objects in the four universes have identical magnitudes, shapes and sizes and if they perform identical relative motions in their universes at all times. These conditions shall be shown to be met in this section.

2.1 Identical magnitudes of masses and of shapes and sizes of the members of every quartet of symmetry-partner particles or objects in the four universes

As illustrated in Fig. 2a or 3a, the one-dimensional intrinsic rest mass (or proper nomass) ϕm_0 "projected" into the projective isotropic one-dimensional proper (or classical) intrinsic space (or proper nospace) $\phi\rho'$, lies directly underneath the three-dimensional rest mass m_0 in the proper (or classical) Euclidean 3-space Σ' of the positive (or our) universe with respect to 3-observers in Σ'. Likewise the "projective" one-dimensional intrinsic rest mass ϕm_0^0 in the projective one-dimensional isotropic proper intrinsic space $\phi\rho^{0\prime}$ lies directly underneath the three-dimensional rest mass m_0^0 in the proper (or classical) Euclidean 3-space $\Sigma^{0\prime}$ of the positive time-universe with respect to 3-observers in $\Sigma^{0\prime}$ in Fig. 2b or 3b.

Now the rest mass m_0 is the outward (or physical) manifestation in the proper (or classical) physical Euclidean 3-space Σ' of the one-dimensional intrinsic rest mass ϕm_0 in the one-dimensional proper (or classical) intrinsic space $\phi\rho'$ lying underneath m_0 in Σ' in Fig. 2a or 3a. It then follows that m_0 and ϕm_0 are equal in magnitude, that is, $m_0 = |\phi m_0|$.

But the one-dimensional intrinsic rest mass ϕm_0 in $\phi\rho'$ along the horizontal is equal in magnitude to the one-dimensional rest mass m_0^0 in the one-dimensional space $\rho^{0\prime}$ along the vertical that 'projects' ϕm_0 contained in $\phi\rho'$ along the horizontal in Fig. 2a or 3a. That is, $m_0^0 = |\phi m_0|$. By combining this with $m_0 = |\phi m_0|$ derived in the preceding paragraph, we have the equality in magnitude of the three-dimensional rest mass m_0 of a particle or object in our proper Euclidean 3-space Σ' and the one-dimensional rest mass m_0^0 of the symmetry-partner particle or object in the one-dimensional proper (or classical) space $\rho^{0\prime}$ (with respect to 3-observers in Σ') in Fig. 2a or 3a. That is, $m_0 = m_0^0$.

Finally the one-dimensional rest mass m_0^0 of a particle or object in the one-dimensional proper space $\rho^{0\prime}$ along the vertical with respect to 3-observers in our proper Euclidean 3-space Σ' in Fig. 2a or 3a, is what 3-observers in the proper Euclidean 3-space $\Sigma^{0\prime}$ of the positive time-universe observe as three-dimensional rest mass m_0^0 of the particle or object in $\Sigma^{0\prime}$. Consequently the one-dimensional rest mass m_0^0 of the particle or object in $\rho^{0\prime}$ in Fig. 2a or 3a is equal in magnitude to the three-dimensional rest mass m_0^0 of the particle or object in the proper Euclidean 3-space $\Sigma^{0\prime}$. This is certainly so since the geometrical contraction of the Euclidean 3-space $\Sigma^{0\prime}$ to one-dimensional space $\rho^{0\prime}$ and the consequent geometrical contraction of the three-dimensional rest mass m_0^0 in $\Sigma^{0\prime}$ to one-dimensional rest mass m_0^0 in $\rho^{0\prime}$ with respect to 3-observers in our Euclidean 3-space Σ', does not alter the magnitude of the rest mass m_0^0.

In summary, we have derived the simultaneous relations $m_0 = |\phi m_0|$ and $m_0^0 = |\phi m_0|$, from which we have, $m_0 = m_0^0$ in the above. Also since m_0^0 in $\Sigma^{0\prime}$ is the outward manifestation of ϕm_0^0 in $\phi\rho^{0\prime}$ in Fig. 2b or 3b, we have the equality in magnitude of m_0^0 and ϕm_0^0, that is, $m_0^0 = |\phi m_0^0|$, which, along with $m_0^0 = |\phi m_0|$ derived above, gives $\phi m_0^0 = \phi m_0$. The conclusion then is that the rest mass m_0 of a particle or object in the proper Euclidean 3-space Σ' of our (or positive) universe with respect to 3-observers in Σ', is equal in magnitude to the rest mass m_0^0 of the symmetry-partner particle or object in the proper Euclidean 3-space $\Sigma^{0\prime}$ of the positive time-universe with respect to 3-observers in $\Sigma^{0\prime}$. The one-dimensional intrinsic rest mass ϕm_0 of the particle or object in our proper intrinsic space $\phi\rho'$ underlying m_0 in Σ' in Fig. 2a, 3a or 4a is equal in magnitude to the intrinsic rest mass ϕm_0^0 of the symmetry-partner particle or object in the proper intrinsic space $\phi\rho^{0\prime}$ underlying m_0^0 in $\Sigma^{0\prime}$ in Fig. 2b, 3b or 4b.

By repeating the derivations done between the positive (or our) universe and the positive time-universe, which lead to the conclusion reached in the foregoing paragraph, between the negative universe and the negative time-universe, (which shall not be done here in order to conserve space), we are also led to the conclusion that the rest mass $-m_0^*$ of a particle or object in the proper Euclidean 3-space $-\Sigma'^*$ of the negative universe with respect to 3-observers in $-\Sigma'^*$, is equal in magnitude to the rest mass $-m_0^{0*}$ of the symmetry-partner particle or object in the proper Euclidean 3-space $-\Sigma^{0\prime*}$ of the negative time-universe with respect to 3-observers in $-\Sigma^{0\prime*}$. The one-dimensional intrinsic rest mass $-\phi m_0^*$ of the particle or object in the proper intrinsic space $-\phi\rho'^*$ of the negative universe underlying $-m_0^*$ in $-\Sigma'^*$, is equal in magnitude to the intrinsic rest mass $-\phi m_0^{0*}$ of the symmetry-partner particle or

object in the proper intrinsic space $-\phi\rho^{0\prime *}$ underlying $-m_0^{0*}$ in $-\Sigma^{0\prime *}$ in the negative time-universe.

The perfect symmetry of state between the positive (or our) universe and the negative universe prescribed in [1], remains a prescription so far. It implies that the rest mass m_0 of a particle or object in the proper Euclidean 3-space Σ' of the positive (or our) universe, is identical in magnitude to the rest mass $-m_0^*$ of the symmetry-partner particle or object in the proper Euclidean 3-space $-\Sigma'^*$ of the negative universe, that is, $m_0 = |-m_0^*|$. The corresponding (prescribed) perfect symmetry of state between positive time-universe and the negative time-universe likewise implies that the rest mass m_0^0 of a particle or object in the proper Euclidean 3-space $\Sigma^{0\prime}$ of the positive time-universe is identical in magnitude to the rest mass$-m_0^{0*}$ of its symmetry-partner in the proper Euclidean 3-space $-\Sigma^{0\prime *}$ of the negative time-universe, that is, $m_0^0 = |-m_0^{0*}|$.

The equality of magnitudes of symmetry-partner rest masses, $m_0 = |-m_0^*|$, that follows from the prescribed perfect symmetry of state between the positive (or our) universe and the negative universe and $m_0^0 = |-m_0^{0*}|$ that follows from the prescribed symmetry of state between the positive time-universe and the negative time-universe, discussed in the foregoing paragraph, are possible of formal proof, as shall be presented elsewhere. By combining these with $m_0 = m_0^0$ and $-m_0^* = -m_0^{0*}$ derived from Figs. 2a and 2b above, we obtain the equality of magnitudes of the rest masses of the four symmetry-partner particles or objects in the four universes, that is, $m_0 = |-m_0^*| = m_0^0 = |-m_0^{0*}|$. Consequently there is equality of magnitudes of the intrinsic rest masses in the one-dimensional intrinsic spaces of the quartet of symmetry-partner particles or objects in the four universes, that is, $|\phi m_0| = |-\phi m_0^*| = |\phi m_0^0| = |-\phi m_0^{0*}|$.

Having demonstrated the equality of magnitudes of the rest masses of the members of every quartet of symmetry-partner particles or objects in the four universes, (to the extent that $m_0 = |-m_0^*|$ between the positive (or our) universe and the negative universe and $m_0^0 = |-m_0^{0*}|$ between the positive and negative time-universes are valid), let us also show their identical shapes and sizes.

Now the rest mass m_0 being the outward manifestation in our proper Euclidean 3-space Σ' of the intrinsic rest mass ϕm_0 of intrinsic length $\Delta\phi\rho'$ in the one-dimensional proper intrinsic space $\phi\rho'$ and the three-dimensional rest mass m_0^0 in the proper Euclidean 3-space $\Sigma^{0\prime}$ with respect to 3-observers in $\Sigma^{0\prime}$, being what geometrically contracts to the one-dimensional rest mass m_0^0 of length $\Delta\rho^{0\prime}$ in $\rho^{0\prime}$ with respect to 3-observers in our Euclidean 3-space Σ' and since $\Delta\rho^{0\prime}$ along the vertical projects $\Delta\phi\rho'$ into Σ' along the horizontal, then the length $\Delta\rho^{0\prime}$ of the one-dimensional rest mass m_0^0 in $\rho^{0\prime}$ has the same magnitude as the intrinsic length $\Delta\phi\rho'$ of the intrinsic rest mass ϕm_0 in $\phi\rho'$, that is, $\Delta\rho^{0\prime} = |\Delta\phi\rho'|$. Consequently the volume $\Delta\Sigma^{0\prime}$ of the Euclidean 3-space $\Sigma^{0\prime}$ occupied by the three-dimensional rest mass m_0^0 with respect to 3-observers in $\Sigma^{0\prime}$ has the same magnitude as the volume $\Delta\Sigma'$ of the Euclidean 3-space Σ' occupied by the rest mass m_0 with respect to 3-observers in Σ'; $\Delta\Sigma'$ occupied by m_0 being the outward manifestation of $\Delta\phi\rho'$ occupied by ϕm_0. In other words, the rest mass m_0 in Σ' has the same size as its symmetry-partner m_0^0 in $\Sigma^{0\prime}$.

Further more, the shape of the outward manifestation of ϕm_0 in the proper Euclidean 3-space Σ', that is, the shape of m_0 in Σ', with respect to 3-observers in Σ', is the same as the shape of the three-dimensional rest mass m_0^0 in the proper Euclidean 3-space $\Sigma^{0\prime}$ with respect to 3-observers in $\Sigma^{0\prime}$. In providing justification for this, let us recall the discussion leading to Fig. 6a and 6b of [1], that the intrinsic rest masses ϕm_0 of particles and objects, which appear as lines of intrinsic rest masses along the one-dimensional isotropic proper intrinsic space $\phi\rho'$ relative to 3-observers in the proper Euclidean 3-space Σ', as illustrated for a few objects in Fig. 6a of [1], are actually three-dimensional intrinsic rest masses ϕm_0 in three-dimensional proper intrinsic space $\phi\Sigma'$ with respect to three-dimensional intrinsic-rest-mass-observers (or 3-intrinsic-observers) in $\phi\Sigma'$, as also illustrated for a few objects in Fig. 6b of [1]. The shape of the three-dimensional intrinsic rest mass ϕm_0 of an object or particle in the three-dimensional intrinsic space $\phi\Sigma'$ with respect to 3-intrinsic-observers in $\phi\Sigma'$, is the same as the shape of its outward manifestation in the proper Euclidean 3-space Σ', that is, the same as the shape of the rest mass m_0 in Σ', with respect to 3-observers in Σ'.

Since the line of intrinsic rest mass ϕm_0 in one-dimensional proper intrinsic space $\phi\rho'$ relative to 3-observers in Σ', (which is a three-dimensional intrinsic rest mass ϕm_0 in three-dimensional proper intrinsic space $\phi\Sigma'$ with respect to 3-intrinsic-observers in $\phi\Sigma'$), is the projection along the horizontal of the line of rest mass m_0^0 in the one-dimensional proper space $\rho^{0\prime}$ along the vertical relative to 3-observers in our proper Euclidean 3-space Σ', (which is a 3-dimensional rest mass m_0^0 in the proper Euclidean 3-space $\Sigma^{0\prime}$ of the positive time-universe with respect to 3-observers in $\Sigma^{0\prime}$), the shape of the three-dimensional intrinsic rest mass ϕm_0 in $\phi\Sigma'$ with respect to 3-intrinsic-observers in $\phi\Sigma'$ is the same as the shape of the three-dimensional rest mass m_0^0 in $\Sigma^{0\prime}$ with respect to 3-observers in $\Sigma^{0\prime}$. It then follows from this and the conclusion (that the shape of ϕm_0 in $\phi\Sigma'$ is the same as the shape of m_0 in Σ') reached in the preceding two paragraphs, that the shapes of the rest masses m_0 in our proper Euclidean 3-space Σ' and m_0^0 in the proper Euclidean 3-space $\Sigma^{0\prime}$ of the positive time-universe are the same, as stated earlier.

The identical sizes and shapes of the the rest mass m_0 of a particle or object in the proper Euclidean 3-space Σ' of our universe and of the rest mass m_0^0 of its symmetry-partner in the proper Euclidean 3-space $\Sigma^{0\prime}$ of the positive time-universe, concluded from the foregoing, is equally true between the rest mass $-m_0^*$ in the Euclidean 3-space $-\Sigma'^*$ of the negative universe and its symmetry-partner $-m_0^{0*}$ in the

Euclidean 3-space $-\Sigma^{0\prime *}$ of the negative time-universe.

When the preceding paragraph is combined with the identical shapes and sizes of the rest mass m_0 of a particle or object in the proper Euclidean 3-space Σ' of the positive (or our) universe and of the rest mass $-m_0^*$ of its symmetry-partner in the proper Euclidean 3-space $-\Sigma'^*$ of the negative universe, which the so far prescribed perfect symmetry of state between our universe and the negative universe implies, as well as the identical shapes and sizes of the rest mass m_0^0 of a particle or object in the proper Euclidean 3-space $\Sigma^{0\prime}$ of the positive time-universe and of the rest mass $-m_0^{0*}$ of its symmetry-partner in the proper Euclidean 3-space $-\Sigma^{0\prime *}$ of the negative time-universe, which the so far prescribed perfect symmetry of state between positive time-universe and the negative time-universe implies, we have the identical shapes and sizes of the four members of the quartet of symmetry-partner particles or objects in the four universes, and this is true for every such quartet of symmetry-partner particles or objects.

2.2 Perfect symmetry of relative motions always among the members of every quartet of symmetry-partner particles or objects in the four universes

As mentioned at the beginning of this section, the second condition that must be met for symmetry of state to obtain among the four universes isolated in part one of this paper [3] and illustrated in Figs. 8a and 8b of that paper namely, the positive (or our) universe, the negative universe, the positive time-universe and the negative time-universe, is that the members of every quartet of symmetry-partner particles or objects in the universes, now shown to have identical magnitudes of masses, identical sizes and identical shapes, are involved in identical motions relative to identical symmetry-partner observers or frames of reference in the universes at all times. The *reductio ad absurdum* method of proof shall be applied to show that this second condition is also met. We shall assume that the quartet of symmetry-partner particles or objects in the four universes are not involved in identical relative motions and show that this leads to a violation of Lorentz invariance.

Let us start with the assumption that the members of a quartet of symmetry-partner particles or objects in the four universes are in arbitrary motions at different speeds relative to the symmetry-partner observers of frames of reference in their respective universes at every given moment. This assumption implies that given an object on earth in our universe in motion at a speed v_{x^+} along the north pole of the earth, say, relative to our earth at a given instant, then its symmetry-partner on earth in the negative universe is in motion at a speed v_{x^-} along the north pole relative to the earth of the negative universe at the same instant; the symmetry-partner object on earth in the positive time-universe is motion at a speed $v_{x^{0+}}$ along the north pole relative to the earth of the positive time-universe at the same instant and the symmetry-partner object on earth in the negative time-universe is in motion at a speed $v_{x^{0-}}$ along the north pole relative to the earth of the negative time-universe at the same instant, where it is being assumed that the speeds v_{x^+}, v_{x^-}, $v_{x^{0+}}$ and $v_{x^{0-}}$ have different magnitudes and each could take on arbitrary values lower than c, including zero. They may as well be assumed to be moving along arbitrary directions on earths in their respective universes.

The geometrical implication of the assumption made in the foregoing paragraph is that the equal intrinsic angle $\phi\psi$ of relative rotations of intrinsic affine space and intrinsic affine time coordinates in the four quadrants, drawn upon the proper (or classical) metric spacetimes/intrinsic spacetimes of the positive (or our) universe and the negative universe in Fig. 8a of [3], as Fig. 10a of that paper, and upon the proper (or classical) metric spacetimes/intrinsic spacetimes of the positive time-universe and negative time-universe in Fig. 8b of [3], as Fig. 10b of that paper, will take on different values $\phi\psi_x^+$, $\phi\psi_x^-$, $\phi\psi_t^+$, $\phi\psi_t^-$, $\phi\psi_{x^0}^+$, $\phi\psi_{x^0}^-$, $\phi\psi_{t^0}^+$ and $\phi\psi_{t^0}^-$ as depicted in Figs. 5a and 5b.

The rotations of $\phi\tilde{x}'$ by intrinsic angle $\phi\psi_x^+$ relative to $\phi\tilde{x}$ along the horizontal in the first quadrant and the rotation of $\phi c\phi\tilde{t}'$ by intrinsic angle $\phi\psi_t^+$ relative to $\phi c\phi\tilde{t}$ along the vertical in the second quadrant are valid with respect to the 3-observer in $\tilde{\Sigma}$ in Fig. 5a, where $\sin\phi\psi_x^+ = \phi v_{x^+}/\phi c$ and $\sin\phi\psi_t^+ = \phi v_{t^+}/\phi c$. On the other hand, the rotation of $-\phi\tilde{x}'^*$ at intrinsic angle $\phi\psi_x^-$ relative to $-\phi\tilde{x}^*$ along the horizontal in the third quadrant and the rotation of $-\phi c\phi\tilde{t}'^*$ by intrinsic angle $\phi\psi_t^-$ relative to $-\phi c\phi\tilde{t}^*$ along the vertical in the fourth quadrant in Fig. 5a are valid with respect to the 3-observer* in $-\tilde{\Sigma}^*$, where $\sin\phi\psi_x^- = \phi v_{x^-}/\phi c$ and $\sin\phi\psi_t^- = \phi v_{t^-}/\phi c$.

The rotations of $\phi\tilde{x}^{0\prime}$ by intrinsic angle $\phi\psi_{x^{0+}}$ relative to $\phi\tilde{x}^0$ along the vertical in the first quadrant and the rotation of $\phi c\phi\tilde{t}^{0\prime}$ by intrinsic angle $\phi\psi_{t^{0+}}$ relative to $\phi c\phi\tilde{t}^0$ along the horizontal in the fourth quadrant are valid with respect to the 3-observer in $\tilde{\Sigma}^0$ in Fig. 5b, where $\sin\phi\psi_{x^0}^+ = \phi v_{x^{0+}}/\phi c$ and $\sin\phi\psi_{t^0}^+ = \phi v_{t^{0+}}/\phi c$. On the other hand, the rotation of $-\phi\tilde{x}^{0\prime *}$ at intrinsic angle $\phi\psi_{x^0}^-$ relative to $-\phi\tilde{x}^{0*}$ along the vertical in the third quadrant and the rotation of $-\phi c\phi\tilde{t}^{0\prime *}$ by intrinsic angle $\phi\psi_{t^0}^-$ relative to $-\phi c\phi\tilde{t}^{0*}$ along the vertical in the second quadrant in Fig. 5b are valid with respect to the 3-observer* in $-\tilde{\Sigma}^{0*}$, where $\sin\phi\psi_{x^0}^- = \phi v_{x^{0-}}/\phi c$ and $\sin\phi\psi_{t^0}^- = \phi v_{t^{0-}}/\phi c$.

Although the intrinsic angles $\phi\psi_x^+$, $\phi\psi_x^-$, $\phi\psi_t^+$ and $\phi\psi_t^-$, which are related to the intrinsic speeds ϕv_{x^+}, ϕv_{x^-}, ϕv_{t^+} and ϕv_{t^-}, as $\sin\phi\psi_x^+ = \phi v_{x^+}/\phi c$; $\sin\phi\psi_x^- = \phi v_{x^-}/\phi c$; $\sin\phi\psi_t^+ = \phi v_{t^+}/\phi c$; and $\sin\phi\psi_t^- = \phi v_{t^-}/\phi c$ respectively in Fig. 5a, are different in magnitude as being assumed and although the intrinsic angles $\phi\psi_{x^0}^+$, $\phi\psi_{x^0}^-$, $\phi\psi_{t^0}^+$, $\phi\psi_{t^0}^-$, which are related to intrinsic speeds $\phi v_{x^{0+}}$, $\phi v_{x^{0-}}$, $\phi v_{t^{0+}}$ and $\phi v_{t^{0-}}$ as $\sin\phi\psi_{x^0}^+ = \phi v_{x^{0+}}/\phi c$; $\sin\phi\psi_{x^0}^- = \phi v_{x^{0-}}/\phi c$; $\sin\phi\psi_{t^0}^+ = \phi v_{t^{0+}}/\phi c$; and $\sin\phi\psi_{t^0}^- = \phi v_{t^{0-}}/\phi c$ respectively in Fig. 5b, are different in magnitude as being assumed, it must be remembered that the intrinsic angles $\phi\psi_x^+$, $\phi\psi_x^-$, $\phi\psi_{t^+}$, $\phi\psi_t^-$ in Fig. 5a are equal to the intrin-

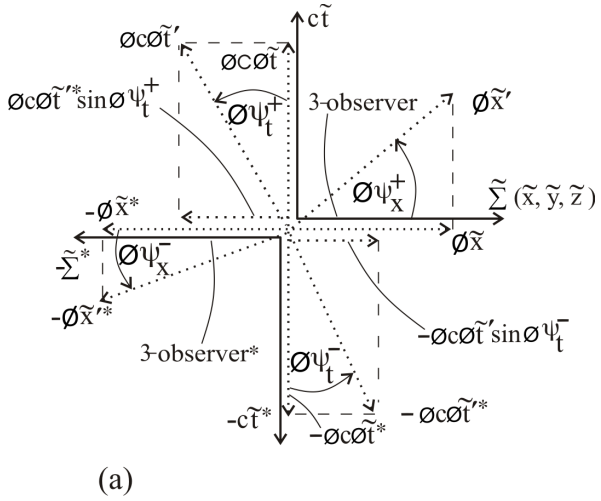

(a)

Fig. 5: (a) Rotations of intrinsic affine spacetime coordinates of intrinsic particle's frame relative to intrinsic observer's frame due to assumed non-symmetrical motions of symmetry-partner particles relative to symmetry-partner observers in the four universes, with respect to 3-observers in the Euclidean 3-spaces in the positive (or our) universe and the negative universe.

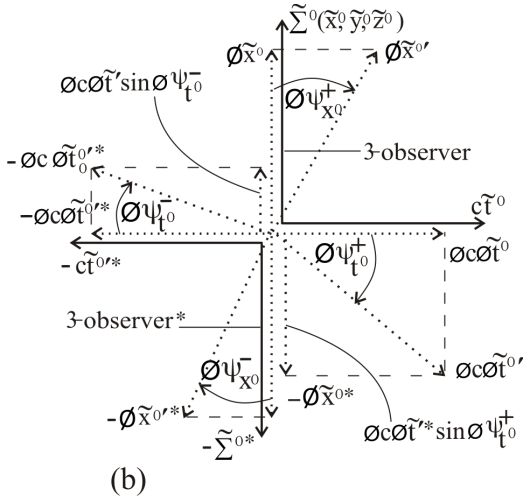

(b)

Fig. 5: (b) Rotations of intrinsic affine spacetime coordinates of intrinsic particle's frame relative to intrinsic observer's frame due to assumed non-symmetrical motions of symmetry-partner particles relative to symmetry-partner observers in the four universes, with respect to 3-observers in the Euclidean 3-spaces in the positive time-universe and the negative time-universe.

sic angles $\phi\psi^+_{t^0}$, $\phi\psi^-_{t^0}$, $\phi\psi^+_{x^0}$, $\phi\psi^-_{x^0}$ respectively in Fig. 5b.

That is, $\phi\psi^+_x = \phi\psi^+_{t^0}$; $\phi\psi^-_x = \phi\psi^-_{t^0}$; $\phi\psi^+_t = \phi\psi^+_{x^0}$ and $\phi\psi^-_t = \phi\psi^-_{x^0}$ in Figs. 5a and 5b. Consequently the intrinsic speeds ϕv_{x^+}, ϕv_{x^-}, ϕv_{t^+} and ϕv_{t^-} in Fig. 5a are equal to $\phi v_{t^{0+}}$, $\phi v_{t^{0-}}$, $\phi v_{x^{0+}}$ and $\phi v_{x^{0-}}$ respectively in Fig. 5b. That is, $\phi v_{x^+} = \phi v_{t^{0+}}$; $\phi v_{x^-} = \phi v_{t^{0-}}$; $\phi v_{t^+} = \phi v_{x^{0+}}$ and $\phi v_{t^-} = \phi v_{x^{0+}}$ in Figs. 5a and 5b.

By following the procedure used to derive partial intrinsic Lorentz transformation with respect to the 3-observer in $\tilde{\Sigma}$ from Fig. 8a of [1], the unprimed intrinsic affine coordinate $\phi\tilde{x}$ along the horizontal is the projection of the inclined $\phi\tilde{x}'$ in the first quadrant in Fig. 5a. That is, $\phi\tilde{x} = \phi\tilde{x}' \cos\phi\psi^+_x$. Hence we can write

$$\phi\tilde{x}' = \phi\tilde{x} \sec\phi\psi^+_x$$

This is all the intrinsic coordinate transformation that could have been possible with respect to the 3-observer in $\tilde{\Sigma}$ along the horizontal in the first quadrant in Fig. 5a, but for the fact that the inclined negative intrinsic coordinate $-\phi c\phi\tilde{t}'^*$ of the negative universe in the fourth quadrant also projects a component $-\phi c\phi\tilde{t}' \sin\phi\psi^-_t$ along the horizontal, which must be added to the right-hand side of the last displayed equation to have

$$\phi\tilde{x}' = \phi\tilde{x} \sec\phi\psi^+_x - \phi c\phi\tilde{t}' \sin\phi\psi^-_t; \qquad (*)$$

w.r.t 3 − observer in $\tilde{\Sigma}$.

As mentioned in the derivation of $(*)$, but for $\phi\psi^+_x = \phi\psi^-_x = \phi\psi$ with Fig. 8a in [1], the dummy star label on the component $-\phi c\phi\tilde{t}'^* \sin\phi\psi^-_t$ projected along the horizontal has been removed, since the projected component is now an intrinsic coordinate in the positive universe.

But $\phi c\phi\tilde{t} = \phi c\phi\tilde{t}' \cos\phi\psi^+_t$ or $\phi c\phi\tilde{t}' = \phi c\phi\tilde{t} \sec\phi\psi^+_t$ along the vertical in the second quadrant in the same Fig. 5a. By replacing $\phi c\phi\tilde{t}'$ by $\phi c\phi\tilde{t} \sec\phi\psi^+_t$ at the right-hand side of $(*)$ we have

$$\phi\tilde{x}' = \phi\tilde{x} \sec\phi\psi^+_x - \phi c\phi\tilde{t} \sec\phi\psi^+_t \sin\phi\psi^-_t; \qquad (9)$$

w.r.t 3 − observer in $\tilde{\Sigma}$. Eq. (9) is the final form of the partial intrinsic Lorentz transformation that the 3-observer in $\tilde{\Sigma}$ in our universe could derive along the horizontal in the first quadrant from Fig. 5a.

By applying the same procedure used to derive Eq. (9) from the first and fourth quadrants of Fig. 5a to the first and second quadrants of Fig. 5b, the counterpart of Eq. (9) that is valid with respect to the 3-observer in $\tilde{\Sigma}^0$ in that figure is the following:

$$\phi\tilde{x}^{0\prime} = \phi\tilde{x}^0 \sec\phi\psi^+_{x^0} - \phi c\phi\tilde{t}^0 \sec\phi\psi^+_{t^0} \sin\phi\psi^-_{t^0}; \qquad (10)$$

w.r.t 3 − observer in $\tilde{\Sigma}^0$. Again Eq. (10) is the final form of the partial intrinsic Lorentz transformation that the 3-observer in $\tilde{\Sigma}^0$ in the positive time-universe could derive along the vertical in the first quadrant from Fig. 5b. By collecting Eqs. (9) and (10) we have

$$\left.\begin{array}{rcl} \phi\tilde{x}' & = & \phi\tilde{x} \sec\phi\psi^+_x - \phi c\phi\tilde{t} \sec\phi\psi^+_t \sin\phi\psi^-_t; \\ & & (\text{w.r.t } 3 - \text{observer in } \tilde{\Sigma}); \\ \phi\tilde{x}^{0\prime} & = & \phi\tilde{x}^0 \sec\phi\psi^+_{x^0} - \phi c\phi\tilde{t}^0 \sec\phi\psi^+_{t^0} \sin\phi\psi^-_{t^0}; \\ & & (\text{w.r.t } 3 - \text{observer in } \tilde{\Sigma}^0) \end{array}\right\}. \qquad (11)$$

However system (11) is useless because it is neither the full intrinsic Lorentz transformation in our (or positive) universe nor in the the positive time-universe. This is so because the second equation of system (11) contains intrinsic coordinates of the positive time-universe, which are elusive to observers in our universe or which cannot appear in physics in our universe. On the other hand, the first equation contains the intrinsic spacetime coordinates of our universe, which cannot appear in physics in the positive time-universe.

In order to make system (11) a valid full intrinsic spacetime coordinate transformation (i.e. to make it full intrinsic Lorentz transformation) in our universe, we must transform the intrinsic spacetime coordinates of the positive time-universe in the second equation into the intrinsic spacetime coordinates of our universe. As derived in part one of this paper [3], we must let $\phi\tilde{x}^{0\prime} \to \phi c\phi\tilde{t}'$, $\phi\tilde{x}^0 \to \phi c\phi\tilde{t}$ and $\phi c\phi\tilde{t}^0 \to \phi\tilde{x}$ in the second equation of system (11), thereby converting system (11) to the following

$$\left.\begin{array}{rcl} \phi\tilde{x}' & = & \phi\tilde{x} \sec\phi\psi^+_x - \phi c\phi\tilde{t} \sec\phi\psi^+_t \sin\phi\psi^-_t; \\ & & (\text{w.r.t } 3 - \text{observer in } \tilde{\Sigma}); \\ \phi c\phi\tilde{t}' & = & \phi c\phi\tilde{t} \sec\phi\psi^+_t - \sec\phi\psi^+_x \sin\phi\psi^-_x; \\ & & (\text{w.r.t } 1 - \text{observer in } c\tilde{t}) \end{array}\right\}. \qquad (12)$$

Fig. 5b cannot serve the role of a complementary diagram to Fig. 5a because it contains spacetime and intrinsic spacetime coordinates of the positive time-universe and negative time-universe that are elusive to observers in our universe and negative universe. This has been discussed for Figs. 10a and 10b of [3]. In order to make Fig. 5b a valid complementary diagram to Fig. 5a, the spacetime/intrinsic spacetime coordinates of the positive and negative time-universes in it must be transformed into those of our universe and the negative universe, as done between Fig. 10b and Fig. 11a of [3], to have Fig. 5c.

Fig. 5c containing spacetime/intrinsic spacetime coordinates of the positive (or our) universe and negative universe (obtained from Fig. 5b) is now a valid complementary diagram to Fig. 5a for the purpose of deriving the ϕLT/LT in our universe and negative universe. Observe that the 3-observers in the Euclidean 3-spaces $\tilde{\Sigma}^0$ and $-\tilde{\Sigma}^{0*}$ of the positive and negative time-universes in Fig. 5b have transformed into 1-observers in the time dimensions $c\tilde{t}$ and $-c\tilde{t}^*$ of our universe and the negative universe in Fig. 5c.

The second equation of system (12) has been derived from Fig. 5c with respect to the 1-observer in the time dimension $c\tilde{t}$

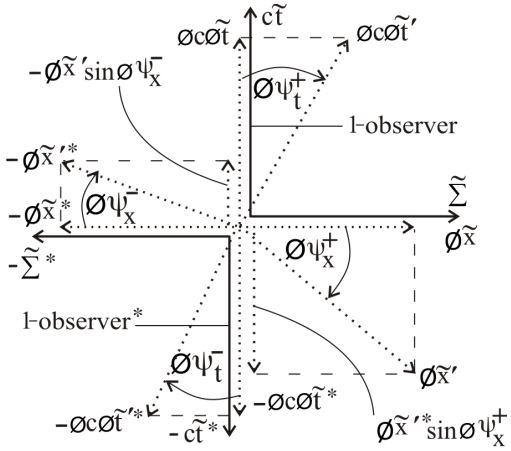

Fig. 5: (c) Complementary diagram to Fig. 5a obtained by transforming the spacetime/intrinsic spacetime coordinates of the positive time-universe and the negative time-universe in Fig. 5b into the spacetime/intrinsic spacetime coordinates of our universe and the negative universe.

in that diagram. It is a valid complementary partial intrinsic spacetime transformation to the first equation of system (12) or to Eq. (10) derived with respect to 3-observer in the Euclidean 3-space $\tilde{\Sigma}$ from Fig. 5a. Thus system (12) is the complete intrinsic Lorentz transformation derivable from Figs. 5a and 5c with respect to 3-observer in $\tilde{\Sigma}$ and 1-observer in $c\tilde{t}$.

By using the definitions given earlier namely,

$$\begin{aligned}
\sin\phi\psi_x^+ &= \sin\phi\psi_{t^0}^+ = \phi v_{x^+}/\phi c;\\
\sin\phi\psi_x^- &= \sin\phi\psi_{t^0}^- = \phi v_{x^-}/\phi c;\\
\sin\phi\psi_{x^0}^+ &= \sin\phi\psi_t^+ = \phi v_{t^+}/\phi c \ \text{ and}\\
\sin\phi\psi_{x^0}^- &= \sin\phi\psi_t^- = \phi v_{t^-}/\phi c;
\end{aligned}$$

system (12) is given explicitly in terms of intrinsic speeds as follows:

$$\left.\begin{aligned}
\phi\tilde{x}' &= \left(1-\frac{\phi v_{x^+}^2}{\phi c^2}\right)^{-\frac{1}{2}}\phi\tilde{x}-\\
&\quad -\left(1-\frac{\phi v_{t^+}^2}{\phi c^2}\right)^{-\frac{1}{2}}(\phi v_{t^-})\phi\tilde{t};\\
&\quad (\text{w.r.t. } 3-\text{observer in } \tilde{\Sigma})\\
\phi\tilde{t}' &= \left(1-\frac{\phi v_{t^+}^2}{\phi c^2}\right)^{-\frac{1}{2}}\phi\tilde{t}-\\
&\quad -\left(1-\frac{\phi v_{x^+}^2}{\phi c^2}\right)^{-\frac{1}{2}}\frac{\phi v_{x^-}}{\phi c^2}\phi\tilde{x};\\
&\quad (\text{w.r.t. } 1-\text{observer in } c\tilde{t})
\end{aligned}\right\} \qquad (13)$$

The outward manifestation on the flat four-dimensional spacetime of systems (12) and (13) are given respectively as follows:

$$\left.\begin{aligned}
\tilde{x}' &= \tilde{x}\sec\psi_x^+ - c\tilde{t}\sec\psi_t^+\sin\psi_t^-;\\
&\quad \tilde{y}'=\tilde{y};\ \tilde{z}'=\tilde{z};\\
&\quad (\text{w.r.t } 3-\text{observer in } \tilde{\Sigma});\\
c\tilde{t}' &= c\tilde{t}\sec\psi_t^+ - \tilde{x}\sec\psi_x^+\sin\psi_x^-;\\
&\quad (\text{w.r.t } 1-\text{observer in } c\tilde{t})
\end{aligned}\right\} \qquad (14)$$

and

$$\left.\begin{aligned}
\tilde{x}' &= \left(1-\frac{v_{x^+}^2}{c^2}\right)^{-\frac{1}{2}}\tilde{x}-\left(1-\frac{v_{t^+}^2}{c^2}\right)^{-\frac{1}{2}}(v_{t^-})\tilde{t};\\
&\quad \tilde{y}'=\tilde{y};\ \tilde{z}'=\tilde{z};\\
&\quad (\text{w.r.t. } 3-\text{observer in } \tilde{\Sigma})\\
\tilde{t}' &= \left(1-\frac{v_{t^+}^2}{c^2}\right)^{-\frac{1}{2}}\tilde{t}-\left(1-\frac{v_{x^+}^2}{c^2}\right)^{-\frac{1}{2}}\frac{v_{x^-}}{c^2}\tilde{x};\\
&\quad (\text{w.r.t. } 1-\text{observer in } c\tilde{t})
\end{aligned}\right\}. \qquad (15)$$

As can be easily shown, system (12) or (13) contradicts (or does not lead to) intrinsic Lorentz invariance (ϕLI) for $\phi\psi_x^+ \neq \phi\psi_x^- \neq \phi\psi_t^+ \neq \phi\psi_t^-$ (or for $\phi v_{x^+} \neq \phi v_{x^-} \neq \phi v_{t^+} \neq \phi v_{t^-}$). System (14) or (15) likewise does not lead to Lorentz invariance (LI) for $\psi_x^+ \neq \psi_x^- \neq \psi_t^+ \neq \psi_t^-$ (or $v_{x^+} \neq v_{x^-} \neq v_{t^+} \neq v_{t^-}$). Even if only one of the four intrinsic angles $\phi\psi_x^+$, $\phi\psi_x^-$, $\phi\psi_t^+$ and $\phi\psi_t^-$ is different from the rest (or if only one of the four intrinsic speeds ϕv_{x^+}, ϕv_{x^-}, ϕv_{t^+} and ϕv_{t^-} is different from the rest), system (12) or (13) still contradicts ϕLI. And even if only one of the four angles ψ_x^+, ψ_x^-, ψ_t^+ and ψ_t^- is different from the rest (or if only one of the four speeds v_{x^+}, v_{x^-}, v_{t^+} and v_{t^-} is different from the rest), system (14) or (15) still contradicts the LI.

The assumption made initially that members of a quartet of symmetry-partner particles or objects in the four universes

are in non-symmetrical relative motions in their universes, which gives rise to Fig. 5a-c, has led to the non-validity of intrinsic Lorentz invariance in intrinsic special relativity (ϕSR) and of Lorentz invariance in special relativity (SR) in our universe and indeed in the four universes. This invalidates the initial assumption, since Lorentz invariance is immutable on the flat four-dimensional spacetime of the special theory of relativity. The conclusion then is that all the four members of every quartet of symmetry-partner particles or objects in the four universes are in identical (or symmetrical) relative motions at all times.

Having shown that the members of every quartet of symmetry-partner particles or objects in the four universes have identical magnitudes of masses, identical shapes and identical sizes, (in so far as the prescribed identical magnitudes of masses, identical shapes and identical sizes of symmetry-partner particles or objets in the positive (or our) universe and the negative universe is valid), in the preceding sub-section and that they are involved in identical relative motions at all times in this sub-section, the perfect symmetry of state among the four universes has been demonstrated. Although gravity is being assumed to be absent in this and the previous papers [1-3], it is interesting to note that gravitational field sources of identical magnitudes of masses, identical sizes and identical shapes, which hence give rise to identical gravitational fields, are located at symmetry-partner positions in spacetimes in the four universes.

3 Summary and conclusion

This section is for the two parts of the initial paper [1] and [2], this paper and its first part [3]. The co-existence in nature of four symmetrical universes identified as positive (or our) universe, negative universe, positive time-universe and negative time-universe in different spacetime/intrinsic spacetime domains, have been exposed in these papers. The four universes exhibit perfect symmetry of natural laws and perfect symmetry of state. This implies that natural laws take on identical forms in the four universes and that all members of every quartet of symmetry-partner particles or objects in the four universes have identical magnitudes of masses, identical shapes and identical sizes and that they are involved in identical relative motions in their universes at all times, as demonstrated. The four universes constitute a four-world background to the special theory of relativity in each universe.

The flat two-dimensional intrinsic spacetime of the intrinsic special theory of relativity (ϕSR), containing one-dimensional intrinsic masses of particles and objects in one-dimensional intrinsic space, which underlies the flat four-dimensional spacetime of the special theory of relativity (SR) containing three-dimensional masses of particles and objects in Euclidean 3-space in each universe, introduced (as *ansatz* in the first paper [1], is isolated in this fourth paper. The two-dimensional intrinsic spacetime is indispensable in special relativity/intrinsic special relativity (SR/ϕSR) in the four-world picture, because the new set of spacetime/intrinsic spacetime diagrams for deriving Lorentz transformation/intrinsic Lorentz transformation (LT/ϕLT) and their inverses in the four-world picture, involve relative rotations of intrinsic spacetime coordinates of two frames in relative motion.

The LT/ϕLT and their inverses are derived from a new set of spacetime/intrinsic spacetime diagrams on the combined spacetimes/intrinsic spacetimes of the positive (or our) universe and the negative universe as one pair of universes and on combined spacetimes/intrinsic spacetimes of the positive time-universe and the negative time-universe as another pair of universes. The two pairs of spacetimes/intrinsic spacetimes co-exist in nature, consequently the spacetime/intrinsic spacetime diagram drawn on one pair co-exists with and must complement the spacetime/intrinsic spacetime diagram drawn on the other pair in deriving the LT/ϕLT and their inverses (with a set of four diagrams in all) in each universe, as done in the first paper [1] and validated formally in the third paper [3].

The proper (or classical) Euclidean 3-space $\Sigma^{0\prime}$ of the positive time-universe with respect to 3-observers in it, is what appears as the proper time dimension ct' of the positive (or our) universe relative to 3-observers in the proper Euclidean 3-space Σ' of our universe and the proper Euclidean 3-space Σ' of the positive (or our) universe with respect to 3-observers in it, is what appears as the proper time dimension $ct^{0\prime}$ of the positive time-universe relative to 3-observers in the proper Euclidean 3-space $\Sigma^{0\prime}$ of the positive time-universe. The proper Euclidean 3-space $-\Sigma^{0\prime *}$ of the negative time-universe is likewise the proper time dimension $-ct'^{*}$ of the negative universe and the proper Euclidean 3-space $-\Sigma'^{*}$ of the negative universe is the proper time dimension $-ct^{0\prime *}$ of the negative time-universe. The important revelation in this is that time is not a fundamental (or "created") concept, but a secondary concept that evolved from the concept of space. Time dimension does not exist in an absolute sense, as does 3-space, but in a relative sense.

The positive time-universe cannot be perceived better than the time dimension ct' of the positive (or our) universe by 3-observers in the Euclidean 3-space Σ' of our universe and the negative time-universe cannot be perceived better than the time dimension $-ct'^{*}$ of the negative universe by 3-observers in the Euclidean 3-space $-\Sigma'^{*}$ of the negative universe. Conversely, the positive (or our) universe cannot be perceived better than the time dimension $ct^{0\prime}$ of the positive time-universe by 3-observers in the Euclidean 3-space $\Sigma^{0\prime}$ of the positive time-universe and the negative universe cannot be perceived better than the time dimension $-ct^{0\prime *}$ of the negative time-universe by 3-observers in the Euclidean 3-space $-\Sigma^{0\prime *}$ of the negative time-universe. It can thus be said that the positive time-universe and the negative time-universe are imperceptibly hidden in the time dimensions of the positive (or our) universe and the negative universe respectively rela-

tive to 3-observers in the Euclidean 3-spaces in our universe and the negative universe and conversely.

Physicists in our (or positive) universe and negative universe can formulate special relativity and special-relativistic physics in general in terms of the spacetime/intrinsic spacetime dimensions (or coordinates) and physical parameters/intrinsic parameters of our universe and the negative universe only. Physicists in the positive time-universe and the negative time-universe can likewise formulate special relativity and special-relativistic physics in general in terms of the spacetime/intrinsic spacetime dimensions (or coordinates) and parameters/intrinsic parameters of the positive and the negative time-universes only. It is to this extent that it can still be said that special relativity and special-relativistic physics in general, pertain to a two-world background, knowing that the two-world picture actually encompasses four universes; two of them being imperceptibly hidden in the time dimensions.

Experimental validation ultimately of the co-existence in nature of four symmetrical universes will give a second testimony to their isolation theoretically in these papers. The next natural step is to investigate the possibility of subsuming the theory of relativistic gravity into the four-world picture.

Acknowledgements

Grateful acknowledgement is made to Dr. Ibukun Omotehinse and Mr. Cyril Ugwu for fully bearing the costs of publication of this and the the previous three papers.

Submitted on February 27, 2010 / Accepted on March 01, 2010

References

1. Adekugbe A. O. J. Two-world background of special relativity. Part I. *Progress in Physics*, 2010, v. 1, 30–48.
2. Adekugbe A. O. J. Two-world background of special relativity. Part II. *Progress in Physics*, 2010, v. 1, 49–61.
3. Adekugbe A. O. J. Re-identification of the many-world background of special relativity as four-world background. Part I. *Progress in Physics*, 2011, v. 1, 3–24.

Missing Measurements of Weak-Field Gravity

Richard J. Benish

Eugene, Oregon, USA. E-mail: rjbenish@teleport.com

For practical and historical reasons, most of what we know about gravity is based on observations made or experiments conducted *beyond the surfaces* of dominant massive bodies. Although the *force* of gravity inside a massive body can sometimes be measured, it remains to demonstrate the *motion* that would be caused by that force through the body's center. Since the idea of doing so has often been discussed as a thought experiment, we here look into the possibility of turning this into a real experiment. Feasibility is established by considering examples of similar experiments whose techniques could be utilized for the present one.

1 Introduction

A recent paper in this journal (M. Michelini [1]) concerned the absence of measurements of Newton's constant, G, within a particular range of vacuum pressures. Important as it may be to investigate the physical reasons for this, a gap of equal, if not greater importance concerns the absence of gravity experiments that probe the *motion* of test objects through the centers of larger massive bodies. As is the case for most measurements of G, the apparatus for the present experimental idea is also a variation of a torsion balance. Before describing the modifications needed so that a torsion balance can measure through-the-center motion, let's consider the context in which we find this gap in experimentation.

Often found in undergraduate physics texts [2–5] is the following problem, discussed in terms of Newtonian gravity: A test object is dropped into an evacuated hole spanning a diameter of an otherwise uniformly dense spherical mass. One of the reasons this problem is so common is that the answer, the predicted equation of motion of the test object, is yet another instance of *simple harmonic motion*. What is rarely pointed out, however, is that we presently lack direct empirical evidence to verify the theoretical prediction. Confidence in the prediction is primarily based on the success of Newton's theory for phenomena that test the *exterior* solution. Extrapolating Newton's law to the interior is a worthwhile mathematical excercise. But a theoretical extrapolation is of lesser value than an empirical fact.

Essentially the same prediction follows from general relativity [6–9]. In this context too, the impression is sometimes given that the predicted effect is a physical fact. A noteworthy example is found in John A. Wheeler's book, *"A Journey into Gravity and Spacetime"*, in which he refers to the phenomenon as "boomeranging". Wheeler devotes a whole (10-page) chapter to the subject because, as he writes, "Few examples of gravity at work are easier to understand in Newtonian terms than boomeranging. Nor do I know any easier doorway to Einstein's concept of gravity as manifestation of spacetime curvature" [10]. But nowhere in Wheeler's book is there any discussion of *empirical evidence* for "boomeranging". No doubt, Newton, Einstein and Wheeler would all have been delighted to see the simple harmonic motion demonstrated as a laboratory experiment.

2 Feasibility

Since the predicted effect has never been observed at all, our initial goal should simply be to ascertain that the oscillation prediction is a correct approximation. After laying out a basic strategy for doing the experiment, this paper concludes with a few additional remarks concerning motivation.

Apparatus that would have sufficed for our purpose were considered in the 1960s–1970s to measure G. Y. T. Chen discusses these through-the-center oscillation devices in his 1988 review paper on G measurements [11]. Each example in this group of proposals was intended for space-borne satellite laboratories. The original motivation for these ideas was to devise ways to improve the accuracy of our knowledge of G by timing the oscillation period of the simple harmonic motion. Though having some advantages over Earth-based G measurements, they also had drawbacks which ultimately prohibited them from ever being carried out.

What distinguishes these proposals from experiments that have actually been carried out in Earth-based laboratories is that the test objects were to be allowed to fall freely back and forth between extremities inside a source mass the whole time. Whereas G measurements conducted on Earth typically involve restricting the test mass's movement and measuring the force needed to do so. The most common, and historically original, method for doing this is to use a torsion balance in which a fiber provides a predetermined resistance to rotation. Torsion balances have also been used to test Einstein's Equivalence Principle (e.g. Gundlach et al. [12]). Another distinguishing characteristic of Earth-based G measurements and Equivalence Principle tests is that the test masses typically remain outside the larger source masses. Since movement of the test masses is restricted to a small range of motion, these tests can be characterized as static measurements. Torsion balance experiments in which the test mass is inside the source mass have also been performed (for example, Spero

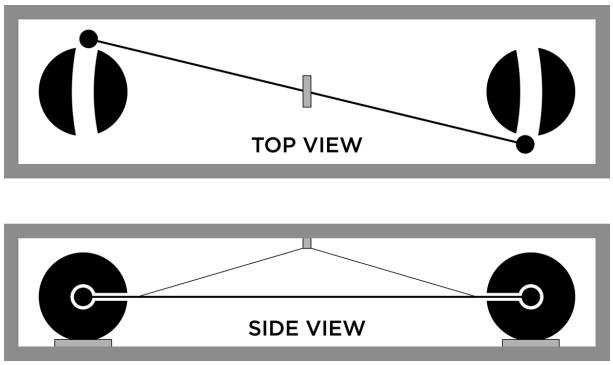

Fig. 1: Schematic of modified Cavendish balance. Since the idea is to demonstrate the simple harmonic motion only as a first approximation, deviation due to the slight arc in the trajectory is inconsequential.

et al. [13] and Hoskins et al. [14]). These latter experiments were tests of the inverse square law.

All three of these types of experiments — G measurements, Equivalence Principle and inverse-square law tests — however, are *static* measurements in the sense that the test masses were not free to move beyond a small distance compared to the size of the source mass. The key innovation in the present proposal is that we want to see an object fall radially as long as it will; we want to eliminate (ideally) or minimize (practically) any obstacle to the radial free-fall trajectory. Space-based experiments would clearly be the optimal way to achieve this. But a reasonably close approximation can be achieved with a modified Cavendish balance in an Earth-based laboratory.

As implied above, the key is to design a suspension system which, instead of providing a restoring force that prevents the test masses from moving very far, allows unrestricted or nearly unrestricted movement. Two available possibilities are fluid suspensions and magnetic suspensions (or a combination of these). In 1976 Faller and Koldewyn succeeded in using a magnetic suspension system to get a G measurement [15, 16]. The experiment's accuracy was not an improvement over that gotten by other methods, but was within 1.5% of the standard value.

As Michelini pointed out in his missing vacuum range discussion, in most G measurements the source masses are located outside an enclosure. Even in the apparatus Cavendish used for his original G measurement at atmospheric pressure, the torsion arm and test masses were isolated from the source masses by a wooden box. In Faller and Koldewyn's experiment the arm was isolated from the source masses by a vacuum chamber. The modified design requires that there be no such isolation, as the arm needs to swing freely through the center of the source masses (see Fig. 1). Given the modest goal of the present proposal, it is reasonable to expect that the technology used by Faller and Koldewyn could be adapted to test the oscillation prediction. Moreover, it seems reasonable to expect that advances in technology since 1976 (e.g. better magnets, better electronics, etc.), would make the experiment quite doable for an institution grade physics laboratory.

3 Motivation: Completeness and Aesthetics

One hardly needs to mention the many successes of Newtonian gravity. By success we mean, of course, that empirical observations match the theoretical predictions. Einsteinian gravity is even more successful. The purpose of many contemporary gravity experiments is to detect physical manifestations of the differences between Newton's and Einstein's theories. In every case Einstein's theory has proven to be more accurate. This is impressive. Given the level of thoroughness and sophistication in gravity experimentation these days, one may be taken aback to realize that Newton's and Einstein's theories *both remain untested* with regard to the problem discussed above. The simple harmonic motion prediction is so common and so obvious that we have come to take it for granted. When discussing the *prediction* for this basic experiment in weak field gravity, it would surely be more satisfactory if we could at the same time cite the *physical evidence*.

The Newtonian explanation for the predicted harmonic motion is that a massive sphere produces a force (or potential) of gravitational attraction. The corresponding general relativistic explanation is that the curvature of spacetime causes the motion. Specifically, the predicted effect is due to the slowing of clock rates toward the center of the sphere. A physical demonstration of the effect would thus indirectly, though convincingly, support general relativity's prediction that the rate of a clock at the body's center is a local minimum — a prediction that has otherwise not yet been confirmed.

In summary, if R represents the surface of a spherical mass, our empirical knowledge of how things move because of the mass within R is essentially confined to the region, $r \gtrsim R$. The region $0 \leq r \lesssim R$ is a rather fundamental and a rather large gap. It is clearly the most ponderable part of the domain. Why not fill this gap?

One of the distinctive features of the kind of experiment proposed above is that its result is, in principle, independent of size. The satellite versions mentioned by Chen were thus referred to as "clock mode" experiments. The determining factor in the oscillation period is the density of the source mass. If the source mass is made of lead (density, $\rho \approx 11,000$ kg/m^3) the oscillation period is about one hour. Would it not be fascinating to observe for an hour, to watch the oscillation take place, knowing that the mass of the larger body is the essential thing making it happen? In my opinion this would be a beautiful sight. Beautiful for completing the domain, $0 \leq r \lesssim R$, and beautiful simply to see what no human being has seen before.

Submitted on September 09, 2010 / Accepted on September 15, 2010

References

1. Michelini M. The Missing Measurements of the Gravitational Constant. *Progress in Physics*, 2009, v. 3, 64–68.
2. Halliday D., Resnick R., Walker J. Fundamentals of Physics. Wiley, New York, 1993.
3. Valens E. G. The Attractive Universe: Gravity and the Shape of Space. World, Cleveland, 1969.
4. Tipler P. A. Physics. Worth, New York, 1982.
5. French A. P. Newtonian Mechanics. Norton, New York, 1971.
6. Misner C. W., Thorne K. and Wheeler J. A. Gravitation. W. H. Freeman, San Francisco, 1973.
7. Tangherlini F. R. An Introduction to the General Theory of Relativity. *Nuovo Cimento Supplement*, 1966, v. 20, 1–86.
8. Epstein L. C. Relativity Visualized. Insight, San Francisco, 1988, pp. 157–158.
9. Taylor N. W. Note on the Harmonic Oscillator in General Relativity. *Australian Journal of Mathematics*, 1961, v. 2, 206–208.
10. Wheeler J. A. A Journey Into Gravity and Spacetime. Scientific American Library, New York, 1990.
11. Chen Y. T. The Measurement of the Gravitational Constant. *International Symposium on Experimental Gravitational Physics*, edited by Michelson P. F., Enke H., Pizzella G. World Scientific, Singapore, 1988, pp. 90–109.
12. Gundlach J. H., Smith G. L., Adelberger E. G., Heckel B. R., Swanson H. E. Short-Range Test of the Equivalence Principle. *Physical Review Letters*, 1997, v. 78, 2523–2526.
13. Spero R. E., Hoskins J. K., Newman R., Pellam J., Schultz J. Test of the Gravitational Inverse-Square Law at Laboratory Distances. *Physical Review Letters*, 1980, v. 44, 1645–1648.
14. Hoskins J. K., Newman R. D., Spero R. E., Schultz J. Experimental tests of the gravitational inverse-square law for mass separations from 2 to 105 cm. *Physical Review D*, 1985, v. 32, 3084–3095.
15. Koldewyn W. A. A New Method for Measuring the Newtonian Gravitational Constant, G. PhD thesis, Wesleyan University, 1976.
16. Faller J. E. A Prototype Measurement of the Newtonian Gravitational Constant Using an Active Magnetic Suspension Torsion Fiber. *Proceedings of the 1983 International School and Symposium on Precision Measurement and Gravity Experiment*, edited by Wei-Tou N., National Tsing Hua University, Hsinchu, Taiwan, 1983, pp. 541–556.

Experimental Investigation of the Fresnel Drag Effect in RF Coaxial Cables

Reginald T. Cahill* and David Brotherton†

*School of Chemical and Physical Sciences, Flinders University, Adelaide 5001, Australia.
E-mail: Reg.Cahill@flinders.edu.au

†Geola Technologies Ltd, Sussex Innovation Centre, Science Park Square, Falmer, East Sussex, BN1 9SB, United Kingdom.
E-mail: dbr@geola.co.uk

An experiment that confirms the Fresnel drag formalism in RF coaxial cables is reported. The Fresnel 'drag' in bulk dielectrics and in optical fibers has previously been well established. An explanation for this formalism is given, and it is shown that there is no actual drag phenomenon, rather that the Fresnel drag effect is merely the consequence of a simplified description of EM scattering within a dielectric in motion wrt the dynamical 3-space. The Fresnel drag effect plays a critical role in the design of various light-speed anisotropy detectors.

1 Introduction

In 2002 it was discovered that the Michelson-Morley 1887 light-speed anisotropy experiment [1], using the interferometer in gas mode, had indeed detected anisotropy, by taking account of both a physical Lorentz length contraction effect for the interferometer arms, and the refractive index effect of the air in the light paths [2, 3]. The observed fringe shifts corresponded to an anisotropy speed in excess of 300 km/s. While confirmed by numerous later experiments, particularly that of Miller [4], see [6] for an overview, the most accurate analysis used the Doppler shifts from spacecraft earth-flybys [5, 6], which gave the solar-system a galactic average speed through 3-space of 486 km/s in the direction $RA = 4.29^h$, $Dec = -75.0°$, a direction within 5° of that found by Miller in his 1925/26 gas-mode Michelson interferometer experiment*. In vacuum mode a Michelson interferometer cannot detect the anisotropy, nor its turbulence effects, as shown by the experiments in [7–12], actually using resonant orthogonal cavities. These experiments show, overall, the difference between Lorentzian Relativity (LR) and Special Relativity (SR). In LR the length contraction effect is caused by motion of a rod, say, through the dynamical 3-space, whereas in SR the length contraction is only a perspective effect, occurring only when the rod is moving relative to an observer. This was further clarified when an exact mapping between Galilean space and time coordinates and the Minkowski-Einstein spacetime coordinates was recently discovered [13]. This demonstrates that the SR time dilation and space contraction effects are merely the result of using an unphysical choice of space and time coordinates that, by construction, makes the speed of light in vacuum an invariant, but only wrt to that choice of coordinates. Such a contrived invariance has no connection with whether light speed anisotropy is detectable or not — that is to be determined by experiments.

*This speed and direction is very different to the CMB speed and direction — which is an unrelated phenomenon.

The detection of light speed anisotropy — revealing a flow of space past the detector, is now entering an era of precision measurements. These are particularly important because experiments have shown large turbulence effects in the flow, and are beginning to characterise this turbulence. Such turbulence can be shown to correspond to what are, conventionally, known as gravitational waves, although not those implied by General Relativity, as they are much larger than these [14–16].

The detection and characterisation of these wave/ turbulence effects requires the development of small and cheap detectors, such as optical fiber Michelson interferometers [18]. However in all detectors the EM signals travel through a dielectric, either in bulk or optical fiber or through RF coaxial cables. For this reason it is important to understand the so-called Fresnel drag effect. In optical fibers the Fresnel drag effect has been established [17]. This is important in the operation of Sagnac optical fiber gyroscopes, for then the calibration is independent of the fiber refractive index. The Fresnel drag speed is a phenomenological formalism that characterises the effect of the absolute motion of the propagation medium upon the speed of the EM radiation within that medium.

The Fresnel drag expression is that a dielectric in absolute motion through space at speed v causes the EM radiation to travel at speed

$$V(v) = \frac{c}{n} + v\left(1 - \frac{1}{n^2}\right) \qquad (1)$$

wrt the dielectric, when V and v have the same direction. Here n is the dielectric refractive index. The 2nd term is known as the Fresnel drag, appearing to show that the moving dielectric "drags" the EM radiation, although below we show that this is a misleading interpretation. That something unusual was happening followed from the discovery of stellar aberration by Bradley in 1725. Here the direction of the telescope must be varied over a year when observing a given star. This is caused by the earth's orbital speed of 30 km/s. Then Airy

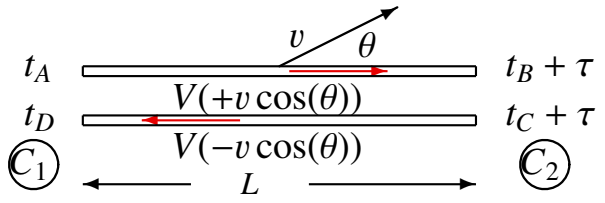

Fig. 1: Schematic layout for measuring the one-way speed of light in either free-space, optical fibers or RF coaxial cables, without requiring the synchronisation of the clocks C_1 and C_2. Here τ is the unknown offset time between the clocks, and $t_A, t_B + \tau, t_C + \tau, t_D$ are the observed clock times, while t_B, t_C are, *a priori*, unknown true times. V is the light speed in (1), and v is the speed of the apparatus through space, in direction θ.

in 1871 demonstrated that the same aberration angle occurs even when the telescope is filled with water. This effect is explained by the Fresnel expression in (1), which was also confirmed by the Fizeau experiment in 1851, who used two beams of light travelling through two tubes filled with flowing water, with one beam flowing in the direction of the water, and the other counterflowing. Interferometric means permitted the measurement of the travel time difference between the two beams, confirming (1), with v the speed of the water flow relative to the apparatus. This arrangement cannot detect the absolute motion of the solar system, as this contribution to the travel time difference cancels because of the geometry of the apparatus.

There have been various spurious "derivations" of (1), some attempting to construct a physical "drag" mechanism, while another uses the SR addition formula for speeds. However that well-known addition formula is merely a mathematical manifestation of using the unphysical Minkowski-Einstein coordinates noted above, and so is nothing but a coordinate effect, unrelated to experiment. Below we give a simple heuristic derivation which shows that there is no actual "drag" phenomenon. But first we show the unusual consequences of (1) in one-way speed of EM radiation experiments. It also plays a role in 2nd order v/c experiments, such as the optical-fiber Michelson interferometer [18].

2 One-way Speed of Light Anisotropy Measurements

Fig.1 shows the arrangement for measuring the one-way speed of light, either in vacuum, a dielectric, or RF coaxial cable. It is usually argued that one-way speed of light measurements are not possible because the clocks cannot be synchronised. Here we show that this is false, and at the same time show an important consequence of (1). In the upper part of Fig.1 the actual travel time t_{AB} from A to B is determined by

$$V(v\cos(\theta))t_{AB} = |\mathbf{L}'| \qquad (2)$$

where $|\mathbf{L}'| = |\mathbf{L} + \mathbf{v}t_{AB}| \approx L + v\cos(\theta)t_{AB} + ..$ is the actual distance travelled, at speed $V(v\cos(\theta))$, using $vt_{AB} \ll L$, giving

$$V(v\cos(\theta))t_{AB} = L + v\cos(\theta)t_{AB} + ... \qquad (3)$$

where the 2nd term comes from, approximately, the end B moving an additional distance $v\cos(\theta)t_{AB}$ during the true time interval t_{AB}. This gives

$$t_{AB} \approx \frac{L}{V(v\cos(\theta)) - v\cos(\theta)} = \frac{nL}{c} + \frac{v\cos(\theta)L}{c^2} + .. \qquad (4)$$

on using (1) and expanding to 1st oder in v/c. If we ignore the Fresnel drag term in (1) we obtain, instead,

$$t_{AB} \approx \frac{L}{c/n - v\cos(\theta)} = \frac{nL}{c} + \frac{n^2 v\cos(\theta)L}{c^2} + .. \qquad (5)$$

The 1st important observation is that the v/c component in (4) is independent of the dielectric refractive index n. This is explained in the next section. If the clocks were synchronised t_{AB} would be known, and by changing direction of the light path, that is varying θ, the magnitude of the 2nd term may be separated from the magnitude of the 1st term. If the clocks are not synchronised, then the measured travel time $\bar{t}_{AB} = (t_B + \tau) - t_A = t_{AB} + \tau$, where τ is the unknown, but fixed, offset between the two clocks. But this does not change the above argument. The magnitude of v and the direction of v can be determined by varying θ. For a small detector the change in θ can be achieved by a direct rotation. But for a large detector, such as De Witte's [19] 1.5 km RF coaxial cable experiment, the rotation was achieved by that of the earth. The reason for using opposing propagation directions, as in Fig.1, and then measuring travel time differences, is that local temperature effects cancel. This is because a common temperature change in the two adjacent cables changes the speed to the same extent, whereas absolute motion effects cause opposite signed speed changes. Then the temperature effects cancel on measuring differences in the travel times, whereas absolute motion effects are additive. Finally, after the absolute motion velocity has been determined, the two spatially separated clocks may be synchronised.

That the v/c term in t_{AB} in (4) is independent of n means that various techniques to do a 1st order in v/c experiment that involves using two dielectrics with different values of n fail. One such experiment was by Trimmer et al [20], who used a triangular interferometer, with the light path split into one beam passing through vacuum, and the other passing through glass. No 1st order effect was seen. This is because the v-dependent travel times through the glass, and corresponding vacuum distance, have the same value to 1st order in v/c. On realising this Trimmer et al. subsequently withdrew their paper, see reference [21]. Cahill [22] performed a dual optical-fiber/RF coaxial cable experiment that was supposedly 1st order in v/c. If the Fresnel drag formalism applies to both optical fibers and RF coaxial cables, then again there could not

have been any v/c signal in that experiment, and the observed effects must have been induced by temperature effects. All this implies that because of the Fresnel drag effect it appears not possible to perform a v/c experiment using one clock — rather two must be used, as in Fig.1. This, as noted above, does not require clock synchronisation, but it does require clocks that very stable. To use one "clock" appears then to require 2nd order in v/c detectors, but then the effect is some 1000 times smaller, and requires interferometric methods to measure the very small travel time differences, as in gas-mode and optical-fiber Michelson interferometers. It is indeed fortuitous that the early experiments by Michelson and Morley, and by Miller, were in gas mode, but not by design.

The Krisher optical fiber 1st order v/c experiment [23] measured the phase differences ϕ_1 and ϕ_2 between the two signals travelling in different directions through very long optical fibers, rather than the travel time variations, as the earth rotated. This involves two phase comparators, with one at each end of the fibers. However the phases always have a multiple of 2π phase ambiguity, and in the Krisher experiment this was overlooked. However the timing of the maxima/minima permitted the Right Ascension (RA) of the direction of v to be determined, as the direction of propagation is changed by rotation, and the result agreed with that found by Miller; see [6] for plots of the Krisher data plotted against local sidereal times.

3 Deriving the Fresnel Drag Formalism

Here we give a heuristic derivation of the Fresnel drag speed formalism in a moving dielectric, with the dielectric modeled by random geometrical-optics paths, see Fig.2. These may be thought of as modelling EM wave scatterings, and their associated time delays. The slab of dielectric has length L and travels through space with velocity $\mathbf{v}$, and with EM radiation traveling, overall, from A to B. The top of Fig.2 shows the microscopic heuristic model of propagation through the dielectric with EM radiation traveling at speed c wrt space between scattering events, being scattered from random sites — atoms, moving through space with velocity $\mathbf{v}$. The bottom of Fig.2 shows the macroscopic description with EM radiation effectively traveling in a straight line directly from A to B, with effective linear speed $V(v\cos(\theta))$, and with the dielectric now described by a refractive index n.

The key insight is that when a dielectric has absolute velocity $\mathbf{v}$ through space, the EM radiation travels at speed c wrt space, between two scattering events within the dielectric. Consider a straight line propagation between scattering events e and f, with angle ϕ to $\mathbf{v}$, see Fig.2. Consider the paths from the rest frame of the space. The EM wave must travel to a point in space f', and then the distance travelled dl', at speed c, is determined by the vector sum $\mathbf{dl}' = \mathbf{dl} + \mathbf{v}dt$, with dl the distance between scattering points e and f, defined in the rest frame of the matter, and $\mathbf{v}dt$ is the displacement of f

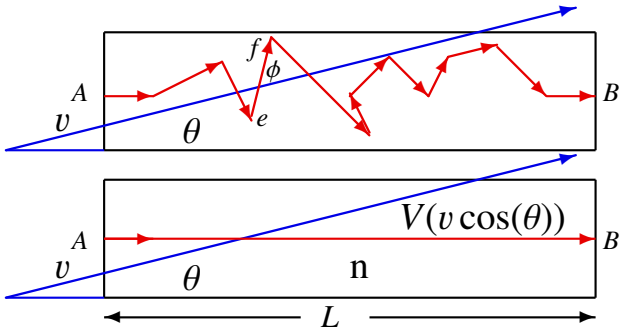

Fig. 2: Slab of dielectric, length L, traveling through space with velocity $\mathbf{v}$, and with EM radiation traveling, overall, from A to B, drawn in rest frame of slab. Top: Microscopic model showing scattering events, with free propagation at speed c relative to the space, between scattering events. Bottom: The derived macroscopic phenomenological description showing the signal travelling at speed $V(v\cos(\theta))$, as given by the Fresnel drag expression in (1). The dielectric refractive index is n.

to f', because of the absolute motion of the scattering atoms. Then the travel time to 1st order in v/c is

$$dt = \frac{dl'}{c} \approx \frac{dl}{c} + \frac{v\cos(\phi)dt}{c} + ..., \quad \text{giving} \tag{6}$$

$$dt \approx \frac{dl}{c} + \frac{vdl\cos(\phi)}{c^2} + ... = \frac{dl}{c} + \frac{\mathbf{v}\cdot\mathbf{dl}}{c^2} + ... \tag{7}$$

We ignore Lorentz length contraction of the slab as this only contributes at 2nd order in v/c. Summing over paths to get total travel time from A to B

$$\begin{aligned} t_{AB} &= \int_A^B \frac{dl}{c} + \int_A^B \frac{\mathbf{v}\cdot\mathbf{dl}}{c^2} + ... \\ &= \frac{l}{c} + \frac{Lv\cos(\theta)}{c^2} + ... \\ &= \frac{nL}{c} + \frac{Lv\cos(\theta)}{c^2} + ..., \end{aligned} \tag{8}$$

where L is the straight line distance from A to B in the matter rest frame, and $n = l/L$ defines the refractive index of the dielectric in this treatment, as when the dielectric is at rest the effective speed of EM radiation through matter in a straight line from A to B is defined to be c/n. Note that t_{AB} does not involve n in the v dependent 2nd term. This effect is actually the reason for the Fresnel drag formalism. The macroscopic treatment, which leads to the Fresnel drag formalism, involves the sum $|\mathbf{L}'| = |\mathbf{L} + \mathbf{v}t_{AB}|$, for the macrosocopic distance traveled, which gives for the travel time

$$\begin{aligned} t_{AB} &= \frac{L'}{V} \approx \frac{L}{V(v\cos(\theta))} + \frac{v\cos(\theta)t_{AB}}{V(v\cos(\theta))}, \quad \text{giving} \\ t_{AB} &= \frac{L}{V(v\cos(\theta))} + \frac{Lv\cos(\theta)}{V(v\cos(\theta))^2} + ... \end{aligned} \tag{9}$$

where $V(v\cos(\theta))$ is the effective linear speed of EM radiation in direction AB at angle θ to $\mathbf{v}$, and $v\cos(\theta)t_{AB}$ is the

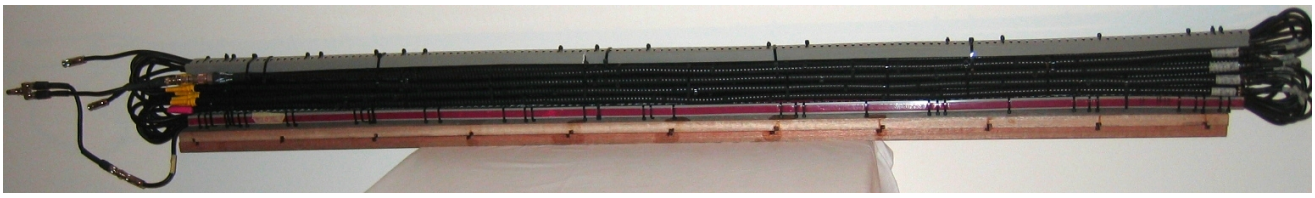

Fig. 3: Photograph of the RF coaxial cables arrangement, based upon 16×1.85 m lengths of phase stabilised Andrew HJ4-50 coaxial cable. These are joined to 16 lengths of FSJ1-50A cable, in the manner shown schematically in Fig.4. The 16 HJ4-50 coaxial cables have been tightly bound into a 4×4 array, so that the cables, locally, have the same temperature, with cables in one of the circuits embedded between cables in the 2nd circuit. This arrangement of the cables permits the cancellation of temperature effects in the cables. A similar array of the smaller diameter FSJ1-50A cables is located inside the grey-coloured conduit boxes. This arrangement has permitted the study of the Fresnel drag effect in RF coaxial cables, and revealed that the usual Fresnel drag speed expression applies.

extra distance travelled, caused by the end B moving. This form assumes that the total distance L' is travelled at speed $V(v\cos(\theta))$. This reproduces the microscopic result (8) only if $V(v) = c/n + v(1 - 1/n^2)$, which is the Fresnel drag expression. The key point is that the Fresnel drag formalism is needed to ensure, despite appearances, that the extra distance traveled due to the absolute motion of the dielectric, is travelled at speed c, and not at speed c/n, even though the propagation is within the dielectric. Hence there is no actual drag phenomenon involved, and so the nomenclature "Fresnel drag" is misleading.

However it was not clear that the same analysis applied to RF coaxial cables, because of the possible effects of the conduction electrons in the inner and outer conductors. The dual coaxial cable experiment reported herein shows that the Fresnel drag expression also applies in this case. The Fresnel drag effect is a direct consequence of the absolute motion of the slab of matter through space, with the speed of EM radiation being c wrt space itself. A more complete derivation based on the Maxwell-Hertz equations is given in Drezet [24].

4 Fresnel Drag Experiment in RF Coaxial Cables

We now come to the 1st experiment that has studied the Fresnel drag effect in RF coaxial cables. This is important for any proposed EM anisotropy experiment using RF coaxial cables. The query here is whether the presence of the conductors forming the coaxial cables affects the usual Fresnel drag expression in (1), for a coaxial cable has an inner and outer conductor, with a dielectric in between.

Fig.4 shows the schematic arrangement using two different RF coaxial cables, with two separate circuits, and Fig.3 a photograph. One measures the travel time difference of two RF signals from a Rubidium frequency standard (Rb) with a Digital Storage Oscilloscope (DSO). In each circuit the RF signal travels one-way in one type of coaxial cable, and returns via a different kind of coaxial cable. Two circuits are used so that temperature effects cancel — if a temperature change alters the speed in one type of cable, and so the travel time, that travel time change is the same in both circuits, and

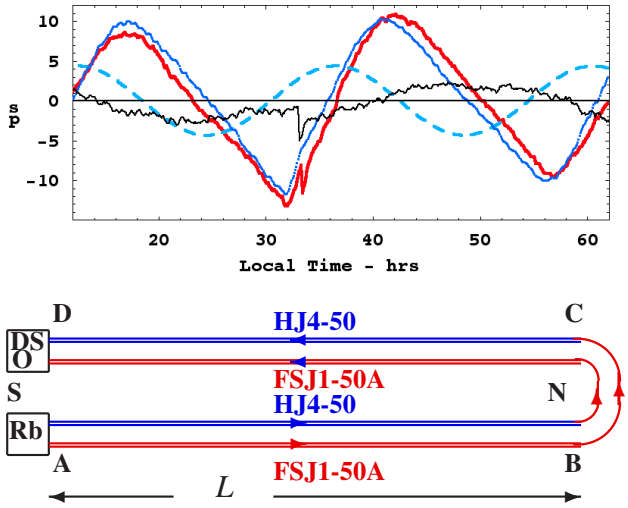

Fig. 4: Top: Data, from May17-19, 2010, from the dual RF coaxial cable experiment enabling Fresnel drag in coaxial cables to be studied: Red plot is relative 10 MHz RF travel times between the two circuits, and blue plot is temperature of the air (varying from 19 to 23°C) passing into the LeCroy DSO, scaled to fit the travel time data. The black plot is travel time differences after correcting for DSO temperature effects. The dashed plot is time variation expected using spacecraft earth-flyby Doppler shift determined velocity, if the Fresnel drag effect is absent in RF coaxial cables. Bottom: Schematic layout of the coaxial cables. This ensures two opposing circuits that enable cancellation of local temperature effects in the cables. In practice the cables are divided further, as shown in Fig.3.

cancels in the difference. Even though phase-stabilised coaxial cables are used, the temperature effects need to be cancelled in order to be able to reliably measure time differences at ps levels. To ensure cancellation of temperature effects, and also for practical convenience, the Andrew HJ4-50 cables are cut into 8×1.85 m shorter lengths in each circuit, corresponding to a net length of $L = 8\times1.85 = 14.8$ m. The curved parts of the Andrew FSJ1-50A cables contribute only at 2nd order in v/c.

To analyse the experimental data we modify the Fresnel

drag speed expression in (1) to

$$V(v) = \frac{c}{n_i} + v\left(1 - \frac{1}{m_i^2}\right) \tag{10}$$

for each cable, $i = 1, 2$, where $m_i = n_i$ gives the normal Fresnel drag, while $m_i = 1$ corresponds to no Fresnel drag. Repeating the derivation leading to (4) we obtain to 1st order in v/c the travel time difference between the two circuits,

$$\Delta t = \frac{2Lv\cos(\theta)}{c^2}\left(\frac{n_1^2}{m_1^2} - \frac{n_2^2}{m_2^2}\right) \tag{11}$$

The apparatus was orientated NS and used the rotation of the earth to change the angle θ. Then θ varies between $\lambda + \delta - 90^\circ = 20^\circ$ and $\lambda - \delta + 90^\circ = 50^\circ$, where $\lambda = 35^\circ$ is the latitude of Adelaide, and $\delta = 75^\circ$ is the declination of the 3-space flow from the flyby Doppler shift analysis, and with a speed of 486 km/s.. Then if $m_i \neq n_i$ a signal with period 24 h should be revealed. We need to compute the magnitude of the time difference signal if there is no Fresnel drag effect. The FSJ1-50A has an effective refractive index $n_1 = 1.19$, while the HJ4-50 has $n_2 = 1.11$, and then Δt would change by 8.7 ps over 24 hours, and have the phase shown in Fig.4. However while cable temperature effects have been removed by the cable layout, another source of temperature effects is from the LeCroy WaveRunner WR6051A DSO. To achieve ps timing accuracy and stability the DSO was operated in Random Interleaved Sampling (RIS) mode. This uses many signal samples to achieve higher precision. However in this mode the DSO temperature compensation re-calibration facility is disabled. To correct for this it was discovered that the timing errors between the two DSO channels very accurately tracked the temperature of the cooling air being drawn into the DSO. Hence during the experiment that air temperature was recorded. The Rb frequency standard was a Stanford Research Systems FS725. The results for 48 hours in mid May, 2010, are shown in Fig. 4: The red plot, with glitch, shows the DSO measured time difference values, while the blue plot shows the temperature variation of the DSO air-intake temperature, scaled to the time data. We see that the time data very closely tracks the air-intake temperature. Subtracting this temperature effect we obtain the smaller plot, which has a range of 5 ps, but showing no 24 h period. The corrected timing data may still have some small temperature effects. The glitch in the timing data near local time of 34 h was probably caused by a mechanical stress-release event in the cables. Hence the data implies that there is no 1st order effect in v/c, and so, from (11), that $n_1/m_1 = n_2/m_2$, with the simplest interpretation being that, in each cable $m = n$. This means that the Fresnel drag effect expression in (1) applies to RF coaxial cables.

5 Conclusions

The first experiment to study the Fresnel drag effect in RF coaxial cables has revealed that these cables exhibit the same effect as seen in bulk dielectrics and in optical fibers, and so this effect is very general, and in the case of the RF coaxial cables, is not affected by the conductors integral to RF coaxial cables. Because this experiment is a null experiment, after correcting for temperature effects in the DSO, its implications follow only when the results are compared with non-null experiments. Here we have compared the results with those from the spacecraft earth-flyby Doppler shift data results. Then we can deduce that the null result is caused by the Fresnel drag effect in the cables, and not by the absence of light speed anisotropy. This is to be understood from the heuristic derivation given herein, where it was shown that the Fresnel drag expression actually involves no drag effect at all, rather its form is such as to ensure that between scatterings the EM waves travel at speed c wrt to the 3-space, that is, that the "speed of light" is not an invariant. This experiment, as have many others, shows that the speed of light, as measured by an observer, actually depends on the speed of that observer wrt to 3-space. We have also shown how the speed of light may be measured in a one-way 1st order in v/c experiment, using spatially separated clocks that are not *a priori* synchronised, by rotating the apparatus. Subsequently, once the velocity of space past the detector is known, the clocks may be synchronised by light speed signalling.

Acknowledgements

Special thanks to Professor Igor Bray for supporting this research.

Submitted on August 23, 2010 / Accepted on September 20, 2010

References

1. Michelson A. A., Morley E. W. On the Relative Motion of the Earth and the Luminiferous Ether, *American Journal of Science*, 1887, v. 34, 333–345.
2. Cahill R. T., Kitto K. Michelson-Morley Experiments Revisited. *Apeiron*, 2003, v. 10, no. 2, 104–117.
3. Cahill R. T. The Michelson and Morley 1887 Experiment and the Discovery of Absolute Motion. *Progress in Physics*, 2005, v. 3, 25–29.
4. Miller D. C. The Ether-Drift Experiments and the Determination of the Absolute Motion of the Earth. *Review of Modern Physics*, 1933, v. 5, 203–242.
5. Anderson J. D., Campbell J. K., Ekelund J. E., Ellis J., Jordan J. F. Anomalous Orbital-Energy Changes Observed during Spaceraft Flybys of Earth. *Physical Review Letters*, 2008, v. 100, 091102.
6. Cahill R. T. Combining NASA/JPL One-Way Optical-Fiber Light-Speed Data with Spacecraft Earth-Flyby Doppler-Shift Data to Characterise 3-Space Flow. *Progress in Physics*, 2009, v. 4, 50–64.
7. Braxmaier C., Müller H., Pradl O., Mlynek J., Peters A., Schiller S. Tests of Relativity Using a Cryogenic Optical Resonator. *Physical Review Letters*, 2002, v. 88, 010401.
8. Müller H., Braxmaier C., Herrmann S., Peters A., Lämmerzahl C. Electromagnetic cavities and Lorentz invariance violation. *Physical Review D*, 2003, v. 67, 056006.
9. Wolf P., Bize S., Clairon A., Santarelli G., Tobar M. E., Luiten A. N. Improved test of Lorentz invariance in electrodynamics. *Physical Review D*, 2004, v. 70, 051902.

10. Wolf P., Bize S., Clairon A., Luiten A. N., Santarelli G., Tobar M. E. Tests of Lorentz Invariance using a Microwave Resonator. *Physical Review Letters*, v. 90, no. 6, 060402.

11. Lipa J. A., Nissen J. A., Wang S., Stricker D. A., Avaloff D. New Limit on Signals of Lorentz Violation in Electrodynamics. *Physical Review Letters*, 2003, v. 90, 060403.

12. Eisle Ch., Nevsky A. Yu., Schiller S. Laboratory Test of the Isotropy of Light Propagation at the 10^{-17} Level. *Physical Review Letters*, 2009, v. 103, 090401.

13. Cahill R. T. Unravelling Lorentz Covariance and the Spacetime Formalism. *Progress in Physics*, 2008, v. 4, 19–24.

14. Cahill R. T. Process Physics: From Information Theory to Quantum Space and Matter. Nova Science Pub., New York, 2005.

15. Cahill R. T. Dynamical 3-Space: A Review, in: Ether space-time and cosmology: New insights into a key physical medium, Duffy M. and Lévy J. (Editors), Apeiron, 2009, pp. 135-200.

16. Cahill R. T. Quantum Foam, Gravity and Gravitational Waves, in: Relativity, Gravitation, Cosmology: New Developments, Dvoeglazov V. (Editor), Nova Science Pub., New York, 2010, pp. 1-55.

17. Wang R., Zhengb Yi., Yaob A., Langley D. Modified Sagnac Experiment for Measuring Travel-time Difference Between Counterpropagating Light Beams in a Uniformly Moving Fiber. *Physics Letters A*, 2003, no. 1-2, 7–10.

18. Cahill R. T., Stokes F. Correlated Detection of sub-mHz Gravitational Waves by Two Optical-Fiber Interferometers. *Progress in Physics*, 2008, v. 2, 103–110.

19. Cahill R. T. The Roland De Witte 1991 Experiment. *Progress in Physics*, 2006, v. 3, 60–65.

20. Trimmer W. S. N. Baierlein R. F., Faller J. E., Hill H. A. Experimental Search for Anisotropy in the Speed of Light. *Physical Review D*, 1973, v. 8, 3321–3326.

21. Trimmer W. S. N. Baierlein R. F., Faller J. E., Hill H. A. Erratum: Experimental Search for Anisotropy in the Speed of Light. *Physical Review D*, 1974, v. 9, 2489.

22. Cahill R. T. A New Light-Speed Anisotropy Experiment: Absolute Motion and Gravitational Waves Detected. *Progress in Physics*, 2006, v. 4, 73–92.

23. Krisher T. P., Maleki L., Lutes G. F., Primas L. E., Logan R. T., Anderson J. D., Will C. M. Test of the Isotropy of the One-Way Speed of Light using Hydrogen-Maser Frequency Standards. *Physical Review D*, 1990, v. 42, 731–734.

24. Drezet A. The Physical Origin of the Fresnel Drag of Light by a Moving Dielectric Medium. *European Physics Journal B*, 2005, v. 45, no. 1, 103–110.

Dynamical 3-Space Gravity Theory: Effects on Polytropic Solar Models

Richard D. May and Reginald T. Cahill

School of Chemical and Physical Sciences, Flinders University, Adelaide 5001, Australia
E-mail: Richard.May@flinders.edu.au, Reg.Cahill@flinders.edu.au

Numerous experiments and observations have confirmed the existence of a dynamical 3-space, detectable directly by light-speed anisotropy experiments, and indirectly by means of novel gravitational effects, such as bore hole g anomalies, predictable black hole masses, flat spiral-galaxy rotation curves, and the expansion of the universe, all without dark matter and dark energy. The dynamics for this 3-space follows from a unique generalisation of Newtonian gravity, once that is cast into a velocity formalism. This new theory of gravity is applied to the solar model of the sun to compute new density, pressure and temperature profiles, using polytrope modelling of the equation of state for the matter. These results should be applied to a re-analysis of solar neutrino production, and to stellar evolution in general.

1 Introduction

It has been discovered that Newton's theory of gravity [1] missed a significant dynamical process, and a uniquely determined generalisation to include this process has resulted in the explanation of numerous gravitational anomalies, such as bore hole g anomalies, predictable black hole masses, flat spiral-galaxy rotation curves, and the expansion of the universe, all without dark matter and dark energy [2–4]. This theory of gravity arises from the dynamical 3-space, described by a dynamical velocity field, when the Schrödinger equation is generalised to take account of the propagation of quantum matter in the dynamical 3-space. So gravity is now an emergent phenomenon, together with the equivalence principle.

The dynamical 3-space has been directly observed using various light-speed anisotropy experiments, dating from the 1st detection by Michelson and Morley in 1887 [5,6], giving a speed in excess of 300 km/s, after re-calibrating the gas-mode interferometer for actual length contraction effects, to the latest using spacecraft earth-flyby Doppler shift data [7]. Overall these experiments reveal that relativistic effects are caused by the absolute motion of rods and clocks wrt the dynamical 3-space, essentially Lorentzian Relativity (LR), rather than the Special Relativity (SR) formalism, which has recently been shown by means of an exact change of space and time variables, to be equivalent to Galilean Relativity [8].

Here we apply the new gravity theory to the internal dynamics of the sun, and compute new density, pressure and temperature profiles, using the polytrope model for the equation of state of the matter. These results should then be applied to a re-analysis of neutrino production [9]. In general the Newtonian-gravity based standard model of stellar evolution also needs re-examination.

2 Dynamical 3-Space

Newton's inverse square law of gravity has the differential form

$$\nabla \cdot \mathbf{g} = -4\pi G\rho, \quad \nabla \times \mathbf{g} = \mathbf{0}, \tag{1}$$

for the acceleration field $\mathbf{g}(\mathbf{r}, t)$, assumed to be fundamental and existing within Newton's model of space, which is Euclidean, static, and unobservable. Application of this to spiral galaxies and the expanding universe has lead to many problems, including, in part, the need to invent dark energy and dark matter*. However (1) has a unique generalisation that resolves these and other problems. In terms of a velocity field $\mathbf{v}(\mathbf{r}, t)$ (1) has an equivalent form [2, 3]

$$\nabla \cdot \left(\frac{\partial \mathbf{v}}{\partial t} + (\mathbf{v} \cdot \nabla)\mathbf{v} \right) = -4\pi G\rho, \quad \nabla \times \mathbf{v} = \mathbf{0}, \tag{2}$$

where now

$$\mathbf{g} = \frac{\partial \mathbf{v}}{\partial t} + (\mathbf{v} \cdot \nabla)\mathbf{v}, \tag{3}$$

is the well-known Galilean covariant Euler acceleration of the substratum that has velocity $\mathbf{v}(\mathbf{r}, t)$. Because of the covariance of $\mathbf{g}$ under a change of the spatial coordinates only relative internal velocities have an ontological existence — the coordinates $\mathbf{r}$ then merely define a mathematical embedding space.

We give a brief review of the concept and mathematical formalism of a dynamical flowing 3-space, as this is often confused with the older dualistic space and aether ideas, wherein some particulate aether is located and moving through an unchanging Euclidean space — here both the space and

*The Friedmann equation for the expanding universe follow trivially from (1), as shown in [4], but then needs "dark matter" and "dark energy" to fit the cosmological data.

the aether were viewed as being ontologically real. The dynamical 3-space is different: here we have only a dynamical 3-space, which at a small scale is a quantum foam system without dimensions and described by fractal or nested homotopic mappings [2]. This quantum foam is not embedded in any space — the quantum foam is all there is, and any metric properties are intrinsic properties solely of that quantum foam. At a macroscopic level the quantum foam is described by a velocity field $\mathbf{v}(\mathbf{r}, t)$, where $\mathbf{r}$ is merely a [3]-coordinate within an embedding space. This embedding space has no ontological existence — it is merely used to (i) record that the quantum foam has, macroscopically, an effective dimension of 3, and (ii) to relate other phenomena also described by fields, at the same point in the quantum foam. The dynamics for this 3-space is easily determined by the requirement that observables be independent of the embedding choice, giving, for zero-vorticity dynamics and for a flat embedding space, and preserving the inverse square law outside of spherical masses, at least in the usual cases, such as planets,

$$\nabla\cdot\left(\frac{\partial\mathbf{v}}{\partial t}+(\mathbf{v}\cdot\nabla)\mathbf{v}\right)+\frac{\alpha}{8}\left((trD)^2-tr(D^2)\right)=-4\pi G\rho,$$

$$\nabla\times\mathbf{v}=\mathbf{0},\quad D_{ij}=\frac{1}{2}\left(\frac{\partial v_i}{\partial x_j}+\frac{\partial v_j}{\partial x_i}\right),\tag{4}$$

where $\rho(\mathbf{r}, t)$ is the matter and EM energy densities, expressed as an effective matter density. Borehole g measurements and astrophysical black hole data has shown that $\alpha\approx 1/137$ is the fine structure constant to within observational errors [2,3,10]. For a quantum system with mass m the Schrödinger equation is uniquely generalised [10] with the new terms required to maintain that the motion is intrinsically wrt the 3-space, and not wrt the embedding space, and that the time evolution is unitary:

$$i\hbar\frac{\partial\psi(\mathbf{r},t)}{\partial t}=-\frac{\hbar^2}{2m}\nabla^2\psi(\mathbf{r},t)-i\hbar\left(\mathbf{v}\cdot\nabla+\frac{1}{2}\nabla\cdot\mathbf{v}\right)\psi(\mathbf{r},t).\tag{5}$$

The space and time coordinates $\{t, x, y, z\}$ in (4) and (5) ensure that the separation of a deeper and unified process into different classes of phenomena — here a dynamical 3-space (quantum foam) and a quantum matter system, is properly tracked and connected. As well the same coordinates may be used by an observer to also track the different phenomena. However it is important to realise that these coordinates have no ontological significance — they are not real. The velocities $\mathbf{v}$ have no ontological or absolute meaning relative to this coordinate system — that is in fact how one arrives at the form in (5), and so the "flow" is always relative to the internal dynamics of the 3-space. A quantum wave packet propagation analysis of (5) gives the acceleration induced by wave refraction to be [10]

$$\mathbf{g}=\frac{\partial\mathbf{v}}{\partial t}+(\mathbf{v}\cdot\nabla)\mathbf{v}+(\nabla\times\mathbf{v})\times\mathbf{v}_R,$$
$$\mathbf{v}_R(\mathbf{r}_o(t),t)=\mathbf{v}_o(t)-\mathbf{v}(\mathbf{r}_o(t),t),\tag{6}$$

where $\mathbf{v}_R$ is the velocity of the wave packet relative to the local 3-space, and where $\mathbf{v}_o$ and $\mathbf{r}_o$ are the velocity and position relative to the observer, and the last term in (6) generates the Lense-Thirring effect as a vorticity driven effect. Together (4) and (6) amount to the derivation of gravity as a quantum effect, explaining both the equivalence principle ($\mathbf{g}$ in (6) is independent of m) and the Lense-Thirring effect. Overall we see, on ignoring vorticity effects, that

$$\nabla\cdot\mathbf{g}=-4\pi G\rho-4\pi G\rho_{DM},\tag{7}$$

where

$$\rho_{DM}=\frac{\alpha}{32\pi G}\left((trD)^2-tr(D^2)\right).\tag{8}$$

This is Newtonian gravity but with the extra dynamical term which has been used to define an effective "dark matter" density. This is not real matter, of any form, but is the matter density needed within Newtonian gravity to explain the flat rotation curves of spiral galaxies, large light bending and lensing effects from galaxies, and other effects. Here, however, it is purely a space self-interaction effect. This new dynamical effect also explains the bore hole g anomalies, and the black hole "mass spectrum". Eqn.(4), even when $\rho = 0$, has an expanding universe Hubble solution that fits the recent supernovae data in a parameter-free manner without requiring "dark matter" nor "dark energy", and without the accelerating expansion artifact [4]. However (7) cannot be entirely expressed in terms of $\mathbf{g}$ because the fundamental dynamical variable is $\mathbf{v}$. The role of (7) is to reveal that if we analyse gravitational phenomena we will usually find that the matter density ρ is insufficient to account for the observed $\mathbf{g}$. Until recently this failure of Newtonian gravity has been explained away as being caused by some unknown and undetected "dark matter" density. Eqn.(7) shows that to the contrary it is a dynamical property of 3-space itself. Significantly the quantum matter 3-space-induced 'gravitational' acceleration in (6) also follows from maximising the elapsed proper time wrt the wave-packet trajectory $\mathbf{r}_o(t)$, see [2],

$$\tau=\int dt\sqrt{1-\frac{\mathbf{v}_R^2(\mathbf{r}_o(t),t)}{c^2}},\tag{9}$$

and then taking the limit $v_R/c\to 0$. This shows that (i) the matter 'gravitational' geodesic is a quantum wave refraction effect, with the trajectory determined by a Fermat maximised proper-time principle, and (ii) that quantum systems undergo a local time dilation effect. Significantly the time dilation effect in (9) involves matter motion wrt the dynamical 3-space, and not wrt the observer, and so distinguishing LR from SR. A full derivation of (9) requires the generalised Dirac equation, with the replacement $\partial/\partial t\to\partial/\partial t+\mathbf{v}\cdot\nabla$, as in (5). In differential form (9) becomes

$$d\tau^2=g_{\mu\nu}dx^\mu dx^\nu=dt^2-\frac{1}{c^2}(d\mathbf{r}-\mathbf{v}(\mathbf{r}(t),t)dt)^2,\tag{10}$$

which introduces a curved spacetime metric $g_{\mu\nu}$ that emerges from (4). However this spacetime has no ontological significance — it is merely a mathematical artifact, and as such hides the underlying dynamical 3-space. This induced metric is not determined by the Einstein-Hilbert equations, which originated as a generalisation of Newtonian gravity, but without the knowledge that a dynamical 3-space had indeed been detected by Michelson and Morley in 1887 by detecting light speed anisotropy. In special circumstances, and with $\alpha = 0$, they do yield the same effective spacetime metric. However the dynamics in (4) is more general, as noted above, and has passed more tests.

3 New Gravity Equation for a Spherically Symmetric System

For the case of zero vorticity the matter acceleration in (6) gives

$$\mathbf{g}(\mathbf{r}, t) = \frac{\partial \mathbf{v}}{\partial t} + \frac{\nabla v^2}{2} \tag{11}$$

For a time independent flow we introduce a generalised gravitational potential, which gives a microscopic explanation for that potential,

$$\Phi(\mathbf{r}) = -\frac{v^2}{2}. \tag{12}$$

For the case of a spherically symmetric and time independent inflow we set $\mathbf{v}(\mathbf{r}, t) = -\hat{\mathbf{r}}v(r)$, then (4) becomes, with $v' = dv/dr$,

$$\frac{\alpha}{2r}\left(\frac{v^2}{2r} + vv'\right) + \frac{2}{r}vv' + (v')^2 + vv'' = -4\pi G\rho \tag{13}$$

which can be written as

$$\frac{1}{r^2}\frac{d}{dr}\left(r^{2-\frac{\alpha}{2}}\frac{d}{dr}\left(r^{\frac{\alpha}{2}}\Phi\right)\right) = 4\pi G\rho \tag{14}$$

This form suggests that the new dynamics can be incorporated into the space metric, in that the 3-space α-term appears to lead to a fractal dimension of $3 - \alpha/2 = 2.996$, see [10]. The velocity flow description of space is completely equivalent to Newtonian gravity when the α dependent term in (4) is removed. In this case setting $\alpha = 0$ reduces (14) to the Poisson equation of Newtonian gravity for the case of spherical symmetry.

4 Solutions to New Gravity Equation for Non-Uniform Density

The solutions to (14) for a uniform density distribution are published in [2]. For variable density $\rho(r)$ the exact solution to (14) is*

$$\begin{aligned}\Phi(r) = - &\frac{\beta}{r^{\frac{\alpha}{2}}} - \frac{G}{(1-\frac{\alpha}{2})r}\int_0^r 4\pi s^2\rho(s)ds \\ - &\frac{G}{(1-\frac{\alpha}{2})r^{\frac{\alpha}{2}}}\int_r^\infty 4\pi s^{1+\frac{\alpha}{2}}\rho(s)ds,\end{aligned} \tag{15}$$

When $\rho(r) = 0$ for $r > R$, this becomes

$$\Phi(r) = \begin{cases} -\dfrac{\beta}{r^{\frac{\alpha}{2}}} - \dfrac{G}{(1-\frac{\alpha}{2})r}\displaystyle\int_0^r 4\pi s^2\rho(s)ds \\ -\dfrac{G}{(1-\frac{\alpha}{2})r^{\frac{\alpha}{2}}}\displaystyle\int_r^R 4\pi s^{1+\frac{\alpha}{2}}\rho(s)ds, \quad 0 < r \le R \\ -\dfrac{\beta}{r^{\frac{\alpha}{2}}} - \dfrac{\gamma}{r}, \qquad r > R \end{cases} \tag{16}$$

where

$$\gamma = \frac{G}{(1-\frac{\alpha}{2})}\int_0^R 4\pi s^2\rho(s)ds = \frac{GM}{(1-\frac{\alpha}{2})} \tag{17}$$

Here M is the total matter mass, and β is a free parameter. The term $\beta/r^{\alpha/2}$ describes an inflow singularity or "black hole" with arbitrary strength. This is unrelated to the putative black holes of General Relativity. This corresponds to a primordial black hole. As well the middle term in (16) also has a $1/r^{\alpha/2}$ inflow-singularity, but whose strength is mandated by the matter density, and is absent when $\rho(r) = 0$ everywhere. This is a minimal "black hole", and is present in all matter systems. The $\beta/r^{\alpha/2}$ term will produce a long range gravitational acceleration $g = \beta/r^{1+\alpha/2}$, as observed in spiral galaxies. For the region outside the sun ($r > R$) Keplerian orbits are known to well describe the motion of the planets within the solar system, apart from some small corrections, such as the Precession of the Perihelion of Mercury, which follow from relativistic effects from (9). Thus is the case $\beta = 0$, and the sun has only an induced 'Minimal Attractor'. These minimal black holes contribute to the external $g = K/r^2$ gravitational acceleration, through an effective mass

$$M_{BH} = \frac{M}{1-\frac{\alpha}{2}} - M = \frac{\alpha}{2}\frac{M}{1-\frac{\alpha}{2}} \approx \frac{\alpha}{2}M \tag{18}$$

as previously reported [2]. These induced black hole " effective" masses have been detected in numerous globular clusters and spherical galaxies and their predicted effective masses have been confirmed in some 19 such cases [11]. These gave the value $\alpha = \approx 1/137$ [12]. The induced black hole dynamics at the center of the sun is responsible for the new density, pressure and temperature profiles computed herein.

*Eqn (14) also permits a $-\overline{\gamma}/r$ term in (16). However this is not valid, as the full [3] version of (14) would then involve a point mass at $r = 0$, because $\nabla^2(1/|r|) = -4\pi\delta(\mathbf{r})$, and in (16) all the mass is accounted for by $\rho(r)$. See [2] for a detailed discussion.

5 Polytropic Models using Dynamical 3-Space Theory

For a star to be in hydrostatic equilibrium the inward force of gravity must match the net outward effect of the pressure,

$$\frac{dP}{dr} = -\frac{d\Phi}{dr}\rho \tag{19}$$

Here we use the polytrope modelling of the pressure-density equation of state.

$$P = K\rho^{1+\frac{1}{n}} \tag{20}$$

where n is the polytropic index, and K is a constant. This was introduced by Eddington, and was extensively used by Chandrasekhar [13–16], but these analyses only apply in the case of Newtonian gravity. The new theory of gravity requires a new treatment.

The polytropic relation between pressure and density (20) gives

$$\frac{dP}{dr} = \frac{K(n+1)}{n}\rho^{\frac{1}{n}}\frac{d\rho}{dr} \tag{21}$$

and (19) gives

$$\frac{d\Phi}{dr} = -\frac{K(n+1)}{n}\rho^{\frac{1}{n}-1}\frac{d\rho}{dr} \tag{22}$$

Integration gives

$$\Phi = -K(n+1)\rho^{\frac{1}{n}} + C \tag{23}$$

Here it will be useful to define the gravitational potential at the sun's surface $\Phi_R = \Phi(R) = C$ as the value of the integration constant, and so we obtain for the density

$$\rho = \left(\frac{\Phi_R - \Phi}{K(n+1)}\right)^n \tag{24}$$

One of the characteristics of the new gravity is that all spherical objects contain induced black holes. In the context of polytrope models this presents the problem that the central value of the potential cannot be used, as in the Lane-Emden equation. We can however impose the polytropic condition from (24) onto numerical solutions to iteratively solve the problem. Multiplying (24) by $4\pi r^2$ and integrating yields

$$M = \int_0^R 4\pi r^2 \rho dr = \int_0^R 4\pi r^2 \left(\frac{\Phi_R - \Phi)}{K(n+1)}\right)^n dr \tag{25}$$

and then

$$K = \frac{1}{(n+1)M^{1/n}}\left(\int_0^R 4\pi r^2(\Phi_R - \Phi)^n dr\right)^{1/n} \tag{26}$$

A new density distribution and K value can now be calculated from an initial density distribution by cycling through the following relations iteratively

$$\begin{aligned}\Phi(r) =& \frac{-G}{(1-\frac{\alpha}{2})}\left(\frac{1}{r}\int_0^r 4\pi s^2\rho(s)ds + \right.\\ &\left. + \frac{1}{r^{\frac{\alpha}{2}}}\int_r^R 4\pi s^{1+\frac{\alpha}{2}}\rho(s)ds\right)\\ K =& \frac{1}{(n+1)M^{1/n}}\left(\int_0^R 4\pi r^2(\Phi_R - \Phi)^n dr\right)^{1/n}\\ \rho(r) =& \left(\frac{\Phi_R - \Phi(r)}{K(n+1)}\right)^n\end{aligned} \tag{27}$$

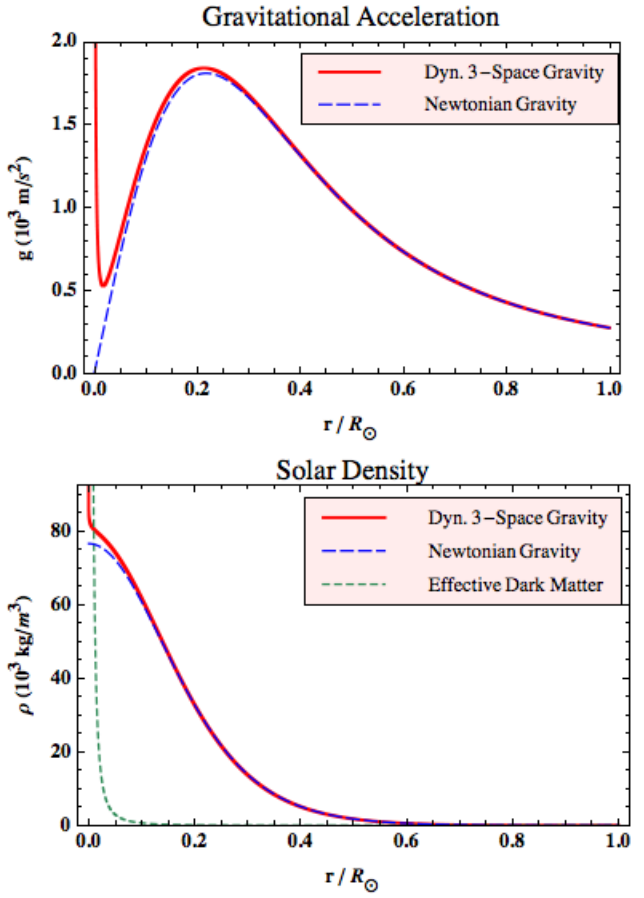

Fig. 1: Gravity and density plots for a polytropic model for the sun with $n = 3$. The effective dark matter distribution is shown in the density plot.

6 Polytropic Solar Models

For the sun a polytrope model with $n = 3$ is known to give a good approximation to conditions in the solar core as compared with the Standard Solar Model [16]. This is known as the Eddington Standard Model. The polytrope model does well in comparison with the Standard Solar Model [17]. To test the calculation method, setting $\alpha = 0$ should reproduce

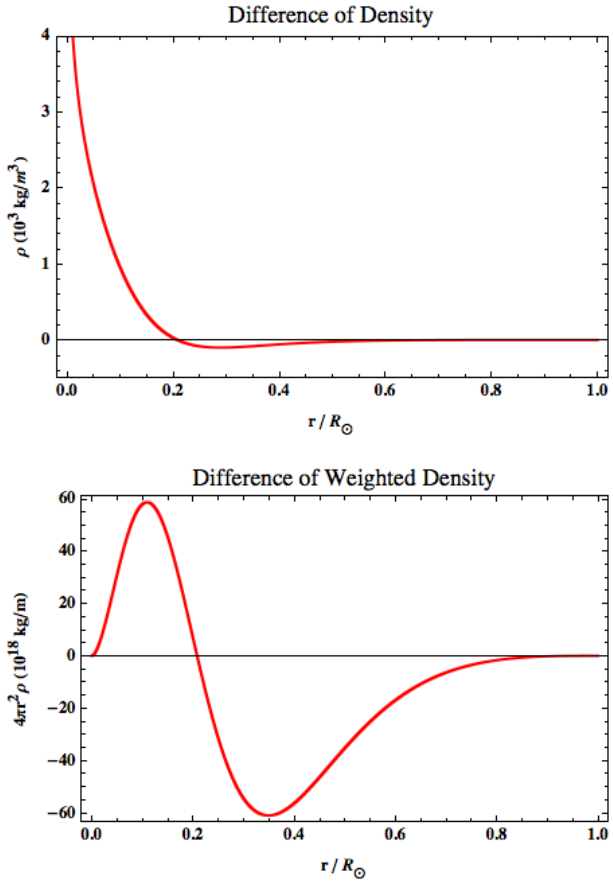

Fig. 2: Top graph shows difference in density $\rho(r)$ between new gravity and Newtonian modeling. Bottom graph show the difference in weighted density $4\pi r^2\rho(r)$.

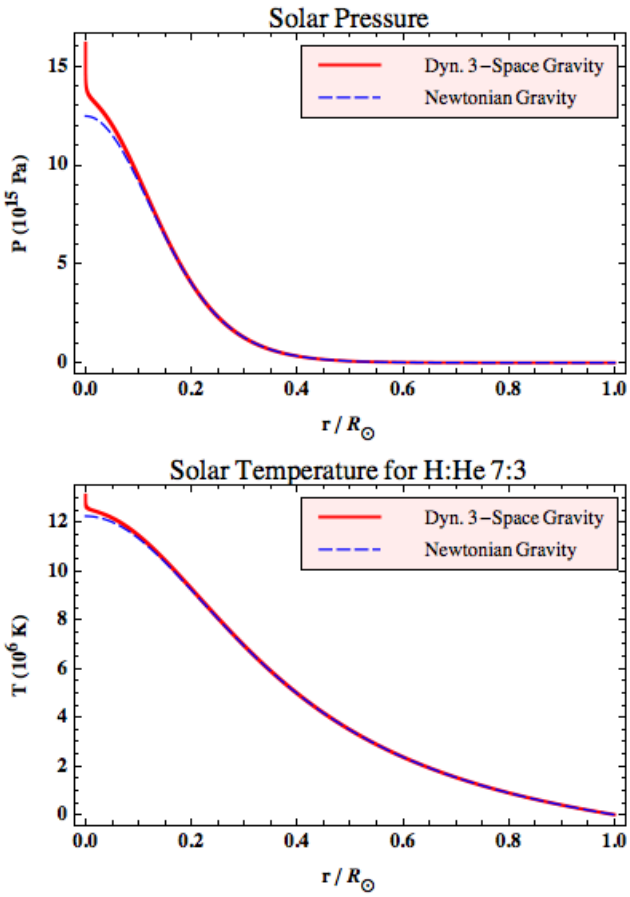

Fig. 3: The pressure and temperature in the center of the sun is predicted to be much larger in the new model.

the results from the Lane-Emden equation, which is based on Newtonian gravity. The results of starting with a uniform density and then iteratively finding the solution agree with the values published by Chandrasekhar [13]. The density distribution also matched numerical solutions produced in Mathematica to the Lane-Emden equation.

Results from solving the equations in (27) iteratively, until convergence was achieved, are shown in Figs.1-3 for various quantities, and compared with the results for Newtonian gravity. For the new gravity ($\alpha = 1/137$) we see a marked increase in the gravity strength $g(r)$ near the center, Fig.1, caused by the induced black hole at the center, which is characteristic of the new gravity theory, and which draws in the matter to enhance the matter density near the center.

The new model of gravity has been used to explain away the need for dark matter in astrophysics [4]. Here we find the effective "dark matter" distribution that would need to be added to the matter distribution to create these gravitational effects in Newtonian Gravity. From (8) and (12) we obtain

$$\rho_{DM}(r) = -\frac{\alpha}{8\pi G r}\left(\frac{\Phi}{r} + \frac{d\Phi}{dr}\right). \qquad (28)$$

Using (16) we then obtain

$$\rho_{DM}(r) = \frac{\alpha}{2} r^{-2-\alpha/2} \int_r^R s^{1+\alpha/2}\rho(s)ds. \qquad (29)$$

This effective "dark matter" distribution is shown in Fig.1 for the polytropic sun model. This then gives the total "dark matter"

$$M_{DM} = \int_0^R 4\pi r^2 \rho_{DM}(r)dr = \frac{\alpha}{2}\frac{M}{1-\frac{\alpha}{2}} \qquad (30)$$

in agreement with (18). The "dark matter" effect is the same as the induced "black hole" effect, in the new gravity theory.

The matter density has increased towards the center, as seen in Fig.2, and so necessarily there is a slightly lower matter density in the inner middle region. This effect is more clearly seen in the plot of $4\pi r^2\rho(r)$. The "dark matter"/"black hole" effect contributes to the external gravitational acceleration, and so the total mass of the sun, defined as its matter content, is lower than computed using Newtonian gravity, see (17). The total mass is now 0.37% ($\equiv \alpha/(2-\alpha)$) smaller.

The pressure and temperature generated by the new gravity is shown in Fig.3. The pressure comes from the poly-

trope relation, (20), and closely follows the density distribution. The temperature can be calculated from the ideal gas equation, with $\mu = 0.62$ corresponding to a ratio of 7:3 of Hydrogen to Helium, to obtain

$$T(r) = \frac{Pm_p\mu}{k\rho} \tag{31}$$

where m_p is the mass of a proton, k is Boltzmann's constant and μ is the mass ratio. Unlike the pressure and density, the temperature is increased in the middle region as well as the inner region.

7 Conclusions

The discovery of the dynamical 3-space changes most of physics. This space has been repeatedly detected in light-speed anisotropy experiments. The dynamics of this space follow from a unique generalisation of Newtonian gravity, once that is expressed in a velocity framework. Then the gravitational acceleration field $\mathbf{g}(\mathbf{r}, t)$ is explained as the local acceleration of the structured space, with evidence that the structure is fractal. This space is the local absolute frame of reference. Uniquely incorporating this space into a generalised Schrödinger equation shows that, up to vorticity effects and relativistic effects, the quantum matter waves are refracted by the space, and yield that quantum matter has the same acceleration as that of space itself. So this new physics provides a quantum theory derivation of the phenomenon of gravity. The 3-space dynamics involves G and the fine structure constant α, with this identification emerging from the bore hole gravity anomalies, and from the masses of the minimal "black holes" reported for globular clusters and spherical galaxies. There are numerous other phenomena that are now accounted for, including a parameter-free account of the supernova red-shift — magnitude data. The occurrence of α implies that we are seeing evidence of a new unified physics, where space and matter emerge from a deeper theory. One suggestion for this theory is *Process Physics*.

Herein we have reported the consequences of the new, emergent, theory of gravity, when applied to the sun. This theory predicts that the solar core, which extends to approximately 0.24 of the radius, is hotter, more dense and of higher pressure than current Newtonian-gravity based models. Thus a new study is now needed on how these changes will affect the solar neutrino output. It is also necessary to revisit the stellar evolution results.

Submitted on August 23, 2010 / Accepted on September 20, 2010

References

1. Newton I. Philosophiae Naturalis Principia Mathematica, 1687.
2. Cahill R. T. Process Physics: From Information Theory to Quantum Space and Matter. Nova Science Pub., New York, 2005.
3. Cahill R. T. Dynamical 3-Space: A Review, in: Ether space-time and cosmology: New insights into a key physical medium, Duffy M. and Lévy J. (Editors), Apeiron, 2009, pp. 135-200.
4. Cahill R. T. Unravelling the Dark Matter — Dark Energy Paradigm, *Apeiron*, 2009, v. 16, no. 3, 323–375.
5. Cahill R. T., Kitto K. Michelson-Morley Experiments Revisited. *Apeiron*, 2003, v. 10, no. 2, 104–117.
6. Cahill R. T. The Michelson and Morley 1887 Experiment and the Discovery of Absolute Motion. *Progress in Physics*, 2005, v. 3, 25–29.
7. Cahill R. T. Combining NASA/JPL One-Way Optical-Fiber Light-Speed Data with Spacecraft Earth-Flyby Doppler-Shift Data to Characterise 3-Space Flow. *Progress in Physics*, 2009, v. 4, 50–64.
8. Cahill R. T. Unravelling Lorentz Covariance and the Spacetime Formalism.*Progress in Physics*, 2008, v. 4, 19–24.
9. Bahcall J. N. Neutrino Astrophysics. Cambridge University Press, Cambridge, England, 1989.
10. Cahill R. T. Dynamical Fractal 3-Space and the Generalised Schrödinger Equation: Equivalence Principle and Vorticity Effects. *Progress in Physics*, 2006, v. 1, 27–34.
11. Cahill R. T. Black Holes and Quantum Theory: The Fine Structure Constant Connection. *Progress in Physics*, 2006, v. 4, 44–50.
12. Cahill R. T. 3-Space Inflow Theory of Gravity: Boreholes, Blackholes and the Fine Structure Constant. *Progress in Physics*, 2006, v. 2, 9–16.
13. Chandrasekhar S. An Introduction to the Study of Stellar Structure. Dover Publications, New York, 1958.
14. Hansen C. J., Kawaler S. D. Trimble V. Stellar Interiors — Physical Principles, Structure and Evolution. Springer, New York, 2004.
15. Horedt G. P. Polytropes. Applications in Astrophysics and Related Fields. Kluwer, Dordrecht, 2004.
16. Kippenhahn R., Weigert A. Stellar Structure and Evolution. Springer, New York, 1994.
17. Bahcall J. N., Basu S., Pinsonneault M. H. How Uncertain are Solar Neutrino Predictions? *Physics Letters B*, 1998, v. 433, 1–8.

Particles and Antiparticles in the Planck Vacuum Theory

William C. Daywitt

National Institute for Standards and Technology (retired), Boulder, Colorado, USA, E-mail: wcdaywitt@earthlink.net

This short note sheds some light on the negative energy vacuum state by expanding the Planck vacuum (PV) model and taking a closer look at the particle-antiparticle nature of the Dirac equation. Results of the development are briefly discussed with regard to the complexity of the PV interaction with the massless free charge, the Dirac electron, and the proton; an exercise that may lead to a better proton model.

The negative energy PV model [1] can be expanded to include negative energy particle states in the following manner: the structure of the PV is related to the string of Compton relations

$$r_e m_e c^2 = \cdots = r_p m_p c^2 = \cdots = r_* m_* c^2 = e_*^2 = c\hbar \qquad (1)$$

where the subscripts represent respectively the electron, proton, Planck particle, and their antiparticles; and where the dots represent any number of intermediate particle-antiparticle states. The r_e and m_e, etc., are the Compton radii and masses of the various particles, c is the speed of light, and $\hbar$ is Planck's constant. The bare charge e_* is assumed to be massless and is related to the elementary charge e observed in the laboratory via $e^2 = \alpha e_*^2$, where α is he fine structure constant. The particle-antiparticle masses are the result of their bare charges being driven by ultra-high-frequency zero-point fields that exist in free space [2, 3]. The charge on the Planck particles within the PV is negative. It is assumed that positive charges are holes that exist within the negative energy PV, an assumption that is supported by the Dirac equation and its negative energy solution [4].

The relation of positive and negative particles and antiparticles to the Compton relations in (1) is easily explained. In the above scheme, negatively charged particles or antiparticles exist in free space and exert a perturbing force [1]

$$\frac{(-e_*)(-e_*)}{r^2} - \frac{mc^2}{r} \qquad (2)$$

on the PV, where m is the particle-antiparticle mass. The first charge on the left is due to the free particle or antiparticle and the second to the Planck particles within the PV. The hole exerts a corresponding force within the PV equal to

$$\frac{(+e_*)(-e_*)}{r^2} - \frac{(-mc^2)}{r} \qquad (3)$$

where the effective positive charge on the left is due to the missing negative charge (the hole) in the PV sea and the negative mass energy $(-mc^2)$ is due to the hole belonging to a negative energy state. The radius r at which (2) and (3) vanish is the particle or antiparticle Compton radius $r_c\,(= e_*^2/mc^2)$. The more complete form for (1) can then be expressed as

$$r_e(\pm\, m_e c^2) = \cdots = r_p(\pm\, m_p c^2) = \cdots = r_*(\pm\, m_* c^2) = \pm\; e_*^2 \qquad (4)$$

which renders its application to both particles and antiparticles more explicit and transparent. The positive mass energies belong to the negatively charged free-space particles or antiparticles, while the negative mass energies belong to the PV holes which are responsible for the ficticious positively charged particles or antiparticles imagined to exist in free space. Both equations in (4) lead back to the single equation (1) which defines $\hbar$.

The preceding ideas are illustrated using the Dirac equation and provide a clearer view of that equation as it is related to the concept of Dirac holes. The Dirac equation for the electron can be expressed as [4, 5]

$$\left(c\,\vec{\alpha}\cdot\widehat{p_e} + \beta m_e c^2\right)\psi_e = E_e\psi_e \qquad (5)$$

where the momentum operator and energy are given by

$$\widehat{p_e} = \frac{\hbar\nabla}{i} = \frac{(-e_*)(-e_*)\nabla}{ic} \text{ and } E_e = +\sqrt{m_e^2c^4 + c^2p_e^2} \qquad (6)$$

and where $\vec{\alpha}$ and β are defined in [5]. The relativistic momentum is $p_e\,(= m_e v/\sqrt{1 - v^2/c^2}\,)$. The shift from the positive-energy electron solution to the negative-energy hole (positron) solution proceeds as follows:

$$E_e \longrightarrow E_h = -E_e \qquad (7)$$

$$m_e c^2 \longrightarrow m_h c^2 = -m_e c^2 \qquad (8)$$

$$p_e = \frac{m_e v}{\sqrt{1 - v^2/c^2}} \rightarrow p_h = \frac{-m_h v}{\sqrt{1 - v^2/c^2}} = -p_e, \qquad (9)$$

$$\widehat{p_e} = \frac{(-e_*)(-e_*)\nabla}{ic} \rightarrow \widehat{p_h} = \frac{(+e_*)(-e_*)\nabla}{ic} = -\widehat{p_e}. \qquad (10)$$

Substituting equations (7) through (10) into (5) yields

$$\left(c\,\vec{\alpha}\cdot\widehat{p_h} + \beta m_h c^2\right)\psi_h = E_h\psi_h \qquad (11)$$

for the hole solution, where $E_h = -(m_h^2c^4 + c^2p_h^2)^{1/2}$. From (5) and (11) and $m_h = m_e$ it follows that the electron and hole satisfy the same Dirac equation of motion with $E_h = -E_e$. Although the hole exists in the PV, it appears experimentally in free space as a positron due to the hole's field permeating that space. In turn, the positron's deflection in a free-space magnetic field is due to that field permeating the PV and affecting the hole.

From the development of the PV theory so far, the Dirac equation appears to be part of a succession of equations involving an increasingly more complicated interaction between the free-space particle and the PV. For example, the interaction of a massless point charge traveling at a constant velocity results in the relativistic electric and magnetic fields (and by inference the Lorentz transformation) that can be easily calculated directly from the charge's Coulomb field (the first term in (2)) and its interaction with the PV [1, Section 4]. The Dirac electron (a massive point charge) is next in complexity to the point charge and perturbs the PV with the total force in (2), leading to the Dirac equation (and the quantum fields associated with it) which represents the PV reaction to the moving Dirac electron [4].

The proton is the next more complex and stable particle whose properties are shaped by its interaction with the PV. Being in essence a more complicated PV hole than the positron, the proton exhibits some structure as witnessed by its three-quark nature associated (it seems correct to assume) with the hole. The calculational difficulties besetting quantum chromodynamics [6, p.70] attest to the idea expressed above that things are getting more complex in the progression from leptons to hadrons and their PV interactions. Perhaps these difficulties can be resolved by a better model for the heavy particles based on the PV theory.

Submitted on September 5, 2010 /Accepted on September 7, 2010

References

1. Daywitt W. C. The Planck vacuum. *Progress in Physics*, 2009, v. 1, 20–26.
2. Puthoff H. E. Gravity as a zero-point-fluctuation force. *Physical Review A*, 1989, v. 39, no. 5, 2333–2342.
3. Daywitt W. C. The source of the quantum vacuum. *Progress in Physics*, 2009, v. 1, 27–32.
4. Daywitt W. C. The Dirac electron in the Planck vacuum theory. *Progress in Physics*, 2010, v. 4, 69–71.
5. Gingrich D. M. Practical quantum electrodynamics. CRC, The Taylor & Francis Group, Boca Raton, 2006.
6. Giunti C., Kim C. W. Fundamentals of neutrino physics and astrophysics. Oxford Univ. Press, Oxford, 2007.

Wave Particle Duality and the Afshar Experiment

Aurélien Drezet
Institut Neel, 25 rue des Martyrs 38042, Grenoble, France. E-mail: aurelien.drezet@grenoble.cnrs.fr

We analyze the experiment realized in 2003-2004 by S. Afshar et al. [1] in order to refute the principle of complementarity. We discuss the general meaning of this principle and show that contrarily to the claim of the authors Bohr's complementarity is not in danger in this experiment.

1 Introduction

In an interesting series of articles published few years ago Afshar and coworkers [1,2] reported an optical experiment in which they claimed to refute the well known N. Bohr principle of complementarity [3,4]. Obviously this result, if justified, would constitute a serious attack against the orthodox interpretation of quantum mechanics (known as the Copenhagen interpretation). This work stirred much debate in different journals (see for examples references [5–12]).

We think however that there are still some important misunderstandings concerning the interpretation of this experiment. In a preprint written originally in 2004 [5] (and following some early discussions with Afshar) we claimed already that the interpretation by Afshar *et al.* can be easily stated if we stay as close as possible from the texts written by Bohr. The aim of the present article (which was initially written in 2005 to precise a bit the thought developed in [5]) is to comment the interpretation discussed in [1]. We will in the following analyze the meaning of Bohr principle and show that far from disproving its content the experiment [1] is actually a complete confirmation of its general validity.

The difficulties associated with the understanding of this principle are not new and actually complementarity created troubles even in Einstein mind [3] so that we are here in good company. To summarize a bit emphatically Bohr's complementarity we here remind that this principle states that if one of a pair of non commuting observables of a quantum object is known for sure, then information about the second (complementary) is lost [3, 4, 15, 16]. This can be equivalently expressed as a kind of duality between different descriptions of the quantum system associated with different experimental arrangements which mutually exclude each other (read in particular [3,4]). Later in the discussion we will try to precise this definition but for the moment it is enough to illustrate the concepts by examples

Consider for instance the well known Young double-pinholes interference experiment made with photons. The discrete nature of light precludes the simultaneous observation of a same photon in the aperture plane and in the interference pattern: the photon cannot be absorbed twice. This is already a trivial manifestation of the principle of Bohr. Here it implies that the two statistical patterns associated with the wave in the aperture plane and its Fourier (i. e., momentum) transform require necessarily different photons for their recording. It is in that sense that each experiment excludes and completes reciprocally the other. In the case considered before the photon is absorbed during the first detection (this clearly precludes any other detection). However even a non-destructive solution for detection implying entanglement with other quantum systems has a radical effect of the same nature: the complementarity principle is still valid. For example, during their debate Bohr and Einstein [3] discussed an ideal *which-way* experiment in which the recoil of the slits is correlated to the motion of the photon. Momentum conservation added to arguments based on the uncertainty relations are sufficient to explain how such entanglement photon-slits can erase fringes [15–19]. It is also important for the present discussion to remind that the principle of complementarity has a perfidious consequence on the experimental meaning of trajectory and path followed by a particle. Indeed the unavoidable interactions existing between photons and detectors imply that a trajectory existing independently of any measurement process cannot be unambiguously defined. This sounds even like a tragedy when we consider once again the two-holes experiment. Indeed for Bohr this kind of experiments shows definitely the essential element of ambiguity which is involved in ascribing conventional physical attributes to quantum systems. Intuitively (i. e., from the point of view of classical particle dynamic) one would expect that a photon detected in the focal plane of the lens must have crossed only one of the hole 1 or 2 before to reach its final destination. However, if this is true, one can not intuitively understand how the presence of the second hole (through which the photon evidently did not go) forces the photon to participate to an interference pattern (which obviously needs an influence coming from both holes). Explanations to solve this paradox have been proposed by de Broglie, Bohm, and others using concepts such as empty waves or quantum potentials [20, 21]. However all these explanations are in agreement with Bohr principle (since they fully reproduce quantum predictions) and can not be experimentally distinguished. Bohr and Heisenberg proposed for all needed purposes a much more pragmatic and simpler answer: *don't bother*, the complementarity principle precludes the simultaneous observation of a photon trajectory and of an interference pattern. For Bohr [3]: *This point is of great logical consequence, since it is only the circumstance that we are presented with a choice of either tracing the path*

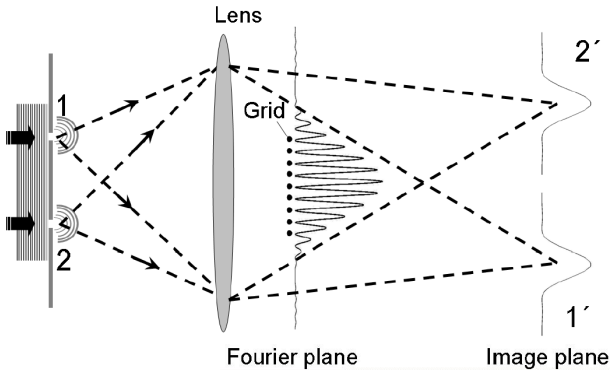

Fig. 1: The experiment described in [1]. Photons coming from pinholes 1 and 2 interfere in the back-focal plane of a lens (Fourier plane) whereas they lead to two isolated narrow spots in the image plane (the image plane is such that its distance p' to the lens is related to the distance p between the lens and the apertures screen by $1/p + 1/p' = 1/f$, where f is the focal length). The wire grid in the back focal plane, distant of f from the lens, is passing through the minima of the interference pattern. The subsequent propagation of the wave is consequently not disturbed by the grid.

of a particle or observing interference effects, which allows us to escape from the paradoxical necessity of concluding that the behaviour of an electron or a photon should depend on the presence of a slit in the diaphragm through which it could be proved not to pass. From such an analysis it seems definitively that Nature resists to deeper experimental investigation of its ontological level. As summarized elegantly by Brian Greene [22]: *Like a Spalding Gray soliloquy, an experimenter's bare-bones measurement are the whole show. There isn't anything else. According to Bohr, there is no backstage*. In spite of its interest it is however not the aim of the present article to debate on the full implications of such strong philosophical position.

2 Complementarity versus the experiments

2.1 A short description of the Afshar *et al.* experiment

The experiment reported in [1] (see Fig. 1) is actually based on a modification of a *gedanken* experiment proposed originally by Wheeler [23]. In the first part of their work, Afshar *et al.* used an optical lens to image the two pinholes considered in the Young interference experiment above mentioned. Depending of the observation plane in this microscope we can then obtain different complementary information.

If we detect the photons in the focal plane of the lens (or equivalently just in front of the lens [24]) we will observe, i.e, after a statistical accumulation of photon detection events, the interference fringes. However, if we record the particles in the image plane of the lens we will observe (with a sufficiently high numerical aperture) two sharp spots 1' and 2' images of the pinholes 1 and 2. Like the initial Young two-holes experiment this example illustrates again very well the principle of Bohr. One has indeed complete freedom for measuring the photon distribution in the image plane instead of detecting the fringes in the back focal plane. However, the two kinds of measurements are mutually exclusive: a single photon can participate only to one of these statistical patterns.

In the second and final part of the experiment, Afshar *et al.* included a grid of thin absorbing wires located in the interference fringes plane. Importantly, in the experiment the wires must be located at the minimum of the interference pattern in order to reduce the interaction with light. In the following we will consider a perfect interference profile (with ideal unit visibility $V = (I_{max} - I_{min})/(I_{max} + I_{min}) = 1$) to simplify the discussion. If additionally the geometrical cross section of each wire tends ideally to zero then the interference behavior will, at the limit, not be disturbed and the subsequent wave propagation will be kept unchanged. This implies that the photon distributions 1' and 2', located in the image plane optically conjugated with the aperture plane, are not modified by the presence, or the absence, of the infinitely thin wire grid. Naturally, from practical considerations an infinitely thin dielectric wire is not interacting with light and consequently produces the same (null) effect whatever its location in the light path (minimum or maximum of the interference for example). In order to provide a sensible probe for the interference pattern, necessary for the aim of the experiment considered, we will suppose in the following idealized wires which conserve a finite absorbtion efficiency and this despite the absence of any geometrical transversal extension. We will briefly discuss later what happens with spatially extended scattering wires with finite cross section, but this point is not essential to understand the essential of the argumentation. With such wires, and if we close one aperture (which implies that there is no interference fringes and thus that a finite field impinges on the wires) the scattering and absorbtion strongly affect the detection behavior in the image plane. As it is seen experimentally [1, 2] the scattering by the wire grid in general produces a complicated diffraction pattern and not only an isolated narrow peak in 1' or 2' as it would be without the grid.

In such conditions, the absence of absorbtion by the wires when the two apertures are open is a clear indication of the existence of the interference fringes zeros, i.e., of a wave-like character, and this even if the photon is absorbed in the image plane in 1' or 2'. Following Afshar *et al.*, this should be considered as a violation of complementarity since the same photons have been used for recording *both* the 'path' and the wave-like information. The essential questions are however what we mean precisely here by path and wave-like information and what are the connections of this with the definition of complementarity. As we will see hereafter it is by finding a clear answer to these questions that the paradox and the contradictions with Bohr's complementarity are going to vanish.

2.2 The wave-particle duality mathematical relation

At that stage, it is important to point out that the principle of complementarity is actually a direct consequence of the mathematical formalism of quantum mechanics and of its statistical interpretation [4]. It is in particular the reason why the different attempts done by Einstein to refute complementarity and the Heisenberg uncertainty relations always failed: the misinterpretations resulted indeed from a non-cautious introduction of classical physics in the fully consistent quantum mechanic formalism [3]. For similar reasons here we show that a problem since Afshar *et al.* actually mixed together, i.e imprudently, argumentations coming from classical and quantum physics. We will show that this mixing results into an apparent refutation of the complementarity principle.

After this remark we now remind that a simple mathematical formulation of complementarity exists in the context of two path interferometry [25–28]. For example in the Young double-apertures experiment considered previously the field amplitudes C_1 and C_2 associated with the two narrow apertures, separated by the distance d, allow us to define the wave function in the two-apertures plane by:

$$\psi(x) \sim C_1\delta(x - d/2) + C_2\delta(x + d/2). \quad (1)$$

From this formula one can easily introduce the "distinguishability"

$$K = \frac{||C_1|^2 - |C_2|^2|}{|C_1|^2 + |C_2|^2}. \quad (2)$$

This quantity can be physically defined by recording the photons distribution in the aperture plane and constitutes an observable measure of the "path" distinguishability (see however section 3.3). The interpretation of K is actually clear, and in particular if $K = 0$ each apertures play a symmetrical role, whereas if $K = 1$ one of the two apertures is necessarily closed. Naturally, like in the Afshar experiment, K can also be measured by recording photons in the image plane of the lens in 1' and 2'. Equations (1) and (2) are still valid, with the only differences that: i) we have now a diffraction spot (like an Airy disk) instead of a Dirac distribution in equation (1), and ii) that the spatial variables are now magnified by the lens.

Instead of the spatial representation one can also consider the Fourier transform corresponding to the far field interference pattern recorded at large distance of the two-slits screen:

$$\psi(k) \sim C_1 \cdot e^{ikd/2} + C_2 \cdot e^{-ikd/2}. \quad (3)$$

Such a wave is associated with an oscillating intensity in the k-space given by

$$I(k) \sim 1 + V\cos(kd + \chi) \quad (4)$$

where $\chi = \arg(C_1) - \arg(C_2)$ and V is the fringe visibility

$$V = \frac{2|C_1| \cdot |C_2|}{|C_1|^2 + |C_2|^2}. \quad (5)$$

This quantity is also a physical observable which can defined by recording the photons in the far-field, or, like in the Afshar *et al.* first experiment, by recording the photons fringes in the back focal plane of the lens (the back focal plane is the plane where the momentum distribution $\hbar k$ is experimentally and rigorously defined [16]). Like it is for K, the meaning of V is also very clear: if $V = 1$ both apertures must play a symmetrical role, whereas if $V = 0$ only one aperture is open.

A direct mathematical consequence of equations (2) and (5) is the relation

$$V^2 + K^2 = 1, \quad (6)$$

which expresses the duality [25, 26] between the two mathematical measures K and V associated with the two mutually exclusive (i.e., complementary) experiments in the direct and Fourier space respectively. A particularly important application of equation (6) concerns which-path experiments. In such experiments, we wish to observe the interference pattern, and to find through each hole each photon is going through. As we explained before, a photon can not be observed twice, and this represents in general a fatal end for such expectations. There is however an important exception in the particular case with only one aperture open (i.e., $K = 1$). Indeed, in such case it is not necessary to record the photon in the aperture plane to know its path since if it is detected (in the back focal plane) it necessarily means that it went through the opened aperture. Of course, from equation (6) we have in counterpart $V = 0$, which means that fringes are not possible.

This dilemma, can not be solved by considering less invasive methods, like those using entanglement between the photon and an other quantum system or an internal degree of freedom (such as polarization or spins). To see that we consider a wave function $|\Psi\rangle$ describing the entanglement between the photon and these others quantum variables defining a which-path detector. We write

$$|\Psi\rangle = \int [C_1\delta(x - d/2)|x\rangle|\gamma_1\rangle + C_2\delta(x + d/2)|x\rangle|\gamma_2\rangle]dx$$
$$= \int [C_1 \cdot e^{ikd/2}|k\rangle|\gamma_1\rangle + C_2 \cdot e^{-ikd/2}|k\rangle|\gamma_2\rangle]dp \quad (7)$$

where $|\gamma_1\rangle$ and $|\gamma_2\rangle$ are the quantum state of the which-path detector if the photon is going through the aperture 1 or 2. Consider now the kind of information one can extract from $|\Psi\rangle$. First, by averaging (tracing) over the detector degrees of freedom we can define the total probability $P(x) = \mathrm{Tr}[\hat{\rho}|x\rangle\langle x|]$ of detecting a photon in the aperture plane in x by

$$P(x) \propto |C_1|^2\langle\gamma_1|\gamma_1\rangle(\delta(x - d/2))^2$$
$$+|C_2|^2\langle\gamma_2|\gamma_2\rangle(\delta(x + d/2))^2. \quad (8)$$

with $\hat{\rho} = |\Psi\rangle\langle\Psi|$ is the total density matrix. By analogy with equation (2) the total distinguishability is then defined by

$$K = \frac{||C_1|^2\langle\gamma_1|\gamma_1\rangle - |C_2|^2\langle\gamma_2|\gamma_2\rangle|}{|C_1|^2\langle\gamma_1|\gamma_1\rangle + |C_2|^2\langle\gamma_2|\gamma_2\rangle}. \quad (9)$$

Same as for equations (3-5) we can define the total probability to detect a photon of (transverse) wave vector k by

$$P(k) = \mathrm{Tr}[\hat{\rho}|k\rangle\langle k|] \propto 1 + V\cos(kx + \phi), \tag{10}$$

where the visibility V is written

$$V = \frac{2|C_1| \cdot |C_2| \cdot |\langle\gamma_1|\gamma_2\rangle|}{|C_1|^2\langle\gamma_1|\gamma_1\rangle + |C_2|^2\langle\gamma_2|\gamma_2\rangle}. \tag{11}$$

By combining V and K we deduce immediately $K^2 + V^2 = \eta^2 \leq 1$ with

$$\eta^2 = 1 - \frac{4|C_1|^2 \cdot |C_2|^2 \cdot (\langle\gamma_1|\gamma_1\rangle\langle\gamma_2|\gamma_2\rangle - |\langle\gamma_1|\gamma_2\rangle|^2)}{(|C_1|^2\langle\gamma_1|\gamma_1\rangle + |C_2|^2\langle\gamma_2|\gamma_2\rangle)^2} \tag{12}$$

and where the inequality results from the Cauchy-Schwartz relation $\langle\gamma_1|\gamma_1\rangle\langle\gamma_2|\gamma_2\rangle - |\langle\gamma_1|\gamma_2\rangle|^2 \geq 0$.
However, we can remark that by tracing over the degrees of freedom associated with the detector we did not consider a which-path experiment but simply decoherence due to entanglement. In order to actually realize such a which-path experiment we need to calculate the joint probability associated with a recording of the photon in the state $|x\rangle$ (or $|k\rangle$) in coincidence with a measurement of the detector in the eigenstate $|\lambda\rangle$ corresponding to one of its observable. These joint probabilities read $P(x,\lambda) = \mathrm{Tr}[\hat{\rho}|x\rangle\langle x||\lambda\rangle\langle\lambda|]$ and $P(k,\lambda) = \mathrm{Tr}[\hat{\rho}|k\rangle\langle k||\lambda\rangle\langle\lambda|$ with

$$\begin{aligned} P(x,\lambda) &\propto |C_1|^2|\langle\lambda|\gamma_1\rangle|^2(\delta(x - d/2))^2 \\ &+|C_2|^2|\langle\lambda|\gamma_2\rangle|^2(\delta(x + d/2))^2 \\ P(k,\lambda) &=\propto 1 + V_\lambda\cos(kx + \phi_\lambda). \end{aligned} \tag{13}$$

Indeed, the aim of such entanglement with a degree of freedom $|\lambda\rangle$ (produced for example by inserting polarization converters like quarter or half wave-plates just after the apertures [32]) is to generate a wave function

$$\psi_\lambda(x) \sim C_{1,\lambda}\delta(x - d/2) + C_{2,\lambda}\delta(x + d/2) \tag{14}$$

with either $C_{1,\lambda}$ or $C_{2,\lambda}$ (but not both) equal to zero. A subsequent projection on $|\lambda\rangle$ will reveal the path information. However, from the duality relation given by equation (5) applied to $\psi_\lambda(x)$ it is now obvious that we did not escape from the previous conclusion. Indeed, while the photon was not destroyed by the entanglement with the which-path detector, we unfortunately only obtained path distinguishability ($K_\lambda = 1$) at the expense of losing the interference behavior ($V_\lambda = 0$).
From all these experiments, it is clear that the discreteness of photon, and more generally of every quantum object, is the key element to understand complementarity. This was evident without entanglement, since the only way to observe a particle is to destroy it. However, even the introduction of a 'which-path' quantum state $|\lambda\rangle$ does not change the rule of the game, since at the end of journey we necessarily need to project, that is to kill macroscopically, the quantum system. This fundamental fact, was already pointed out many times by Bohr in his writings when he considered the importance of separating the macroscopic world of the observer from the microscopic quantum system observed, and also when he insisted on the irreversible act induced by the observer on the quantum system during any measurement process [4].

Let now return to the interpretation of Afshar *et al*. experiments. In the configuration with the lens and without the grid, we have apparently a new aspect of the problem since the fringes occur in a plane located before the imaging plane. Contrarily to the which-path experiments above mentioned, where the destructive measurements occurred in the interference plane, we have a priori here the freedom to realize a 'fringes-interaction free-experiment' which aim is to observe the fringes without detecting the particle in the back focal plane whereas the destructive measurement will occur in the image plane (i.e., in 1' or 2'). The role of the grid is expected to provide such information necessary for the interference reconstruction. Due to the absence of disturbance by the grid, Afshar *et al*. logically deduce that the field equals zero at the wires locations. If we *infer* the existence of an interference pattern with visibility V we must have

$$V = \frac{(I_{max} - I_{min})}{(I_{max} + I_{min})} = \frac{(I_{max} - 0)}{(I_{max} + 0)} = 1, \tag{15}$$

since $I_{min} = 0$. This means that we can obtain the value of the visibility only from the two assumptions that (i) the form of the profile should be a 'cos' function given by equation (4), and that (ii) no photon have been absorbed by the wires. Finally in this experiment, we record the photons in the area 1' (or 2') and consequently we have at the same time the path information. Importantly, following Afshar *et al*. we here only consider one image spot 1' or 2' (since each photon impinges one only one of these two regions) and we deduce therefore $K = 1$. Together with the interference visibility $V = 1$ this implies

$$K^2 + V^2 = 2, \tag{16}$$

in complete contradiction with the bound given by equation (6).

In the previous analysis we only considered the infinitely thin wires to simplify the discussion. Actually, this is however the only experimental configuration in which the Afshar experiment is easily analyzable since it is only in such case that the duality relation can be defined. Indeed, scattering by the wire always results into complicated diffraction pattern in the image plane and the simple mathematical derivation [25–28] leading to equations 2, 5, and 6 is not possible. We will then continue to consider the idealized case of the infinitely thin wires in the rest of the paper since it is this ideal limit that the authors of [1]wanted obviously to reach.

3 The rebuttal: Inference and Complementarity

3.1 Duality again

There are several reasons why the analysis by Afshar *et al.* actually fails. First, from a mathematical point of view it is not consistent to write $K^2 + V^2 = 2$. Indeed, in all the experiments previously discussed (excluding the Afshar experiments) it was necessary to consider statistics on all the recorded photons in order to observe either the interference or the path information (in the case were entanglement was involved only the photons tagged by $|\lambda\rangle$ have to be considered). Same here, if one consider all the detected photons one will deduce $K = 0$ and equation (6) will be respected. Actually, this results directly from the experimental method considered by the authors of [1]. Indeed, if somebody is accepting the existence of an interference pattern he or she needs to know the complete distribution 1' *and* 2' recorded in the image plane. This is necessary in order to deduce that the wire grid didn't caused any disturbances on the propagation. Indeed, the disturbance could have no consequence in 1' but yet have some effects in 2'. Consequently, ignoring 2' does not allow us to deduce that the experiment with the grid is interaction-free. For this reason, it is unjustified to write $K = 1$, that is to consider only one half of the detected photon population, while we actually need both pinhole images to deduce the value of V (this is also in agreement with the obvious fact that an interference pattern requires the two apertures 1 and 2 opened for its existence).

There is an other equivalent way to see why the choice $K = 0$ is the only one possible. Indeed, having measured in the image plane the two distributions 1' and 2' with intensity $|C_1|^2$ and $|C_2|^2$ we can, by applying the laws of optics, propagate backward in time the two converging beams until the interference plane (this was done by Afshar *et al.*). In this plane equation (4) and (5), which are a direct consequence of these above mentioned optical laws, are of course valid. Since we have $|C_1|^2 = |C_2|^2$, we deduce (from equations (2) and (5)) that $K = 0$ and $V = 1$ in full agreement with the duality relation (6). It is important to remark that since the phase of C_1 and C_2 are not know from the destructive measurements in the image plane, we cannot extrapolate the value of $\chi = \arg(C_1) - \arg(C_2)$. However, the presence of the grid give us access to this missing information since it provides the points where $I(k) = 0$ (for example if $I(\pi/d) = 0$ then $\chi = 2\pi \cdot N$ with N =0, 1, ...). We can thus define completely the variable V and χ without recording any photon in the Fourier plane. It is clear, that this would be impossible if the duality condition $K^2 + V^2 = 1$ was not true since this relation is actually a direct consequence of the law of optics used in our derivations as well as in the one by Afshar *et al.*.

To summarize the present discussion, we showed that Afshar *et al.* reasoning is obscured by a misleading interpretation of the duality relation given by equation (6). We however think that this problem is not so fundamental for the discussion of the experiment. Actually, we can restate the complete reasoning without making any reference to this illusory violation of equation (6). After doing this we think that the error in the deductions by Afshar *et al.* should become very clear. Let then restate the story:

A) First, we record individuals photons in the regions 1' and 2'. We can then keep a track or a list of each detection event, so that, for each photon, we can define its 'path' information. However, this individual property of each photon is not entering in conflict with the statistical behavior, which in the limit of large number, give us the two narrow distribution in 1' and 2'. That is, the value $K = 0$ is not in conflict with the existence of a which-path information associated with each photon. This situation differs strongly from usual which-path experiments in which the path detection, or tagging, is done *before* the interference plane. As we explained before in these experiments the value $K = 1$ was a necessary consequence of the preselection procedure done on the photon population. This point also means that we have to be very prudent when we use the duality relation in experimental situations different from the ones for which a consensus has already been obtained.

B) Second, we apply the laws of optics backward in time to deduce the value of the visibility V. Inferring the validity of such optical laws we can even reconstruct completely the interference profile thanks to the presence of wire grid.

C) Finally, we can check that indeed $K^2+V^2 = 1$ in agreement with the duality relation.

Having elucidated the role of the duality relation, the question that we have still to answer is what are the implications of this experiment for complementarity. What has indeed been shown by Afshar *et al.* is that each photon detected in the image plane is associated with a wave behavior since none of them crossed the wires. Using the laws of optics backward in time allow us to deduce the precise shape of intensity profile in the back focal plane but this is a theoretical inference and actually not a measurement. We will now show that this is the weak point.

3.2 Classical versus quantum inferences

In classical physics, such an inference (i.e., concerning interference) is of no consequence since we can always, at least in principle, imagine a test particle or detector to check the validity of our assumptions concerning the system. However, in quantum mechanics we are dealing with highly sensitive systems and this modify the rules of the game.

In quantum mechanics it is common to say that the wave function represents the catalog of all the potentiality accessible to the system. Due to the very nature of this theory there are however some (complementary) pages which can not be read at the same time without contradictions. In the Afshar experiment, we do not have indeed the slightest experimental proof that the observed photons did participate to the "cos"

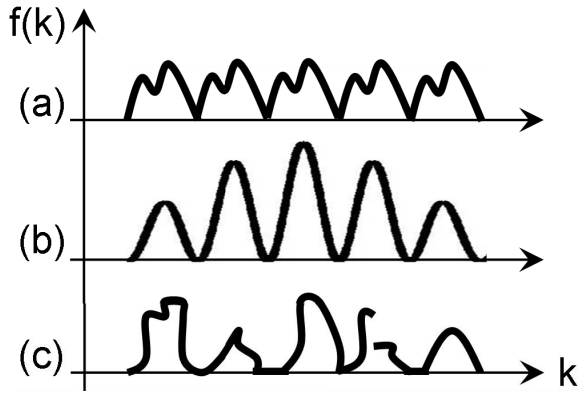

Fig. 2: Different possible intensity profiles in the Fourier plane. Each profile $f(k)$ obeys to the condition $f(k) = 0$ on the wires. (a) A continuous periodic function. (b) The diffractive interference profile predicted by quantum mechanics. (c) A discontinuous profile intensity. Each profile is 'apriori' equiprobable for an observer which has no knowledge in optics and quantum mechanics.

interference pattern given by equations (3) and (4). Furthermore, by detecting the photons in the image plane, we only know from the experiment that the photons never crossed the wires but this is not sufficient to rebuild objectively the complete interference pattern.

We can go further in this direction by using information theory. Indeed, from the point of view of the information theory of Gibbs [33], Shannon [34], and Jaynes [35], every interference patterns, such that $I(k) = 0$ on the wires, are equiprobable (see Fig. 2). However, there are an infinity of such profiles, so that our information is rather poor. More precisely, let write $\rho[f(k)]$ the functional giving the density of probability associated with the apriori likelihood of having the interference profile $f(k)$ located in an infinitely small (functional) volume $\mathcal{D}[f(k)]$. We write $\Sigma[f(x)]$ the space of all this interference profiles obeying to the condition $f(k) = 0$ on the wires. We have thus $\rho[f(k)] = 1/\Sigma$ (equiprobability) for the function f contained in Σ, and $\rho[f(k)] = 0$ for the function outside Σ (that are functions which do not satisfy the requirements $f(k) = 0$ on the wires). The Shannon entropy [33–35] $S[f(x)]$ associated with this distribution is given by

$$S[f(x)] = -\int_{(\Sigma)} \mathcal{D}[f(k)]\rho[f(k)] \ln(\rho[f(k)]) = \ln(\Sigma[f(k)]) \to +\infty, \qquad (17)$$

which expresses our absence of objective knowledge concerning $f(k)$. In this reasoning, we used the concept of probability taken in the Bayesian sense, that is in the sense of decision-maker theory used for example by poker players. For an observer which do not have any idea concerning quantum mechanics and the laws of optics, this equiprobability is the most reasonable guess if he wants only to consider the photons he actually detected. Of course, by considering a different experiment, in which the photons are recorded in the Fourier plane, the observer might realize what is actually the interference pattern. However (and this is essential for understanding the apparent paradox discussed in reference 1) it will be only possible by considering different recorded photons in full agreement with the principle of complementarity.

Let now summarize a bit our analysis. We deduced that in the experiment discussed in [1] the photons used to *measure* objectively the interference pattern i.e. to calculate the visibility $V = 1$ are not the same than those used to *measure* the distribution in the image plane and calculate the distinguishability $K = 0$. This is strictly the same situation than in the original two-holes experiment already mentioned. It is in that sense that the relationship (6) represents indeed a particular formulation of complementarity [25–28]. Actually (as we already commented before) the value $V = 1$ obtained in [1] does not result from a measurement but from an extrapolation. Indeed, from their negative measurement Afshar et al. recorded objectively $I_{min} = 0$. If we suppose that there is a hidden sinusoidal interference pattern in the plane of the wires we can indeed write

$$V = (I_{max} - I_{min}) / (I_{max} + I_{min}) = I_{max}/I_{max} = 1. \qquad (18)$$

However to prove experimentally that such sinusoidal interference pattern actually exists we must definitively record photons in the rest of the wires plane. This is why the experiment described in [1] does not constitutes a violation of complementarity.

It is finally interesting to remark that similar analysis could be easily done already in the Young two-holes experiment. Indeed, suppose that we record the photon interference fringes after the holes. We can thus measure $V = 1$. However, if we suppose that the sinusoidal oscillation of the intensity results from the linear superposition of waves coming from holes 1 and 2 then from equation 5 we deduce $|C_1|^2 + |C_2|^2 - 2|C_1||C_2| = 0$ i. e., $|C_1| = |C_2|$. From equation 2 this implies $K = 0$. Reasoning like Afshar *et al.* we could be tempted to see once again a violation of complementarity since we deduced the distinguishability without disturbing the fringes! However, we think that our previous analysis sufficiently clarified the problem so that paradoxes of that kind are now naturally solved without supplementary comments.

3.3 The objectivity of trajectory in quantum mechanics

At the end of section 2.1 we shortly pointed that the concept of trajectory is a key issue in the analysis of the experiment reported in reference 1. This was also at the core of most commentaries (e.g. references [6–14]) concerning the work by Afshar *et al.*. As a corollary to the previous analysis we will now make a brief comment concerning the concept of path and trajectory in quantum mechanics since we think that a lot of confusion surrounds this problem. This is also important because Afshar *et al.* claimed not only that they can

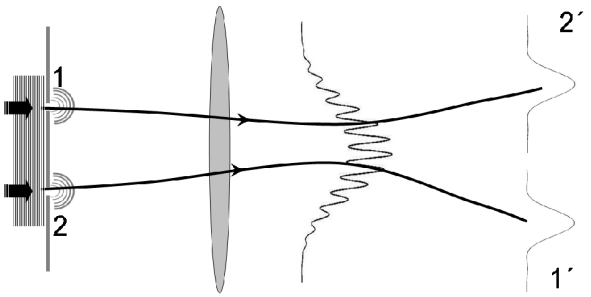

Fig. 3: Illustration of the counterintuitive paths followed by photons if we accept the ontological interpretation given by de Broglie and Bohm. The photons coming from aperture 1 or 2 reach the 'wrong' detector 2' or 1'.

circumvent complementarity but that additionally they determine the *path* chosen by the particle. Following here an intuitive assumption they accepted that with the two pinholes open a photon trajectory (if trajectory there is) connects necessarily a pinhole to its optical image like it is in geometrical optics. They called that intuition (probably in analogy with what occurs in classical physics) a 'consequence of momentum conservation'. However, the meaning of momentum and trajectory is not the same in quantum and classical mechanics. Actually, as it was realized by several physicists the connection 1 to 1' and 2 to 2' is a strong hypothesis which depends of our model of (hidden) reality and which can not in general be experimentally tested (read for example [29, 36]).

Actually nothing in this experiment with two holes forbids a photon coming from one pinhole to go in the *wrong* detector associated with the second pinhole. This is the case for example in the *hidden variable* theory of de Broglie-Bohm in which every photons coming from the aperture 1 (respectively 2) is reaching the wrong image spot 2'(respectively 1') [29, 36] as shown in figure 3. This is counter intuitive but not in contradiction with experiments since we can not objectively test such hidden variable model [36]. In particular closing one pinhole will define unambiguously the path followed by the particle. However this is a different experiment and the model shows that the trajectories are modified (in general non locally) by the experimental context. The very existence of a model like the one of de Broglie and Bohm demonstrates clearly that in the (hidden) quantum reality a trajectory could depend of the complete context of the experiment. For this reason we must be very prudent and conservative when we interpret an experiment: Looking the image of a pinhole recorded in a statistical way by a cascade of photon will not tell us from which pinhole an individual photon come from but only how many photons crossed this pinhole. In counterpart of course we can not see the fringes and the complementarity principle of Bohr will be, as in every quantum experiment, naturally respected. It is thus in general dangerous to speak unambiguously of a which-path experiment and this should preferably be avoided from every discussions limited to empirical facts. As claimed by Bohr the best empirical choice is in such conditions to accept that *it is wrong to think that the task of physics is to find out how Nature is. Physics concerns what we can say about Nature* [4].

4 Conclusion

To conclude, in spite of some claims we still need at least two complementary experiments in order to exploit the totality of the phenomenon in Young-like interferometers. Actually, as pointed out originally by Bohr, we can not use information associated with a same photon event to reconstruct in a statistical way (i.e. by a accumulation of such events) the two complementary distributions of photons in the image plane of the lens and in the interference plane. The presence of the wires inserted in reference 1 does not change anything to this fact since the information obtained by adding the wires is too weak and not sufficient to rebuild objectively (i. e. , unambiguously from experimental data) the whole interference pattern. The reasoning of Afshar *et al.* is therefore circular and the experiment is finally in complete agreement with the principle of complementarity.

Submitted on September 12, 2010 / Accepted on September 15, 2010

References

1. Afshar S., Flores E., McDonalds K. F., Knoesel E. Paradox in wave-particle duality. *Foundations of Physics*, 2007, v. 37, 295-–305.
2. Afshar S. Violation of Bohr's complementarity: one slit or both? *AIP Conference Proceedings*, 2006 v. 810, 294-–299.
3. Bohr N. Discussions with Einstein on epistemological problems in atomic physics. Albert Einstein philosopher-scientist, edited by P. A. Schilpp, The library of living philosophers, Evanston, 1949, pp. 200–241.
4. Bohr N. Can quantum-mechanical description of physical reality be considered complete? *Physical Review*, 1935, v. 48, 696–702.
5. Drezet A. Complementarity and Afshar's experiment. arXiv:quant-ph/0508091v3.
6. Kastner R. Why the Afshar experiment does not refute complementarity? *Studies in history and philosophy of modern physics*, 2005 v. 36, 649–658.
7. Kastner R. On Visibility in the Afshar Two-Slit Experiment. *Foundations of Physics*, 2009, v. 39, 1139–1144.
8. Steuernagel O. Afshar's Experiment Does Not Show a Violation of Complementarity. *Foundations of Physics*, 2007, v. 37, 1370–1385.
9. Qureshi T. Complementarity and the Afshar Experiment. arXiv:quant-ph/0701109v2.
10. Flores E. V. Reply to Comments of Steuernagel on the Afshar's Experiment. *Foundations of Physics*, 2008, v. 38, 778–781.
11. Flores E. V., Knoesel E. Why Kastner analysis does not apply to a modified Afshar experiment. arXiv:quant-ph/0702210.
12. Jacques V. et al. Illustration of quantum complementarity using single photons interfering on a grating. *New Journal of Physics*, 2008, v. 10, 123009.
13. Georgiev D. D. Single photon experiments and quantum complementarity. *Progress in Physics*, 2007, v. 2, 97–103; Ibid 2007, v. 3, 28.

14. Unruh W. G. Comment on "single photon experiments and quantum complementarity" by D. Georgiev. *Progress in Physics*, 2007, v. 3, 27–27. See also: http://axion.physics.ubc.ca/rebel.html
15. Feynman R. P., Leighton R., Sand M. The Feynman Lectures on Physics. Vol. 3, Adisson Wesley, Reading, 1965.
16. Zeilinger A. Experiment and the foundations of quantum physics. *Review of Modern Physics*, 1999, v. 71, S288–S297.
17. Scully M. O., Englert B. G., Walther H. Quantum optical tests of complementarity. *Nature*, 1991, v. 351, 111–116.
18. Drezet A., Hohenau H., Krenn J. R. Heisenberg optical near-field microscope. *Physical Review A*, 2006, v. 73, 013402.
19. Drezet A., Hohenau H., Krenn J. R. Momentum transfer for momentum transfer-free which-path experiments. *Physical Review A*, 2006, v. 73, 062112.
20. de Broglie L. Ondes et Mouvements. Gauthier-Villars, Paris, 1926.
21. Bohm D. A Suggested Interpretation of the Quantum Theory in Terms of "Hidden" Variables. Part 1 and 2. *Physical Review* 1952, v. 85, 166–179 and 180–193.
22. Greene B. The fabric of the cosmos. Alfred A. Knopf, New York 2004.
23. Wheeler J. A. Mathematical Foundations of Quantum Physics. A. R. Marlow (Editor), Academic, NewYork, 1978.
24. In the actual experimental setup considered in [1] the lens is located far away from the two pinholes so that it is in practice equivalent to observe the fringes in front of the lens or in its back focal plane.
25. Englert B. G. Fringe Visibility and Which-Way Information: An Inequality. *Physical Review Letters*, 1996, v. 77, 2154–2157.
26. Greenberger D. M., Yasin A. Simultaneous wave and particle knowledge in a neutron interferometer. *Physics Letters A*, 1988, v. 128, 391–394.
27. Wooters W. K., Zurek W. H. Complementarity in the double-slit experiment: Quantum nonseparability and a quantitative statement of Bohr's principle. *Physical Review D*, 1979, v. 19, 473–484.
28. Jaeger G., Shimony A., Vaidman L. Two interferometric complementarities. *Physical Review A*, 1995, v. 51, 54–67.
29. Englert B.-G., Scully M. O., Süssmann G., Walther H. Surrealistic Bohm trajectories. *Zeitschrift für Naturforschung A*, 1992, v. 47, 1175–1186.
30. Vaidman L. The reality in bohmian quantum mechanics or can you kill with an empty wave bullet? *Foundations of Physics*, 2005, v. 35, 299–312.
31. Bohm D. J., Dewdney C., Hiley B. H. A quantum potential approach to the Wheeler delayed-choice experiment. *Nature*, 1985, v. 315, 294–297.
32. Bartell L. S. Complementarity in the double-slit experiment: On simple realizable systems for observing intermediate particle-wave behavior. *Physical Review D*, 1980, v. 21, 1698–1699.
33. Gibbs J. W. Elementary Principles in Statiscal Mechanics. Longmans Green and Company, NewYork, 1928.
34. Shannon C. E., Weaver W. The mathematical theory of communications. University of Illinois Press, Urbana,1949.
35. Jaynes E. T. Information theory and statistical mechanics. *Physical Review*, 1957 v. 106, 620–630.
36. Hiley B. J. and Callaghan R. E. What is Erased in the Quantum Erasure? *Foundations of Physics*, 2007, v.36, 1869-1883.

Noise and Fano-factor Control in AC-Driven Aharonov-Casher Ring

Walid A. Zein*, Nabil A. Ibrahim†, and Adel H. Phillips*

*Faculty of Engineering, Ain-Shams University, Cairo, Egypt
†Higher Technological Institute, Ramadan Tenth City, Egypt
E-mail: adel_phillips@yahoo.com

The spin dependent current and Fano factor of Aharonov-Casher semiconducting ring is investigated under the effect of microwave, infrared, ultraviolet radiation and magnetic field. Both the average current and the transport noise (Fano factor) characteristics are expressed in terms of the tunneling probability for the respective scattering channels. For spin transport induced by microwave and infrared radiation, a random oscillatory behavior of the Fano factor is observed. These oscillations are due to constructive and destructive spin interference effects. While for the case of ultraviolet radiation, the Fano factor becomes constant. This is due to that the oscillations has been washed out by phase averaging (i.e. ensemble dephasing) over the spin transport channels. The present investigation is very important for quantum computing and information processing.

1 Introduction

The field of spintronics is devoted to create, store, manipulate at a given location, and transport coherent electron spin states through dilute magnetic semiconductors and conventional semiconductor heterostructure [1]. The two principle challenges for new generation of spintronics devices are efficient injection of spins into various semiconductor nanostructures and coherent control of spin. In particular, preserving spin coherence, which enables coherent superpositions of states $a|\uparrow\rangle + b|\downarrow\rangle$ and corresponding quantum-interference effects, is essential for both quantum computing with spin-based qubits [2, 3]. The electrical control of spin via Rashba spin-orbit coupling [4], which arises due to inversion asymmetry of the confining electric potential for tow-dimensional electron gas (2DEG), is very important physical parameter when dealing with semiconductor spintronics. The pursuit of fundamental spin interference effects, as well as spin transistors with unpolarized charge currents [3, 5–10] has generated considerable interest to demonstrate the Aharonov-Casher effect via transport experiments in spin-orbit coupled semiconductor nanostructures [7, 11].

The ballistic spin-resolved shot noise and consequently Fano factor in Aharonov-Casher semiconducting ring is investigated in the present paper. The effects of both electromagnetic field of wide range of frequencies and magnetic field are taken into consideration.

2 Theoretical Formulation

It is well known that shot noise and consequently Fano factor is a powerful quantity to give information about controlling decoherence of spin dependent phenomena [12, 13]. So we shall deduce an expression for both shot noise and Fano factor for spintronic device considered in the paper [10]. This device is modeled as follows: Aharonov-Casher interferometer ring in which a semiconductor quantum dot is embedded

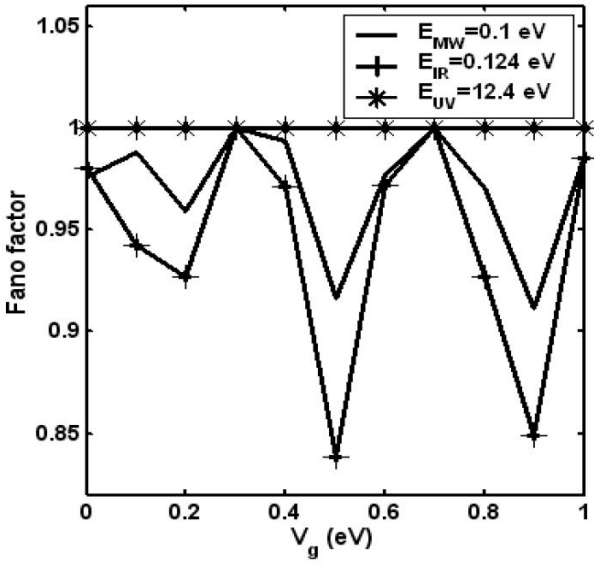

Fig. 1: The variation of Fano factor with gate voltage at different photon energies.

in one arm of the ring. The form of the confining potential is modulated by an external gate electrode allowing for direct control of the electron spin-orbit coupling. The effect of electromagnetic field of wide range of frequencies (microwave, infrared, ultraviolet) is taken into consideration.

The spin dependent shot noise $S_{\alpha\beta}^{\sigma\sigma'}(t-t')$ is expressed in terms of the spin resolved currents $I(\uparrow)$, and $I(\downarrow)$ due to the flow of spin-up $\uparrow$ and spin-down $\downarrow$ electrons through the terminals of the present device [14] as

$$S_{\alpha\beta}^{\sigma\sigma'}(t-t') = \frac{1}{2}\left\langle \delta\hat{I}_{\alpha}^{\sigma}(t)\,\delta\hat{I}_{\beta}^{\sigma'}(t') + \delta\hat{I}_{\beta}^{\sigma'}(t')\,\delta\hat{I}_{\alpha}^{\sigma}(t)\right\rangle \quad (1)$$

where $\hat{I}_{\alpha}^{\sigma}(t)$ is the quantum mechanical operator of the spin resolved ($\sigma \Rightarrow \uparrow, \downarrow$) current in left lead α, $\hat{I}_{\beta}^{\sigma'}(t')$ is the same

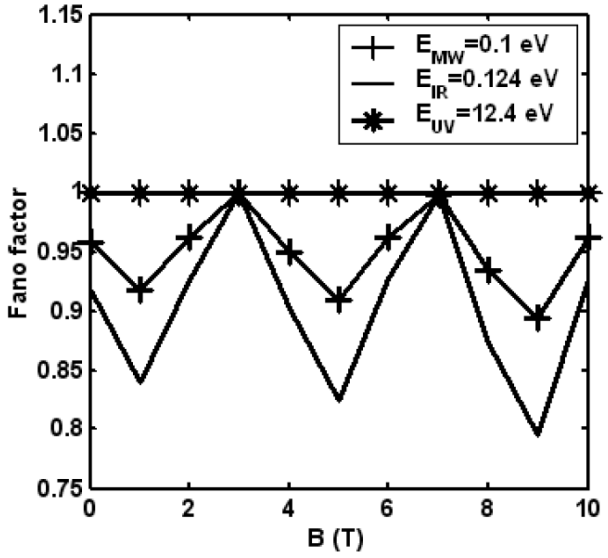

Fig. 2: The variation of Fano factor with magnetic field at different photon energies.

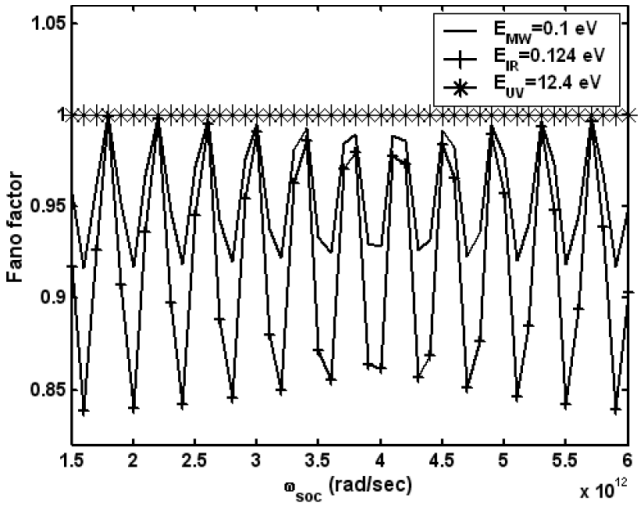

Fig. 3: The variation of Fano factor with frequency ω_{Soc} at different photon energies.

definition of $\hat{I}^{\sigma}_{\alpha}(t)$, but for the right lead β. In Eq. (1), the parameter $\delta\hat{I}^{\sigma}_{\alpha}(t)$ represents the current fluctuation operator at time t in the left lead α with spin state σ (up or down) and is given by

$$\delta\hat{I}^{\sigma}_{\alpha}(t) = \hat{I}^{\sigma}_{\alpha}(t) - \left\langle \hat{I}^{\sigma}_{\alpha}(t) \right\rangle \tag{2}$$

where $\langle --\rangle$ denotes an ensemble average. The Fourier transform of Eq.(1), which represents the spin resolved noise power between the left and right terminals of the device, is given by

$$S^{\sigma\sigma'}_{\alpha\beta}(\omega) = 2\int d(t-t')\, e^{-i\omega(t-t')} S^{\sigma\sigma'}_{\alpha\beta}(t-t'). \tag{3}$$

Since the total spin dependent current is given by

$$I_{\alpha} = I^{\uparrow}_{\alpha} + I^{\downarrow}_{\alpha}, \tag{4}$$

the corresponding noise power is expressed as

$$S_{\alpha\beta}(\omega) = S^{\uparrow\uparrow}_{\alpha\beta}(\omega) + S^{\downarrow\downarrow}_{\alpha\beta}(\omega) + S^{\uparrow\downarrow}_{\alpha\beta}(\omega) + S^{\downarrow\uparrow}_{\alpha\beta}(\omega). \tag{5}$$

Now, expressing the spin-resolved current $\hat{I}^{\sigma}_{\alpha}(t)$ in terms of the creation and annihilation operators of the incoming electrons $\hat{a}^{\sigma+}_{\alpha}(E)$, $\hat{a}^{\sigma}_{\alpha}(E')$ and for the outgoing electrons $\hat{b}^{\sigma+}_{\alpha}(E+n\hbar\omega)$, $\hat{b}^{\sigma}_{\alpha}(E'+n\hbar\omega)$ [15], as follows:

$$\hat{I}^{\sigma}_{\alpha}(t) = \frac{e}{h}\sum_{n}\int\int dE dE' e^{i(E-E')t/\hbar} \times \left[\hat{a}^{\sigma+}_{\alpha}(E)\,\hat{a}^{\sigma}_{\alpha}(E') - \hat{b}^{\sigma+}_{\alpha}(E+n\hbar\omega)\,\hat{b}^{\sigma}_{\alpha}(E'+n\hbar\omega)\right]. \tag{6}$$

Now, in order to evaluate the shot noise spectrum $S_{\alpha\beta}(\omega)$ this can be achieved by substituting Eq.(6) into Eq.(1), and using the transmission eigenfunctions [10] through the present spintronic device, we can determine the expectation value [15, 16]. We get an expression for the shot noise spectrum $S_{\alpha\beta}(\omega)$ as follows:

$$S_{\alpha\beta}(\omega) = \frac{2eP_0}{h}\sum_{\sigma}\int_{0}^{\infty} dE \left|\Gamma_{\mu\ with\ photon}(E)\right|^2 \times f_{\alpha FD}(E) \times \left[1 - f_{\beta FD}(E+n\hbar\omega)\right] \tag{7}$$

where $\left|\Gamma_{\mu\ with\ photon}(E)\right|^2$ is the tunneling probability induced by the external photons, and $f_{\alpha FD}(E)$, $f_{\beta FD}(E+n\hbar\omega)$ are the Fermi distribution functions, and P_0 is the Poissonian shot noise spectrum [15].

The tunneling probability $\left|\Gamma_{\mu\ with\ photon}(E)\right|^2$ has been determined previously by the authors [10]

The Fano factor, F, of such mesoscopic device is given by [17]:

$$F = \frac{S_{\alpha\beta}(\omega)}{2eI}. \tag{8}$$

The explicit expression for the Fano factor, F, can be written as, after some algebraic computation of Eqs.(7, 8), [18, 19]:

$$F = \frac{\left[\sum_{n}\sum_{\mu}\left|\Gamma_{\mu\ with\ photon}(E)\right|^2\left(1 - \left|\Gamma_{\mu\ with\ photon}(E)\right|^2\right)\right]}{\sum_{n}\sum_{\mu}\left|\Gamma_{\mu\ with\ photon}(E)\right|^2}. \tag{9}$$

3 Results and Discussion

The Fano factor F Eq.(9) has been computed numerically as a function of the gate voltage V_g magnetic field B and function of the frequency ω_{Soc} due to spin-orbit coupling. These calculations are performed over a wide range of frequencies

of the induced electromagnetic field (microwave, MW, infrared, IR, and ultraviolet, UV). We use the semiconductor heterostructures as *InGaAs/InAlAs* as in the paper [10]. The main features of the present obtained results are:

(1) Fig.1, shows the dependence of Fano factor on the gate voltage V_g at photon energies for microwave, infrared, and ultraviolet. As shown from the figure that, the Fano factor fluctuates between maximum and minimum values for the two cases microwave and infrared irradiation. While for the case of ultraviolet irradiation, the Fano factor is constant and approximately equals $\sim$1.

(2) Fig.2, shows the dependence of Fano factor on the magnetic field B at photon energies for microwave, infrared, and ultraviolet. The trend of this dependence is similar in a quite fair to the trend and behavior of Fig.1.

(3) Fig.3, shows the dependence of Fano factor on the frequency ω_{Soc} associated with the spin-orbit coupling at photon energies for microwave, infrared, and ultraviolet. An oscillatory behavior for this dependence for the two cases microwave and infrared are shown. While for the case of ultraviolet, the Fano factor is constant and approximately equals $\sim$1 as in Figs. 1, 2.

These results might be explained as follows: Computations show that the average current suppression is accompanied by a noise maxima and remarkably low minima (Fano factor). These cases are achieved when the electron spin transport is influenced by both microwave and infrared photons. Such results have been observed previously by the authors [20–22]. The random oscillatory behavior of the Fano factor can be understood as the strength of the spin-orbit coupling is modified by the gate electrode covering the Aharonov-Casher ring to tune constructive and destructive spin interference effect [10]. For the case of the induced ultraviolet radiation, the results show that the Fano factor becomes approximately constant. These results have been observed previously by the authors [23,24]. The constancy of Fano factor might be due to washing out of the oscillations by phase averaging (i.e. ensemble dephasing) over the spin transport channels [23, 24].

We conclude that these phenomena can be used to devise novel spintronic devices with a priori controllable noise levels. The present investigation is very important for quantum computing and quantum information processing.

Submitted on September 9, 2010 / Accepted on September 14, 2010

References

1. Zutic I., Fabian J., Das Sarma S. Spintronics: Fundamentals and Applications. *Review of Modern Physics*, 2004, v. 76, 323–410.
2. Nikolic B. K., Zarbo L. P., Souma S. Imaging Mesoscopic Spin Hall Flow: Spatial Distribution of Local Spin Currents and Spin Densities in and out of Multiterminal Spin-Orbit Coupled Semiconductor Nanostructures. *Physical Review B*, 2006, v. 73, 075303.
3. Fabian J., Matos-Abiaguea A., Ertlera C., Stano P., Zutic I. Semiconductor Spintronics. *Acta Physica Slovaca*, 2007, v. 57, 565–907.
4. Rashba E. I. Electron Spin Operation by Electric Fields: Spin Dynamics and Spin Injection. *Physica E*, 2004, v. 20, 189–195.
5. Nitta J., Meijer F. E., Takayanagi H. Spin Interference Device. *Applied Physics Letters*, 1999, v. 75, 695–697.
6. Nitta J., Bergsten T. Time Reversal Aharonov-Casher Effect Using Rashba Spin-Orbit Interaction. *New Journal of Physics*, 2007, v.9, 341–352.
7. Frustaglia D., Richter K. Spin Interference Effects in Ring Conductors Subject to Rashba Coupling. *Physical Review B*, 2004, v.69, 235310.
8. Zein W. A., Phillips A. H., Omar O. A. Quantum Spin Transport in Mesoscopic Interferometer. *Progress in Physics*, 2007, v. 4, 18–21.
9. Zein W. A., Phillips A. H., Omar O. A. Spin Coherent Transport in Mesoscopic Interference Device. *NANO*, 2007, v. 2, no. 6, 389–392.
10. Zein W. A., Ibrahim N. A., Phillips A. H. Spin Dependent Transport through Aharonov-Casher Ring Irradiated by an Electromagnetic Field. *Progress in Physics*, 2010, v. 4, 78–81.
11. Konig M., Tschetschetkin A., Hankiewicz E. M., Sinova J., Hock V., Daumer V., Schafer M., Beacker C. R., Buhmann H., Molenkamp L. W. Direct Observation of the Aharonov-Casher Phase. *Physical Review Letters*, 2006, v. 96, 076804.
12. Awschalom D. D., Flatte M. E. Challenges for Semiconductor Spintronics. *Nature Physics*, 2007, v. 3, 153–159.
13. Sukhorukov E. V., Burkard G., Loss D. Noise of a Quantum dot System in the Cotunneling Regime. *Physical Review B*, 2001, v. 63, 125315.
14. Sauret O., Feinberg D. Spin-Current Shot Noise as a probe of Interactions in Mesoscopic Systems. *Physical Review Letters*, 2004, v. 92, 106601.
15. Mina A. N., Phillips A. H. Frequency Resolved Detection over a Large Frequency Range of the Fluctuations in an Array of Quantum Dots. *Progress in Physics*, 2006, v. 4, 11–17.
16. Beenakker C. W. J., Buttiker M. Suppression of Shot Noise in Metallic Diffusive Conductors. *Physical Review B*, 1992, v. 46, R1889.
17. Blanter Ya. M., Buttiker M., Shot Noise in Mesoscopic Conductors. *Physics Reports*, 2000, v. 336, 1–166.
18. Dragomirova R. L., Nikolic B. K. Shot Noise of Spin Polarized Charge Currents as a Probe of Spin Coherence in Spin-Orbit Coupled Nanostructures. *Physical Review B*, 2007, v. 75, 085328.
19. Liang-Zhong L., Rui Z., Wen-Ji D. Shot Noise in Aharonov-Casher Rings. *Chinese Physics Letters*, 2010, v. 27, no. 6, 067306.
20. Camalet S., Lehmann J., Kohler S., Hanggi P. Current Noise in ac-driven Nanoscale Conductors. *Physical Review Letters*, 2003, v. 90, 210602.
21. Camalet S., Kohler S., Hanggi P. Shot Noise Control in AC-driven Nanoscale Conductors. *Physical Review B*, 2004, v. 70, 155326.
22. Sanchez R., Kohler S., Platero G. Spin Correlation in Spin Blockade. *New Journal of Physics*, 2008, v. 10, 115013.
23. Souma S., Nikolic B. K. Modulating unpolarized Current in Quantum Spintronics: Visibility of Spin Interfering Effects in Multichannel Aharonov-Casher Mesoscopic Rings. *Physical Review B*, 2004, v. 70, 195346.
24. Padurariu C., Amin A. F., Kleinekathofer U. Laser-Assisted Electron Transport in Nanoscale Devices, in: Radons G., Rumpf B., Schuster H. G (Editors), Nonlinear Dynamics of Nanosystems, Wiley-VCH, 2009.

Smarandache's Minimum Theorem in the Einstein Relativistic Velocity Model of Hyperbolic Geometry

Cătălin Barbu
"Vasile Alecsandri" College — Bacău, str. Vasile Alecsandri, nr.37, 600011, Bacău, Romania. E-mail: kafka_mate@yahoo.com.

In this note, we present a proof to the Smarandache's Minimum Theorem in the Einstein Relativistic Velocity Model of Hyperbolic Geometry.

1 Introduction

Hyperbolic Geometry appeared in the first half of the 19^{th} century as an attempt to understand Euclid's axiomatic basis of Geometry. It is also known as a type of non-Euclidean Geometry, being in many respects similar to Euclidean Geometry. Hyperbolic Geometry includes similar concepts as distance and angle. Both these geometries have many results in common but many are different. There are known many models for Hyperbolic Geometry, such as: Poincaré disc model, Poincaré half-plane, Klein model, Einstein relativistic velocity model, etc. Here, in this study, we give hyperbolic version of Smarandache minimum theorem in the Einstein relativistic velocity model of hyperbolic geometry. The well-known Smarandache minimum theorem states that if ABC is a triangle and AA', BB', CC' are concurrent cevians at P, then

$$\frac{PA}{PA'} \cdot \frac{PB}{PB'} \cdot \frac{PC}{PC'} \geq 8$$

and

$$\frac{PA}{PA'} + \frac{PB}{PB'} + \frac{PC}{PC'} \geq 6$$

(see [1]).

Let D denote the complex unit disc in complex z-plane, i.e.

$$D = \{z \in \mathbb{C} : |z| < 1\}.$$

The most general Möbius transformation of D is

$$z \to e^{i\theta} \frac{z_0 + z}{1 + \overline{z_0} z} = e^{i\theta}(z_0 \oplus z),$$

which induces the Möbius addition $\oplus$ in D, allowing the Möbius transformation of the disc to be viewed as a Möbius left gyrotranslation

$$z \to z_0 \oplus z = \frac{z_0 + z}{1 + \overline{z_0} z}$$

followed by a rotation. Here $\theta \in \mathbb{R}$ is a real number, $z, z_0 \in D$, and $\overline{z_0}$ is the complex conjugate of z_0. Let $Aut(D, \oplus)$ be the automorphism group of the grupoid $(D, \oplus)$. If we define

$$gyr : D \times D \to Aut(D, \oplus), gyr[a, b] = \frac{a \oplus b}{b \oplus a} = \frac{1 + a\overline{b}}{1 + \overline{a}b},$$

then is true gyrocommutative law

$$a \oplus b = gyr[a, b](b \oplus a).$$

A gyrovector space $(G, \oplus, \otimes)$ is a gyrocommutative gyrogroup $(G, \oplus)$ that obeys the following axioms:
(1) $gyr[\mathbf{u}, \mathbf{v}]\mathbf{a} \cdot gyr[\mathbf{u}, \mathbf{v}]\mathbf{b} = \mathbf{a} \cdot \mathbf{b}$ for all points $\mathbf{a}, \mathbf{b}, \mathbf{u}, \mathbf{v} \in G$.
(2) G admits a scalar multiplication, $\otimes$, possessing the following properties. For all real numbers $r, r_1, r_2 \in \mathbb{R}$ and all points $\mathbf{a} \in G$:
(G1) $1 \otimes \mathbf{a} = \mathbf{a}$
(G2) $(r_1 + r_2) \otimes \mathbf{a} = r_1 \otimes \mathbf{a} \oplus r_2 \otimes \mathbf{a}$
(G3) $(r_1 r_2) \otimes \mathbf{a} = r_1 \otimes (r_2 \otimes \mathbf{a})$
(G4) $\frac{|r| \otimes \mathbf{a}}{\|r \otimes \mathbf{a}\|} = \frac{\mathbf{a}}{\|\mathbf{a}\|}$
(G5) $gyr[\mathbf{u}, \mathbf{v}](r \otimes \mathbf{a}) = r \otimes gyr[\mathbf{u}, \mathbf{v}]\mathbf{a}$
(G6) $gyr[r_1 \otimes \mathbf{v}, r_1 \otimes \mathbf{v}] = 1$
(3) Real vector space structure $(\|G\|, \oplus, \otimes)$ for the set $\|G\|$ of onedimensional "vectors"

$$\|G\| = \{\pm \|\mathbf{a}\| : \mathbf{a} \in G\} \subset \mathbb{R}$$

with vector addition $\oplus$ and scalar multiplication $\otimes$, such that for all $r \in \mathbb{R}$ and $\mathbf{a}, \mathbf{b} \in G$,
(G7) $\|r \otimes \mathbf{a}\| = |r| \otimes \|\mathbf{a}\|$
(G8) $\|\mathbf{a} \oplus \mathbf{b}\| \leqslant \|\mathbf{a}\| \oplus \|\mathbf{b}\|$

Theorem 1. ***(Ceva's theorem for hyperbolic triangles).*** *If M is a point not on any side of an gyrotriangle ABC in a gyrovector space $(V_s, \oplus, \otimes)$, such that AM and BC meet in A', BM and CA meet in B', and CM and AB meet in C', then*

$$\frac{\gamma_{|AC'|}\,|AC'|}{\gamma_{|BC'|}\,|BC'|} \cdot \frac{\gamma_{|BA'|}\,|BA'|}{\gamma_{|CA'|}\,|CA'|} \cdot \frac{\gamma_{|CB'|}\,|CB'|}{\gamma_{|AB'|}\,|AB'|} = 1,$$

where $\gamma_{\mathbf{v}} = \frac{1}{\sqrt{1 - \frac{\|\mathbf{v}\|^2}{s^2}}}$.

(See [2, p. 564].) For further details we refer to the recent book of A.Ungar [3].

Theorem 2. ***(Van Aubel's theorem in hyperbolic geometry).*** *If the point P does lie on any side of the hyperbolic triangle ABC, and BC meets AP in D, CA meets BP in E, and AB meets CP in F, then*

$$\frac{\gamma_{|AP|}\,|AP|}{\gamma_{|PD|}\,|PD|} = \frac{\gamma_{|BC|}\,|BC|}{2}\left(\frac{\gamma_{|AE|}\,|AE|}{\gamma_{|EC|}\,|EC|} \cdot \frac{1}{\gamma_{|BD|}\,|BD|}\right) + \frac{\gamma_{|BC|}\,|BC|}{2}\left(\frac{\gamma_{|FA|}\,|FA|}{\gamma_{|FB|}\,|FB|} \cdot \frac{1}{\gamma_{|CD|}\,|CD|}\right).$$

(See [4].)

2 Main result

In this section, we prove Smarandache's minimum theorem in the Einstein relativistic velocity model of hyperbolic geometry.

Theorem 3. *If ABC is a gyrotriangle and AA', BB', CC' are concurrent cevians at P, then*

$$\frac{\gamma_{|AP|}\,|AP|}{\gamma_{|PA'|}\,|PA'|}\cdot\frac{\gamma_{|BP|}\,|BP|}{\gamma_{|PB'|}\,|PB'|}\cdot\frac{\gamma_{|CP|}\,|CP|}{\gamma_{|PC'|}\,|PC'|}\geqslant 1,$$

and

$$\frac{\gamma_{|AP|}\,|AP|}{\gamma_{|PA'|}\,|PA'|}+\frac{\gamma_{|BP|}\,|BP|}{\gamma_{|PB'|}\,|PB'|}+\frac{\gamma_{|CP|}\,|CP|}{\gamma_{|PC'|}\,|PC'|}\geqslant 3.$$

Proof. We set

$$|A'C|=a_1,|BA'|=a_2,|B'A|=b_1,$$

$$|B'C|=b_2,|C'B|=c_1,|C'A|=c_2,$$

$$\frac{\gamma_{|AP|}\,|AP|}{\gamma_{|PA'|}\,|PA'|}\cdot\frac{\gamma_{|BP|}\,|BP|}{\gamma_{|PB'|}\,|PB'|}\cdot\frac{\gamma_{|CP|}\,|CP|}{\gamma_{|PC'|}\,|PC'|}=P,$$

$$\frac{\gamma_{|AP|}\,|AP|}{\gamma_{|PA'|}\,|PA'|}+\frac{\gamma_{|BP|}\,|BP|}{\gamma_{|PB'|}\,|PB'|}+\frac{\gamma_{|CP|}\,|CP|}{\gamma_{|PC'|}\,|PC'|}=S.$$

If we use the Van Aubel's theorem in the gyrotriangle ABC (See Theorem 2), then

$$\frac{\gamma_{|AP|}|AP|}{\gamma_{|PA'|}|PA'|}=\frac{\gamma_{|BC|}|BC|}{2}\left(\frac{\gamma_{|AB'|}|AB'|}{\gamma_{|CB'|}|CB'|}\cdot\frac{1}{\gamma_{|BA'|}|BA'|}\right)+\frac{\gamma_{|BC|}|BC|}{2}\left(\frac{\gamma_{|AC'|}|AC'|}{\gamma_{|BC'|}|BC'|}\cdot\frac{1}{\gamma_{|CA'|}|CA'|}\right)$$

$$=\frac{\gamma_a a}{2}\left[\frac{\gamma_{b_1}b_1}{\gamma_{b_2}b_2}\cdot\frac{1}{\gamma_{a_2}a_2}+\frac{\gamma_{c_2}c_2}{\gamma_{c_1}c_1}\cdot\frac{1}{\gamma_{a_1}a_1}\right],\qquad(1)$$

and

$$\frac{\gamma_{|BP|}|BP|}{\gamma_{|PB'|}|PB'|}=\frac{\gamma_{|CA|}|CA|}{2}\left(\frac{\gamma_{|BC'|}|BC'|}{\gamma_{|AC'|}|AC'|}\cdot\frac{1}{\gamma_{|CB'|}|CB'|}\right)+\frac{\gamma_{|CA|}|CA|}{2}\left(\frac{\gamma_{|BA'|}|BA'|}{\gamma_{|CA'|}|CA'|}\cdot\frac{1}{\gamma_{|AB'|}|AB'|}\right)$$

$$=\frac{\gamma_b b}{2}\left[\frac{\gamma_{c_1}c_1}{\gamma_{c_2}c_2}\cdot\frac{1}{\gamma_{b_2}b_2}+\frac{\gamma_{a_2}a_2}{\gamma_{a_1}a_1}\cdot\frac{1}{\gamma_{b_1}b_1}\right],\qquad(2)$$

and

$$\frac{\gamma_{|CP|}|CP|}{\gamma_{|PC'|}|PC'|}=\frac{\gamma_{|AB|}|AB|}{2}\left(\frac{\gamma_{|CA'|}|CA'|}{\gamma_{|BA'|}|BA'|}\cdot\frac{1}{\gamma_{|AC'|}|AC'|}\right)+\frac{\gamma_{|AB|}|AB|}{2}\left(\frac{\gamma_{|CB'|}|CB'|}{\gamma_{|AB'|}|AB'|}\cdot\frac{1}{\gamma_{|BC'|}|BC'|}\right)$$

$$=\frac{\gamma_c c}{2}\left(\frac{\gamma_{a_1}a_1}{\gamma_{a_2}a_2}\cdot\frac{1}{\gamma_{c_2}c_2}+\frac{\gamma_{b_2}b_2}{\gamma_{b_1}b_1}\cdot\frac{1}{\gamma_{c_1}c_1}\right).\qquad(3)$$

If we use the Ceva's theorem in the gyrotriangle ABC (See Theorem 1), we have

$$\frac{\gamma_{|CA'|}\,|CA'|}{\gamma_{|BA'|}\,|BA'|}\cdot\frac{\gamma_{|AB'|}\,|AB'|}{\gamma_{|CB'|}\,|CB'|}\cdot\frac{\gamma_{|BC'|}\,|BC'|}{\gamma_{|AC'|}\,|AC'|}=\frac{\gamma_{a_1}a_1}{\gamma_{a_2}a_2}\cdot\frac{\gamma_{b_1}b_1}{\gamma_{b_2}b_2}\cdot\frac{\gamma_{c_1}c_1}{\gamma_{c_2}c_2}=1.\qquad(4)$$

From (1) and (4), we have

$$\frac{\gamma_{|AP|}\,|AP|}{\gamma_{|PA'|}\,|PA'|}=\frac{\gamma_a a}{2}\left(\frac{\gamma_{b_1}b_1\gamma_{c_2}c_2}{\gamma_{a_2}a_2\gamma_{b_2}b_2\gamma_{c_2}c_2}\right)+\frac{\gamma_a a}{2}\left(\frac{\gamma_{b_1}b_1\gamma_{c_2}c_2}{\gamma_{a_1}a_1\gamma_{b_1}b_1\gamma_{c_1}c_1}\right)=\frac{\gamma_a a}{2}\cdot\frac{2\gamma_{b_1}b_1\gamma_{c_2}c_2}{\gamma_{a_2}a_2\gamma_{b_2}b_2\gamma_{c_2}c_2}$$

$$=\frac{\gamma_a a\gamma_{b_1}b_1\gamma_{c_2}c_2}{\gamma_{a_2}a_2\gamma_{b_2}b_2\gamma_{c_2}c_2}.\qquad(5)$$

Similary we obtain that

$$\frac{\gamma_{|BP|}\,|BP|}{\gamma_{|PB'|}\,|PB'|}=\frac{\gamma_b b\gamma_{c_1}c_1\gamma_{a_2}a_2}{\gamma_{a_2}a_2\gamma_{b_2}b_2\gamma_{c_2}c_2},\qquad(6)$$

and

$$\frac{\gamma_{|CP|}\,|CP|}{\gamma_{|PC'|}\,|PC'|}=\frac{\gamma_c c\gamma_{a_1}a_1\gamma_{b_2}b_2}{\gamma_{a_2}a_2\gamma_{b_2}b_2\gamma_{c_2}c_2}.\qquad(7)$$

From the relations (5), (6) and (7) we get

$$P=\frac{\gamma_a a\gamma_{b_1}b_1\gamma_{c_2}c_2\cdot\gamma_b b\gamma_{c_1}c_1\gamma_{a_2}a_2\cdot\gamma_c c\gamma_{a_1}a_1\gamma_{b_2}b_2}{\left(\gamma_{a_2}a_2\gamma_{b_2}b_2\gamma_{c_2}c_2\right)^3}=\frac{\gamma_a a\gamma_b b\gamma_c c}{\gamma_{a_2}a_2\gamma_{b_2}b_2\gamma_{c_2}c_2}\qquad(8)$$

and

$$S=\frac{\gamma_a a\gamma_{b_1}b_1\gamma_{c_2}c_2+\gamma_b b\gamma_{c_1}c_1\gamma_{a_2}a_2+\gamma_c c\gamma_{a_1}a_1\gamma_{b_2}b_2}{\gamma_{a_2}a_2\gamma_{b_2}b_2\gamma_{c_2}c_2}.\qquad(9)$$

Because $\gamma_a\geqslant\gamma_{a_2},\gamma_b\geqslant\gamma_{b_2}$, and $\gamma_c\geqslant\gamma_{c_2}$ result

$$\gamma_a\gamma_b\gamma_c\geqslant\gamma_{a_2}\gamma_{b_2}\gamma_{c_2}.\qquad(10)$$

Therefore

$$\frac{\gamma_a a\gamma_b b\gamma_c c}{\gamma_{a_2}a_2\gamma_{b_2}b_2\gamma_{c_2}c_2}\geqslant 1.\qquad(11)$$

From the relations (8) and (11), we obtain that $P \geqslant 1$. If we use the inequality of arithmetic and geometric means, we obtain

$$S \geqslant 3\sqrt[3]{\frac{\gamma_a a\gamma_{b_1} b_1\gamma_{c_2} c_2 \cdot \gamma_b b\gamma_{c_1} c_1\gamma_{a_2} a_2 \cdot \gamma_c c\gamma_{a_1} a_1\gamma_{b_2} b_2}{\left(\gamma_{a_2} a_2\gamma_{b_2} b_2\gamma_{c_2} c_2\right)^3}} =$$

$$= 3\sqrt[3]{\frac{\gamma_a a\gamma_b b\gamma_c c}{\gamma_{a_2} a_2\gamma_{b_2} b_2\gamma_{c_2} c_2}}. \qquad (12)$$

From the relations (11) and (12), we obtain that $S \geqslant 3$. □

3 Conclusion

The special theory of relativity as was originally formulated by Einstein in 1905, [8], to explain the massive experimental evidence against ether as the medium for propagating electromagnetic waves, and Varičak in 1908 discovered the connection between special theory of relativity and hyperbolic geometry, [9]. The Einstein relativistic velocity model is another model of hyperbolic geometry. Many of the theorems of Euclidean geometry are relatively similar form in the Einstein relativistic velocity model, Smarandache minimum theorem is an example in this respect. In the Euclidean limit of large s, $s \to \infty$, gamma factor γ_v reduces to 1, so that the gyroinequalities (11) and (12) reduces to the

$$\frac{PA}{PA'} \cdot \frac{PB}{PB'} \cdot \frac{PC}{PC'} \geqslant 1,$$

and

$$\frac{PA}{PA'} + \frac{PB}{PB'} + \frac{PC}{PC'} \geqslant 3,$$

in Euclidean geometry. We observe that the previous inequalities are "weaker" than the inequalities of Smarandache's theorem of minimum.

References

1. Smarandache F. Nine Solved and Nine Open Problems in Elementary Geometry. arxiv.org/abs/1003.2153.
2. Ungar A. A. Analytic Hyperbolic Geometry and Albert Einstein's Special Theory of Relativity. Hackensack, NJ: World Scientific, 2008.
3. Ungar A. A. A Gyrovector Space Approach to Hyperbolic Geometry. Morgan & Claypool Publishers, 2009.
4. Barbu C., Pişcoran L. Van Aubel's Theorem in the Einstein Relativistic Velocity Model of Hyperbolic Geometry. Analele Universităţii din Timişoara, (to appear).
5. Ungar A. A. Analytic Hyperbolic Geometry Mathematical Foundations and Applications. World Scientific, Hackensack, 2005.
6. Barbu C. Fundamental Theorems of Triangle Geometry. Ed. Unique, Bacău, 2008 (in romanian).
7. Smarandache F. Problémes avec et sans... probléms! Somipress, Morocoo, 1983.
8. Einstein A. Relativity the special and general theory. Crown Publishers, New York, 1961.
9. Varičak V. Beitrage zur nichteuklidischen Geometrie. Jahresberichte des Deutschen Mathematiker Verein, 1908.

S-Denying a Theory

Florentin Smarandache
Department of Mathematics, University of New Mexico, Gallup, NM 87301, USA. E-mail: smarand@unm.edu

In this paper we introduce the operators of *validation* and *invalidation* of a proposition, and we extend the operator of *S-denying* a proposition, or an axiomatic system, from the geometric space to respectively any theory in any domain of knowledge, and show six examples in geometry, in mathematical analysis, and in topology.

1 Definitions

Let **T** be a theory in any domain of knowledge, endowed with an ensemble of sentences **E**, on a given space **M**.

E can be for example an axiomatic system of this theory, or a set of primary propositions of this theory, or all valid logical formulas of this theory, etc. **E** should be closed under the logical implications, i.e. given any subset of propositions $\mathbf{P_1}$, $\mathbf{P_2}$, ... in this theory, if **E** is a logical consequence of them then **Q** must also belong to this theory.

A sentence is a logic formula whose each variable is quantified {i.e. inside the scope of a quantifier such as: $\exists$ (*exist*), $\forall$ ($forall$), modal logic quantifiers, and other various modern logics' quantifiers}.

With respect to this theory, let **P** be a proposition, or a sentence, or an axiom, or a theorem, or a lemma, or a logical formula, or a statement, etc. of **E**.

It is said that **P** is *S-denied*[*] on the space **M** if **P** is valid for some elements of **M** and invalid for other elements of **M**, or **P** is only invalid on **M** but in at least two different ways.

An ensemble of sentences **E** is considered *S-denied* if at least one of its propositions is *S-denied*.

And a theory **T** is *S-denied* if its ensemble of sentences is *S-denied*, which is equivalent to at least one of its propositions being *S-denied*.

The proposition **P** is partially or totally denied/negated on **M**. The proposition **P** can be simultaneously validated in one way and invalidated in (finitely or infinitely) many different ways on the same space **M**, or only invalidated in (finitely or infinitely) many different ways.

The **invalidation** can be done in many different ways.

For example the statement **A** = "$x \neq 5$" can be invalidated as "$x = 5$" (total negation), but "$x \in \{5, 6\}$" (partial negation).

(Use a notation for *S-denying*, for invalidating in a way, for invalidating in another way a different notation; consider it as an operator: neutrosophic operator? A notation for invalidation as well.)

But the statement **B** = "$x > 3$" can be invalidated in many ways, such as "$x \leq 3$", or "$x = 3$", or "$x < 3$", or "x = -7", or "$x = 2$", etc. A negation is an invalidation, but not reciprocally – since an invalidation signifies a (partial or total) degree of negation, so invalidation may not necessarily be a complete negation. The negation of **B** is $\neg\mathbf{B}$ = "$x \leq 3$", while "x = -7" is a partial negation (therefore an invalidation) of **B**.

Also, the statement **C** = "John's car is blue and Steve's car is red" can be invalidated in many ways, as: "John's car is yellow and Steve's car is red", or "John's car is blue and Steve's car is black", or "John's car is white and Steve's car is orange", or "John's car is not blue and Steve's car is not red", or "John's car is not blue and Steve's car is red", etc.

Therefore, we can *S-deny* a theory in finitely or infinitely many ways, giving birth to many partially or totally denied versions/deviations/alternatives theories: $\mathbf{T_1}$, $\mathbf{T_2}$, ... These new theories represent **degrees of negations** of the original theory **T**.

Some of them could be useful in future development of sciences.

Why do we study such ***S-denying* operator**? Because our reality is heterogeneous, composed of a multitude of spaces, each space with different structures. Therefore, in one space a statement may be valid, in another space it may be invalid, and invalidation can be done in various ways. Or a proposition may be false in one space and true in another space or we may have a degree of truth and a degree of falsehood and a degree of indeterminacy. Yet, we live in this mosaic of distinct (even opposite structured) spaces put together.

S-denying involved the creation of the multi-space in geometry and of the *S-geometries* (1969).

It was spelt *multi-space*, or *multispace*, of *S-multispace*, or *mu-space*, and similarly for its: *multi-structure*, or *multistructure*, or *S-multistructure*, or *mu-structure*.

[*]The multispace operator S-denied (*Smarandachely-denied*) has been inherited from the previously published scientific literature (see for example Ref. [1] and [2]).

2 Notations

Let <A> be a statement (or proposition, axiom, theorem, etc.).

a) For the classical Boolean logic *negation* we use the same notation. The negation of <A> is noted by $\neg\mathbf{A}$ and $\neg\mathbf{A} = <nonA>$.

An *invalidation* of <A> is noted by **i(A)**, while a *validation* of <A> is noted by **v(A)**:

$$i(A) \subseteq 2^{<nonA>} \setminus \{\emptyset\} \text{ and } v(A) \subseteq 2^{<A>} \setminus \{\emptyset\}$$

where 2^X means the power-set of X, or all subsets of X.

All possible invalidations of <A> form a set of invalidations, notated by $I(A)$. Similarly for all possible validations of <A> that form a set of validations, and noted by $V(A)$.

b) *S-denying* of <A> is noted by $\mathbf{S\neg(A)}$. S-denying of <A> means some validations of <A> together with some invalidations of <A> in the same space, or only invalidations of <A> in the same space but in many ways.

Therefore, $S\neg(A) \subseteq V(A) \cup I(A)$ or $S\neg(A) \subseteq I(A)^k$, for $k \geq 2$.

3 Examples

Let's see some models of *S-denying*, three in a geometrical space, and other three in mathematical analysis (calculus) and topology.

3.1 The first *S-denying* model was constructed in 1969. This section is a compilation of ideas from paper [1].

An axiom is said *Smarandachely denied* if the axiom behaves in at least two different ways within the same space (i.e., validated and invalided, or only invalidated but in multiple distinct ways).

A *Smarandache Geometry* [SG] is a geometry which has at least one Smarandachely denied axiom.

Let's note any point, line, plane, space, triangle, etc. in such geometry by s-point, s-line, s-plane, s-space, s-triangle respectively in order to distinguish them from other geometries.

Why these hybrid geometries? Because in reality there do not exist isolated homogeneous spaces, but a mixture of them, interconnected, and each having a different structure.

These geometries are becoming very important now since they combine many spaces into one, because our world is not formed by perfect homogeneous spaces as in pure mathematics, but by non-homogeneous spaces. Also, SG introduce the degree of negation in geometry for the first time [for example an axiom is denied 40% and accepted 60% of the space] that's why they can become revolutionary in science and it thanks to the idea of partial denying/accepting of axioms/propositions in a space (making multi-spaces, i.e. a space formed by combination of many different other spaces), as in fuzzy logic the degree of truth (40% false and 60% true).

They are starting to have applications in physics and engineering because of dealing with non-homogeneous spaces.

The first model of S-denying and of SG was the following:

The axiom that through a point exterior to a given line there is only one parallel passing through it [Euclid's Fifth Postulate], was S-denied by having in the same space: no parallel, one parallel only, and many parallels.

In the Euclidean geometry, also called parabolic geometry, the fifth Euclidean postulate that there is only one parallel to a given line passing through an exterior point, is kept or validated.

In the Lobachevsky-Bolyai-Gauss geometry, called hyperbolic geometry, this fifth Euclidean postulate is invalidated in the following way: there are infinitely many lines parallels to a given line passing through an exterior point.

While in the Riemannian geometry, called elliptic geometry, the fifth Euclidean postulate is also invalidated as follows: there is no parallel to a given line passing through an exterior point.

Thus, as a particular case, Euclidean, Lobachevsky-Bolyai-Gauss, and Riemannian geometries may be united altogether, in the same space, by some SG's. These last geometries can be partially Euclidean and partially Non-Euclidean simultaneously.

3.2 Geometric Model (particular case of SG)

Suppose we have a rectangle $ABCD$.

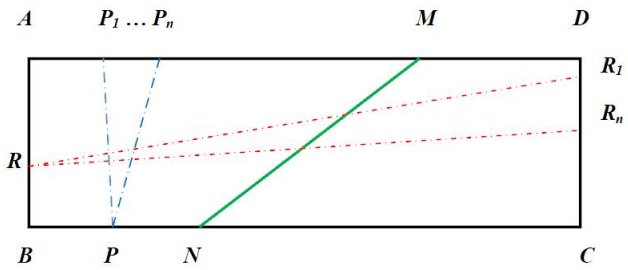

Fig. 1.

In this model we define as:

Point = any point inside or on the sides of this rectangle;

Line = a segment of line that connects two points of opposite sides of the rectangle;

Parallel lines = lines that do not have any common point (do not intersect);

Concurrent lines = lines that have a common point.

Let's take the line MN, where M lies on side AD and N on side BC as in the above *Fig. 1*. Let P be a point on side BC, and R a point on side AB.

Through P there are passing infinitely many parallels (PP_1, ..., PP_n, ...) to the line MN, but through R there is no parallel to the line MN (the lines RR_1, ..., RR_n cut line MN).

Therefore, the Fifth Postulate of Euclid (that though a point exterior to a line, in a given plane, there is only one parallel to that line) in *S-denied* on the space of the rectangle *ABCD* since it is invalidated in two distinct ways.

3.3 Another Geometric Model (another particular case of SG)

We change a little the Geometric Model 1 such that:

The rectangle *ABCD* is such that side *AB* is smaller than side *BC*. And we define as *line* the arc of circle inside (and on the borders) of *ABCD*, centered in the rectangle's vertices *A*, *B*, *C*, or *D*.

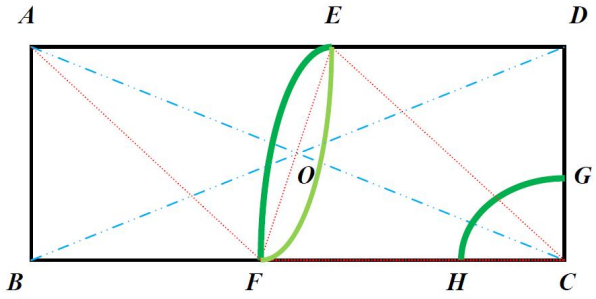

Fig. 2.

The axiom that: through two distinct points there exists only one line that passes through is S-denied (in three different ways):

a) Through the points *A* and *B* there is **no passing line** in this model, since there is no arc of circle centered in *A*, *B*, *C*, or *D* that passes through both points. See *Fig. 2*.

b) We construct the perpendicular $EF \perp AC$ that passes through the point of intersection of the diagonals *AC* and *BD*. Through the points *E* and *F* there are **two distinct lines** the dark green (left side) arc of circle centered in *C* since $CE \equiv FC$, and the light green (right side) arc of circle centered in *A* since $AE \equiv AF$, and because the right triangles $\sqcup\, COE$, $\sqcup\, COF$, $\sqcup\, AOE$, and $\sqcup\, AOF$ are all four congruent, we get $CE \equiv FC \equiv AE \equiv AF$.

c) Through the points *G* and *H* such that $CG \equiv CH$ (their lengths are equal) there is only **one passing line** (the dark green arc of circle *GH*, centered in *C*) since $AG \neq AH$ (their lengths are different), and similarly $BG \neq BH$ and $DG \neq DH$.

3.4 Example for the Axiom of Separation

The Axiom of Separation of Hausdorff is the following:

$$\forall\, x,y \in M\ \exists\, N(x), N(y)\colon\ N(x) \cap N(y) = \emptyset,$$

where *N(x)* is a neighborhood of *x*, and respectively *N(y)* is a neighborhood of *y*.

We can *S-deny* this axiom on a space *M* in the following way:

a) $\exists\, x_1, y_1 \in M$: $\exists\, N_1(x_1), N_1(y_1)$: $N_1(x_1) \cap N_1(y_1) = \emptyset$ where $N_1(x_1)$ is a neighborhood of x_1, and respectively $N_1(y_1)$ is a neighborhood of y_1; [validated].

b) $\exists\, x_2, y_2 \in M$: $\forall\, N_2(x_2), N_2(y_2)$: $N_2(x_2) \cap N_2(y_2) \neq \emptyset$; where $N_2(x_2)$ is a neighborhood of x_2, and respectively $N_2(y_2)$ is a neighborhood of y_2; [invalidated].

Therefore we have two categories of points in *M*: some points that verify The Axiom of Separation of Hausdorff and other points that do not verify it. So *M* becomes a partially separable and partially inseparable space, or we can see that *M* has some **degrees of separation**.

3.5 Example for the Norm

If we remove one or more axioms (or properties) from the definition of a notion <*A*> we get a pseudo-notion <*pseudoA*>.

For example, if we remove the third axiom (inequality of the triangle) from the definition of the <*norm*> we get a <*pseudonorm*>.

The axioms of a **norm** on a real or complex vectorial space *V* over a field *F*, $x \mapsto \|.\|$, are the following:

a) $\|x\| = 0 \Leftrightarrow x = 0$.

b) $\forall\, x \in V, \forall\, \alpha \in F, \|\alpha \cdot x\| = |\alpha| \cdot \|x\|$.

c) $\forall\ x,\ y \in V,\ \|x + y\| \leq \|x\| \cdot \|y\|$ (inequality of the triangle).

For example, a **pseudo-norm** on a real or complex vectorial space *V* over a field *F*, $x \mapsto_p \|.\|$, may verify only the first two above axioms of the norm.

A pseudo-norm is a particular case of an *S-denied norm* since we may have vectorial spaces over some given scalar fields where there are some vectors and scalars that satisfy the third axiom [validation], but others that do not satisfy [invalidation]; or for all vectors and scalars we may have either $\|x + y\| = 5 \cdot \|x\| \cdot \|y\|$ or $\|x + y\| = 6 \cdot \|x\| \cdot \|y\|$, so invalidation (since we get $\|x + y\| > \|x\| \cdot \|y\|$) in two different ways.

Let's consider the complex vectorial space

$$\mathscr{C} = \{\ a+b \cdot i, \text{ where } a, b \in \mathbb{R},\ i = \sqrt{-1}\ \}$$

over the field of real numbers $\mathbb{R}$.

If $z = a+b \cdot i \in \mathscr{C}$ then its pseudo-norm is $\| z \| = \sqrt{a^2 + b^2}$. This verifies the first two axioms of the norm, but does not satisfy the third axiom of the norm since:

For $x = 0 + b \cdot i$ and $y = a + 0 \cdot i$ we get:

$$\|x + y\| = \|a + b \cdot i\| = \sqrt{a^2 + b^2} \leq \|x\| \cdot \|y\|$$
$$= \|0 + b \cdot i\| \cdot \|a + 0 \cdot i\| = |a \cdot b|, \text{ or } a^2 + b^2 \leq a^2 \cdot b^2.$$

But this is true for example when $a = b \geq \sqrt{2}$ (validation), and

false if one of a or b is zero and the other is strictly positive (invalidation).
Pseudo-norms are already in use in today's scientific research, because for some applications the norms are considered too restrictive.

Similarly one can define a pseudo-manifold (relaxing some properties of the manifold), etc.

3.6 Example in Topology

A topology $\mathcal{O}$ on a given set E is the ensemble of all parts of E verifying the following properties:

a) E and the empty set $\emptyset$ belong to $\mathcal{O}$.
b) Intersection of any two elements of $\mathcal{O}$ belongs to $\mathcal{O}$ too.
c) Union of any family of elements of $\mathcal{O}$ belongs to $\mathcal{O}$ too.

Let's go backwards. Suppose we have a topology $\mathcal{O}_1$ on a given set E_1, and the second or third (or both) previous axioms have been *S-denied*, resulting an ***S-denied topology*** $S\neg(\mathcal{O}_1)$ on the given set E_1.

In general, we can go back and "recover" (reconstruct) the original topology $\mathcal{O}_1$ from $S\neg(\mathcal{O}_1)$ by recurrence: if two elements belong to $S\neg(\mathcal{O}_1)$ then we set these elements and their intersection to belong to $\mathcal{O}_1$, and if a family of elements belong to $S\neg(\mathcal{O}_1)$ then we set these family elements and their union to belong to $\mathcal{O}_1$; and so on: we continue this recurrent process until it does not bring any new element to $\mathcal{O}_1$.

Conclusion

Decidability changes in an *S-denied theory*, i.e. a defined sentence in an S-denied theory can be partially deducible and partially undeducible (we talk about **degrees of deducibility of a sentence** in an *S-denied theory*).

Since in classical deducible research, a theory T of language L is said complete if any sentence of L is decidable in T, we can say that an *S-denied theory* is partially complete (or has some **degrees of completeness** and degrees of incompleteness).

Submitted on September 22, 2010 / Accepted on September 26, 2010

References

1. Kuciuk L., Antholy M. An Introduction to Smarandache Geometries. Mathematics Magazine, Aurora, Canada, v. 12, 2003.
2. Mao, Linfan, An introduction to Smarandache geometries on maps. 2005 International Conference on Graph Theory and Combinatorics, Zhejiang Normal University, Jinhua, Zhejiang, P. R. China, June 25-30, 2005.
3. Rabounski D. Smarandache Spaces as a New Extension of the Basic Space-Time of General Relativity. *Progress in Physics*, 2010, v. 2, L1-L2.
4. Smarandache F. Paradoxist Geometry. State Archives from Valcea, Rm. Valcea, Romania, 1969; and in "Paradoxist Mathematics", Collected Papers (Vol. II), Kishinev University Press, Kishinev, 1997, pp. 5-28.
5. Smarandache F. Multi-Space and Multi-Structure, in: "Neutrosophy. Neutrosophic Logic, Set, Probability and Statistics", American Research Press, 1998.
6. Szudzik M., "Sentence", from *MathWorld* – A Wolfram Web Resource, created by Eric W. Weisstein, http://mathworld.wolfram.com/Sentence.html.

On the Quantum Mechanical State of the Δ^{++} Baryon

Eliahu Comay

Charactell Ltd. P.O. Box 39019, Tel Aviv 61390 Israel, E-mail: elicomay@post.tau.ac.il

The Δ^{++} and the Ω^{-} baryons have been used as the original reason for the construction of the Quantum Chromodynamics theory of Strong Interactions. The present analysis relies on the multiconfiguration structure of states which are made of several Dirac particles. It is shown that this property, together with the very strong spin-dependent interactions of quarks provide an acceptable explanation for the states of these baryons and remove the classical reason for the invention of color within Quantum Chromodynamics. This explanation is supported by several examples that show a Quantum Chromodynamics' inconsistency with experimental results. The same arguments provide an explanation for the problem called the proton spin crisis.

1 Introduction

It is well known that writing an atomic state as a sum of terms, each of which belongs to a specific configuration is a useful tool for calculating electronic properties of the system. This issue has already been recognized in the early days of quantum mechanics [1]. For this purpose, mathematical tools (called angular momentum algebra) have been developed mainly by Wigner and Racah [2]. Actual calculations have been carried out since the early days of electronic computers [3]. Many specific properties of atomic states have been proven by these calculations. In particular, these calculations have replaced guesses and conjectures concerning the mathematical form of atomic states by evidence based on a solid mathematical basis. In this work, a special emphasis is given to the following issue: Contrary to a naive expectation, even the ground state of a simple atom is written as a sum of more than one configuration. Thus, the apparently quite simple closed shell ground state of the two electron He atom, having $J^{\pi} = 0^{+}$, *disagrees* with the naive expectation where the two electrons are just in the $1s^2$ state. Indeed, other configurations where individual electrons take higher angular momentum states (like $1p^2$, $1d^2$, etc.) have a non-negligible part of the state's description [3]. The multiconfiguration description of the ground state of the He atom proves that shell model notation of state is far from being complete. Notation of this model can be regarded as an anchor configuration defining the J^{π} of the state. Therefore, all relevant configurations must have the same parity and their single-particle angular momentum must be coupled to the same J.

This paper discusses some significant elements of this scientific knowledge and explains its crucial role in a quantum mechanical description of the states of the Δ^{++}, the Δ^{-} and the Ω^{-} baryons. In particular, it is proved that these baryons do not require the introduction of new structures (like the $SU(3)$ color) into quantum mechanics. A by-product of this analysis is the settlement of the "proton spin crisis" problem.

The paper is organized as follows. The second section describes briefly some properties of angular momentum algebra. It is proved in the third section that ordinary laws of quantum mechanics explain why the states of the Δ^{++}, Δ^{-} and Ω^{-} baryons are consistent with the Pauli exclusion principle. This outcome is used in the fourth section for showing that QCD does not provide the right solution for hadronic states. The problem called "proton spin crisis" is explained in the fifth section. The last section contains concluding remarks.

2 Some Features of Angular Momentum Algebra

Consider the problem of a bound state of N Dirac particles. (Baryonic states are extremely relativistic. Therefore, a relativistic formulation is adopted from the beginning.) This system is described as an eigenfunction of the Hamiltonian. Thus, the time variable is removed and one obtains a problem of $3N$ spatial variables for each of the four components of a Dirac wave function. It is shown here how angular momentum algebra can be used for obtaining a dramatic simplification of the problem.

The required solution is constructed as a sum of terms, each of which depends on all the independent variables mentioned above. Now angular momentum is a good quantum number of a closed system and parity is a good quantum number for systems whose state is determined by strong or electromagnetic interactions. Thus, one takes advantage of this fact and uses only terms that have the required angular momentum and parity, denoted by J^{π}. (Later, the lower case j^{π} denotes properties of a bound spin-1/2 single particle.)

The next step is to write each term as a product of N single particle Dirac functions, each of which has a well defined angular momentum and parity. The upper and lower parts of a Dirac function have opposite parity [4, see p. 53]. The angular coordinates of the two upper components of the Dirac function have angular momentum l and they are coupled with the spin to an overall angular momentum $j = l \pm 1/2$ ($j > 0$). The two lower components have angular momentum $(l \pm 1) \geq 0$ and together with the spin, they are coupled to the same j. The spatial angular momentum eigenfunctions having an eignevalue l, make a set of $(2l + 1)$ members de-

noted by $Y_{lm}(\theta, \phi)$, where θ, ϕ denote the angular coordinates and $-l \le m \le l$ [2].

It is shown below how configurations can be used for describing a required state whose parity and overall spin are known.

3 The Δ^{++} State

The purpose of this section is to describe how the state of each of the four Δ baryons can be constructed in a way that abides by ordinary quantum mechanics of a system of three fermions. Since the $\Delta^{++}(1232)$ baryon has 3 valence quarks of the u flavor, the isospin $I = 3/2$ of all four Δ baryons is fully symmetric. Therefore, the space-spin components of the 3-particle terms must be antisymmetric. (An example of relevant nuclear states is presented at the end of this section.) Obviously, each of the 3-particle terms must have a total spin $J = 3/2$ and an even parity. For writing down wave functions of this kind, single particle wave functions having a definite j^π and appropriate radial functions are used. A product of n specific j^π functions is called a configuration and the total wave function takes the form of a sum of terms, each of which is associated with a configuration. Here n=3 and only even parity configurations are used. Angular momentum algebra is applied to the single particle wave functions and yields an overall $J = 3/2$ state. In each configuration, every pair of the Δ^{++} u quarks must be coupled to an antisymmetric state. r_j denotes the radial coordinate of the jth quark.

Each of the A-D cases described below contains one configuration and one or several antisymmetric 3-particle terms. The radial functions of these examples are adapted to each case.

Notation: $f_i(r_j)$, $g_i(r_j)$, $h_i(r_j)$ and $v_i(r_j)$ denote radial functions of Dirac single particle $1/2^+$, $1/2^-$, $3/2^-$ and $3/2^+$ states, respectively. The index i denotes the excitation level of these functions. Each of these radial functions is a two-component function, one for the upper 2-component spin and the other for the lower 2-component spin that belong to a 4-component Dirac spinor.

A. In the first example all three particles have the same j^π,

$$f_0(r_0)f_1(r_1)f_2(r_2)\ 1/2^+\ 1/2^+\ 1/2^+. \qquad (1)$$

Here the spin part is fully symmetric and yields a total spin of 3/2. The spatial state is fully antisymmetric. It is obtained from the 6 permutations of the three orthogonal $f_i(r_j)$ functions divided by $\sqrt{6}$. This configuration is regarded as the anchor configuration of the state.

B. A different combination of $j_i = 1/2$ can be used,

$$f_0(r_0)g_0(r_1)g_1(r_2)\ 1/2^+\ 1/2^-\ 1/2^-. \qquad (2)$$

Here, the two single particle $1/2^-$ spin states are coupled symmetrically to j=1 and they have two orthogonal radial functions g_i. The full expression can be antisymmetrized.

C. In this example, just one single particle is in an angular excitation state,

$$f_0(r_0)f_0(r_1)v_0(r_2)\ 1/2^+\ 1/2^+\ 3/2^+. \qquad (3)$$

Here we have two $1/2^+$ single particle functions having the same non-excited radial function. These spins are coupled antisymmetrically to a spin zero two particle state. These spins have the same non-excited radial function. The third particle yields the total $J = 3/2$ state. The full expression can be antisymmetrized.

D. Here all the three single particle j^π states take different values. Therefore, the radial functions are free to take the lowest level,

$$f_0(r_0)g_0(r_1)h_0(r_2)\ 1/2^+\ 1/2^-\ 3/2^-. \qquad (4)$$

Due to the different single particle spins, the antisymmetrization task of the spin coordinates can easily be done. (The spins can be coupled to a total $J = 3/2$ state in two different ways. Hence, two different terms belong to this configuration.)

The examples A-D show how a Hilbert space basis for the $J^\pi = 3/2^+$ state can be constructed for three identical fermions. Obviously, more configurations can be added and the problem can be solved by ordinary spectroscopic methods. It should be noted that unlike atomic states, the very strong spin dependent interactions of hadrons are expected to yield a higher configuration mixture.

It is interesting to note that a similar situation is found in nuclear physics. Like the u,d quarks, the proton and the neutron are spin-1/2 fermions belonging to an isospin doublet. This is the basis for the common symmetry of isospin states described below. Table 1 shows energy levels of each of the four A=31 nuclei examined [5, see p. 357]. Each of these nuclei has 14 protons and 14 neutrons that occupy a set of inner closed shells and three nucleons outside these shells. (The closed shells are $1/2^+$, $3/2^-$, $1/2^-$, and $5/2^+$. The next shells are the $1/2^+$ that can take 2 nucleons of each type and the

Table 1: Nuclear A=31 Isospin State Energy levels (MeV)

J^π	I (T)[a]	^{31}Si	^{31}P	^{31}S	^{31}Cl[b]
$1/2^+$	1/2	—	0	0	—
$3/2^+$	3/2	0	6.38	6.27	0
$1/2^+$	3/2	0.75	7.14	7.00	—

[a] I,T denote isospin in particle physics and nuclear physics, respectively.
[b] The ^{31}Cl data is taken from [6].

$3/2^+$ shell that is higher than the $1/2^+$ shell. [7, See p. 245]. The state is characterized by these three nucleons that define the values of total spin, parity and isospin. The first line of table 1 contains data of the ground states of the $I = 1/2$ ^{31}P and ^{31}S nuclei. The second line contains data of the lowest level of the $I = 3/2$ state of the four nuclei. The quite small energy difference between the ^{31}P and ^{31}S excited states illustrates the quite good accuracy of the isospin approximation. The third line of the table shows the first excited $I = 3/2$ state of each of the four nuclei. The gap between states of the third and the second lines is nearly, but not precisely, the same. It provides another example of the relative goodness of the isospin approximation.

The nuclear states described in the first and the second lines of table 1 are relevant to the nucleons and the Δ baryons of particle physics. Indeed, the states of both systems are characterized by three fermions that may belong to two different kinds and where isospin is a useful quantum number. Here the neutron and the proton correspond to the ground state of ^{31}P and ^{31}S, respectively, whereas energy states of the second line of the table correspond to the four Δ baryons. Every nuclear energy state of table 1 has a corresponding baryon that has the same spin, parity, isospin and the I_z isospin component. Obviously, the dynamics of the nuclear energy levels is completely different from hadronic dynamics. Indeed, the nucleons are composite spin-1/2 particles whose state is determined by the strong nuclear force. This is a residual force characterized by a rapidly decaying attractive force at the vicinity of the nucleon size and a strong repulsive force at a smaller distance [7, see p. 97]. On the other hand, the baryonic quarks are elementary pointlike spin-1/2 particles whose dynamics differs completely from that of the strong nuclear force. However, both systems are made of fermions and the spin, parity and isospin analogy demonstrates that *the two systems have the same internal symmetry.*

The following property of the second line of table 1 is interesting and important. Thus, all nuclear states of this line have the same *symmetric* $I = 3/2$ state. Hence, due to the Pauli exclusion principle, all of them have the same *antisymmetric space-spin state.* Now, for the ^{31}P and ^{31}S nuclei, this state is an excited state because they have lower states having $I = 1/2$. However, the ^{31}Si and ^{31}Cl nuclei have no $I = 1/2$ state, because their $I_z = 3/2$. Hence, the second line of table 1 shows *the ground state of the* $I_z = 3/2$ *nuclei*. It will be shown later that this conclusion is crucial for having a good understanding of an analogous quark system. Therefore it is called *Conclusion A*.

Now, the ^{31}Si has three neutrons outside the 28 nucleon closed shells and the ^{31}Cl has three protons outside these shells. Hence, the outer shell of these two nuclear states consists of three identical fermions which make the required ground state. Relying on this nuclear physics example, one deduces that *the Pauli exclusion principle is completely consistent with three identical fermions in a* $J^\pi = 3/2^+$ *and* $I = 3/2$ *ground state.* The data of table 1 are well known in nuclear physics.

A last remark should be made before the end of this section. As explained in the next section, everything said above on the isospin quartet $J^\pi = 3/2^+$ states of the three *ud* quark flavor that make the four Δ baryons, holds for the full decuplet of the three *uds* quarks, where, for example, the Ω^- state is determined by the three *sss* quarks. In particular, like the Δ^{++} and the Δ^-, *the* Ω^- *baryon is the ground state of the three sss quarks and each of the baryons of the decuplet has an antisymmetric space-spin wave function.*

4 Discussion

It is mentioned above that spin-dependent interactions are much stronger in hadronic states than in electronic states. This point is illustrated by a comparison of the singlet and triplet states of the positronium [8] with the π^0 and ρ^0 mesons [9]. The data are given in table 2. The fourth column of the table shows energy difference between each of the $J^\pi = 1^-$ states and the corresponding $J^\pi = 0^-$ state. The last column shows the ratio between this difference and the energy of the $J^\pi = 0^-$ state.

Both electrons and quarks are spin-1/2 pointlike particles. The values of the last column demonstrate a clear difference between electrically charged electrons and quarks that participate in strong interactions. Indeed, the split between the two electronic states is *very small*. This is the reason for the notation of *fine structure* for the spin dependent split between electronic states of the same excitation level [10, see p. 225]. Table 2 shows that the corresponding situation in quark systems is larger by more than 9 orders of magnitude. Hence, spin dependent interactions in hadrons are very strong and make an important contribution to the state's energy.

Now, electronic systems in atoms satisfy the Hund's rules [10, see p. 226]. This rule says that in a configuration, the state having the highest spin is bound stronger. Using this rule *and* the very strong spin-dependent hadronic interaction which is demonstrated in the last column of table 2, one con-

Table 2: Positronium and meson energy (MeV)

Particle	J^π	Mass	$M(1^-) - M(0^-)$	$\Delta M/M(0^-)$
e^+e^-	0^-	~ 1.022	—	—
e^+e^-	1^-	~ 1.022	8.4×10^{-10}	8.2×10^{-10}
π^0	0^-	135	—	—
ρ^0	1^-	775	640	4.7

cludes that the anchor configuration A of the previous section really describes a very strongly bound state of the Δ^{++} baryon. In particular, the isospin doublet $J^\pi = 1/2^+$ state of the neutron and the proton correspond to the same $J^\pi = 1/2^+$ of the ground state of the $A = 31$ nuclei displayed in the first line of table 1. The isospin quartet of the Δ baryons correspond to the isospin quartet of the four nuclear states displayed in the second line of table 1.

Here the significance of Conclusion A of the previous section becomes clear. Indeed, an analogy is found between the two nuclear states of the $I = 3/2$ and $I_z = \pm 1/2$, namely the ^{31}P and the ^{31}S are *excited states* of these nuclei whereas the $I = 3/2$ and $I_z = \pm 3/2$, namely the ^{31}Si and the ^{31}Cl states are the *ground states* of these nuclei. The same pattern is found in the particle physics analogue. The Δ^+ and the Δ^0 are *excited states* of the proton and the neutron, respectively. This statement relies on the fact that both the proton and the Δ^+ states are determined by the *uud* quarks. Similarly, the neutron and the Δ^0 states are determined by the *udd* quarks. On the other hand, in the case of the ^{31}Si and the ^{31}Cl nuclei, the $I = 3/2$ and $J^\pi = 3/2^+$ states are the *ground states* of these nuclei. The same property holds for the Δ^{++} and the Δ^-, which are the *ground states* of the *uuu* and *ddd* quark systems, respectively.

The relationship between members of the lowest energy $J^\pi = 1/2^+$ baryonic octet and members of the $J^\pi = 3/2^+$ baryonic decuplet can be described as follows. There are 7 members of the decuplet that are excited states of corresponding members of the octet. Members of each pair are made of the same specific combination of the *uds* quarks. The Δ^{++}, Δ^- and Ω^- baryons have no counterpart in the octet. Thus, in spite of being a part of the decuplet whose members have space-spin antisymmetric states, these three baryons are the *ground state* of the *uuu, ddd* and *sss* quarks, respectively.

This discussion can be concluded by the following statements: *The well known laws of quantum mechanics of identical fermions provide an interpretation of the* Δ^{++}, Δ^- *and* Ω^- *baryons, whose state is characterized by three uuu, ddd and sss quarks, respectively. There is no need for any fundamental change in physics in general and for the invention of color in particular. Like all members of the decuplet, the states of these baryons abide by the Pauli exclusion principle.* Hence, one wonders why particle physics textbooks regard precisely the same situation of the four Δ baryons as a fiasco of the Fermi-Dirac statistics [11, see p. 5].

The historic reasons for the QCD creation are the states of the Δ^{++} and the Ω^- baryons. These baryons, each of which has three quarks of the same flavor, are regarded as the *classical reason* for the QCD invention [12, see p. 338]. The analysis presented above shows that this argument does not hold water. For this reason, one wonders whether QCD is really a correct theory. This point is supported by the following examples which show that QCD is inconsistent with experimental results.

1. The interaction of hard real photons with a proton is practically the same as its interaction with a neutron [13]. This effect cannot be explained by the photon interaction with the nucleons' charge constituents, because these constituents take different values for the proton and the neutron. The attempt to recruit Vector Meson Dominance (VMD) for providing an explanation is unacceptable. Indeed, Wigner's analysis of the irreducible representations of the Poincare group [14] and [15, pp. 44–53] proves that VMD, which mixes a massive meson with a massless photon, is incompatible with Special relativity. Other reasons of this kind also have been published [16].
2. QCD experts have predicted the existence of strongly bound pentaquarks [17, 18]. In spite of a long search, the existence of pentaquarks has not been confirmed [19]. By contrast, correct physical ideas used for predicting genuine particles, like the positron and the Ω^-, have been validated by experiment after very few years (and with a technology which is very very poor with respect to that used in contemporary facilities).
3. QCD experts have predicted the existence of chunks of Strange Quark Matter (SQM) [20]. In spite of a long search, the existence of SQM has not been confirmed [21].
4. QCD experts have predicted the existence of glueballs [22]. In spite of a long search, the existence of glueballs has not been confirmed [9].
5. For a very high energy, the proton-proton (*pp*) total and elastic cross section increase with collision energy [9] and the ratio of the elastic cross section to the total cross section is nearly a constant which equals about 1/6. This relationship between the *pp* cross sections is completely different from the high energy electron-proton (*ep*) scattering data where the total cross section decreases for an increasing collision energy and the elastic cross section's portion becomes negligible [23]. This effect proves that the proton contains a quite solid component that can take the heavy blow of the high energy collision and keep the entire proton intact. This object cannot be a quark, because in energetic *ep* scattering, the electron strikes a single quark and the relative part of elastic events is negligible. QCD has no explanation for the *pp* cross section data [24].

5 The Proton Spin Crisis

Another problem which is settled by the physical evidence described above is called *the proton spin crisis* [25, 26]. Here polarized muons have been scattered by polarized protons. The results prove that the instantaneous quark spin sums up to a very small portion of the entire proton's spin. This outcome, which has been regarded as a surprise [26], was later

supported by other experiments. The following lines contain a straightforward explanation of this phenomenon.

The four configurations A-D that are a part of the Hilbert space of the Δ^{++} baryon are used as an illustration of the problem. Thus, in configuration A, all single particle spins are parallel to the overall spin. The situation in configuration B is different. Here the single particle function $j^{\pi} = 1/2^{-}$ is a coupling of $l = 1$ and $s = 1/2$. This single particle coupling has two terms whose numerical values are called Clebsh-Gordan coefficients [2]. In one of the coupling terms, the spin is parallel to the overall single particle angular momentum and in the other term it is antiparallel to it. This is an example of an internal partial cancellation of the contribution of the single particle spin to the overall angular momentum. (As a matter of fact, this argument also holds for the lower pair of components of each of Dirac spinor of configuration A. Here the lower pair of the high relativistic system is quite large and it is made of $l = 1$ $s = 1/2$ coupled to $J = 1/2$.) In configuration C one finds the same effect. Spins of the first and the second particles are coupled to $j_{01} = 0$ and cancel each other. In the third particle the $l = 2$ spatial angular momentum is coupled with the spin to $j = 3/2$. Here one also finds two terms and the contribution of their single-particle spin-1/2 partially cancels. The same conclusion is obtained from an analogous analysis of the spins of configuration D.

It should be pointed out that the very large hadronic spin-dependent interaction which is demonstrated by the data of table 2, proves that in hadronic states, one needs many configurations in order to construct a useful basis for the Hilbert space of a baryon. It follows that in hadrons the internal single particle cancellation seen in configurations of the previous section, is expected to be quite large.

Obviously, the configuration structure of the proton relies on the same principles. Here too, many configurations, each of which has the quantum numbers $J^{\pi} = 1/2^{+}$, are needed for the Hilbert space. Thus, a large single particle spin cancellation is obtained. Therefore, the result of [25] is obvious. It should make neither a crisis nor a surprise.

On top of what is said above, the following argument indicates that the situation is more complicated and the number of meaningful configurations is even larger. Indeed, it has been shown that beside the three valence quarks, the proton contains additional quark-antiquark pair(s) whose probability is about 1/2 pair [23, see p. 282]. It is very reasonable to assume that all baryons share this property. The additional quark-antiquark pair(s) increase the number of useful configurations and of their effect on the Δ^{++} ground state and on the proton spin as well.

6 Concluding Remarks

Relying on the analysis of the apparently quite simple ground state of the He atomic structure [3], it is argued here that *many* configurations are needed for describing a quantum mechanical state of more than one Dirac particle. This effect is much stronger in baryons. where, as shown in table 2, spin-dependent strong interactions are very strong indeed. This effect and the multiconfiguration basis of hadronic states do explain the isospin quartet of the $J = 3/2^{+}$ Δ baryons. Here the Δ^0 and the Δ^+ are *excited states* of the neutron and the proton, respectively whereas their isospin counterparts, the Δ^{++} and the Δ^- are *ground states* of the *uuu* and the *ddd* quark systems, respectively. Analogous conclusions hold for all members of the $J = 3/2^{+}$ baryonic decuplet that includes the Ω^- baryon. It is also shown that states of four $A = 31$ nuclei are analogous to the nucleons and the Δs isospin quartet (see table 1).

The discussion presented above shows that there is no need for introducing a new degree of freedom (like color) in order to settle the states of Δ^{++}, Δ^- and Ω^- baryons with the Pauli exclusion principle. Hence, there is no reason for the QCD invention. Several inconsistencies of QCD with experimental data support this conclusion.

Another aspect of recognizing implications of the multi-configuration structure of hadrons is that the proton spin crisis experiment, which shows that instantaneous spins of quarks make a little contribution to the proton's spin [25], creates neither a surprise nor a crisis.

Submitted on November 7, 2010 / Accepted on November 9, 2010

References

1. Wong S. S. M. Nuclear Physics. Wiley, New York, 1998.
2. de-Shalit A. and Talmi I. Nuclear Shell Theory. Academic, New York, 1963.
3. Weiss A. W. Configuration Interaction in Simple Atomic Systems. *Physcal Review*, 1961, v. 122, 1826–1836.
4. Bjorken J. D. and Drell S. D. Relativistic Quantum Mechanics. McGraw, New York, 1964.
5. Endt P. M. Energy Levels of A = 21–44 Nuclei (VII). *Nuclear Physics A*, 1990, v. 521, 1–830.
6. Kankainen A. et al. Excited states in ^{31}S studied via beta decay of ^{31}Cl. *The European Physical Journal A — Hadrons and Nuclei*, 2006, v. 27, 67–75.
7. Wong S. S. M. Nuclear Physics. Wiley, New York, 1998.
8. Berko S. and Pendleton H. N. Positronium. *Annual Review of Nuclear and Particle Science*, 1980, v. 30, 543–581.
9. Nakamura K. et al. (Particle Data Group), Review of Particle Physics 075021. *Journal of Physics G: Nuclear and Particle Physics*, 2010, v. 37, 1–1422.
10. Landau L. D. and Lifshitz E. M. Quantum Mechanics. Pergamon, London, 1959.
11. Halzen F. and Martin A. D. Quarks and Leptons. Wiley, New York, 1984.
12. Close F. E. An Introduction to quarks and Partons. Academic, London, 1979.
13. Bauer T. H., Spital R. D., Yennie D. R. and Pipkin F. M. The Hadronic Properties of the Photon in High-Energy Interactions. *Reviews of Modern Physics*, 1978, v. 50, 261–436.
14. Wigner E. P. On Unitary Representations of the Inhomogeneous Lorentz Group. *The Annals of Mathematics*, 1939, v. 40, 149–204.

15. Schweber S. S. An Introduction to Relativistic Quantum Field Theory. Harper & Row, New York, 1964.
16. Comay E. Remarks on Photon-Hadron Interactions. *Apeiron*, 2003, v. 10 (2), 87–103.
17. Gignoux C., Silvestre-Brac B. and Richard J. M. Possibility of Stable Multiquark Baryons. *Physics Letters B*, 1987, v. 193, 323–326.
18. Lipkin H. J. New Possibilities for Exotic Hadrons–Anticharmed Strange Baryons. *Physics Letters B*, 1987, v. 195, 484–488.
19. Whol C. G. In the 2009 report of PDG at http://pdg.lbl.gov/2009/reviews/rpp2009-rev-pentaquarks.pdf
20. Witten E. Cosmic Separation of Phases. *Physical Review D*, 1984, v. 30, 272–285.
21. Han K. et al. Search for Stable Strange Quark Matter in Lunar Soil. *Physical Review Letters*, 2009, v. 103, 092302-1–092302-4.
22. Frauenfelder H. and Henley E. M. Subatomic Physics. Prentice Hall, Englewood Cliffs, 1991.
23. Perkins D. H. Introductions to High Energy Physics. Addison-Wesley, Menlo Park, 1987.
24. Arkhipov A. A. On Global Structure of Hadronic Total Cross Sections. arXiv: hep-ph/9911533v2
25. Ashman J. et al. (EMC) A Measurement of the Spin Asymmetry and Determination of the Structure Function g_1 in Deep Inelastic Muon-Proton Scattering. *Physics Letters B*, 1988, v. 206, 364–370.
26. Myhrer F. and Thomas A. W. Understanding the Proton's Spin Structure. *Journal of Physics G*, 2010, v. 37, 023101-1–023101–12.

Sound-Particles and Phonons with Spin 1

Vahan Minasyan and Valentin Samoilov
Scientific Center of Applied Research, JINR, Dubna, 141980, Russia
E-mails: mvahan@scar.jinr.ru; scar@off-serv.jinr.ru

We present a new model for solids which is based on the stimulated vibration of independent neutral Fermi-atoms, representing independent harmonic oscillators with natural frequencies, which are excited by actions of the longitudinal and transverse elastic waves. Due to application of the principle of elastic wave-particle duality, we predict that the lattice of a solid consists of two type Sound Boson-Particles with spin 1 with finite masses. Namely, these lattice Boson-Particles excite the longitudinal and transverse phonons with spin 1. In this letter, we estimate the masses of Sound Boson-Particles which are around 500 times smaller than the atom mass.

1 Introduction

The original theory proposed by Einstein in 1907 was of great historical relevance [1]. In the Einstein model, each atom oscillates relatively to its neighbors in the lattice which execute harmonic motions around fixed positions, the knots of the lattice. He treated the thermal property of the vibration of a lattice of N atoms as a $3N$ harmonic independent oscillator by identical own frequency Ω_0 which was quantized by application of the prescription developed by Plank in connection with the theory of Black Body radiation. The Einstein model could obtain the Dulong and Petit prediction at high temperature but could not reproduce an adequate representation of the the lattice at low temperatures. In 1912, Debye proposed to consider the model of the solid [2], by suggestion that the frequencies of the $3N$ harmonic independent oscillators are not equal as it was suggested by the Einstein model. In addition to his suggestion, the acoustic spectrum of solid may be treated as if the solid represented a homogeneous medium, except that the total number of independent elastic waves is cut off at $3N$, to agree with the number of degrees of freedom of N atoms. In this respect, Debye stated that one longitudinal and two transverse waves are excited in solid. These velocities of sound cannot be observed in a solid at frequencies above the cut-off frequency. Also, he suggested that phonon is a spinless. Thus, the Debye model correctly showed that the heat capacity is proportional to the T^3 law at low temperatures. At high temperatures, he obtained the Dulong-Petit prediction compatible to experimental results.

In this letter, we propose a new model for solids which consists of neutral Fermi-atoms, fixed in the knots of lattice. In turn, within the formalism of Debye, we may predict that lattice represents as the Bose-gas of Sound-Particles with finite masses m_l and m_t, corresponding to a longitudinal and a transverse elastic field. In this sense, the lattice is considered as a new substance of matter consisting of Sound-Particles, which excite the one longitudinal and one transverse elastic waves (this approach is differ from Debye one). These waves act on the Fermi-atoms which are vibrating with the natural frequencies Ω_l and Ω_t. Thus, there are stimulated vibrations of the Fermi-atoms by under action of longitudinal and transverse phonons with spin 1. In this context, we introduce a new principle of elastic wave-particle duality, which allows us to build the lattice model. The given model leads to the same results as presented by Debye's theory.

2 Analysis

As we suggest, the transfer of heat from one part of the body to another occurs through the lattice. This process is very slow. Therefore, we can regard any part of the body as thermally insulated, and there occur adiabatic deformations. In this respect, the equation of motion for an elastic continuum medium [3] represents as

$$\varrho\ddot{\vec{u}}(\vec{r},t) = c_t^2\nabla^2\vec{u}(\vec{r},t) + (c_l^2 - c_t^2)\, grad \cdot div\, \vec{u}(\vec{r},t) \qquad (1)$$

where $\vec{u} = \vec{u}(\vec{r},t)$ is the vector displacement of any particle in solid; c_l and c_t are the velocities of a longitudinal and a transverse ultrasonic wave, respectively.

We shall begin by discussing a plane longitudinal elastic wave with condition $\mathrm{curl}\,\vec{u}(\vec{r},t) = 0$ and a plane transverse elastic wave with condition $\mathrm{div}\,\vec{u}(\vec{r},t) = 0$ in an infinite isotropic medium. In this respect, in direction of vector $\vec{r}$ can be propagated two transverse and one longitudinal elastic waves. The vector displacement $\vec{u}(\vec{r},t)$ is the sum of the vector displacements of a longitudinal $u_l(\vec{r},t)$ and of a transverse ultrasonic wave $u_t(\vec{r},t)$:

$$\vec{u}(\vec{r},t) = \vec{u}_l(\vec{r},t) + \vec{u}_t(\vec{r},t) \qquad (2)$$

where $\vec{u}_l(\vec{r},t)$ and $\vec{u}_t(\vec{r},t)$ are perpendicular with each other or $\vec{u}_l(\vec{r},t)\cdot\vec{u}_t(\vec{r},t) = 0$.

In turn, the equations of motion for a longitudinal and a transverse elastic wave take the form of the wave-equations:

$$\nabla^2\vec{u}_l(\vec{r},t) - \frac{1}{c_l^2}\frac{\partial^2\vec{u}_l(\vec{r},t)}{\partial t^2} = 0 \qquad (3)$$

$$\nabla^2\vec{u}_t(\vec{r},t) - \frac{1}{c_t^2}\frac{\partial^2\vec{u}_l(\vec{r},t)}{\partial t^2} = 0. \qquad (4)$$

It is well known, in quantum mechanics, a matter wave is determined by electromagnetic wave-particle duality or de Broglie wave of matter [4]. We argue that in an analogous manner, we may apply the elastic wave-particle duality. This reasoning allows us to present a model of elastic field as the Bose-gas consisting of the Sound Bose-particles with spin 1 and non-zero rest masses, which are interacting with each other. In this respect, we may express the vector displacement of a longitudinal ultrasonic wave $u_l(\vec{r},t)$ via the second quantization vector wave functions of one Sound Boson of the longitudinal wave. In analogy manner, vector displacement of a transverse ultrasonic waves $u_t(\vec{r},t)$ is expressed via the second quantization vector wave functions of one Sound Boson of the transverse wave:

$$\vec{u}_l(\vec{r},t) = u_l\Big(\phi(\vec{r},t) + \phi^+(\vec{r},t)\Big) \tag{5}$$

and

$$\vec{u}_t(\vec{r},t) = u_t\Big(\psi(\vec{r},t) + \psi^+(\vec{r},t)\Big) \tag{6}$$

where u_l and u_t are, respectively, the norm coefficients for longitudinal and transverse waves; $\vec{\phi}(\vec{r},t)$ and $\vec{\phi}^+(\vec{r},t)$ are, respectively, the second quantization wave vector functions for "creation" and "annihilation" of one Sound-Particle of the longitudinal wave, in point of coordinate $\vec{r}$ and time t whose direction $\vec{l}$ is directed toward to wave vector $\vec{k}$; $\vec{\psi}(\vec{r},t)$ and $\vec{\psi}^+(\vec{r},t)$ are, respectively, the second quantization wave vector functions for "creation" and "annihilation" of one Sound-Particle of the transverse wave, in point of coordinate $\vec{r}$ and time t, whose direction $\vec{t}$ is perpendicular to the wave vector $\vec{k}$:

$$\vec{\phi}(\vec{r},t) = \frac{1}{\sqrt{V}}\sum_{\vec{k},\sigma}\vec{a}_{\vec{k},\sigma}e^{i(\vec{k}\vec{r}-kc_lt)} \tag{7}$$

$$\vec{\phi}^+(\vec{r},t) = \frac{1}{\sqrt{V}}\sum_{\vec{k},\sigma}\vec{a}^+_{\vec{k},\sigma}e^{-i(\vec{k}\vec{r}-kc_lt)} \tag{8}$$

and

$$\vec{\psi}(\vec{r},t) = \frac{1}{\sqrt{V}}\sum_{\vec{k},\sigma}\vec{b}_{\vec{k},\sigma}e^{i(\vec{k}\vec{r}+-kc_lt)} \tag{9}$$

$$\vec{\psi}^+(\vec{r},t) = \frac{1}{\sqrt{V}}\sum_{\vec{k},\sigma}\vec{b}^+_{\vec{k},\sigma}e^{-i(\vec{k}\vec{r}-kc_lt)} \tag{10}$$

with condition

$$\begin{aligned}&\int\phi^+(\vec{r},\sigma)\phi(\vec{r},\sigma)dV + \int\psi^+(\vec{r},\sigma)\psi(\vec{r},\sigma)dV = \\ &= n_o + \sum_{\vec{k}\neq0,\sigma}\hat{a}^+_{\vec{k},\sigma}\hat{a}_{\vec{k},\sigma} + \sum_{\vec{k}\neq0,\sigma}\hat{b}^+_{\vec{k},\sigma}\hat{b}_{\vec{k},\sigma} = \hat{n}\end{aligned} \tag{11}$$

where $\vec{a}^+_{\vec{k},\sigma}$ and $\vec{a}_{\vec{k},\sigma}$ are, respectively, the Bose vector-operators of creation and annihilation for one free longitudinal Sound Particle with spin 1, described by a vector $\vec{k}$ whose direction coincides with the direction $\vec{l}$ of the longitudinal wave; $\vec{b}^+_{\vec{k},\sigma}$ and $\vec{b}_{\vec{k},\sigma}$ are, respectively, the Bose vector-operators of creation and annihilation for one free transverse Sound Particles with spin 1, described by a vector $\vec{k}$ which is perpendicular to the direction $\vec{t}$ of the transverse wave; $\hat{n}$ is the operator of total number of the Sound Particles; $\hat{n}_0 = n_{0,l} + n_{0,t}$ is the total number of Sound Particles in the condensate level with wave vector $\vec{k} = 0$ which consists of a number of Sound Particles $n_{0,l}$ of the longitudinal wave and a number of Sound Particles $n_{0,t}$ of the transverse wave.

The energies of longitudinal $\frac{\hbar^2k^2}{2m_l}$ and transverse $\frac{\hbar^2k^2}{2m_t}$ free Sound Particles have the masses of Sound Particles m_l and m_t and the value of its spin z-component $\sigma = 0;\pm1$. In this respect, the vector-operators $\vec{a}^+_{\vec{k},\sigma}$, $\vec{a}_{\vec{k},\sigma}$ and $\vec{b}^+_{\vec{k},\sigma}$, $\vec{b}_{\vec{k},\sigma}$ satisfy the Bose commutation relations as:

$$\Big[\hat{a}_{\vec{k},\sigma},\hat{a}^+_{\vec{k}',\sigma'}\Big] = \delta_{\vec{k},\vec{k}'}\cdot\delta_{\sigma,\sigma'}$$

$$[\hat{a}_{\vec{k},\sigma},\hat{a}_{\vec{k}',\sigma'}] = 0$$

$$[\hat{a}^+_{\vec{k},\sigma},\hat{a}^+_{\vec{k}',\sigma'}] = 0$$

and

$$\Big[\hat{b}_{\vec{k},\sigma},\hat{b}^+_{\vec{k}',\sigma'}\Big] = \delta_{\vec{k},\vec{k}'}\cdot\delta_{\sigma,\sigma'}$$

$$[\hat{b}_{\vec{k},\sigma},\hat{b}_{\vec{k}',\sigma'}] = 0$$

$$[\hat{b}^+_{\vec{k},\sigma},\hat{b}^+_{\vec{k}',\sigma'}] = 0$$

Thus, as we see, the vector displacements of a longitudinal $\vec{u}_l$ and of a transverse $\vec{u}_t$ ultrasonic wave satisfy the wave-equations of (3) and (4) and have the forms:

$$\vec{u}_l(\vec{r},t) = u_{\vec{0},l} + \frac{u_l}{\sqrt{V}}\sum_{\vec{k}\neq0,\sigma}\left(\vec{a}_{\vec{k},\sigma}e^{i(\vec{k}\vec{r}-kc_lt)} + \vec{a}^+_{\vec{k},\sigma}e^{-i(\vec{k}\vec{r}-kc_lt)}\right) \tag{12}$$

and

$$\vec{u}_t(\vec{r},t) = u_{\vec{0},t} + \frac{u_t}{\sqrt{V}}\sum_{\vec{k}\neq0,\sigma}\left(\vec{b}_{\vec{k},\sigma}e^{i(\vec{k}\vec{r}-kc_lt)} + \vec{b}^+_{\vec{k},\sigma}e^{-i(\vec{k}\vec{r}-kc_lt)}\right). \tag{13}$$

While investigating superfluid liquid, Bogoliubov [5] separated the atoms of helium in the condensate from those atoms, filling states above the condensate. In an analogous manner, we may consider the vector operators $\hat{a}_0 = \vec{l}\sqrt{n_{0,l}}$, $\hat{b}_0 = \vec{t}\sqrt{n_{0,t}}$ and $\hat{a}^+_0 = \vec{l}\sqrt{n_{0,l}}$, $\hat{b}^+_0 = \vec{t}\sqrt{n_{0,t}}$ as c-numbers (where $\vec{l}$ and $\vec{t}$ are the unit vectors in the direction of the longitudinal and transverse elastic fields, respectively, and also $\vec{l}\cdot\vec{t} = 0$) within the approximation of a macroscopic number of Sound Particles in

the condensate $n_{0,l} \gg 1$ and $n_{0,t} \gg 1$. This assumptions lead to a broken Bose-symmetry law for Sound Particles of longitudinal and transverse waves in the condensate. In fact, we may state that if a number of Sound Particles of longitudinal and transverse waves fills a condensate level with the wave vector $\vec{k} = 0$, then they reproduce the constant displacements $\vec{u}_{0,l} = \frac{2u_l\vec{e}\sqrt{n_{0,l}}}{\sqrt{V}}$ and $\vec{u}_{0,t} = \frac{2u_t\vec{e}\sqrt{n_{0,t}}}{\sqrt{V}}$.

In this context, we may emphasize that the Bose vector operators $\vec{a}^{+}_{\vec{k},\sigma}$, $\vec{a}_{\vec{k},\sigma}$ and $\vec{b}^{+}_{\vec{k},\sigma}$ and $\vec{b}_{\vec{k},\sigma}$ communicate with each other because the vector displacements of a longitudinal $\vec{u}_l(\vec{r},t)$ and a transverse ultrasonic wave $\vec{u}_t(\vec{r},t)$ are independent, and in turn, satisfy to the Bose commutation relation $[\vec{u}_l(\vec{r},t), \vec{u}_t(\vec{r},t)] = 0$.

Now, we note that quantization of elastic field means that this field operator does not commute with its momentum density. Taking the commutators gives

$$\left[\vec{u}_l(\vec{r},t), \vec{p}_l(\vec{r}',t)\right] = i\hbar\delta^3_{\vec{r}-\vec{r}'} \tag{14}$$

and

$$\left[\vec{u}_t(\vec{r},t), \vec{p}_t(\vec{r}',t)\right] = i\hbar\delta^3_{\vec{r}-\vec{r}'} \tag{15}$$

where the momentums of the longitudinal and transverse waves are defined as

$$\vec{p}_l(\vec{r},t) = \rho_l(\vec{r})\frac{\partial\vec{u}_l(\vec{r},t)}{\partial t} \tag{16}$$

and

$$\vec{p}_t(\vec{r},t) = \rho_t(\vec{r})\frac{\partial\vec{u}_t(\vec{r},t)}{\partial t} \tag{17}$$

where $\rho_l(\vec{r})$ and $\rho_t(\vec{r})$ are, respectively, the mass densities of longitudinal and transverse Sound Particles in the coordinate space, which are presented by the equations

$$\rho_l(\vec{r}) = \rho_{0,l} + \sum_{\vec{k}\neq 0}\rho_l(\vec{k})e^{i\vec{k}\vec{r}} \tag{18}$$

and

$$\rho_t(\vec{r}) = \rho_{0,t} + \sum_{\vec{k}\neq 0}\rho_t(\vec{k})e^{i\vec{k}\vec{r}}. \tag{19}$$

The total mass density $\rho(\vec{r})$ is

$$\rho(\vec{r}) = \rho_0 + \sum_{\vec{k}\neq 0}\rho_l(\vec{k})e^{i\vec{k}\vec{r}} + \sum_{\vec{k}\neq 0}\rho_t(\vec{k})e^{i\vec{k}\vec{r}} \tag{20}$$

where $\rho_l(\vec{k})$ and $\rho_t(\vec{k})$ are, respectively, the fluctuations of the mass densities of the longitudinal and transverse Sound Particles which represent as the symmetrical function from wave vector $\vec{k}$ or $\rho_l(\vec{k}) = \rho_l(-\vec{k})$; $\rho_t(\vec{k}) = \rho_t(-\vec{k})$; $\rho_0 = \rho_{0,l} + \rho_{0,t}$ is the equilibrium density of Sound Particles.

Applying (12) and (13) to (16) and (17), and taking (18) and (19), we get

$$\vec{p}_l(\vec{r},t) = -\frac{ic_lu_l}{\sqrt{V}}\sum_{\vec{k}'}\sum_{\vec{k},\sigma}k\rho_l(\vec{k}')\Big(\vec{a}_{\vec{k},\sigma}e^{-ikc_lt} - \vec{a}^{+}_{-\vec{k},\sigma}e^{ikc_lt}\Big)e^{i(\vec{k}+\vec{k}')\vec{r}} \tag{21}$$

$$\vec{p}_t(\vec{r},t) = -\frac{ic_lu_l}{\sqrt{V}}\sum_{\vec{k}'}\sum_{\vec{k},\sigma}\rho_t(\vec{k}')k\Big(\vec{b}_{\vec{k},\sigma}e^{-ikc_lt} - \vec{b}^{+}_{-\vec{k},\sigma}e^{ikc_lt}\Big)e^{i(\vec{k}+\vec{k}')\vec{r}} \tag{22}$$

Application of (12), (21) and (13), (22) to (14) and (15), and taking the Bose commutation relations presented above, we obtain

$$\left[\vec{u}_l(\vec{r},t), \vec{p}_l(\vec{r}',t)\right] = \frac{2iu_l^2c_l}{V}\sum_{\vec{k}}k\rho_l(\vec{k})e^{i\vec{k}(\vec{r}-\vec{r}')} \tag{23}$$

and

$$\left[\vec{u}_t(\vec{r},t), \vec{p}_t(\vec{r}',t)\right] = \frac{2iu_t^2c_t}{V}\sum_{\vec{k}}k\rho_t(\vec{k})e^{i\vec{k}(\vec{r}-\vec{r}')} \tag{24}$$

The right sides of Eqs. (14) and (23) as well as Eqs. (15) and (24) coincide when

$$\rho_l(\vec{k}) = \frac{\hbar}{2ku_l^2c_l} \tag{25}$$

and

$$\rho_t(\vec{k}) = \frac{\hbar}{2ku_t^2c_t} \tag{26}$$

by using

$$\frac{1}{V}\sum_{\vec{k}}e^{i\vec{k}(\vec{r}-\vec{r}')} = \delta^3_{\vec{r}-\vec{r}'}$$

3 Sound-Particles and Phonons

The Hamiltonian operator $\hat{H}$ of the system, consisting of the vibrated Fermi-atoms with mass M, is represented by the following form

$$\hat{H} = \hat{H}_l + \hat{H}_t \tag{27}$$

where

$$\hat{H}_l = \frac{MN}{2V}\int\left(\frac{\partial\vec{u}_l}{\partial t}\right)^2dV + \frac{NM\Omega_l^2}{2V}\int(\vec{u}_l)^2dV \tag{28}$$

and

$$\hat{H}_t = \frac{MN}{2V}\int\left(\frac{\partial\vec{u}_t}{\partial t}\right)^2dV + \frac{NM\Omega_t^2}{2V}\int(\vec{u}_t)^2dV \tag{29}$$

with Ω_l and Ω_t which are, respectively, the natural frequencies of the atom by action of longitudinal and transverse elastic waves.

To find the Hamiltonian operator $\hat{H}$ of the system, we use the framework of Dirac [6] for the quantization of electromagnetic field:

$$\frac{\partial \vec{u}_l(\vec{r},t)}{\partial t} = -\frac{ic_l u_l}{\sqrt{V}} \sum_{\vec{k},\sigma} k\left(\vec{a}_{\vec{k},\sigma} e^{-ikc_l t} - \vec{a}^{+}_{-\vec{k},\sigma} e^{ikc_l t}\right) e^{i\vec{k}\vec{r}} \quad (30)$$

and

$$\frac{\partial \vec{u}_t(\vec{r},t)}{\partial t} = -\frac{ic_t u_t}{\sqrt{V}} \sum_{\vec{k},\sigma} k\left(\vec{b}_{\vec{k},\sigma} e^{-ikc_t t} - \vec{b}^{+}_{-\vec{k},\sigma} e^{ikc_t t}\right) e^{i\vec{k}\vec{r}} \quad (31)$$

which by substituting into (28) and (29) using (12) and (13), we obtain the reduced form for the Hamiltonian operators $\hat{H}_l$ and $\hat{H}_t$:

$$\hat{H}_l = \sum_{\vec{k},\sigma}\left[\left(\frac{MNu_l^2c_l^2k^2}{V} + \frac{MNu_l^2\Omega_l^2}{V}\right)\vec{a}^{+}_{\vec{k},\sigma}a_{\vec{k},\sigma} - \left(\frac{MNu_l^2c_l^2k^2}{V} - \frac{MNu_l^2\Omega_l^2}{V}\right)\left(\vec{a}_{-\vec{k},\sigma}\vec{a}_{\vec{k},\sigma} + \vec{a}^{+}_{\vec{k},\sigma}\vec{a}^{+}_{-\vec{k},\sigma}\right)\right] \quad (32)$$

and

$$\hat{H}_t = \sum_{\vec{k},\sigma}\left[\left(\frac{MNu_t^2c_t^2k^2}{V} + \frac{MNu_t^2\Omega_t^2}{V}\right)\vec{a}^{+}_{\vec{k},\sigma}a_{\vec{k},\sigma} - \left(\frac{MNu_t^2c_t^2k^2}{V} - \frac{MNu_l^2\Omega_t^2}{V}\right)\left(\vec{a}_{-\vec{k},\sigma}\vec{a}_{\vec{k},\sigma} + \vec{a}^{+}_{\vec{k},\sigma}\vec{a}^{+}_{-\vec{k},\sigma}\right)\right] \quad (33)$$

where u_l and u_t are defined by the first term in right side of (32) and (33) which represent as the kinetic energies of longitudinal Sound Particle $\frac{\hbar^2k^2}{2m_l}$ and transverse Sound Particles $\frac{\hbar^2k^2}{2m_t}$. Therefore, u_l and u_l are found, if we suggest:

$$\frac{MNu_l^2c_l^2k^2}{V} = \frac{\hbar^2k^2}{2m_l} \quad (34)$$

and

$$\frac{MNu_t^2c_t^2k^2}{V} = \frac{\hbar^2k^2}{2m_t} \quad (35)$$

which in turn determine

$$u_l = \frac{\hbar}{c_l\sqrt{2m_l\rho}}$$

and

$$u_t = \frac{\hbar}{c_t\sqrt{2m_t\rho}}$$

where $\rho = \frac{MN}{V}$ is the density of solid.

$$\hat{H}_l = \sum_{\vec{k},\sigma}\left[\left(\frac{\hbar^2k^2}{2m_l} + \frac{\hbar^2\Omega_l^2}{2m_lc_l^2}\right)\vec{a}^{+}_{\vec{k},\sigma}a_{\vec{k},\sigma} + \frac{U_{\vec{k},l}}{2}\left(\vec{a}_{-\vec{k},\sigma}\vec{a}_{\vec{k},\sigma} + \vec{a}^{+}_{\vec{k},\sigma}\vec{a}^{+}_{-\vec{k},\sigma}\right)\right] \quad (36)$$

and

$$\hat{H}_t = \sum_{\vec{k}}\left[\left(\frac{\hbar^2k^2}{2m} + \frac{\hbar^2\Omega_t^2}{2m_tc_t^2}\right)\vec{b}^{+}_{\vec{k},\sigma}b_{\vec{k},\sigma} + \frac{U_{\vec{k},t}}{2}\left(\vec{b}_{-\vec{k},\sigma}\vec{b}_{\vec{k},\sigma} + \vec{b}^{+}_{\vec{k},\sigma}\vec{b}^{+}_{-\vec{k},\sigma}\right)\right] \quad (37)$$

$U_{\vec{k},l}$ and $U_{\vec{k},t}$ are the interaction potentials between identical Sound Particles.

In analogous manner, as it was done in letter [7] regarding the quantization of the electromagnetic field, the boundary wave numbers $k_l = \frac{\Omega_l}{c_l}$ for the longitudinal elastic field and $k_t = \frac{\Omega_t}{c_t}$ for the transverse one are determined by suggestion that identical Sound Particles interact with each other by the repulsive potentials $U_{\vec{k},l}$ and $U_{\vec{k},t}$ in wave vector space

$$U_{\vec{k},l} = -\frac{\hbar^2k^2}{2m_l} + \frac{\hbar^2\Omega_l^2}{2m_lc_l^2} > 0$$

and

$$U_{\vec{k},t} = -\frac{\hbar^2k^2}{2m_t} + \frac{\hbar^2\Omega_t^2}{2m_tc_t^2} > 0$$

As results, there are two conditions for wave numbers of longitudinal $k < k_l$ and transverse $k < k_t$ Sound Particles which are provided by property of the model of hard spheres [8]. Indeed, there is a request of presence of repulsive potential interaction between identical kind of particles (recall S-wave repulsive pseudopotential interaction between atoms in the superfluid liquid ^{4}He in the model of hard spheres [8]).

On the other hand, it is well known that at absolute zero $T = 0$, the Fermi atoms fill the Fermi sphere in momentum space. As it is known, the total numbers of the Fermi atoms with opposite spins are the same, therefore, the Fermi wave number k_f is determined by a condition:

$$\frac{V}{2\pi^2}\int_0^{k_f} k^2dk = \frac{N}{2} \quad (38)$$

where N is the total number of Fermi-atoms in the solid. This reasoning together with the model of hard spheres claims the important condition as introduction the boundary wave number $k_f = \left(\frac{3\pi^2N}{V}\right)^{\frac{1}{3}}$ coinciding with k_l and k_t. Thus we claim that all Fermi atoms had one natural wavelength

$$\lambda_0 = \frac{2\pi}{k_f} = \frac{2\pi}{k_l} = \frac{2\pi}{k_t} \quad (39)$$

This approach is a similar to the Einstein model of solid where he suggested that all atoms have the same natural frequencies.

Now, to evaluate of the energy levels of the operator $\hat{H}_l$ (36) and $\hat{H}_t$ (37) in diagonal form, we use a new transformation of the vector-Bose-operators presented in [6]:

$$\vec{a}_{\vec{k},\sigma} = \frac{\vec{c}_{\vec{k},\sigma} + L_{\vec{k}}\vec{c}^{+}_{-\vec{k},\sigma}}{\sqrt{1 - L^2_{\vec{k}}}} \quad (40)$$

and

$$\vec{b}_{\vec{k},\sigma} = \frac{\vec{d}_{\vec{k},\sigma} + M_{\vec{k}}\vec{d}^{+}_{-\vec{k},\sigma}}{\sqrt{1 - M^2_{\vec{k}}}} \tag{41}$$

where $L_{\vec{k}}$ and $M_{\vec{k}}$ are, respectively, the real symmetrical functions of a wave vector $\vec{k}$. Consequently:

$$\hat{H}_l = \sum_{k<k_f,\sigma} \varepsilon_{\vec{k},l}\vec{c}^{+}_{\vec{k},\sigma}\vec{c}_{\vec{k},\sigma} \tag{42}$$

and

$$\hat{H}_t = \sum_{k<k_f,\sigma} \varepsilon_{\vec{k},t}\vec{d}^{+}_{\vec{k},\sigma}\vec{d}_{\vec{k},\sigma}. \tag{43}$$

Hence, we infer that the Bose-operators $\vec{c}^{+}_{\vec{k},\sigma}$, $\vec{c}_{\vec{k},\sigma}$ and $\vec{d}^{+}_{\vec{k},\sigma}$, $\vec{d}_{\vec{k},\sigma}$ are, respectively, the vector of "creation" and the vector of "annihilation" operators of longitudinal and transverse phonons with spin 1 and having the energies:

$$\varepsilon_{\vec{k},l} = \sqrt{\left(\frac{\hbar^2k^2}{2m_l} + \frac{\hbar^2\Omega_l^2}{2m_lc_l^2}\right)^2 - \left(\frac{\hbar^2k^2}{2m_l} - \frac{\hbar^2\Omega_l^2}{2m_lc_l^2}\right)^2} = \hbar kc_l \tag{44}$$

and

$$\varepsilon_{\vec{k},t} = \sqrt{\left(\frac{\hbar^2k^2}{2m_t} + \frac{\hbar^2\Omega_t^2}{2m_tc_t^2}\right)^2 - \left(\frac{\hbar^2k^2}{2m_t} - \frac{\hbar^2\Omega_l^2}{2m_tc_t^2}\right)^2} = \hbar kc_t \tag{45}$$

where the mass of longitudinal Sound Particle equals to

$$m_l = \frac{\hbar\Omega_l}{c_l^2} \tag{46}$$

but the mass of transverse Sound Particle is

$$m_t = \frac{\hbar\Omega_t}{c_t^2}. \tag{47}$$

Thus, we may state that there are two different Sound Particles with masses m_l and m_t which correspond to the longitudinal and transverse waves.

4 Thermodynamic property of solid

Now, we demonstrate that the herein presented theory leads to same results which were obtained by Debye in his theory investigating the thermodynamic properties of solids. So that, at the statistical equilibrium, the average energy of solid equals to

$$\overline{H} = \sum_{k<k_f,\sigma} \varepsilon_{\vec{k},l}\overline{\vec{c}^{+}_{\vec{k},\sigma}\vec{c}_{\vec{k},\sigma}} + \sum_{k<k_f,\sigma} \varepsilon_{\vec{k},t}\overline{\vec{d}^{+}_{\vec{k},\sigma}\vec{d}_{\vec{k},\sigma}} \tag{48}$$

where $\overline{\hat{c}^{+}_{\vec{k},\sigma}\hat{c}_{\vec{k},\sigma}}$ and $\overline{\hat{d}^{+}_{\vec{k},\sigma}\hat{d}_{\vec{k},\sigma}}$ are, respectively, the average number of phonons with the wave vector $\vec{k}$ corresponding to the longitudinal and transverse fields at temperature T:

$$\overline{\hat{c}^{+}_{\vec{k},\sigma}\hat{c}_{\vec{k},\sigma}} = \frac{1}{e^{\frac{\varepsilon_{\vec{k},l}}{kT}} - 1}$$

and

$$\overline{\hat{d}^{+}_{\vec{k},\sigma}\hat{d}_{\vec{k},\sigma}} = \frac{1}{e^{\frac{\varepsilon_{\vec{k},t}}{kT}} - 1}.$$

Thus, at thermodynamic limit, the average energy of solid may rewritten down as

$$\overline{H} = \frac{3Vk^4T^4}{2\pi^2\hbar^3c_l^3}\int_0^{\frac{\Theta_l}{T}} \frac{x^3dx}{e^x - 1} + \frac{3Vk^4T^4}{2\pi^2\hbar^3c_t^3}\int_0^{\frac{\Theta_t}{T}} \frac{x^3dx}{e^x - 1} \tag{49}$$

where $\Theta_l = \frac{\hbar k_f c_l}{k}$ and $\Theta_t = \frac{\hbar k_f c_t}{k}$ are, respectively, the characteristic temperatures for solid corresponding to longitudinal and transverse waves; k is the Boltzmann constant. In our theory we denote

$$\frac{1}{c_l^3} + \frac{1}{c_t^3} = \frac{2}{c^3}$$

where c is the average velocity of phonons with spin 1 in the given theory; $\Theta_B = \frac{\hbar k_f c}{k}$ is the new characteristic temperature.

Hence, we may note that the coefficient with number 3 must be appear before both integrals on the right side of equation (49) because it reflects that phonons of longitudinal and transverse waves have number 3 quantities of the value of spin z-component $\sigma = 0; \pm 1$. At $T \ll \Theta_l$ and $T \ll \Theta_t$, the equation (49) takes the form:

$$\overline{H} = \frac{3\pi^4}{5}\frac{NkT^4}{2}\left(\frac{1}{\Theta_l^3} + \frac{1}{\Theta_t^3}\right) \tag{50}$$

where $\int_0^\infty \frac{x^3dk}{e^x-1} = \frac{\pi^4}{15}$.

Thus, Eq.(50) may be rewritten as

$$\overline{H} \approx \frac{3\pi^4}{5}\frac{RT^4}{\Theta_B^3} \tag{51}$$

where $R = Nk$ is the gas constant. Hence, we may note that at $T \gg \Theta_l$ and $T \gg \Theta_t$, the equation (49) takes the form:

$$\overline{H} = 3RT. \tag{52}$$

In this context, the heat capacity is determined as

$$C_V = \left(\frac{d\overline{H}}{dT}\right)_V \tag{53}$$

which obviously, at $T \ll \Theta_l$ and $T \ll \Theta_t$, the equation (53) with (51) reflects the Debye law T^3 at low temperatures:

$$C_V \approx \frac{12\pi^4}{5}\frac{RT^3}{\Theta_B^3}. \tag{54}$$

But at high temperatures $T \gg \Theta_l$ and $T \gg \Theta_t$, the equation (53) with (52) recovers the Dulong-Petit law:

$$C_V \approx 3R. \tag{55}$$

Obviously, the average velocity of phonon c and new characteristic temperature Θ_B are differ from their definition in Debye theory because the average energy of solid in Debye theory is presented as

$$\overline{H}_D = \frac{3Vk^4T^4}{2\pi^2\hbar^3c_l^3}\int_0^{\frac{\Theta_l}{T}}\frac{x^3dx}{e^x-1} + \frac{3Vk^4T^4}{\pi^2\hbar^3c_t^3}\int_0^{\frac{\Theta_t}{T}}\frac{x^3dx}{e^x-1} \qquad (56)$$

where $\Theta_l = \frac{\hbar k_D c_l}{k}$ and $\Theta_t = \frac{\hbar k_D c_t}{k}$ are, respectively, the characteristic temperatures for solid corresponding to one longitudinal and two transverse waves:

$$\frac{1}{c_l^3} + \frac{2}{c_t^3} = \frac{3}{v_0^3} \qquad (57)$$

where v_0 is the average velocity of spinless phonons in Debye theory; $k_D = \left(\frac{6\pi^2N}{V}\right)^{\frac{1}{3}}$ is the Debye wave number; $\Theta_D = \frac{\hbar k_D v_0}{k}$ is the Debye characteristic temperature which is

$$\frac{1}{\Theta_l^3} + \frac{2}{\Theta_t^3} = \frac{3}{\Theta_D^3} \qquad (58)$$

As we see the average energy of solid $\overline{H}_D$ in (56) is differ from one in (49) by coefficient 2 in ahead of second term in right side of Eq.(56) (which is connected with assumption of presence two transverse waves), as well as introduction of Debye wave number k_D. So that due to definition of the average velocity v_0 of spinless phonons by (57), Debye may accept a phonon as spinless quasiiparticle.

5 Concussion

Thus, in this letter, we propose new model for solids which is different from the well-known models of Einstein and Debye because: 1), we suggest that the atoms are the Fermi particles which are absent in the Einstein and Debye models; 2), we consider the stimulated oscillation of atoms by action of longitudinal and transverse waves in the solid. The elastic waves stimulate the vibration of the fermion-atoms with one natural wavelength, we suggested that atoms have two independent natural frequencies corresponding to a longitudinal and a transverse wave, due to application of the principle of the elastic wave-particle duality, the model of hard spheres and considering the atoms as the Fermi particles. In accordance to this reasoning, there is an appearance of a cut off in the energy spectrum of phonons; 3), In our model, we argue that the photons have spin 1 which is different from models presented by Einstein and Debye. On the other hand, we suggest that only one longitudinal and one transverse wave may be excited in the lattice of the solid which is different from Debye who suggested a presence of two sorts of transverse waves.

The quantization of the elastic wave by our theory leads to a view of the lattice as the diffraction picture. Within our theory, the mass density $\rho(\vec{r})$ in coordinate space, due to substituting $\rho_l(\vec{r},t)$ and $\rho_l(\vec{r},t)$ from (25) and (26) into (20), represents as

$$\rho(\vec{r}) = \rho_0 + \frac{8\pi\hbar k_f^2}{u_l^2 c_l}\left(\frac{\sin k_f r}{k_f r}\right)^2 + \frac{8\pi\hbar k_f^2}{u_t^2 c_t}\left(\frac{\sin k_f r}{k_f r}\right)^2 \qquad (59)$$

which implies that the lattice has the diffraction picture.

Now, we try to estimate the masses of the Sound Particles in substance as Aluminium Al. In this respect, we use of (46) and (47) with introducing of the Fermi momentum $p_f = \hbar k_f = \frac{\hbar\Omega_l}{c_l} = \frac{\hbar\Omega_t}{c_t}$, for instance, for such material as Al with $c_l = 6.26\cdot 10^3\frac{m}{sec}$ and $c_t = 3.08\cdot 10^3\frac{m}{sec}$ at room temperature [9], and $p_f = 1.27\cdot 10^{-24}\frac{kg\cdot m}{sec}$ we may estimate $m_l = \frac{p_f}{c_l} = 2\cdot 10^{-28}kg$ and $m_t = \frac{p_f}{c_t} = 4\cdot 10^{-28}kg$.

It is well known that the mass of atom Al is $M = 10^{-25}kg$ which is around 500 time more in regard to the masses of Sound Particles.

In this context, we remark that the new characteristic temperature Θ_B almost coincide with the Debye temperature Θ_D. Indeed, by our theory for Al:

$$\Theta_B = \frac{2^{\frac{1}{3}}p_f c_l}{k\left(1+\frac{c_l^3}{c_t^3}\right)^{\frac{1}{3}}} \approx 400K$$

but Debye temperature equals to $\Theta_D = 418K$.

Acknowledgements

We are particularly grateful to Dr. Andreas Ries for valuable scientific support and for help with the English.

Submitted on October 20, 2010 / Accepted on November 9, 2010

References

1. Einstein A. Die Plancksche Theorie der Strahlung und die Theorie der spezifischen Waerme. *Annalen der Physik*, 1907, v. 22, 180–190.
2. Debye P. Zur Theorie der spezifischen Waerme. *Annalen der Physik*, 1912, v. 39, no. 4, 789–839.
3. Landau L. D., Lifshiz E. M. Theory of Elasticity. *Theoretical Physics* 1987, v. V11, 124–127.
4. de Broglie L. Researches on the quantum theory. *Annalen der Physik*, 1925, v. 3, 22–32.
5. Bogoliubov N. N. On the theory of superfludity. *Journal of Physics (USSR)*, 1947, v. 11, 23–32.
6. Dirac P. A. M. The Principles of Quantum Mechanics. Clarendon Press, Oxford, 1958.
7. Minasyan V. N., Samoilov V. N. Two Type Surface Polaritons Excited into Nanoholes in Metal Films. *Progress in Physics*, 2010, v. 2, 3–6.
8. Huang K. Statistical Mechanics. John Wiley, New York, 1963.
9. Kittel Ch., Introduction to Solid State Physics. John Wiley, New York, 1990.

Applying Adjacent Hyperbolas to Calculation of the Upper Limit of the Periodic Table of Elements, with Use of Rhodium

Albert Khazan

E-mail: albkhazan@gmail.com

In the earlier study (Khazan A. Upper Limit in Mendeleev's Periodic Table — Element No. 155. 2nd ed., Svenska fysikarkivet, Stockholm, 2010) the author showed how Rhodium can be applied to the hyperbolic law of the Periodic Table of Elements in order to calculate, with high precision, all other elements conceivable in the Table. Here we obtain the same result, with use of fraction linear functions (adjacent hyperbolas).

1 Introduction

In the theoretical deduction of the hyperbolic law of the Periodic Table of Elements [1], the main attention was focused onto the following subjects: the equilateral hyperbola with the central point at the coordinates (0; 0), its top, the real axis, and the line tangential to the normal of the hyperbola. All these were created for each element having the known or arbitrary characteristics. We chose the top of the hyperbolas, in order to describe a chemical process with use of Lagrange's theorem; reducing them to the equation $Y = K/X$ was made through the scaling coefficient 20.2895, as we have deduced.

The upper limit of the Table of Elements, which is the heaviest (last) element of the Table, is determined within the precision we determine the top of its hyperbola [1]. Therefore hyperbolas which are related to fraction linear functions were deduced. These hyperbolas are equilateral as well, but differ in the coordinates of their centre: $x = 0$, $y = 1$. To avoid possible mistakes in the future, the following terminology has been assumed: hyperbolas of the kind $y = k/x$ are referred to as *straight*; equilateral hyperbolas of the kind $y = (ax + b)/(cx + d)$ are referred to as *adjacent*. The latter ones bear the following properties: such a hyperbola intersects with the respective straight hyperbola at the ordinate $y = 0.5$ and the abscissa equal to the double mass of the element; the line $y = 0.5$ is the axis of symmetry for the arcs; the real and tangential lines of such hyperbolas meet each other; the normal of such a hyperbola is the real axis and the tangential line of another hyperbola of this kind.

The found common properties of the hyperbolas provided a possibility to use them for determination of the heaviest (last) element in another way than earlier.

2 Method of calculation

Once drawing straight hyperbolas for a wide range of the elements, according to their number from 1 to 99 in the Table of Elements, where the atomic masses occupy the scale from Hydrogen (1.00794) to Einsteinium (252), one can see that the real axis of each straight hyperbola is orthogonal to the real axis of the respective adjacent hyperbola, and they cross each other at the point $y = 0.5$.

Then we draw the intersecting lines from the origin of the adjacent hyperbolas (0; 1). The lines intersect the straight hyperbolas at two points, and also intersect the real axis and the abscissa axis where they intercept different lengths.

Connection to molecular mass of an element (expressed in the Atomic Units of Mass) differs between the abscissas of the lengths selected by the intersecting lines and the abscissas of transection of the straight and adjacent hyperbolas. Therefore, the line which is tangent to the straight in the sole point (102.9055; 205.811) is quite complicated. These coordinates mean the atomic mass of Rhodium and the half of the atomic mass of the heaviest (last) element of the Periodic Table.

The right side of the line can easily be described by the 4th grade polynomial equation. However the left side has a complicate form, where the maximum is observed at the light elements (Nitrogen, Oxygen) when lowered to (102.9055; 0) with the increase in atomic mass.

According to our calculation, the straight and adjacent hyperbolas were determined for Rhodium. The real axes go through the transecting points of the hyperbolas to the axis X and the line $Y = 1$, where they intercept the same lengths 411.622. This number differs for 0.009% from 411.66.

Thus, this calculation verified the atomic mass 411.66 of the heaviest element (upper limit) of the Periodic Table of Elements, which was determined in another way in our previous study [1].

3 Algorithm of calculation

The algorithm and results of the calculation without use of Rhodium were given in detail in Table 3.1 of the book [1]. The calculation is produced in six steps.

Step 1. The data, according to the Table of Elements, are written in columns 1, 2, 3.

Step 2. Square root is taken from the atomic mass of each element. Then the result transforms, through the scaling coefficient 20.2895, into the coordinates of the tops of straight hyperbolas along the real axis. To do it, the square root of the data of column 3 is multiplied by 20.2895 (column 4), then is divided by it (column 3).

Step 3. We draw transecting lines from the centre (0; 1) to

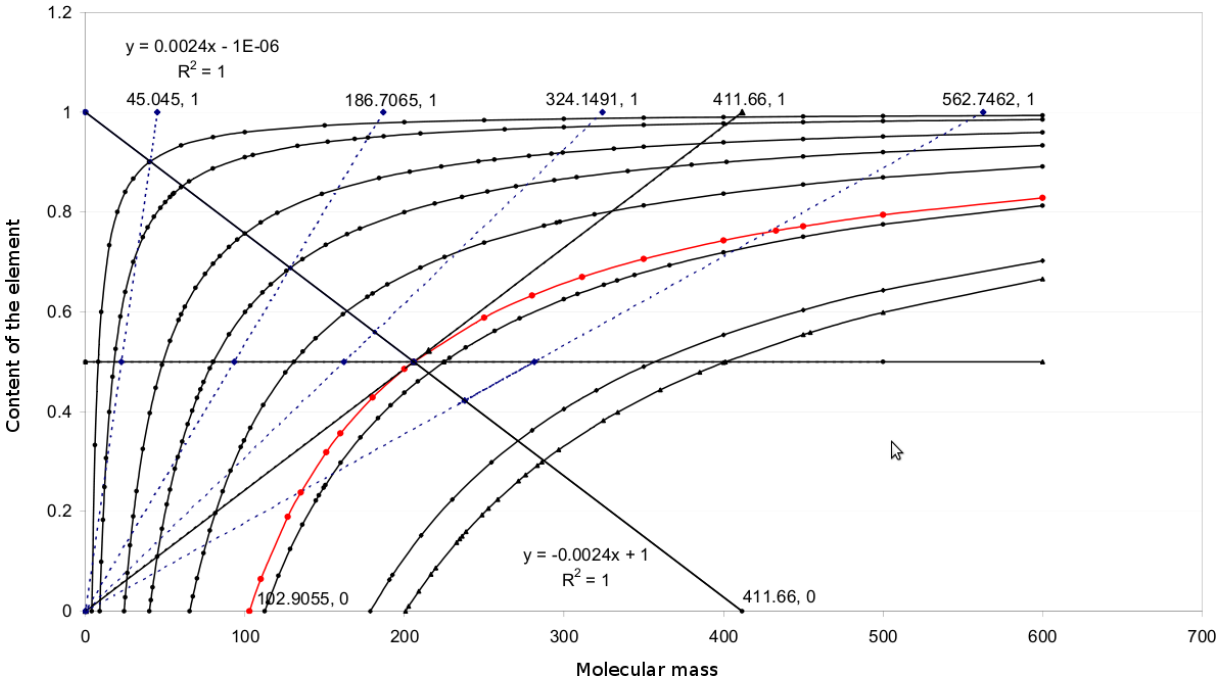

Fig. 1: Calculation with the centre at the point (0;0).

the transections with the line $y = 0.5$, with the real axis at the point $(X_0; Y_0)$, and so forth up to the axis X. To determine the abscissa of the intersection points, we calculate the equation of a straight line of each element. This line goes through two points: the centre (0; 1) and a point located in the line $y = 0.5$ or in the axis X: $(X - 0)/(X_0 - 0) = (Y - 1)/(Y_0 - 1)$. For instance, consider Magnesium. After its characteristics substituted, we obtain the equation $(X - 0)/(100.0274 - 0) = (Y - 1)/(0.242983 - 1)$, wherefrom the straight line equation is obtained: $Y = 1 - 0.007568\,X$. Thus, the abscissa of the transecting line, in the line $y = 0.5$, is 66.0669 (column 6).

Step 4. We write, in column 7, the abscissas of the points of transection of the straight and adjacent hyperbolas. The abscissas are equal to the double atomic mass of the element under study.

Step 5. We look for the region, where the segment created by a hyperbola and its transecting line is as small as a point (of the hyperbola and its transecting line). To find the coordinates, we subtract the data of column 7 from the respective data of column 6. Then we watch where the transecting line meets the real axis. The result is given by column 8. Here we see that the numerical value of the segments increases, then falls down to zero, then increases again but according to another law.

Step 6. Column 9 gives tangent of the inclination angle of the straights determined by the equations, constructed for two coordinate points of each element: $Y = -KX + 1$, where K is the tangent of the inclination angle.

4 Using adjanced hyperbolas in the calculation

Because straight and adjacent hyperbolas are equilateral, we use this fact for analogous calculations with another centre, located in the point (0; 0). The result has been shown in Fig. 1. In this case X_0 remains the same, while the ordinate is obtained as difference between 1 and Y_0. The straight line equation is obtained between two points with use of the data of column 9, where tangent should be taken with the opposite sign. As a result, we obtain an adjacent hyperbola of Rhodium. For example, consider Calcium. We obtain $X_0 = 128.4471$, $Y_0 = 0.31202$ (the ordinate for the straight hyperbola of Calcium), and $Y_0 = 1 - 0.31202 = 0.68798$ (for the adjacent hyperbola). The straight line equation between these two points is $Y = 0.005356\,X$. Thus, we obtain $x = 186.7065$ under $y = 1$, and $x = 93.3508$ under $y = 0.5$.

The new calculations presented here manifest that determining the heaviest (last) element of the Periodic Table of Elements is **correct for both ways of calculation**: the way with use of Lagrange's theorem and the scaling coefficient [1], and also the current method of the hyperbolas adjacent to that of Rhodium (method of adjacent hyperbolas). As one can see, the calculation results obtained via these two methods differ only in thousand doles of percent.

Submitted on October 22, 2010 / Accepted on December 12, 2010

References

1. Khazan A. Upper Limit in Mendeleev's Periodic Table — Element No. 155, 2nd edition, Svenska fysikarkivet, Stockholm, 2010.

How Black Holes Violate the Conservation of Energy

Douglas L. Weller
Email: physics@dougweller.com

Black holes produce more energy than they consume thereby violating the conservation of energy and acting as perpetual motion machines.

1 Introduction

According to Stephen Hawking and Leonard Mlodinow [1]: "Because there is a law such as gravity, the Universe can and will create itself from nothing." Such views of gravity are usually attributed as being rooted in Einstein's general-relativistic space-time.

However, the field equations Einstein [2] used to describe the general-relativistic space-time are founded on the conservation of momentum and energy. How can a space-time derived based on the conservation of momentum and energy provide an ex nihilo source of energy sufficient to create a universe?

The answer is found in Karl Schwarzschild's solution [3] to the field equations, usually called the Schwarzschild metric. The Schwarzschild metric describes a gravitational field outside a spherical non-rotating mass. When the mass is compacted within its Schwarzschild radius it is commonly referred to as a black hole.

Herein the terms of the Schwarzschild metric are rearranged to display limits in the Schwarzschild metric that necessarily result from the conservation of momentum and energy. Then is shown how black holes violate the limits, acting as perpetual motion machines that produce more energy than they consume.

2 Expressing the Schwarzschild metric using velocities

In this section, the Schwarzschild metric is rearranged so as to be expressed using velocities measured with reference coordinates. This rearrangement, which appears as equation (8) at the end of this section, will make very clear the limits imposed within the Schwarzschild metric by the conservation of momentum and energy.

Einstein [4] originally expressed the principles of special relativity using velocities measured with reference coordinates. However, Einstein [2, Equations 47] expressed the field equations in more abstract terms, using tensors. Einstein was careful to show that the field equations, nevertheless, correspond to the conservation of momentum and energy [2, Equations 47a] and thus have a nexus to physical reality.

The Schwarzschild metric, as a solution to the field equations, also corresponds to the conservation of momentum and energy. Arrangement of the Schwarzschild metric as in (8) allows for an intuitive comprehension of exactly how momentum and energy is conserved.

For a compact mass M with a Schwarzschild radius R, the Schwarzschild metric is often expressed using reference space coordinates (r, θ, ϕ), coordinate time t and local time τ (often referred to as proper time τ), as

$$c^2 d\tau^2 = c^2 \left(1 - \frac{R}{r}\right) dt^2 - \frac{dr^2}{(1 - R/r)} - r^2 d\theta^2 - (r sin\theta)^2 d\phi^2. \quad (1)$$

The Schwarzschild metric as shown in (1) can be rearranged to form (8), as shown below. To obtain (8) from (1), begin by multiplying both sides of (1) by $\left(\frac{1}{dt}\right)^2$ yielding

$$\begin{aligned} c^2 \left(\frac{d\tau}{dt}\right)^2 &= c^2 \left(1 - \frac{R}{r}\right)\left(\frac{dt}{dt}\right)^2 - \frac{1}{1 - R/r}\left(\frac{dr}{dt}\right)^2 \\ &- r^2 \left(\frac{d\theta}{dt}\right)^2 - (r sin\theta)^2 \left(\frac{d\phi}{dt}\right)^2, \end{aligned} \quad (2)$$

which allows motion in all dimensions to be measured with respect to the reference coordinates (r, θ, ϕ, t). The terms of (2) can be rearranged as

$$\begin{aligned} c^2 &= c^2 \left(\frac{d\tau}{dt}\right)^2 + c^2 \frac{R}{r} + \frac{1}{1 - R/r}\left(\frac{dr}{dt}\right)^2 \\ &+ r^2 \left(\frac{d\theta}{dt}\right)^2 + (r sin\theta)^2 \left(\frac{d\phi}{dt}\right)^2. \end{aligned} \quad (3)$$

The terms in (3) can be grouped by defining three different velocities. A velocity through the three dimensions of curved space can be defined as

$$v_S = \sqrt{\frac{1}{1 - R/r}\left(\frac{dr}{dt}\right)^2 + r^2 \left(\frac{d\theta}{dt}\right)^2 + (r sin\theta)^2 \left(\frac{d\phi}{dt}\right)^2}. \quad (4)$$

A velocity of local time through a time dimension can be defined as

$$v_\tau = c \frac{d\tau}{dt}. \quad (5)$$

A gravitational velocity can be defined as

$$v_G = c \sqrt{\frac{R}{r}}. \quad (6)$$

Using the definitions in (4), (5) and (6), (3) reduces to

$$c^2 = v_\tau^2 + v_G^2 + v_S^2. \quad (7)$$

Equation (7) can be expressed using orthogonal vectors $\vec{v}_\tau$, $\vec{v}_G$ and $\vec{v}_S$ where $v_\tau = |\vec{v}_\tau|$, $v_G = |\vec{v}_G|$ and $v_S = |\vec{v}_S|$, and where

$$c = \left|\vec{v}_\tau + \vec{v}_G + \vec{v}_S\right|. \quad (8)$$

Equation (8) is mathematically equivalent to (1) and expresses the Schwarzschild metric as a relationship of vector velocities. The conservation of momentum and energy, as expressed in the Schwarzschild metric, requires that the magnitude of the sum of the velocities is always equal to the constant c. Before exploring the full implication of this relationship, the next section confirms that (8) conforms with what is predicted by special relativity.

3 Equation (8) and special relativity

In the previous section, the Schwarzschild metric in (1) has been rearranged as (8) to provide a more concrete picture of the relationships necessary for conservation of momentum and energy.

Here is confirmed (8) is in accord with the case of special relativity for unaccelerated motion.

When there is no acceleration and therefore no gravity field, $R = 0$ and thus according to (6), $v_G = 0$ so that (8) reduces to

$$c = \left|\vec{v}_\tau + \vec{v}_S\right|. \tag{9}$$

When $R = 0$,

$$v_{S,R=0} = \sqrt{\left(\frac{dr}{dt}\right)^2 + r^2\left(\frac{d\theta}{dt}\right)^2 + (rsin\theta)^2\left(\frac{d\phi}{dt}\right)^2}, \tag{10}$$

which expressed in Cartesian coordinates is the familiar form of velocity used in special relativity,

$$v_{S,R=0} = \sqrt{\left(\frac{dx}{dt}\right)^2 + \left(\frac{dy}{dt}\right)^2 + \left(\frac{dz}{dt}\right)^2}. \tag{11}$$

Equation (9) accurately reproduces the relationship of velocity and time known from special relativity. As velocity v_S in the space dimensions increases, there is a corresponding decline in the velocity v_τ in the orthogonal time dimension. When velocity in the time dimension reaches its minimum value (i.e., $v_\tau = 0$) this indicates a maximum value (i.e., $v_S = c$) in the space dimensions has been reached.

Equation (9) can be rearranged to confirm it portrays exactly the relationship between coordinate time and local time that is known to occur in the case of special relativity. Specifically, from the relationship of the orthogonal vectors $\vec{v}_\tau$, and $\vec{v}_S$ in (9), it must be true that

$$c^2 = v_\tau^2 + v_S^2. \tag{12}$$

and thus from (5)

$$c^2 = c^2\left(\frac{d\tau}{dt}\right)^2 + v_S^2, \tag{13}$$

and therefore

$$\frac{d\tau}{dt} = \sqrt{1 - \frac{v_S^2}{c^2}}, \tag{14}$$

which is a form of the well known Laplace factor indicating the relationship between local time and coordinate time for special relativity.

4 Equation (8) and limits imposed by the conservation of momentum and energy

The arrangement of the Schwarzschild metric in (8) allows for a more concrete explanation of the limitations inherent in the Schwarzschild metric that necessarily result from the conservation of momentum and energy.

The vector sum of $\vec{v}_\tau$, $\vec{v}_G$ and $\vec{v}_S$ establishes a maximum value of c for each individual vector velocity.

When $\vec{v}_\tau = 0$ and $\vec{v}_S = 0$, $\vec{v}_G$ reaches its maximum value of c. Gravitational velocity $\vec{v}_G$ cannot exceed its maximum value of c without violating (8).

According to the definition of v_G in (6), when $v_G = c$, then $r = R$. When $r < R$, then $v_G > c$; therefore, according to (8), $r < R$ never occurs. As shown by Weller [5], matter from space can never actually reach $r = R$, but if it could, it would go no farther. At $r = R$ and $v_G = c$, all motion through space stops ($\vec{v}_S = 0$) and local time stops ($\vec{v}_\tau = 0$, so $d\tau/dt = 0$). Without motion in time or space, matter cannot pass through radial location $r = R$.

This section has shown that because of the conservation of momentum and energy — as expressed by the Schwarzschild metric arranged as in (8) — matter from space cannot cross the Schwarzschild radius R to get to a location where $r < R$.

The following sections consider conservation of energy equivalence in the Schwarzschild metric and the result when energy conservation is not followed.

5 Apportionment of energy equivalence

Einstein [6] pioneered apportioning energy differently based on reference frames, using such an apportionment in his initial calculations deriving the value for the energy equivalence of a mass (i.e., $E = mc^2$).

This notion of apportionment of energy equivalence is a helpful tool in understanding the implications of violating the conservation of energy and momentum in the Schwarzschild metric. When considering apportionment of energy equivalence in the Schwarzschild metric, it is helpful to keep in mind how Einstein makes a distinction between "matter" and a "matterless" gravitational field defined by the field equations or by the Schwarzschild metric. According to the Einstein [2, p. 143], everything but the gravitation field is denoted as "matter". Therefore, matter when added to the matterless field includes not only matter in the ordinary sense, but the electromagnetic field as well.

How the Schwarzschild metric apportions energy equivalence can be understood from

$$c^2 = v_\tau^2 + c^2\frac{R}{r} + v_S^2. \tag{15}$$

which is (7) modified so as to replace v_G with its equivalent given in (6). Equation (15) is mathematically equivalent to (1), just rearranged to aid in the explanation of the apportionment of energy equivalence.

Equation (15) can be put into perhaps more familiar terms by introducing a particle of mass m into the gravitation field. The energy equivalence mc^2 of the mass m is apportioned according to (15) as

$$mc^2 = mv_\tau^2 + mc^2\frac{R}{r} + mv_S^2. \tag{16}$$

In order to provide insight into the nature of the gravitational energy component c^2R/r in (15) —which appears as mc^2R/r in (16) — the next section discusses briefly how this term came to reside in the Schwarzschild metric.

6 Schwarzschild's description of gravity

One of the issues Schwarzschild [3, see §4] faced when deriving the Schwarzschild metric was how to describe the effects of gravity. He chose to do so using a positive integration constant that depends on the value of the mass at the origin. As a result the Newtonian gravitational constant G appears in the Schwarzschild metric. In (1) the gravitational constant G appears as part of the definition of the Schwarzschild radius R. In both Newtonian physics and the Schwarzschild metric, the Schwarzschild radius (R) — the location where Newtonian escape velocity (i.e., v_G) is equal to c — is defined as

$$R = \frac{2GM}{c^2}. \tag{17}$$

When the Schwarzschild metric is arranged as in (15), gravitational energy component c^2R/r increases toward infinity as radial location r decreases toward zero. This suggests the location of an unlimited energy source within the Schwarzschild metric; however, total gravitational energy is limited by the requirement that energy be conserved, as illustrated by the hypothetical described in the next section.

7 A hypothetical illustrating the conservation of energy equivalence in the Schwarzschild metric

The total energy-equivalence of a system comprised of a mass M can be defined as

$$E_M = Mc^2, \tag{18}$$

where the energy of magnetic fields is included in M, or neglected. If a mass m is added to the system, the additional energy E added to the system as a result of the presence of mass m is also well known to be

$$E = mc^2. \tag{19}$$

Thus if the system consisting of mass M and mass m were dissolved into radiation, the total resulting energy would be equal to

$$E_M + E = Mc^2 + mc^2. \tag{20}$$

In order for the conservation of energy to be maintained in the system as a whole, any gravitational energy E_G or any energy from motion E_K that is added to the system as a result of the presence of mass m must be included as part of the additional energy E described in (19). Therefore, the additional energy E present in the system as a result of adding mass m can be expressed as

$$E = mc^2 = E_K + E_G + E_\tau, \tag{21}$$

where E_τ is the portion of energy E that is not represented by gravitational energy component E_G or motion energy component E_K.

Equation (21) is the apportionment of energy equivalence shown in (16). To confirm this, in (21) set $E_G = mc^2R/r$, $E_K = mv_S^2$ and $E_\tau = mv_\tau^2$ to obtain (16).

The apportionment of energy equivalence in (16) and (21) indicates why crossing the Schwarzschild radius R violates the conservation of energy. When the particle reaches the Schwarzschild radius R — i.e., $r = R$ — the entire energy equivalence of mass m, is consumed by the gravitation component, i.e., $E_G = mc^2R/R = mc^2$. There is no energy left for mass m to travel in time (i.e., $E_\tau = 0$) or in space (i.e., $E_K = 0$). Therefore at locations $r = R$, all motion in time and space must stop, preventing mass m from ever crossing the critical radius.

If mass m were from space to cross the Schwarzschild radius R, the gravitational energy component $E_G = mc^2R/r$ would exceed the total energy equivalence $E = mc^2$ violating the conservation of energy.

If the particle were allowed to reach $r = 0$, gravitational energy component $E_G = mc^2R/r$ would approach infinity before becoming undefined.

8 How black holes act as perpetual motion machines

A perpetual motion machine is a hypothetical machine that violates the conservation of energy by producing more energy than it consumes.

According to the conservation of momentum and energy described by the Schwarzschild metric, see (8) and (15), a particle can never from space cross the Schwarzschild radius R of a compact mass M.

When a black hole is formed from a compacting mass M, the last particle on the surface of the mass that reaches and crosses the Schwarzschild radius R violates (8). Every particle thereafter that from space crosses R violates (8).

Further, from (16), each particle of mass m that reaches a radial location $r < R$, produces an amount of gravitational energy ($E_G = mc^2R/r$) that is greater than its total energy equivalence mc^2, as can only happen in a perpetual motion machine. When a particle is allowed to approach and reach $r = 0$, the ultimate perpetual motion machine is created which from the finite energy equivalence mc^2 of the particle produces an unlimited amount of gravitational energy as the particle approaches $r = 0$.

9 Concluding Remarks

Describing the effects of gravity using a gravitational constant and violating the conservation of momentum and energy described by the Schwarzschild metric can hypothetically result in black holes that act as perpetual motion machines able to produce an unlimited amount of energy. However, the existence of such perpetual motion machines is not in accordance with the conservation of momentum and energy as expressed in Einstein's general-relativistic space-time.

Special mathematical calculations, including use of specially selected coordinates, have been used to explain how a particle can cross the Schwarzschild radius allowing black holes to form. Critiquing these mathematical calculations is beyond the scope of this short paper. The author has directly addressed some of this subject matter in a companion paper [5].

Submitted on November 16, 2010 / Accepted on December 15, 2010

References

1. Hawking S., Mlodinow L. The grand design. Bantom Books, New York, 2010, p. 180.
2. Einstein A. The foundation of the general theory of relativity. The Principle of Relativity. Dover Publications, New York, 1923. pp. 111–164.
3. Schwarzschild K. On the gravitational field of a mass point according to Einstein's theory. Translated by S. Antoci, A. Loinger, 1999, arXiv:Physics/9905030.
4. Einstein A. On the electrodynamics of moving bodies. The Principle of Relativity. Dover Publications, New York, 1923, pp. 37–65.
5. Weller D. Five fallacies used to link black holes to Einstein's relativistic space-time. *Progress in Physics*, 2011, v. 1, 93–97.
6. Einstein A. Does the inertia of a body depend upon its energy-content? The Principle of Relativity. Dover Publications, New York, 1923, pp. 69–71.

Five Fallacies Used to Link Black Holes to Einstein's Relativistic Space-Time

Douglas L. Weller
E-mail: physics@dougweller.com

For a particle falling radially toward a compact mass, the Schwarzschild metric maps local time to coordinate time based on radial locations reached by the particle. The mapping shows the particle will not cross a critical radius regardless of the coordinate used to measure time. Herein are discussed five fallacies that have been used to make it appear the particle can cross the critical radius.

1 Introduction

Einstein [1] sets out field equations that describe a matter-free field. A German military officer, Karl Schwarzschild [2], shortly before he died, derived a solution of the field equations for a static gravitational field of spherical symmetry. Schwarzschild's solution is referred to as the Schwarzschild metric.

Einstein [3] showed that matter cannot be compacted below a critical radius defined by the Schwarzschild metric. Weller [4] shows that compacting matter below the critical radius to form a black hole results in a violation of the conservation of momentum and energy.

Why, then, do many believe that black holes exist in Einstein's relativistic space time? The belief appears to have arisen based, at least partly, on an incorrect description of the journey of a particle falling radially towards a hypothetical mass compacted below the critical radius. The description is incorrect in that the particle reaches and crosses the critical radius.

Herein are discussed five fallacies used in the description of the particle's journey. Preliminary to addressing the fallacies, it is shown why the particle will never reach the critical radius.

2 Mapping coordinate time t to local time τ

For a particle falling radially toward a hypothetical mass compacted below a critical radius, a mapping of the coordinate time t of a distant observer to a local time τ of the particle based on a radial distance r is shown in Fig. 1. The data shown in Fig. 1 can be obtained using the Schwarzschild metric.

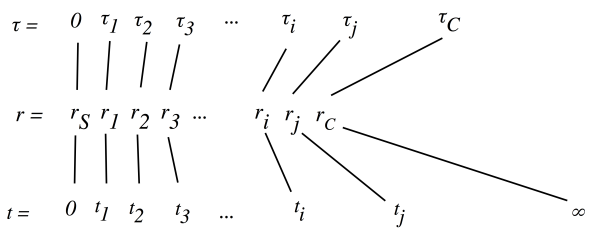

Fig. 1: For a particle falling radially, the Schwarschild Metric maps every value of the coordinate time t of a distant observer — where $0 \le t \le \infty$ — into a corresponding value of the local time τ of the particle — where $0 \le \tau \le \tau_C$.

Particularly, for a compact mass M with a Schwarzschild radius R, the Schwarzschild metric can be expressed using reference space coordinates (r, θ, ϕ), a coordinate time t and a local time τ (often referred to as proper time τ), i.e.,

$$c^2 d\tau^2 = c^2\left(1-\frac{R}{r}\right)dt^2 - \frac{dr^2}{(1-R/r)} - r^2 d\theta^2 - (r^2 sin^2\theta)d\phi^2. \quad (1)$$

Reference coordinates (r, θ, ϕ, t) are the space and time coordinates used by the distant observer to make measurements while the particle detects passage of time using local time coordinate τ. For a particle falling radially

$$d\theta = d\phi = 0, \quad (2)$$

so the Schwarzschild metric in (1) reduces to

$$c^2 d\tau^2 = c^2\left(1-\frac{R}{r}\right)dt^2 - \frac{dr^2}{(1-R/r)}, \quad (3)$$

which expresses a relationship between radial location r, local time τ and coordinate time t.

According to the relationship expressed by (3), for every radial location r_i reached from a starting location r_S, the coordinate time t_i to reach radial location r_i can be calculated using an integral

$$t_i = \int_{r_S}^{r_i} dt = \int_{r_S}^{r_i} f_1(r)dr, \quad (4)$$

where $f_1(r)$is a function of r derived from (3) [5, p. 667].

The local time τ_i required to reach the radial location r_i can be calculated using an integral

$$\tau_i = \int_{r_S}^{r_i} d\tau = \int_{r_S}^{r_i} f_2(r)dr, \quad (5)$$

where $f_2(r)$is a function of r derived from (3) [5, p. 663].

When the radial location r_i is set equal to a critical radius r_C, the integrand $f_1(r)$ for the integral in (4) and the integrand $f_2(r)$ for the integral in (5) are undefined; however, the integral in (5) converges while the integral in (4) does not. This

indicates that the critical radius r_C is reached in a finite local time τ_C but cannot be reached in finite Schwarzschild coordinate time.

The results of calculations using the integral of (4) and the integral of (5) are summarized in Fig. 1. As shown by Fig. 1, based on the integrals in (4) and (5), any value of coordinate time t, $0 \le t \le \infty$, can be mapped into a corresponding value for local time τ, $0 \le \tau \le \tau_C$ based on radial location r.

3 A pause to check correctness of Fig. 1

At this point the reader is encouraged to stop, look at Fig. 1, and perform an obviousness check to confirm why the data in Fig. 1 must be correct. The salient points are as follows:

- It takes infinite coordinate time (i.e., $t = \infty$) to reach the critical radius r_C;
- It takes finite local time τ_C to reach the critical radius r_C;
- Both local time τ and coordinate time t monotonically progress with decreasing r;
- To reach each radial location r_i will take a coordinate time t_i to complete and a local time τ_i to complete;
- Based on radial location r_i, a value of coordinate time t_i is mapped to a local time τ_i.

A reader who understands why Fig. 1 must be an accurate description of data derived from the Schwarzschild metric has already made a paradigm shift which if held to provides an intuitive foundation from which to understand the remainder of the paper. There is only one slight modification to Fig. 1 that is necessary to reveal why the critical radius can never be crossed. That is the subject of the next section.

4 Fig. 1 modified to take into account the finite duration of the compact mass

Fig. 1 depicts data from the Schwarzschild metric for a hypothetical compact mass that is presumed to exist forever in coordinate time. But what happens when the compact mass is replaced by an entity that more closely approximates reality in that it has a finite lifetime? For example, replace the compact mass with a theoretical black hole that has a finite lifetime. The result is shown in Fig. 2.

Because of Hawking radiation [6], it is estimated that a black hole will evaporate well within 10^{100} years. Therefore, added to Fig. 2 is finite coordinate time t_E which is the coordinate time required for a hypothetical black hole to completely evaporate [7]. Using the mapping shown in Fig. 1, it is possible to identify a radial location r_E — where $r_E > r_C$ — the particle will have reached simultaneous with the black hole evaporating at coordinate time t_E.

Fig. 2 shows a local time τ_E that represents the local time required for the particle to reach r_E. Local time τ_E corresponds with coordinate time t_E — the coordinate time required for a black hole to completely evaporate. Local time

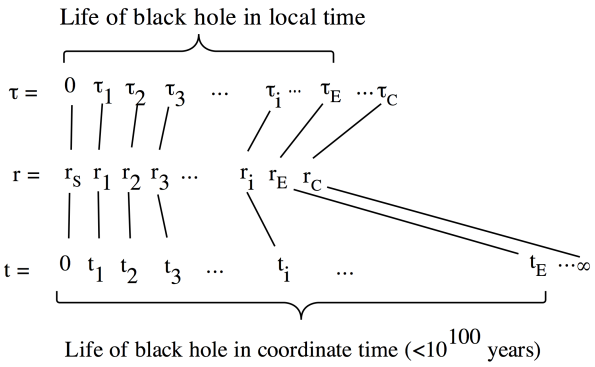

Fig. 2: According to the mapping of coordinate time to local time performed using the Schwarschild metric, the local time required to reach the critical radius of a black hole (τ_C) is longer than the life of the black hole (τ_E).

τ_C, as calculated by (5), represents the local time required for the particle to reach critical radius r_C. Because $\tau_E < \tau_C$, the particle will experience in local time τ that the black hole will evaporate before the critical radius can be reached.

5 The significance of Fig. 2

Fig. 2, based on the data from the Schwarzschild metric, shows a radially falling particle will never cross the critical radius of the compact mass regardless of what coordinate is used to measure the passage of time. For every radial location reached by the particle (i.e., $r_S \ge r \ge r_E$, there is a corresponding coordinate time t to reach the radial location and a corresponding local time τ to reach the radial location. The final destination of the particle is not dependent upon which measure of time is used to time the journey.

Fig. 2 presents a paradigm that is in conformance with the fundamental requirement of general relativity — and indeed a coherent universe — that there is a single reality with a logical sequence of events. The logical sequence of events does not vary based upon the reference frame from which observations are made.

Fig. 2 is meant to be an anchor from which can be shown how each of the five fallacies discussed below entices a departure from a coherent reality, where the logical sequence of events is consistent for every reference frame, into an incoherent reality where physical events differ based on reference frames from which observations are made.

In the following discussion of fallacies, evaporation of black holes is used as a convenient way to account for the finite lifetime of a hypothetical mass compacted below the critical radius. However, as should be clear from Fig. 2, a particle cannot cross the critical radius and therefore, as pointed out by [3], a mass will never compact below its critical radius. For the implication of this for collapsing stars, see the discussion of fallacy 4 below.

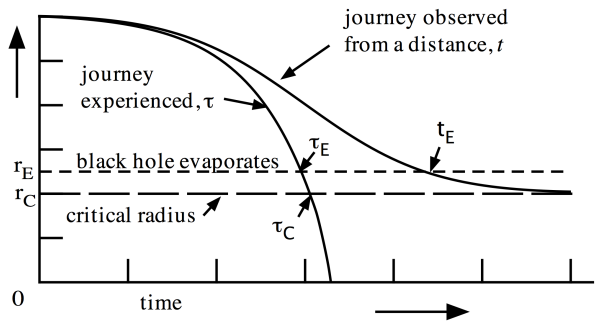

Fig. 3: Fig. 3 arranges the data shown in Fig. 2 in a different format. The trace extending to $r = 0$ incorrectly suggests that it is physically possible to cross the critical radius.

6 Fallacy 1: Showing a particle crosses the critical radius after evaporation of a black hole

For the journey of a particle to a black hole, elapsed time calculated using (4) and (5) is typically not represented as set out in Fig. 2, but rather as set out in Fig. 3 [5, p. 667].

Fig. 3, like Fig. 1 and Fig. 2, is a graphic representation of data obtained from (4) and (5). However, Fig. 3 qualifies as a fallacy because Fig. 3 includes extra data, not shown in Fig. 1 or Fig. 2., that incorrectly portrays the journey of the particle. Particularly, in Fig. 3, the trace representing local time τ extends beyond τ_C, the local time required to reach critical radius r_C.

Ordinary rules of mathematics cannot be used to generate the extra data for local time τ that occur after critical radius r_C is reached. This is because the integrand in (5) is undefined at r_C. Nevertheless, a novel "cycloid principle" [5, See pp. 663–664] has been used to generate this extra data.

But merely showing how the extra data can be mathematically generated does not overcome the logical sequencing problem introduced by adding the extra data to Fig. 3. The extra data suggests r_C can be reached and crossed in local time τ_C. However, this is impossible because as shown in Fig. 2, a black hole will evaporate in local time τ_E, so that critical radius r_C will cease to exist before it can be reached by the particle.

A horizontal line has been included in Fig. 3 to indicate where in Fig. 3 the evaporation of a black hole occurs. As shown by Fig. 3, evaporation of a black hole at radial location r_E, local time τ_E and coordinate time t_E logically occurs before reaching radial location r_C, local time τ_C and coordinate time $t = \infty$.

Fig. 3 should be corrected to show that a physical journey of a particle towards a black hole must end at radial location r_E — short of the critical radius r_C — when the black hole evaporates at local time τ_E and coordinate time t_E. The end of the journey occurs at r_E whether time is measured using coordinate time t or local time τ.

7 Fallacy 2: Declaring coordinates to be "pathological"

Fig. 3 suggests an impossible picture of physical reality. The particle cannot finally arrive at different destinations ($r = 0$ and $r = r_C$) merely based on the coordinate used to measure time.

As discussed in the last section, the logical sequence of events that occurs in all time frames, as out in Fig. 2, makes clear what is wrong with Fig. 3 and how it can be corrected. However, another competing explanation has been put forth.

The infinite coordinate time t required to reach the critical radius has been explained as the result of a "pathology" in the coordinates used to express the Schwarzschild metric. [5, See pp. 820-823].

Declaring coordinates to be pathological is a fallacy because it is a violation of general relativity at its most fundamental level. According to general relativity, all coordinates (reference frames) will observe the same reality. As Einstein [1, p. 117] made clear when setting out the basis for the theory of general relativity: "... all imaginable systems of coordinates, on principle, [are] equally suitable for the description of nature".

If general relativity is true, the events that occur during the journey of the particle occur in the same logical sequence irrespective of the coordinates used to observe the journey. Fig. 2 shows that the logical sequence of events that happens when time is measured using coordinate time t also happens in the same logical order when time is measured using local time τ. The next section shows that even when making observation from specially selected coordinates, the logical sequence of events does not differ from that shown in Fig. 2.

8 Fallacy 3: Use of specially selected coordinates

Fallacy 3 is an attempt to find coordinates that will show the particle can reach and cross the critical radius. The specially selected coordinates achieve this purpose based on a logical fallacy called begging the question in which the thing to be proved is assumed in a premise.

The thing to be proved is that a free falling particle can reach and cross the critical radius. The premise is that the specially selected coordinates can reach and cross the critical radius. When the specially selected coordinates are used as the reference coordinates in the Schwarzschild metric, and it is assumed the specially selected coordinates can cross the critical radius, it is possible to "show" the particle also can cross the critical radius.

But the premise is false. In the Schwarzschild metric, no reference frame can cross its critical radius because to do so would be a violation of the conservation of momentum and energy [4]. Below are considered two classes of specially selected coordinates:

- Coordinates that use the same reference frame as the free falling particle (e.g., the Novikov coordinates);

- Coordinates that use the reference frame of a radially traveling photon, (e.g., ingoing Eddington-Finkelstein coordinates and the Kruskal-Szekeres coordinates).

For each class of specially selected coordinates it is shown that their reference frame cannot cross a critical radius within the time it takes a black hole to evaporate.

Coordinates that use the reference frame of the free falling particle: Coordinates, such as the Novikov coordinates, that share a reference frame with the particle, also share the same time coordinate. Thus the local time coordinate τ measures the passage of time for both the local coordinates and the reference frame of the Novikov coordinates [5, p. 826].

The time required for a black hole to evaporate as measured by the time coordinate τ — which is the time coordinate for the reference frame shared by the Novikov coordinates shared and the local coordinates — has already been shown to be τ_E. See Fig. 2. As discussed above, $\tau_E < \tau_C$, indicating a black hole will evaporate at local time τ_E before the reference frame for the Novikov coordinates and the particle will be able to reach the critical radius at local time τ_C.

Coordinates that use the reference frame of a photon: The reference frame for ingoing Eddington-Finkelstein coordinates and the Kruskal-Szekeres coordinates is a radially traveling photon. [5, See pp. 826–832].

The coordinate time t for the photon to reach its critical radius can be very simply calculated from the Schwarzschild metric in (1). Because the photon is traveling radially, $d\theta = d\phi = 0$. Because local time for a photon does not progress, $d\tau = 0$. Therefore, the form of the Schwarzschild metric used to calculate values for coordinate time t is obtained by setting $d\theta = d\phi = d\tau = 0$ in (1) yielding

$$0 = c^2\left(1 - \frac{R}{r}\right)dt^2 - \frac{dr^2}{(1 - R/r)}. \qquad (6)$$

The integral in (4) can be used to calculate elapsed coordinate time t for the photon based on radial distance. Integrand $f_1(r)$ is obtained by rearranging the terms in (6), i.e.,

$$f_1(r) = \frac{dt}{dr} = \frac{1}{c(1 - R/r)}. \qquad (7)$$

When the photon reaches $r = R$, the integrand in (7) is undefined and the integral in (4) does not converge. Therefore the radially traveling photon will not reach R in finite coordinate time.

A black hole that evaporates in finite coordinate time t_E, will evaporate when the photon reaches a radial location r_L that is outside R. When the photon reaches radial location r_L at coordinate time t_E, the ingoing particle will be at radial location r_E, outside the critical radius r_C, as shown by Fig. 2.

In the reference frame of a photon, the black hole will evaporate when the photon reaches radial location r_L, before the photon reaches its critical radius R. As in all reference frames of the Schwarzschild metric, the reference frame of the photon is not able to reach the critical radius before the black hole evaporates.

9 Fallacy 4: Claiming the existence of surfaces trapped below a surface of last influence

Misner et al. [5, pp. 873–874] makes the argument that once the surface of a collapsing star crosses a critical radius, light reflecting from the surface remains trapped below the critical radius. This is a fallacy because the surface of a collapsing star will never cross the critical radius [3]. The very last particle on the surface to cross the critical radius can be approximately modeled by the radially falling particle of Fig. 2. From the perspective of the distant observer (coordinate time in Fig. 2), the collapsing star evaporates in finite time, before the infinite coordinate time required for the last particle on the surface to cross the critical radius.

From the perspective of a particle on the surface (local time in Fig. 2), the collapsing star evaporates very suddenly as the particle nears the critical radius. It is intriguing to imagine the experience of the particle as the surface of the collapsing star immediately disintegrates into radiation near the critical radius. Such an inferno of unimaginable proportions would tend to be masked from a distant observer by the extreme gravity near the critical radius. But as the surface burns away reducing the mass of the collapsing star — causing the critical radius to retreat farther below the surface of the collapsing star — a less time dilated view of the inferno might be released, perhaps providing an explanation for the sudden appearance of quasars.

Since the surface of a collapsing star cannot cross its critical radius in finite coordinate time t, Misner et al. [5, pp. 873–874] measures time from the reference frame for the ingoing Eddington-Finkelstein coordinates. As discussed in the prior section, use of ingoing Eddington-Finkelstein coordinates to prove the critical radius can be crossed just begs the question. The ingoing Eddington-Finkelstein coordinates will not cross the Schwarzschild metric of the collapsing star before the collapsing star evaporates. This should be especially clear for the example of a collapsing star since the surface, located outside its critical radius, will be an impenetrable barrier that will prevent any photon, serving as a reference frame for the ingoing Eddington-Finkelstein coordinates, from reaching its critical radius at R.

10 Fallacy 5: Claiming the infinite coordinate time to reach the critical radius is an optical illusion

It has been asserted that as measured by proper time, a free-falling traveler quickly reaches the critical radius. To the distant observer it appears to take an infinite amount of coordinate time to reach the critical radius as a result of an optical illusion caused by light propagation introducing a delay in communicating that the critical radius has been reached [5,

pp. 874–875]. Fallacy 5 is a departure from general relativity because in general relativity the difference between local time and coordinate time is not merely the result of delay introduced by light propagation. In the theory of general relativity, time progresses at different rates depending on the strength of the gravity field in which measurements are made.

Einstein [8, p. 106] explains: "we must use clocks of unlike constitution, for measuring time at places with differing gravitational potential." This principle of relativity is embodied in the Schwarzschild metric where gravity changes the rate at which time progresses [2]. For a precise description of how in the Schwarzschild metric gravity affects time based on the conservation of momentum and energy, see [4, Eq. 8].

Because fallacy 5 does not properly account for the effect gravity has on time, and is therefore not in accord with general relativity or the Schwarzschild metric, the results predicted by fallacy 5 do not agree with results calculated using the Schwarzschild metric. This is illustrated by a hypothetical in the following section.

11 A hypothetical illustrating the logical contradictions introduced by fallacy 5

According to fallacy 5, as measured by proper time, a radially falling traveler quickly reaches and crosses the critical radius of a black hole. The reality that the traveler quickly reaches the critical radius appears to the distant observer to take an infinite amount of time because of the propagation of light.

Fallacy 5's portrayal of reality is not consistent with calculations made using the Schwarzschild metric.

For example, put a reflector on the back of the traveler and have the distant observer periodically shine a light beam at the traveler. Use the Schwarzschild metric to calculate the radial location at which the faster moving light beam will overtake the slower moving traveler and reflect back to indicate the location of the traveler to the distant observer.

No matter how much of a head start the traveler has before the light is turned on (even trillions of years or longer, as measured using coordinate time), according to the Schwarzschild metric the light will always overtake the traveler before the critical radius is reached. The radial location at which the traveler is overtaken is the same whether local time or coordinate time is used to make the calculations, provided start time and overtake time for each light beam are measured with the same time coordinate. This result is inevitable based on the pattern of the data obtained from the Schwarzschild metric, as shown in Fig. 1.

As shown by Fig. 2, the distant observer can continue to shine light beams at the traveler until the distant observer observes the black hole evaporates. The feedback from the reflected light beams will tell the distant observer that the traveler remains outside the black hole as the black hole evaporates slowly in coordinate time, and quickly in local time. This contradicts the assertion of fallacy 5 that the traveler easily reaches and crosses the critical radius.

The distant observer does not even need to shine a light beam for this experiment as background radiation reflecting from the traveler provides exactly the same information.

Hawking radiation also provides the same information. While the distant observer sees the traveler outside the critical radius, the distant observer will also observe Hawking radiation from the evaporating black hole, which will first have to pass through the radial location of the traveler before reaching the distant observer. This indicates to the distant observer that the traveler will have experienced, before the distant observer, radiation emitted during the disintegration of the black hole. Further, the radiation passing by the traveler will continuously bring information to the distant observer about the location of the traveler confirming the information from the light beams. Each photon of radiation from the evaporating black hole that passes by the traveler is a progress report on the traveler's location that will confirm to the distant observer that the traveler had not yet passed through the critical radius when that photon of radiation passed the traveler. Such progress reports will continue until the black hole completely evaporates.

Light beams from the distant observer, background radiation and Hawking radiation will all intercept the traveler outside the critical radius — according to the Schwarzschild metric — regardless of the coordinates used to make measurements. This result contradicts the assertion of fallacy 5 that the critical radius is quickly crossed and only appears to the distant observer to take infinite time because of light propagation.

Submitted on November 16, 2010 / Accepted on December 15, 2010

References

1. Einstein A. The foundation of the general theory of relativity. The Principle of Relativity. Dover Publications, New York, 1923. pp. 111–164.
2. Schwarzschild K. On the gravitational field of a mass point according to Einstein's theory. Translated by S. Antoci, A. Loinger, 1999, arXiv:Physics/9905030.
3. Einstein A. On a stationary system with spherical symmetry consisting of many gravitating masses. *Annals of Mathematics*, 1939, v. 40, no. 4, 922–936.
4. Weller D. How black holes violate the conservation of energy. *Progress in Physics*, 2011, v. 1, 89–92.
5. Misner C., Thorne K., Wheeler J. Gravitation, W.H. Freeman & Co, New York, 1973.
6. Hawking S. W. Black Hole Explosions? *Nature*, 1974, v. 248, no. 5443, 30–31.
7. Vachaspati T., Stojkovic D., Krauss L. Observation of incipient black holes and the information loss problem. *Physical Review D*, 2007, v. 76, 024005.
8. Einstein A. On the Influence of gravitation on the propagation of light. The Principle of Relativity. Dover Publications, New York, 1923, pp. 99–108.

Lee Smolin Five Great Problems and Their Solution without Ontological Hypotheses

Gunn Quznetsov

Chelyabinsk State University, Chelyabinsk, Ural, Russia. E-mail: gunn@mail.ru, quznets@yahoo.com

Solutions of Lee Smolin Five Great Problems from his book *The Trouble with Physics: the Rise of String Theory, the Fall of a Science, and What Comes Next* are described. These solutions are obtained only from the properties of probability without any ontological hypotheses.

Introduction

In his book [1] Lee Smolin, professor of Perimeter Institute, Canada, has formulated the following five problems which he named Great Problems:

> *Problem 1: Combine general relativity and quantum theory into a single theory that claim to be the complete theory of nature.*
>
> *Problem 2: Resolve the problems in the foundations of quantum mechanics, either by making sense of the theory as it stands or by inventing a new theory that does make sense. ...*
>
> *Problem 3: Determine whether or not the various particles and forces can be unified in a theory that explain them all as manifestations of a single, fundamental entity. ...*
>
> *Problem 4: Explain how the values of of the free constants in the standard model of particle physics are chosen in nature. ...*
>
> *Problem 5: Explain dark matter and dark energy. Or if they don't exist, determine how and why gravity is modified on large scales. ...*

Solution

Let us consider the free Dirac Lagrangian:

$$\mathcal{L} := \psi^{\dagger}\left(\beta^{[k]}\partial_k + m\gamma^{[0]}\right)\psi. \qquad (1)$$

Here*

$$\beta^{[\nu]} := \begin{bmatrix} \sigma_\nu & 0_2 \\ 0_2 & -\sigma_\nu \end{bmatrix} \quad , \gamma^{[0]} := \begin{bmatrix} 0_2 & 1_2 \\ 1_2 & 0_2 \end{bmatrix}$$

where σ_1, σ_2, σ_3 are the Pauli matrices.

Such Lagrangian is not invariant [2] under the SU(2) transformation with the parameter α:

$$\psi^{\dagger}U^{\dagger}(\alpha)\left(\beta^{[k]}\partial_k + m_1\gamma^{[0]}\right)U(\alpha)\psi = \psi^{\dagger}\left(\beta^{[k]}\partial_k + (m\cos\alpha)\,\gamma^{[0]}\right)\psi,$$

the mass member is changed under this transformation.

Matrices $\beta^{[\nu]}$ and $\gamma^{[0]}$ are anticommutative. But it turns out that there exists a fifth matrix $\beta^{[4]}$ anticommuting with all these four matrices:

$$\beta^{[4]} := \mathrm{i}\begin{bmatrix} 0_2 & 1_2 \\ -1_2 & 0_2 \end{bmatrix}.$$

And the term with this matrix should be added to this Lagrangian mass term:

$$\underline{\mathcal{L}} := \psi^{\dagger}\left(\beta^{[k]}\partial_k + m_1\gamma^{[0]} + m_2\beta^{[4]}\right)\psi$$

where $\sqrt{m_1^2 + m_2^2} = m$.

Let $U(\alpha)$ be any SU(2)-matrix with parameter α and let $\mathbf{U}$ be the space in which $U(\alpha)$ acts. In such case $U(\alpha)$ divides the space $\mathbf{U}$ into two orthogonal subspaces $\mathbf{U}_o$ and $\mathbf{U}_x$ such that for every element ψ of $\mathbf{U}$ there exists an element ψ_o of $\mathbf{U}_o$ and an element ψ_x of $\mathbf{U}_x$ which fulfills the following conditions [3, 4]:

1.
$$\psi_o + \psi_x = \psi,$$

2.
$$\begin{aligned}&\psi_o^{\dagger}U^{\dagger}(\alpha)\left(\beta^{[k]}\partial_k + m_1\gamma^{[0]} + m_2\beta^{[4]}\right)U(\alpha)\psi_o = \\ =\ &\psi_o^{\dagger}(\beta^{[k]}\partial_k + (m_1\cos\alpha - m_2\sin\alpha)\,\gamma^{[0]} + \\ &+ (m_2\cos\alpha + m_1\sin\alpha)\,\beta^{[4]})\psi_o,\end{aligned} \qquad (2)$$

3.
$$\begin{aligned}&\psi_x^{\dagger}U^{\dagger}(\alpha)\left(\beta^{[k]}\partial_k + m_1\gamma^{[0]} + m_2\beta^{[4]}\right)U(\alpha)\psi_x = \\ =\ &\psi_x^{\dagger}(\beta^{[k]}\partial_k + (m_1\cos\alpha + m_2\sin\alpha)\,\gamma^{[0]} + \\ &+ (m_2\cos\alpha - m_1\sin\alpha)\,\beta^{[4]})\psi_x.\end{aligned} \qquad (3)$$

In either case, m does not change.

I call these five ($\beta := \left\{\beta^{[\nu]}, \beta^{[4]}, \gamma^{[0]}\right\}$) anticommuting matrices *Clifford pentad*. Any sixth matrix does not anticommute with all these five.

There exist only six Clifford pentads (for instance, [5, 6]): I call one of them (the pentad β) *the light pentad*, three (ζ, η, θ) — *the chromatic pentads*, and two ($\underline{\Delta}$, $\underline{\Gamma}$) — *the gustatory pentads*.

*$0_2 := \begin{bmatrix} 0 & 0 \\ 0 & 0 \end{bmatrix}, 1_2 := \begin{bmatrix} 1 & 0 \\ 0 & 1 \end{bmatrix}, \beta^{[0]} := -1_4 := -\begin{bmatrix} 1_2 & 0_2 \\ 0_2 & 1_2 \end{bmatrix}$, $k \in \{0, 1, 2, 3\}$, $\nu \in \{1, 2, 3\}$.

The light pentad contains three diagonal matrices ($\beta^{[\nu]}$) corresponding to the coordinates of 3-dimensional space, and two antidiagonal matrices ($\beta^{[4]}$, $\gamma^{[0]}$) relevant to mass terms (2,3) — one for the lepton state and the other for the neutrino state of this lepton.

Each chromatic pentad also contains three diagonal matrices corresponding to three coordinates and two antidiagonal mass matrices - one for top quark state and the other — for bottom quark state.

Each gustatory pentad contains a single diagonal coordinate matrix and two pairs of antidiagonal mass matrices [6] — these pentads are not needed yet.

Let* $\langle \rho_A \mathrm{c},\, j_{A,\nu} \rangle$ be a 1+3-vector of probability density of a pointlike event A.

For any A the set of four equations with an unknown complex 4×1 matrix function $\varphi(x_k)$

$$\left\{ \begin{array}{c} \rho_A = \varphi^\dagger \varphi, \\ \dfrac{j_{A,\nu}}{\mathrm{c}} = -\varphi^\dagger \beta^{[\nu]} \varphi \end{array} \right|$$

has solution [3].

If† $\rho_{\mathfrak{A}}(x_k) = 0$ for all x_k such that $|x_k| > (\pi \mathrm{c}/\mathrm{h})$ then φ obeys the following equation [10]:

$$\begin{aligned} &\Big(-\left(\partial_0 + \mathrm{i}\Theta_0 + \mathrm{i}\Upsilon_0\gamma^{[5]}\right) + \beta^{[\nu]}\left(\partial_\nu + \mathrm{i}\Theta_\nu + \mathrm{i}\Upsilon_\nu\gamma^{[5]}\right) + \\ &\qquad + 2\left(\mathrm{i}M_0\gamma^{[0]} + \mathrm{i}M_4\beta^{[4]}\right)\Big)\varphi + \\ &+\Big(-\left(\partial_0 + \mathrm{i}\Theta_0 + \mathrm{i}\Upsilon_0\gamma^{[5]}\right) - \zeta^{[\nu]}\left(\partial_\nu + \mathrm{i}\Theta_\nu + \mathrm{i}\Upsilon_\nu\gamma^{[5]}\right) + \\ &\qquad + 2\left(-\mathrm{i}M_{\zeta,0}\gamma^{[0]}_\zeta + \mathrm{i}M_{\zeta,4}\zeta^{[4]}\right)\Big)\varphi + \\ &+\Big(\left(\partial_0 + \mathrm{i}\Theta_0 + \mathrm{i}\Upsilon_0\gamma^{[5]}\right) - \eta^{[\nu]}\left(\partial_\nu + \mathrm{i}\Theta_\nu + \mathrm{i}\Upsilon_\nu\gamma^{[5]}\right) + \\ &\qquad + 2\left(-\mathrm{i}M_{\eta,0}\gamma^{[0]}_\eta - \mathrm{i}M_{\eta,4}\eta^{[4]}\right)\Big)\varphi + \\ &+\Big(-\left(\partial_0 + \mathrm{i}\Theta_0 + \mathrm{i}\Upsilon_0\gamma^{[5]}\right) - \theta^{[\nu]}\left(\partial_\nu + \mathrm{i}\Theta_\nu + \mathrm{i}\Upsilon_\nu\gamma^{[5]}\right) + \\ &\qquad + 2\left(\mathrm{i}M_{\theta,0}\gamma^{[0]}_\theta + \mathrm{i}M_{\theta,4}\theta^{[4]}\right)\Big)\varphi = \\ &= \ 0 \end{aligned}$$

with real
$\Theta_k(x_k)$, $\Upsilon_k(x_k)$, $M_0(x_k)$, $M_4(x_k)$, $M_{\zeta,0}(x_k)$, $M_{\zeta,4}(x_k)$, $M_{\eta,0}(x_k)$, $M_{\eta,4}(x_k)$, $M_{\theta,0}(x_k)$, $M_{\theta,4}(x_k)$
and with

$$\gamma^{[5]} := \left[\begin{array}{cc} 1_2 & 0_2 \\ 0_2 & -1_2 \end{array} \right].$$

*c = 299792458.

†h := $6.6260755 \cdot 10^{-34}$

The first summand of this equation contains elements of the light pentad only. And the rest summands contain elements of the chromatic pentads only.

This equation can be rewritten in the following way:

$$\begin{aligned} &\beta^{[k]}\left(-\mathrm{i}\partial_k + \Theta_k + \Upsilon_k\gamma^{[5]}\right)\varphi + \\ &+(M_0\gamma^{[0]} + M_4\beta^{[4]} - \\ &-M_{\zeta,0}\gamma^{[0]}_\zeta + M_{\zeta,4}\zeta^{[4]} - \\ &-M_{\eta,0}\gamma^{[0]}_\eta - M_{\eta,4}\eta^{[4]} + \\ &+M_{\theta,0}\gamma^{[0]}_\theta + M_{\theta,4}\theta^{[4]})\varphi = \\ = \ &0 \end{aligned} \tag{4}$$

because

$$\zeta^{[\nu]} + \eta^{[\nu]} + \theta^{[\nu]} = -\beta^{[\nu]}.$$

This equation is a generalization of the Dirac's equation with gauge fields $\Theta_k(x_k)$ and $\Upsilon_k(x_k)$ and with eight mass members. The mass members with elements of the light pentad (M_0 and M_4) conform to neutrino and its lepton states. And six mass members with elements of the chromatic pentads conform to three pairs (up and down) of chromatic states (red, green, blue).

Let this equation not contains the chromatic mass nembers:

$$\left(\beta^{[k]}\left(-\mathrm{i}\partial_k + \Theta_k + \Upsilon_k\gamma^{[5]}\right) + M_0\gamma^{[0]} + M_4\beta^{[4]}\right)\varphi = 0. \tag{5}$$

If function φ is a solution of this equation then φ represents the sum of functions $\varphi_{n,s}$ which satisfy the following conditions [3, 62–71]:

n and s are integers;

each of these functions obeys its equation of the following form:

$$\left(\beta^{[k]}\left(\mathrm{i}\partial_k - \Theta_0 - \Upsilon_0\gamma^{[5]}\right) - \frac{\mathrm{h}}{\mathrm{c}}\left(\gamma^{[0]}n + \beta^{[4]}s\right)\right)\varphi_{n,s} = 0; \tag{6}$$

for each point x_k of space-time: or this point is empty (for all n and s: $\varphi_{n,s}(x_k) = 0$), or in this point is placed a single function (for x_k there exist integers n_0 and s_0 such that $\varphi_{n_0,s_0}(x_k) \neq 0$ and if $n \neq n_0$ and/or $s \neq s_0$ then $\varphi_{n,s}(x_k) = 0$).

In this case if $m := \sqrt{n^2 + s^2}$ then m is a natural number. But under the SU(2)-transformation with parameter α (2, 3):
$m \to \left((n\cos\alpha - s\sin\alpha)^2 + (s\cos\alpha + n\sin\alpha)^2\right)^{0.5}$,
$(n\cos\alpha - s\sin\alpha)$ and $(s\cos\alpha + n\sin\alpha)$ must be integers too. But it is impossible.

But for arbitrarily high accuracy in distant areas of the natural scale there exist such numbers m that for any α some natural numbers n' and s' exist which obey the following conditions: $n' \approx (n\cos\alpha - s\sin\alpha)$ and $s' \approx (s\cos\alpha + n\sin\alpha)$. These numbers m are separated by long intervals and determine the mass spectrum of the generations of elementary particles. Apparently, this is the way to solve Problem 4 because

the masses are one of the most important constants of particle physics.

The Dirac's equation for leptons with gauge members which are similar to electroweak fields is obtained [4, p. 333–336] from equations (5, 6). Such equation is invariant under electroweak transformations. And here the fields W and Z obey the Klein-Gordon type equation with nonzero mass.

If the equation (4) does not contain lepton's and neutrino's mass terms then the Dirac's equation with gauge members which are similar to eight gluon's fields is obtained. And oscillations of the chromatic states of this equation bend space-time. This bend gives rise to the effects of redshift, confinement and asymptotic freedom, and Newtonian gravity turns out to be a continuation of subnucleonic forces [10]. And it turns out that these oscillations bend space-time so that at large distances the space expands with acceleration according to Hubble's law [7]. And these oscillations bend space-time so that here appears the discrepancy between the quantity of the luminous matter in the space structures and the traditional picture of gravitational interaction of stars in these structures. Such curvature explains this discrepancy without the Dark Matter hypothesis [8] (Problem 5).

Consequently, the theory of gravitation is a continuation of quantum theory (Problem 1 and Problem 3).

Thus, concepts and statements of Quantum Theory are concepts and statements of the probability of pointlike events and their ensembles.

Elementary physical particle in vacuum behaves like these probabilities. For example, according to doubleslit experiment [9], if a partition with two slits is placed between a source of elementary particles and a detecting screen in vacuum then interference occurs. But if this system will be put in a cloud chamber, then trajectory of a particle will be clearly marked with drops of condensate and any interference will disappear. It seems that a physical particle exists only in the instants of time when some events happen to it. And in the other instants of time the particle does not exist, but the probability of some event to happen to this particle remains.

Thus, if no event occurs between an event of creation of a particle and an event of detection of it, then the particle does not exist in this period of time. There exists only the probability of detection of this particle at some point. But this probability, as we have seen, obeys the equations of quantum theory and we get the interference. But in a cloud chamber events of condensation form a chain meaning the trajectory of this particle. In this case the interference disappears. But this trajectory is not continuous — each point of this line has an adjacent point. And the effect of movement of this particle arises from the fact that a wave of probability propagates between these points.

Consequently, the elementary physical particle represents an ensemble of pointlike events associated with probabilities. And charge, mass, energy, momentum, spins, etc. represent parameters of distribution of these probabilities. It explains all paradoxes of quantum physics. Schrödinger's cat lives easily without any superposition of states until the microevent awaited by everyone occurs. And the wave function disappears without any collapse in the moment when event probability disappears after the event occurs.

Hence, entanglement concerns not particles but probabilities. That is when the event of the measuring of spin of Alice's electron occurs then probability for these entangled electrons is changed instantly in the whole space. Therefore, nonlocality acts for probabilities, not for particles. But probabilities can not transmit any information (Problem 2).

Conclusion

Therefore, Lee Smolin's Five Great Problems do have solution only using the properties of probabilities. These solutions do not require any dubious ontological hypotheses such as superstrings, spin networks, etc.

Submitted on December 15, 2010 / Accepted on December 16, 2010

References

1. Smolin L. The trouble with physics: the rise of string theory, the fall of a science, and what comes next. Houghton Mifflin, Boston, 2006.
2. Kane G. Modern Elementary Particle Physics. Addison-Wesley Publ. Comp., 1993, p. 93.
3. Quznetsov G. Probabilistic Treatment of Gauge Theories, in series *Contemporary Fundamental Physics*, ed. Dvoeglazov V., Nova Sci. Publ., N.Y., 2007.
4. Quznetsov G. It is not Higgs. *Prespacetime Journal*, 2010, v. 1, 314–343.
5. Madelung E. Die Mathematischen Hilfsmittel des Physikers. Springer Verlag, Berlin, Gottingen, Heidelberg, 1957, p. 12.
6. Quznetsov G. Logical Foundation of Theoretical Physics. Nova Sci. Publ., N.Y., 2006.
7. Quznetsov G. A. Oscillations of the Chromatic States and Accelerated Expansion of the Universe. *Progress in Physics*, 2010, v. 2, 64–65.
8. Quznetsov G. Dark Matter and Dark Energy are Mirage. *Prespacetime Journal*, October 2010, v. 1, Issue 8, 1241–1248, arXiv: 1004.4496 2.
9. Quznetsov G. Double-Slit Experiment and Quantum Theory Event-Probability Interpretation, arXiv: 1002.3425.
10. Quznetsov G. A. 4X1-Marix Functions and Dirac's Equation. *Progress in Physics*, 2009, v. 2, 96–106.

On the Failure of Particle Dark Matter Experiments to Yield Positive Results

Joseph F. Messina
Topical Group in Gravitation, American Physical Society,
P.O. Box 130520, The Woodlands, TX 77393, USA.
Email: jfmessina77@yahoo.com

It is argued that the failure of *particle* dark matter experiments to verify its existence may be attributable to a *non-Planckian* "action", which renders dark matter's behavior contradictory to the consequences of quantum mechanics as it applies to luminous matter. It is pointed out that such a possibility cannot be convincingly dismissed in the absence of a physical law that prohibits an elementary "action" smaller than Planck's. It is further noted that no purely dark matter measurement of Planck's constant exists. Finally, the possibility of a non-Planckian cold dark matter particle is explored, and found to be consistent with recent astronomical observations.

The search for dark matter (DM) remains one of the most vexing of the unresolved problems of contemporary physics. While the existence of DM is no longer in dispute, its composition is a matter of lively debate. A variety of subatomic particles with exotic properties have been proposed as possible candidates. However, as is well known by now, after more than three decades of experimentation, and considerable expenditure, none have yet been detected. If the past is any guide, such negative results often force us to radically reexamine some of the basic tenets underlying physical concepts. It is the purpose of this paper to propose a plausible, experimentally verifiable, explanation for the persistent failure of *particle* DM experiments to yield positive results.

Since DM's existence is inferred solely from its gravitational effects, and its nature is otherwise unknown, one cannot rule-out the possibility that DM's behavior may be contradictory to the consequences of quantum mechanics as it applies to luminous matter (LM), which is particularly troubling since it necessarily brings into question the applicability of Planck's constant as a viable "action" in this *non-luminous* domain. It is important to point out that *no* purely DM measurement of Planck's constant exists. Indeed, all that we know about Planck's constant is based on electromagnetic and strong interaction experiments, whose particles and fields account for only 4.6% of the mass-energy density of the observable universe, which pales when compared to the 23.3% attributable to DM.

While it is true that very little is known about DM, some progress has been made on the astronomical front. Recent observations have revealed important new clues regarding its behavior. Particularly important, an analysis of cosmic microwave background observables has provided conclusive evidence that DM is made up of slow-moving particles [1], a development that has firmly established the cold DM paradigm as the centerpiece of the standard cosmology. Equally revealing, large aggregates of DM have been observed passing right through each other without colliding [2–3], which is clearly significant since it essentially rules out the idea that particles of DM can somehow interact and collide with each other. Taken together these astronomical findings are suggestive of a non-relativistic, non-interacting, particle whose coherent mode of behavior is a characteristic of *classical light*. Clearly, for such a particle, the condition of quantization can only become a physical possibility if its "action" is considerably *smaller* than Planck's.

Upon reflection one comes to the realization that such a possibility can be accommodated in the context of the framework of quantum mechanics, whose formalism allows for *two* immutable "actions". Namely, Planck's familiar constant, h, which has been shown experimentally to play a crucial role in the microphysical realm, and the more diminutive, less familiar "action" e^2/c where e is the elementary charge, and c is the velocity of light in a vacuum (denoted by the symbol j for simplicity of presentation). While this *non-Planckian* constant appears to have no discernible role in our luminous world, it is, nevertheless, clearly of interest since it may be sufficiently *smaller* than Planck's constant to account for DM's astronomical behavior; a possibility that cannot be convincingly dismissed in the absence of a physical law that prohibits an *elementary* "action" smaller than Planck's.

Whether or not we know DM's nature, the undisputed fact remains that *all* elementary particles exhibit wavelike properties. Hence, if DM's behavior is orchestrated by this *non-Planckian* "action" it should be possible to describe such particle waves quantum mechanically. In order to facilitate matters we shall assume that DM's non-Planckian *particle/wave* properties are consistent with both the Einstein relation for the total energy of a particle, in the form

$$E = jf = mc^2 = \frac{m_0 c^2}{\sqrt{1 - v^2/c^2}} \tag{1}$$

and the de Broglie relation for the momentum

$$p = \frac{j}{\lambda} = mv = \frac{m_0 v}{\sqrt{1 - v^2/c^2}}\,, \tag{2}$$

where $j = 7.6956 \times 10^{-30}$ erg s is the conjectured DM "action" quantum, which may be compared with the Planck constant,

h, found in our luminous world (i.e., 6.6260×10^{-27} erg s). Now, since the relation between energy and momentum in *classical* mechanics is simply

$$E = \frac{1}{2m}\, p^2 \tag{3}$$

we can replace E and p with the differential operators

$$E = i\,\frac{j}{2\pi}\,\frac{\partial}{\partial t} \tag{4}$$

and

$$p = -\,i\,\frac{j}{2\pi}\,\frac{\partial}{\partial x} \tag{5}$$

and operate with the result on the wave function $\psi(x,t)$ that represents the de Broglie wave. We then obtain

$$i\,\frac{j}{2\pi}\,\frac{\partial\psi}{\partial t} = -\frac{(j/2\pi)^2}{2m}\,\frac{\partial^2\psi}{\partial x^2}\,, \tag{6}$$

which is Schrödinger's general wave equation for a non-relativistic *free* particle. Its solution describes a *non-Planckian* particle that is the quantum mechanical analog of a non-interacting *classical* particle that is moving in the x direction with constant velocity; a result that closely mirrors DM's elusive behavior, and can be simply explained in the context of this generalization. That is, the *classical* concept of two particles exerting a force on each other corresponds to the quantum mechanical concept that the de Broglie wave of one particle influences the de Broglie wave of another particle. However, this is only possible if the de Broglie wave propagates *non-linearly,* in sharp contrast with Schrödinger's general wave equation for which the propagation of waves is described by a *linear* differential equation. Hence the presence of one wave *does not* affect the behavior of another wave, allowing them to pass right through each other without colliding, which is consistent with the results of the aforementioned astronomical observations [2–3].

If it exists, this non-Planckian particle would easily have eluded detection because of the diminutive magnitude of the non-Planckian "action". More succinctly, the closer one comes to the *classical* limit the *less* pronounced are the quantum effects. As a result, its behavior is expected to be *more* wave-like than particlelike, which is consistent with the observed coherent mode of behavior of large aggregates of DM [2–3]. Clearly, the detection of this non-Planckian particle in a terrestrial laboratory setting will, almost certainly, require the use of a wholly different set of experimental tools than those presently employed in conventional DM experiments, which are, after all, specifically designed to detect *particle* interactions.

While, as has been shown, DM's behavior in the astronomical arena can be satisfactorily accounted for quantum mechanically, in terms of this non-Planckian "action", the detailed implications remain to be worked out. Nevertheless, the introduction of this *non-Planckian cold DM particle* in the context of quantum mechanics, provides a fundamentally plausible means of explaining the failure of *conventional* experiments to provide conclusive evidence for the *particle* nature of DM. After these many decades of null experimental results, the time has come to acknowledge the possibility that DM's behavior may be orchestrated by a richer variety of fundamentally different mechanisms than previously recognized.

Appendix

I have taken note of the fact that if the reader is to grapple with some of the concepts generated by this paper, it would be advisable to ascribe an appropriate name to this non-Planckian particle. Clearly, the basic aspect that one should be mindful of is this particle's indispensable role in enabling the *warping* of spacetime sufficiently enough to cradle whole galaxies. Hence, I believe *"warpton"* would be the name of choice.

It is hoped that the experimental community can be sufficiently motivated to make a determined search for this provocative particle.

Submitted on December 14, 2010 / Accepted on December 15, 2010.

References

1. Lewis A.D., Buote D.A., Stocke J.T. Chandra Observations of A2029: The Dark Matter Profile Down to below $0.01r_{\rm vir}$ in an Unusually Relaxed Cluster. *The Astrophysical Journal*, 2003, v. 586, 135–142.
2. Clowe D., Bradac M., Gonzalez A.H., Markevitch M., Randall S.W., Jones C., Zaritsky D. A Direct Empirical Proof of the Existence of Dark Matter. *The Astrophysical Journal*, 2006, v. 648(2), L109–L113.
3. Natarajan P., Kneib J.-P. Smail I., Ellis R. Quantifying Substructure Using Galaxy-Galaxy Lensing in Distant Clusters. arXiv: astro-ph/0411426.

Application of the Model of Oscillations in a Chain System to the Solar System

Andreas Ries and Marcus Vinicius Lia Fook
Universidade Federal de Campina Grande, Unidade Acadêmica de Engenharia de Materiais, Rua Aprígio Veloso 882, 58429-140 Campina Grande — PB, Brazil

E-mail: andreasries@yahoo.com

A numerical analysis revealed that masses, radii, distances from the sun, orbital periods and rotation periods of celestial bodies can be expressed on the logarithmic scale though a systematic set of numbers: $4e$, $2e$, e, $\frac{e}{2}$, $\frac{e}{4}$, $\frac{e}{8}$ and $\frac{e}{16}$. We analyzed these data with a fractal scaling model originally published by Müller in this journal, interpreting physical quantities as proton resonances. The data were expressed in continued fraction form, where all numerators are Euler's number. From these continued fractions, we explain the volcanic activity on Venus, the absence of infrared emission of Uranus and why Jupiter and Saturn emit more infrared radiation than they receive as total radiation energy from the Sun. We also claim that the Kuiper cliff was not caused by a still unknown planet. It can be understood why some planets have an atmosphere and others not, as well as why the ice on dwarf planet Ceres does not evaporate into space through solar radiation. The results also suggest that Jupiter and Saturn have the principal function to capture asteroids and comets, thus protecting the Earth, a fact which is well-reflected in the high number of their irregular satellites.

1 Introduction

Recently in three papers of this journal, Müller [1–3] suggested a chain of similar harmonic oscillators as a general model to describe physical quantities as proton resonance oscillation modes. In this model, the spectrum of eigenfrequencies of a chain system of many proton harmonic oscillators is given by a continuous fraction equation [2]:

$$f = f_p \exp S \tag{1}$$

where f is any natural oscillation frequency of the chain system, f_p the oscillation frequency of one proton and S the continued fraction corresponding to f. S was suggested to be in the canonical form with all partial numerators equal 1 and the partial denominators are positive or negative integer values.

$$S = n_0 + \cfrac{1}{n_1 + \cfrac{1}{n_2 + \cfrac{1}{n_3 + \ldots}}} \tag{2}$$

Particularly interesting properties arise when the nominator equals 2 and all denominators are divisible by 3. Such fractions divide the logarithmic scale in allowed values and empty gaps, i.e. ranges of numbers which cannot be expressed with this type of continued fractions. He showed that these continued fractions generate a self-similar and discrete spectrum of eigenvalues [1], that is also logarithmically invariant. Maximum spectral density areas arise when the free link n_0 and the partial denominators n_i are divisible by 3.

In a previous article [5] we slightly modified this model, substituting all nominators by Euler's number. In that way we confirmed again that elementary particles are proton resonance states, since most masses were found to be located close to spectral nodes and definitively not random.

In this article we investigated various solar system data, such as masses, sizes and distances from the Sun, rotation and orbital periods of celestial bodies on the logarithmic scale. We showed that continued fractions with Euler's number as nominator are adequate to describe the solar system. From these continued fractions we derived claims regarding specific properties of planets. It became evident, that the solar system possesses a hidden fractal structure.

2 Data sources and computational details

All solar system data, such as distances, masses, radii, orbital and rotation periods of celestial bodies, were taken from the NASA web-site. The km was converted into the astronomical unit via 1 AU = 149, 597, 870.7 km. The mean distance of an object from the central body is understood as $\frac{1}{2}(Aphelion - Periphelion)$. Numerical values of continued fractions were always calculated using the the Lenz algorithm as indicated in reference [4].

3 Results and discussion

3.1 Standard numerical analysis

Before doing any numerical analysis, one always has to be aware of the fact that the numerical value of a quantity depends on the physical unit. In this particular analysis we decided to choose practical units which were made exclusively by nature. Such units are the astronomical unit (AU) for lengths, the earth mass for planetary masses, as well as the year and the day for orbit and rotation periods. As can be seen, this particular choice leads to quite interesting regularities.

In a previous article [5], we had already done a similar analysis of elementary particle masses on the logarithmic

scale and detected a set of systematic mass gaps: $2e$, e, $\frac{e}{2}$, $\frac{e}{4}$, $\frac{e}{8}$ and $\frac{e}{16}$. Therefore, our numerical analysis was focused on these numbers and in a similar way, we detected this set of expressions again.

When looking from the Earth in direction away from the Sun, it can be noted that there are two principal zones, where mass accumulation into heavy planets seems to be forbidden. The existing mass is scattered in the form of asteroids and large bodies cannot become more than dwarf planets. The first such zone is the so-called Asteroid belt, located between Mars and Jupiter. Its population has already been well investigated, especially to confirm the orbital resonance effects manifesting in the Kirkwood gaps. Most asteroids have semi-major axes between 2.1 and 3.5 AU.

The second scattered-mass zone is the Kuiper belt, located from the orbit of Neptune (30 AU) to 55 AU distance from the Sun.

The Oort cloud is also such a scattered-mass zone. Due to its giant distance from the center of the solar system, there is no well-confirmed lower and upper limit, so we did not include it into the numerical analysis.

Table 1: Mean distances of celestial bodies (d) from the Sun expressed through e on the logarithmic scale and absolute values of corresponding numerical errors.

Object d [AU] ln(d)	Expression	Numerical error
Mercury 0.3871044 -0.9491	$-\left(\frac{e}{4}+\frac{e}{8}\right)$	0.0703
Venus 0.723339 -0.3239	$-\frac{e}{8}$	0.0159
Earth 0.9999808 0.0000	$0e$	0.0000
Mars 1.523585 0.4211	$\frac{e}{8}$	0.0812
Ceres 2.7663 1.0175	$\frac{e}{4}+\frac{e}{8}$	0.0019
Jupiter 5.204419 1.6495	$\frac{e}{2}+\frac{e}{8}$	0.0494
Saturn 9.582516 2.2599	$\frac{e}{2}+\frac{e}{4}+\frac{e}{16}$	0.0513
Uranus 19.201209 2.9550	$e+\frac{e}{16}$	0.0668
Neptune 30.04762 3.4028	$e+\frac{e}{4}$	0.0049
Pluto 39.486178 3.6758	$e+\frac{e}{4}+\frac{e}{8}$	0.0618

Table 2: Equatorial radii (r) of celestial bodies expressed through e on the logarithmic scale and absolute values of corresponding numerical errors.

Object r [AU] ln(r)	Expression	Numerical error
Mercury 1.6308×10^{-5} -11.0238	$-\left(4e+\frac{e}{16}\right)$	0.0192
Venus 4.0454×10^{-5} -10.1154	$-\left(2e+e+\frac{e}{2}+\frac{e}{4}\right)$	0.0782
Earth 4.2635×10^{-5} -10.0628	$-\left(2e+e+\frac{e}{2}+\frac{e}{8}+\frac{e}{16}\right)$	0.0391
Mars 2.2708×10^{-5} -10.6928	$-\left(2e+e+\frac{e}{2}+\frac{e}{4}+\frac{e}{8}+\frac{e}{16}\right)$	0.0104
Ceres 3.2574×10^{-6} -12.6346	$-\left(4e+e+\frac{e}{2}+\frac{e}{8}\right)$	0.0625
Jupiter 4.7789×10^{-4} -7.6461	$-\left(2e+\frac{e}{2}+\frac{e}{4}+\frac{e}{16}\right)$	0.0010
Saturn 4.0287×10^{-4} -7.8169	$-\left(2e+\frac{e}{2}+\frac{e}{4}+\frac{e}{8}\right)$	0.0018
Uranus 1.709×10^{-4} -8.6747	$-\left(2e+e+\frac{e}{8}+\frac{e}{16}\right)$	0.0102
Neptune 1.6554×10^{-4} -8.7063	$-\left(2e+e+\frac{e}{8}+\frac{e}{16}\right)$	0.0418
Pluto 7.6940×10^{-6} -11.7751	$-\left(4e+\frac{e}{4}+\frac{e}{16}\right)$	0.0525
Sun 4.649×10^{-3} -5.3817	$-2e$	0.0549

Table 3: Sidereal orbital periods (T) of celestial bodies expressed through e on the logarithmic scale and absolute values of corresponding numerical errors.

Object T [y] ln(T)	Expression	Numerical error
Mercury 0.2408467 -1.4236	$-\frac{e}{2}$	0.0645
Venus 0.61519726 -0.4858	$-\left(\frac{e}{8}+\frac{e}{16}\right)$	0.0239
Earth 1.0000174 0.0000	$0e$	0.0000
Mars 1.8808476 0.6317	$\frac{e}{4}$	0.0479
Ceres 4.60 1.5261	$\frac{e}{2}+\frac{e}{16}$	0.0029
Jupiter 11.862615 2.4734	$\frac{e}{2}+\frac{e}{4}+\frac{e}{8}+\frac{e}{16}$	0.0750
Saturn 29.447498 3.3826	$e+\frac{e}{4}$	0.0153
Uranus 84.016846 4.4310	$e+\frac{e}{2}+\frac{e}{8}$	0.0138
Neptune 164.79132 5.1047	$e+\frac{e}{2}+\frac{e}{4}+\frac{e}{8}$	0.0079
Pluto 247.92065 5.5131	$2e$	0.0765

Table 4: Sidereal rotation periods (T) of celestial bodies (retrograde rotation ignored) expressed through e on the logarithmic scale and absolute values of corresponding numerical errors.

Object T [d] ln(T)	Expression	Numerical error
Mercury 58.6462 4.0715	$e+\frac{e}{2}$	0.0059
Venus 243.018 5.4931	$2e$	0.0565
Earth 0.99726968 -0.0027	$0e$	0.0027
Mars 1.02595676 0.0256	$0e$	0.0256
Ceres 0.3781 -0.9726	$-\left(\frac{e}{4}+\frac{e}{8}\right)$	0.0468
Jupiter 0.41354 -0.8830	$-\left(\frac{e}{4}+\frac{e}{16}\right)$	0.0335
Saturn 0.44401 -0.8119	$-\left(\frac{e}{4}+\frac{e}{16}\right)$	0.0376
Uranus 0.71833 -0.3308	$-\frac{e}{8}$	0.0090
Neptune 0.67125 -0.3986	$-\frac{e}{4}$	0.0588
Pluto 6.3872 1.8543	$\frac{e}{2}+\frac{e}{8}+\frac{e}{16}$	0.0145
Sun 25.05 3.2209	$e+\frac{e}{8}+\frac{e}{16}$	0.0071

It can be seen that the distance between Ceres (the largest Asteroid belt object) and Pluto (the largest Kuiper belt object) matches Euler's number quite accurately. Table 1 summarizes the mean distances of the most important celestial bodies from the Sun together with the corresponding natural logarithms. It was found that all logarithms can be expressed as a sum of $2e$, e, $\frac{e}{2}$, $\frac{e}{4}$, $\frac{e}{8}$ and $\frac{e}{16}$. Most distances could even expressed as multiples of $\frac{e}{8}$ since they do not contain the summand $\frac{e}{16}$. The numerical errors on the logarithmic scale are significantly lower than $\frac{e}{16}$.

Analogously, we expressed the equatorial radii, sidereal orbital periods, sidereal rotation periods and masses of celestial bodies on the logarithmic number line (see Tables 2–5). In very few cases it was necessary to introduce $4e$ into the set of summands.

From these results we conclude that all these numerical values of planetary data are definitively not a set of random numbers. The repeatedly occurring summands strongly support the idea of a self-similar, fractal structure as Müller already claimed in reference [2].

In the present form, these results are obtained only when considering nature-made units, which underlines their importance.

Table 5: Masses (m) of celestial bodies, rescaled by earth mass and expressed through e on the logarithmic scale and absolute values of corresponding numerical errors.

Object m [$\times 10^{24}$ kg] $\ln(\frac{m}{m_{Earth}})$	Expression	Numerical error
Mercury 0.330104 -2.8950	$-\left(e+\frac{e}{16}\right)$	0.0068
Venus 4.86732 -0.2046	$-\frac{e}{16}$	0.0347
Earth 5.97219 0.0000	$0e$	0.0000
Mars 0.641693 -2.2312	$-\left(\frac{e}{2}+\frac{e}{4}+\frac{e}{16}\right)$	0.0226
Ceres 0.000943 -8.7403	$-\left(2e+e+\frac{e}{8}+\frac{e}{16}\right)$	0.0758
Jupiter 1898.13 5.7615	$2e+\frac{e}{8}$	0.0148
Saturn 568.319 4.5556	$e+\frac{e}{2}+\frac{e}{8}+\frac{e}{16}$	0.0315
Uranus 86.8103 2.6766	e	0.0416
Neptune 102.410 2.8419	$e+\frac{e}{16}$	0.0463
Pluto 0.01309 -6.1193	$-\left(2e+\frac{e}{4}\right)$	0.0032
Sun 1989100 12.7161	$4e+\frac{e}{2}+\frac{e}{8}+\frac{e}{16}$	0.0258

3.2 Continued fraction analysis

Due to the fact that all the solar system data can be expressed by multiples of $\frac{e}{16}$, it is consistent to set all partial numerators in Müller's continued fractions (given in equation(2)) to Euler's number. We further follow the formalism of previous publications [5, 6] and introduce a phase shift p in equation (2). According to [6] the phase shift can only have the values 0 or ±1.5. So we write for instance for the masses of the celestial bodies:

$$\ln\frac{mass}{proton\ mass}=p+S \tag{3}$$

where S is the continued fraction

$$S=n_0+\cfrac{e}{n_1+\cfrac{e}{n_2+\cfrac{e}{n_3+...}}}. \tag{4}$$

We abbreviate $p+S$ as $[p; n_0 \mid n_1, n_2, n_3, \ldots]$. The free link n_0 and the partial denominators n_i are integers divisible by 3. For convergence reason, we have to include $|e{+}1|$ as allowed partial denominator. This means the free link n_0 is allowed to be $0, \pm 3, \pm 6, \pm 9 \ldots$ and all partial denominators n_i can take the values $e{+}1, -e{-}1, \pm 6, \pm 9, \pm 12 \ldots$.

Analogously we write for the planetary mean distances from the Sun:

$$\ln\frac{mean\ distance}{\lambda_C}=p+S \tag{5}$$

where $\lambda_C = \frac{h}{2\pi mc}$ is the reduced Compton wavelength of the proton with the numerical value $2.103089086\times 10^{-16}$ m. Since the exact diameter or radius of the proton is unknown, some other proton related parameter is used, which can be determined accurately. The same applies for the equatorial radii. For orbital and rotational periods we write:

$$\ln\frac{time\ period}{\tau}=p+S \tag{6}$$

where $\tau = \frac{\lambda_C}{c}$ is the oscillation period of a hypothetical photon with the reduced Compton wavelength of the proton and traveling with light speed (numerical value $7.015150081\times 10^{-25}$ s).

For the calculation of the continued fractions we did not consider any standard deviation of the published data. Practically, we developed the continued fraction and determined only 18 partial denominators. Next we calculated repeatedly the data value from the continued fraction, every time considering one more partial denominator. As soon as considering further denominators did not improve the experimental data value significantly (on the linear scale), we stopped considering further denominators and gave the resulting fraction in Tables 6-10. This means we demonstrate how accurately the published solar system data can be expressed through continued fractions. Additionally we gave also the numerical error, which is defined as absolute value of the difference between NASA's published data value and the value calculated from the continued fraction representation.

The continued fraction representations of the masses of celestial bodies are given in Table 6. As can be seen, the absolute value of the first partial denominator is frequently high, which locates the mass very close to the principal node.

Table 6: Continued fraction representation of masses (m) of celestial bodies according to equation (3) and absolute values of corresponding numerical errors.

Object m [kg]	Continued fraction representation Numerical error [kg]
Mercury 0.330104×10^{24}	[1.5; 114 | 9, -12, -e-1, e+1] $5.5e + 19$
Venus 4.86732×10^{24}	[1.5; 117 | -305223] 1.6×10^{14}
Earth 5.97219×10^{24}	[1.5; 117 | 12, e+1, -e-1, e+1] 3.0×10^{22}
Mars 0.641693×10^{24}	[0; 117 | -6, e+1, -6, 33, -60, -e-1, e+1, -e-1] 1.1×10^{15}
Ceres 9.43×10^{20}	[1.5; 108 | 6, 99, e+1, -e-1, e+1, -6, e+1, e-1] 3.4×10^{12}
Jupiter 1.89813×10^{27}	[1.5; 123 | -81, e+1, -e-1, -e-1, -e-1, e+1, -9, -e-1] 3.6×10^{18}
Saturn 5.68319×10^{26}	[0; 123 | 9, e+1, -e-1] 8.1×10^{24}
Uranus 8.68103×10^{25}	[1.5; 120 | -24, e+1, -e-1, e+1] 7.0×10^{22}
Neptune 1.0241×10^{26}	[1.5; 120 | 60, -e-1, e+1, -e-1] 3.9×10^{22}
Pluto 1.309×10^{22}	[1.5; 111 | 33, 9, -e-1, e+1, -18, e+1, e+1, -15] 3.2×10^{12}
Sun 1.9891×10^{30}	[0; 132 | -e-1, -e-1, e+1, -e-1, 12, -e-1] 5.0×10^{25} [1.5; 129 | e+1, -e-1, 15, e+1] 6.2×10^{26}

Table 7: Continued fraction representation of mean distances of celestial bodies from the Sun according to equation (5) and absolute values of corresponding numerical errors.

Object mean distance [km]	Continued fraction representation Numerical error
Mercury 57.91×10^6	[0; 60 | e+1, -e-1, -e-1, -e-1, 6, 6, -9, -e-1] 1 km
Venus 108.21×10^6	[1.5; 60 | 513, 6, -9, e+1] 260 m
Earth 149.595×10^6	[1.5; 60 | 9, -e-1, 51, e+1, 6, 6] 873 m
Mars 227.925×10^6	[0; 63 | -e-1, 30, -e-1, -15, 6, 9, -9] 0.4 m
Ceres 413.833×10^6	[0; 63 | -18, 9, e+1, -e-1, e+1, -e-1, e+1, -e-1] 5854 km
Jupiter 778.57×10^6	[0; 63 | 6, -9, 6, -e-1, e+1, -e-1, -6, 54] 372 m
Saturn 1433.525×10^6	[1.5; 63 | -6, -e-1, -e-1, -15, -48, e+1, -e-1] 8.7 km
Uranus 2872.46×10^6	no continued fraction found
Neptune 4495.06×10^6	[0; 66 | -e-1, 15, 15, 54, 9, -e-1, e+1, -e-1] 46 m [1.5; 63 | e+1, -597, -9, e+1] 181 km
Pluto 5906.375×10^6	[0; 66 | -6, 6, -e-1, -6, -15, -e-1, -12, -e-1] 7.2 km

In case of the Venus, the mass is almost exactly located in a node. Notably two low-weight bodies, Ceres and Mars, are most distant from the principal nodes. A preferred accumulation of planetary masses in nodes in agreement with results previously published by Müller [2]. This author published already a continued fraction analysis of planetary masses, however, the continued fractions were in the canonical form with all nominators equal 1. Interestingly, his result is principally not changed substituting the nominators for e. The only exception is the Sun, here even two continued fractions can be given and the mass is located in a non-turbulent zone between the principal nodes 129+1.5 and 132. This indicates that the probability of mass changes of the Sun is extremely low, so one can expect that all astrophysical parameters of the Sun will not show any evolution for a long time. We conclude that it seems to be a general property of mass to accumulate close to the nodes. Apparently no specific properties of the celestial bodies can be correlated to these data.

Table 7 displays the continued fraction representations of the mean distances from the Sun of the considered celestial bodies. When analyzing the denominators, it is directly clear that there is no general behavior of the planetary distances. For instance Venus is located almost in a node (n_1 very high), while Mercury, Mars and Neptune are far away from a node ($n_1 = e+1$ or $-e-1$). Uranus is even in a gap. Earth, Jupiter, Saturn and Pluto are moderately close to a node. This opens a door to associate a specific property of these bodies to the continued fraction representation. In this particular case we relate the mean distance to seismic activity of a solid object or heat release of a gas planet. The oscillation process inside Venus is turbulent, and it is known that Venus has an extreme

Table 8: Continued fraction representation of equatorial radii of celestial bodies according to equation (5) and absolute values of corresponding numerical errors.

Object Equatorial radius [km]	Continued fraction representation Numerical error
Mercury 2439.7	[0; 51 | -15, e+1, -e-1, e+1, -e-1] 1.6 km
Venus 6051.8	[0; 51 | e+1, 30, 9] 98 m
Earth 6378.14	[0; 51 | e+1, -15, -e-1, e+1, e+1] 57 m [1.5; 51 | -e-1, 207] 58 m
Mars 3397	[0; 51 | 21, -e-1, e+1, -e-1, e+1] 1.8 km
Ceres 487.3	[1.5; 48 | -9, 27, 9, 18] 0.01 m
Jupiter 71492	[0; 54 | 15, -18, -24, -6] 2 m
Saturn 60268	[0; 54 | 222, -6, -e-1] 46 m
Uranus 25559	[0; 54 | -e-1, 6, -e-1, -e-1, 9] 898 m [1.5; 51 | e+1, 6, 12, -e-1, e+1, -6] 44 m
Neptune 24764	[0; 54 | -e-1, e+1, e+1, 9, -e-1, 9] 22 m [1.5; 51 | e+1, e+1, 6, -6, -213] 0.05 m
Pluto 1151	[0; 51 | -e-1, e+1, -6, e+1, e+1] 475 m
Sun 6.955×10^5	[0; 57 | -6, e+1, -e-1, e+1, -e-1, -e-1, 12, -6] 49 m [1.5; 54 | e+1, -e-1, e+1, e+1, e+1 -e-1, e+1, -e-1, e+1] 21 km

volcanic activity [7,8]. Scientists also believe that the volcanism on Venus has been changing over time [7], so changes in trend may occur. The data also suggest that seismic activity on Earth is higher than on Mars, Mercury or Pluto.

For the gas planets Jupiter, Saturn and Neptune, it has been known that they produce more heat internally than they receive from the Sun [9, 10]. Contrary to this, Uranus is a relatively cold planet, radiating very little more energy than received. The principal source of this heating is believed to be a liberation of thermal energy from precipitation of Helium or other compounds in the interior of the planet while simultaneously gravitational potential energy is released.

Physically, such processes should exist in all gas planets, this means only the process kinetics can be associated to the continued fraction representation. We assume that the rate of this process is influenced by oscillations in the planet. For Uranus, which is located in a gap, the oscillation capability is low, which means the heat-releasing process occurred faster and is already almost completed. Jupiter and Saturn, located in proximity to the nodes 63 and 1.5+63, are in a fluctuation zone. So here the heat releasing process is disturbed and they are yet in a more early phase of process development, whereas Neptune (away from nodes) is in an already more advanced phase. From this we can predict that one day in future, first Neptune stops releasing excess heat, while Jupiter and Saturn will do this much later.

A very special situation is the continued fraction representation of dwarf planet Ceres. As can be seen, it has an exceptional high numerical error, actually this must be interpreted as "no continued fraction found". We report the fraction here only in order to demonstrate that the whole Asteroid belt is in a fluctuation zone around the node 63, which translates to $\lambda_C exp(63) = 3.22$ AU. This value is not acceptable as an average for the distances of the Asteroid belt objects from the Sun. Actually most Asteroids can be found between 2.1 and 3.5 AU. From this it can be concluded that most Asteroids accumulate in the compression zone before the principal node 63. Similarly is the situation for the Kuiper belt. All Kuiper belt objects are located before the node 66, $\lambda_C exp(66) = 64.77$ AU. The Astrophysics textbooks always teach the belt is located from the orbit of Neptune (30 AU) to 50 or 55 AU distance from the Sun. So again, the celestial bodies accumulate before a principal node.

Since Ceres is the largest Asteroid belt object, it is reasonable to claim Ceres is located in a gap, even inside a fluctuation zone. We interpret these fluctuations as the cause of the observed mass scattering in the whole Asteroid belt.

More research must still be done regarding the distribution of Kuiper belt objects. Brunini and Melita [11] suggested a Mars like object around 60 AU distance from the Sun in order to explain the Kuiper cliff, a sudden drop off of space rocks beyond 50 AU. Later, numerical simulations of Lykawka and Mukai showed that such a body would not reproduce the observed orbital distribution in the Kuiper belt [12], however these authors did not completely exclude the possibility of an unknown planet. Now, from our continued fraction analysis we suggest that there is indeed no unknown planet, it is just so that the compression zone before the principal node acts as accumulation site of these relatively light Kuiper belt objects. If there was such a solid planet in the fluctuation zone, it should possess volcanic activity similarly to Venus, and consequently should be very easy to detect, because of emission of infrared radiation. So this argument again confirms the absence of such a planet. Anyway, a detailed continued fraction analysis of Trans-Neptunian objects

combined with Kuiper belt objects would be very useful.

Table 8 displays analogously the continued fraction representations of planetary equatorial radii. From these data, some statements regarding the atmosphere of solid planets can be derived. We interprete an atmosphere as an extension of a planet with the effect to increase its radius. On the other hand, an atmosphere is also governed by the chemical composition of a planet and its temperature and these parameters are more decisive. Such an analysis cannot be applied to gaseous planets, since they always have a very dense atmosphere, regardless of their radii.

The most dense atmospheres can be found on Earth and on Venus. The first partial denominator in the continued fraction representation of Venus is e+1. this means the radius of Venus is in an expansion zone and far away from the node. An increase in radius is favored and any probabilities of trend changes are low. This is in agreement with the observed high density of the atmosphere on Venus, with a pressure of 95 bar at the surface [8]. In the case of our planet Earth, two continued fractions can be given, so the radius is influenced by the two nodes 51 and 51+1.5. Both first partial denominators put the radius far away from the corresponding nodes into a non-fluctuation zone. Here does not exist any specific trend and the formation of the atmosphere is solely governed by chemical composition and temperature.

Pluto is with a negative first partial denominator in a compression zone, so the expansion of its radius by an atmosphere is not favored. Indeed Pluto has only a very thin atmosphere in the micro-bar range [13]. According to reference [14], Pluto's atmosphere at perihelion extends to depths greater than Earth's atmosphere and may even enclose the moon Charon. The atmosphere is thought to be actively escaping, so Pluto is the only planet in the solar system actively losing its atmosphere now.

The same is true for Mercury. In agreement with the observations, Mercury does not have an atmosphere [8], which can also be alternatively explained by its high surface temperature.

Mars is with the positive number 21 of the first partial denominator in an expansion zone, so the formation of an atmosphere is favored. At the same time the radius is also close to the node 51 in a fluctuation zone. This means changes in process trends may occur. Considering the formation of an atmosphere as the relevant process, this process can be interrupted or inverted over long time periods. As a consequence, one would expect an atmosphere, but significantly thinner than that on Venus. Actually the surface pressure on Mars is close to 1% to that of the Earth and there are speculations that the atmosphere on Mars has experienced major changes in the past [8].

Ceres is a low density object consisting of rock and ice with mean density of only 2 g/cm^3, which supports the presence of a lot of ice. The "frost line" in our solar system — the distance where ice will not evaporate — is roughly at 5 AU from the Sun [15]. So one must ask why Ceres does not have already lost all his ice through sublimation. From the continued fraction representation, the radius of Ceres is in a compression zone and the formation of an atmosphere is not favored. Through evaporation of the ice, at least temporarily an atmosphere will form. For this reason we believe Ceres is able to continue for a long time as an icy dwarf planet.

When looking at the data it turns out that the gaseous planets seem to prefer radii that can be described by two con-

Table 9: Continued fraction representation of sidereal orbital periods of celestial bodies according to equation (6) and absolute values of corresponding numerical errors.

Planet T [s]	Continued fraction representation Numerical error
Mercury 7595370	[0; 72 | -6, e+1, -e-1, e+1, -30, -e-1, -33, -6] 0.002 s [1.5; 69 | e+1, -e-1, e+1, 6, -12, 6, -e-1, e+1, -15] 0.01 s
Venus 19400861	[0; 72 | 6, e+1, -6, 6, e+1, -e-1, e+1, -e-1, e+1] 128 s
Earth 31536549	[0; 72 | e+1, -e-1, -6, e+1, -6, -6, -e-1, 9, -6] 0.1 s [1.5; 72 | -e-1, -e-1, -12, 45, e+1, -6, -e-1, -24] 0.0003 s
Mars 59314410	[1.5; 72 | 183, -e-1, 12, -e-1, e+1, -e-1] 13 s
Ceres 145065600	[0; 75 | -e-1, -e-1, e+1, 6, -e-1, 6, -6, -18, e+1] 0.3 s [1.5; 72 | e+1, -e-1, -225, -e-1, e+1, -e-1, -9, -e-1] 0.06 s
Jupiter 374099427	no continued fraction found
Saturn 928656297	[1.5; 75 | -12, 6, e+1, -e-1, 33, e+1, -e-1, e+1, -e-1] 74 s
Uranus 2649555255	[0; 78 | -e-1, -12, e+1, -e-1, 12, -e-1, -69, -9] 0.9 s
Neptune 5196859068	[0; 78 | -225, e+1, -9, e+1, -6, e+1, 48] 0.04 s
Pluto 7818425618	no continued fraction found

tinued fractions. For the Sun, Uranus and Neptune it can be said that they are influenced by two neighbored nodes. This indicates their sizes will remain constant over a longe time. The only exceptions are Jupiter and Saturn, which are in an expansion zone. One would expect their sizes increasing. How could this be achieved in practice? There is only one possibility, Jupiter and Saturn must capture some asteroids or comets preferentially from the Kuiper belt. When looking at the number of their moons, it can be assumed that such a process has already been progressing for a long time. A moon can be interpreted as an incomplete capture, this means the object was captured without crashing into the planet and increasing its size. Indeed Jupiter and Saturn have 63 and 62 confirmed moons, while Uranus has 27, and Neptune only 13 moons. Normally one would expect that Uranus and Neptune should have the most moons, since they are much closer located to the Kuiper belt. Notably 55 of Jupiter's moons are irregular satellites with high eccentricities and inclinations, while Saturn has just 38 of such satellites. It is assumed that these irregular satellites were captured from other orbits.

In Table 9, the continued fraction representations of the orbital periods are given. When analyzing these fractions, their interpretation is problematic: One has to bear in mind that Kepler's 3rd law relates the orbital period to the semi-major axis (for most planets close to the mean distance), so these parameters are not independent from each other.

Regarding oscillation properties, it is clearly visible that the continued fraction representations of the orbital periods do not provide a similar image of planetary features than the representations of the corresponding mean distances. For instance, the orbital periods of Mars and Neptune are located in a highly turbulent zone. This is contrary to to the continued fraction representation of its mean distances given in Table 7, where both planets are far away from a node. Since for the mean distances a meaningful continued fraction representation exists, the orbital periods do not fit anymore in this model and their mathematical representation in continued fractions, as presented here, is physically meaningless.

Luckily, the situation is easier for the rotation periods of the celestial bodies (see Table 10). As can be seen, the rotation periods prefer values far away from the nodes in non-fluctuating zones. There are only three exceptions: Jupiter Saturn and Ceres have periods located in a principal node. This means the rotation periods are in an early stage of development, which can be justified with a specific process inside the celestial bodies.

For the gas planets Jupiter and Saturn it has been known that heat is generated from precipitation of Helium or other compounds in the interior of the planet while simultaneously gravitational potential energy is released. Through such a process, the moment of inertia of the planet changes gradually and the rotation period evolves. From the analysis of the mean distances of Jupiter and Saturn, we have already stated that their heat release processes are still in an early phase of development. Exactly the same can be derived from the analysis of rotation periods. The rotation of the Sun is also not yet completely evolved, however here this effect is minor. Any internal structuring of plasma fluxes could be responsible for this.

Table 10: Continued fraction representation of sidereal rotation periods (T) of celestial bodies according to equation (6) and absolute values of corresponding numerical errors.

Planet T [s]	Continued fraction representation Numerical error
Mercury 5067032	[0; 72 | -e-1, e+1, -6, 6, -15, -e-1, e+1, -e-1, e+1] 3 s
Venus 20996755	[0; 72 | 6, -9, -12, 18, -9, e+1] 0.1 s
Earth 86164	[0;66 | e+1, -e-1, e+1, -6, e+1, e+1, -e-1, 21] 0.02 s [1.5; 66 | -6, e+1, -15, -e-1, -6] 0.07 s
Mars 88643	[1.5; 66 | -6, 6, -18, -12] 0.04 s
Ceres 32668	[0; 66 | 255, -e-1, e+1, -e-1, e+1] 0.17 s
Jupiter 35730	[0; 66 | 27, 27, -21] 0.005 s
Saturn 38362	[0; 66 | 15, e+1, -e-1, -e-1, e+1, -e-1] 2 s
Uranus 62064	[0; 66 | e+1, 6, 39, -12] 0.02 s [1.5; 66 | -e-1, 6, -e-1, -9, -e-1, 48] 0.001 s
Neptune 57996	[0; 66 | e+1, e+1, -e-1, 9, -9, -18] 0.003 s [1.5; 66 | -e-1, e+1, -30, -e-1, e+1, -e-1] 4 s
Pluto 551854	no continued fraction found
Sun 2164320	[1.5; 69 | -9, -15, e+1, e+1, -6, 9] 0.003 s

Ceres has an unusual location inside the Asteroid belt, which is a turbulent zone as can be derived from the continued fraction analysis of its mean distance from the Sun. Knowing this, we speculate that the evolution of its rotation period could have been influenced by the fluctuating population of the belt through collisions of an early Ceres with many smaller asteroids over a long time. According to reference [15], there are possibly volatile compounds in the interior of Ceres. Ceres could have accreted from rocky and icy planetesimals. This has taken some time, we speculate that

possibly Ceres had less time for the evolution of its rotation than other planets.

An other reference [16] speculates regarding a subsurface ocean and mentions a modeling predicting that ice in the outer 10 km of Ceres would always remain frozen, although the frozen crust would be gravitationally unstable and likely overturn, melt, and re-freeze. Such repeatedly occurring movements of heavy masses on Ceres could have interfered with the evolution of its rotation period.

4 Conclusions

Numerical investigation of solar system data revealed that masses, radii, distances of celestial bodies from the Sun, orbital periods and rotation periods can be expressed as multiples of $\frac{e}{16}$ on the logarithmic number line, which proves that they are not a set of random numbers. Through application of a fractal scaling model, we set these numerical values in relation to proton resonances and correlated numerous features of celestial bodies with their oscillation properties. From this it can be concluded that the continued fraction representations with all nominators equal e are adequate and Müller's fractal model turned out to be a powerful tool to explain the fractal nature of the solar system. If some day in future, a further planet will be discovered in our solar system, it should be possible to derive analogously some of its features from its orbital parameters.

Acknowledgments

The authors greatly acknowledge the financial support from the Brazilian governmental funding agencies FAPESQ and CNPq.

Submitted on December 26, 2010 / Accepted on December 27, 2010

References

1. Müller H. Fractal scaling Models of resonant oscillations in chain systems of harmonic oscillators. *Progress in Physics*, 2009, v. 2 72–76.
2. Müller H. Fractal scaling models of natural oscillations in chain systems and the mass distribution of the celestial bodies in the solar system. *Progress in Physics*, 2010, v. 1 62–66.
3. Müller H. Fractal scaling models of natural oscillations in chain systems and the mass distribution of particles. *Progress in Physics*, 2010, v. 3 61–66.
4. Press W. H., Teukolsky S. A., Vetterling W. T., Flannery B. P. Numerical recipes in C. Cambridge University Press, Cambridge, 1992.
5. Ries A., Fook M. V. L. Fractal structure of nature's preferred masses: Application of the model of oscillations in a chain system. *Progress in Physics*, 2010, v. 4, 82–89.
6. Otte R., Müller H.. German patent No. DE102004003753A1, date: 11.08.2005
7. Basilevsky A. T., Head J. W. Venus: Timing and rates of geologic activity. *Geology*, 2002, v. 30, no. 11, 1015-–1018.
8. Gregersen E. (Editor). The inner solar system: the Sun, Mercury, Venus, Earth, and Mars. Britannica Educational Publishing, New York, 2010.
9. Elkins-Tanton L. T. Jupiter and Saturn. Chelsea House, New York, 2006.
10. Gregersen E. (Editor). The outer solar system: Jupiter, Saturn, Uranus, Neptune, and the dwarf planets. Britannica Educational Publishing, New York, 2010.
11. Brunini A., Melita M. D. The Existence of a Planet beyond 50 AU and the Orbital Distribution of the Classical Edgeworth-Kuiper-Belt Objects. *Icarus*, 2002, v. 160, no. 1, 32–43.
12. Patryk S. Lykawka P. S., Mukai T. An Outer Planet beyond Pluto and the Origin of the Trans-Neptunian belt Architecture. *The Astronomical Journal*, 2008, v. 135, 1161-–1200.
13. Lellouch E., Sicardy B., de Bergh C., Käufl H.-U., Kassi S., Campargue A. Pluto's lower atmosphere structure and methane abundance from high-resolution spectroscopy and stellar occultations. arXiv:0901.4882v1, [astro-ph.EP], 30 Jan 2009.
14. Elkins-Tanton L. T. Uranus, Neptune, Pluto, and the Outer Solar System. Chelsea House, New York, 2006.
15. Carry B., Dumas C., Fulchignoni M., Merline W. J., Berthier J., Hestroffer D., Fusco T., Tamblyn P. Near-Infrared Mapping and Physical Properties of the Dwarf-Planet Ceres. arXiv:0711.1152v1, [astro-ph], 7 Nov 2007.
16. Rivkin A. S., Volquardsen E. L., Clark B. E. The surface composition of Ceres: Discovery of carbonates and iron-rich clays. *Icarus*, 2006, v. 185, 563–567.

Photon-Assisted Resonant Chiral Tunneling Through a Bilayer Graphene Barrier

Aziz N. Mina* and Adel H. Phillips†
*Faculty of Science, Beni-Suef University, Beni-Suef, Egypt
†Faculty of Engineering, Ain-Shams University, Cairo, Egypt

E-mail: adel_phillips@yahoo.com

The electronic transport property of a bilayer graphene is investigated under the effect of an electromagnetic field. We deduce an expression for the conductance by solving the Dirac equation. This conductance depends on the barrier height for graphene and the energy of the induced photons. A resonance oscillatory behavior of the conductance is observed. These oscillations are strongly depends on the barrier height for chiral tunneling through graphene. This oscillatory behavior might be due to the interference of different central band and sidebands of graphene states. The present investigation is very important for the application of bilayer graphene in photodetector devices, for example, far-infrared photodevices and ultrafast lasers.

1 Introduction

Two-dimensional graphene monolayer and bilayer exhibit fascinating electronic [1–4] and optical properties [5, 6] due to zero energy gap and relativistic-like nature of quasiparticle dispersion close to the Fermi-level. With recent improvements in nanofabrication techniques [7] the zero-energy gap of graphene can be opened via engineering size, shape, character of the edge state and carrier density, and this in turn offers possibilities to simultaneously control electronic [8, 9] magnetic [10, 11] and optical [6, 12] properties of a single material nanostructure. Recent studies have also addressed electronic properties of confined graphene structure like dots, rings or nanoribbons. In particular, nanoribbons have been suggested as potential candidates for replacing electronic components in future nanoelectronic and spintronic devices [3, 13]. Recent research shows that graphene [14] is a suitable candidate to examine the photon-assisted tunneling and quantum pumps in the Dirac system.

The purpose of the present paper is to investigate the angular dependence of the chiral tunneling through double layer graphene under the effect of the electromagnetic field of wide range of frequencies.

2 Theoretical Formulation

In this section, we shall derive an expression for the conductance of a bilayer graphene by solving the eigenvalue problem Dirac equation. The chiral fermion Hamiltonian operates in space of the two-component eigenfunction, ψ, where Dirac eigenvalue differential equation is given by [14, 15]:

$$-i v_F \vec{\sigma} \cdot \vec{\nabla} \psi(r) = E\psi(r), \tag{1}$$

where $\vec{\sigma}$ are the Pauli-matrices, V_F is the Fermi-velocity, and E is the scattered energy of electrons. It is well known that graphene junction have finite dimensions [14, 15], the motion of chiral fermions is quantized. This quantization imposes additional constrains on the directional tunneling diagram. So, accordingly, the value of the angle of incidence of electrons on the barrier could be obtained from boundary conditions along the y-direction as we will see below.

In order to solve Eq.(1), we propose a potential barrier of width, L, and height, V_0,. The eigenfunction, $\psi_L(r)$ in the left of the potential barrier is given by:

$$\psi_L(r) = \sum_{n=-\infty}^{\infty} J_n\left(\frac{eV_{ac}}{\hbar\omega}\right)\left\{e^{[i(k_x x+k_y y)]} + \right.$$
$$\left. + \frac{R_n(E)}{\sqrt{2}}\begin{pmatrix}1\\ s\, e^{i(\pi-\phi)}\end{pmatrix} e^{[i(-ik_x x+k_y y)]}\right\}, \tag{2}$$

where the angle $\phi = \tan^{-1}(\frac{k_y}{k_x})$, in which $k_x = k_f \cos(\phi)$ and $k_v = k_F \sin(\phi)$,and k_F is the Fermi-wave number, and J_n is the n^{th} order Bessel function, V_{ac} is the amplitude of the induced photons of the electromagnetic field with frequency, ω, and $R_n(E)$ is the energy-dependent reflection coefficient.

The eigenfunction, $\psi_b(r)$, inside the potential barrier is given by:

$$\psi_b(r) = \sum_{n=-\infty}^{\infty} J_n\left(\frac{eV_{ac}}{\hbar\omega}\right)\left\{\frac{a}{\sqrt{2}}\begin{pmatrix}1\\ s'\, e^{i\theta}\end{pmatrix} e^{[i(q_x x+k_y y)]} + \right.$$
$$\left. + \frac{b}{\sqrt{2}}\begin{pmatrix}1\\ s'\, e^{i(\pi-\theta)}\end{pmatrix} e^{[i(-q_x x+k_y y)]}\right\}, \tag{3}$$

where the angle $\theta = \tan^{-1}(\frac{k_y}{q_x})$, and the wave number qx is expressed as:

$$q_x = \sqrt{\frac{(V_0-\varepsilon)^2}{v_F^2} - k_y^2} \tag{4}$$

and $\varepsilon = E - eV_g - \hbar\omega$, V_0 is the barrier height, E is the energy of the scattered electrons, V_g is the gate voltage and $\hbar\omega$ is the photon energy.

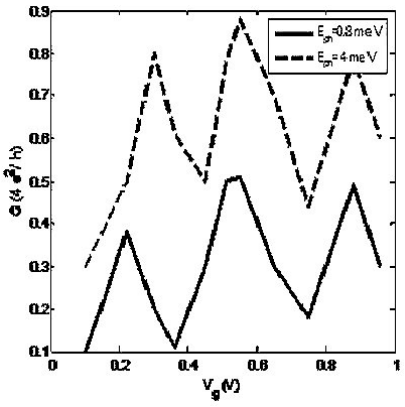

Fig. 1: The variation of the conductance, G, with gate voltage V_g, at different photon energies, E_{ph}.

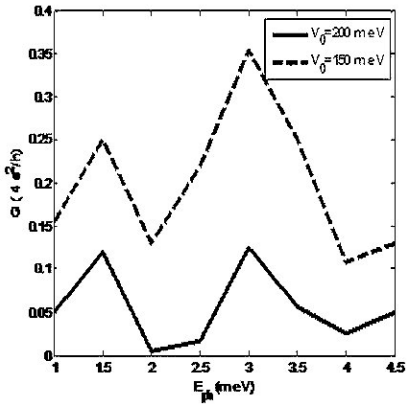

Fig. 2: The variation of the conductance, G, with the photon energy, E_{ph}, at different values of barrier height, V_0.

The eigenfunction, $\psi_R(r)$, in the right region to the potential barrier which represents the transmitted electrons is given by:

$$\psi_R(r) = \sum_{n=-\infty}^{\infty} J_n\left(\frac{eV_{ac}}{\hbar\omega}\right)\left\{\frac{\Gamma_n(E)}{\sqrt{2}}\begin{pmatrix}1\\ s\,e^{i\theta}\end{pmatrix}e^{[i(k_x x+k_y y)]}\right\}, \quad (5)$$

where $\Gamma_n(E)$ are the transmitted electron waves through the barrier. The parameters s and s' are expressed as:

$$s = \mathrm{sgn}\,(E) \qquad \text{and} \qquad s' = \mathrm{sgn}\,(E - V_0)\,. \quad (6)$$

Now, the coefficients $R_n(E), a, b, \Gamma_n(E)$ could be determined by applying the continuity conditions of the eigenfunctions, Eqs.(2,3,5), at the boundaries as follows:

$$\left.\begin{aligned}&\psi_L\,(x=0,\,y) = \psi_b\,(x=0,\,y)\\ &\text{and}\\ &\psi_b\,(x=L,\,y) = \psi_R\,(x=L,\,y)\end{aligned}\right\}. \quad (7)$$

So, the transmission probability, $|\Gamma_n(E)|^2$, could be determined from the boundary conditions Eq.(7) and is given by:

$$|\Gamma_n(E)|^2 = \sum_{n=-\infty}^{\infty} J_n^2\left(\frac{eV_{ac}}{\hbar\omega}\right)\times$$
$$\times\left\{\frac{\cos^2(\theta)\cos^2(\phi)}{[[\cos(Lq_x)\cos\phi\cos\theta]^2+\sin^2(Lq_x)(1-ss'\sin\phi\sin\theta)^2]}\right\}. \quad (8)$$

The conductance, G, is given by [16, 17]:

$$G(E) = \frac{4e^2}{h}\int dE\,|\Gamma_n(E)|^2\left(-\frac{\partial f_{FD}}{\partial E}\right), \quad (9)$$

where f_{FD} is the Fermi-Dirac distribution function. Now, substituting Eq.(8) into Eq.(9), we get a complete expression for conductance which depends on the angles ϕ, θ, and on the barrier height, V_0, and its width, the gate voltage, V_g, and the photon energy, $\hbar\omega$.

3 Results and Discussions

The conductance, G, has been computed numerically as a function of the gate voltage, V_g, and photon energy, $E_{ph} = \hbar\omega$ of the induced electromagnetic field. For the bilayer graphene, the effective mass of the fermion quasiparticle m^* equals approximately 0.054 m_e [14, 15]. The parameter m_e is the free mass of the electron. The main features of the present results are:

(1) Fig.(1) shows the variation of the conductance, with the gate voltage, V_g, at different values of the photon energies of the induced electromagnetic field. We notice an oscillatory behavior of the conductance. The electromagnetic field induces resonant peaks in the photon-assisted chiral tunneling conductance.

(2) Fig.(2) shows the dependence of the conductance on the energy of the induced photons at different values of the barrier height, V_0. An oscillation of the conductance is observed.

The observed oscillations in conductance for Figs.(1,2) can be explained as Follows: For grapheme under the effect of the electromagnetic field, the chiral tunneling of electrons can undergo transitions between the central band to several sidebands by means of photon emission or absorption. Such process is referred to as photo-assisted tunneling [18–20]. Also, the phase correlations during chiral tunneling can be directly tuned by applying of an external electromagnetic field leads to a resonance trend in the conductance of a bilayer graphene.

The present results show a good concordant with those in the literature [21–23].

4 Conclusion

The present investigation shows that the chiral tunneling of Dirac electrons through graphene enables ultra-wide band tunability. The rise of graphene in photonics and optoelectronics is shown by several results ranging from photo-detectors, light emitted devices, solar cells and ultra-fast lasers [23, 24].

Submitted on December 12, 2010 / Accepted on December 19, 2010

References

1. Novoselov K.S., Geim A.K., Morozov S.V., Jiang D., Katsnelson M.I., Grigoriev I.V., Dubonos S.V. and Firsov A.A. Two-dimensional gas of massless Dirac fermions in graphene. *Nature*, 2005, v.438, 197.
2. Zhang Y.B., Tan Y.W., Stormer H.L., and Kim P. Experimental observation of the quantum Hall effect and Berry's phase in graphene. *Nature*, 2005, v.438, 2001.
3. Geim A.K. and Novoselov K.S. The rise of graphene. *Nature Materials*, 2007, v.6, 183.
4. Tworzydlo J., Trauzettel B., Titov M. Rycerz A. and Beenakker C.W.J. Quantum limited shot noise in graphene. *Physical Review Letters*, 2006, v.96, 246802.
5. Sadowski M.L., Martinez G., Potemski M., Berger C. and de Haar W.A. Landau level spectroscopy of ultra thin graphite layers. *Physical Review Letters*, 2006, v.97, 266405.
6. Mueller T., Xia F. N. A., and Avouris P. Graphene photo-detectors for high speed optical communications. *Nature Photonics*, 2010, v.4, 297.
7. Campos L.C., Manfrinato V. R., Sanchez-Yamagishi J.D., Kong J., and Jarillo-Herrero P. Anisotropic etching and nanoribbon formation in single layer graphene. *Nano Letters*, 2009, v.9, 2600.
8. Libish F., Stampfer C., and Bugdorfer J. Graphene quantum dots: beyond a Dirac billiard. *Physical Review B*. 2009, v.79, 115423.
9. Ezawa M. Dirac fermions in a graphene nanodisk and a graphene corner: Texture of vortices with an unusual winding number. *Physical Review B*, 2010, v.81, 201402.
10. Ezawa M. Metallic graphene nanodisks: Electrical and magnetic properties. *Physical Review B*, 2007, v.76, 245415.
11. Wang W. L., Meng S. and Kaxiras E. Graphene nanoflakes with large spin. *Nano Letters*, 2008, v.8, 241.
12. Yan X., Cui X., Li B.S., and Li L.S. Large solution processable graphene quantum dots as light absorber for photovoltaics. *Nano Letters*, 2010, v.10, 1869.
13. Son J.W., Cohen M. L. and Louie S. G. Half-metallic graphene nanoribbons. *Nature*, 2006, v.444, 347.
14. Castro Neto A.H., Guinea F., Peres N.M.R., Novoselov K.S. and Geim A.K. The electronic properties of graphene. *Reviews of Modern Physics*, 2009, v.81, 109.
15. Beenakker C.W. J. Andreev reflection and Klein tunneling in graphene. *Reviews of Modern Physics*, 2008,v.80, 1337.
16. Datta S. Electronic transport in mesoscopic systems. Cambridge University Press, 1997, Cambridge.
17. McEuen P.L., Bockrath M., Cobden D.H., Yoon Y.G., and Louie S.G. Disorder, pseudospin, and back scattering in carbon nanotubes. *Physical Review Letters*, 1999, v.83, 5098.
18. Platero G. and Aguado R. Photon-assisted transport in semiconductor nanostructures. *Physics Reports*, 2004, v.394, 1.
19. Mina A.N., Awadalla A.A., Phillips A.H., and Ahmed R.R.. Microwave spectroscopy of carbon nanotube field effect transistor. *Progress in Physics*, 2010, v.4, 61.
20. Awadalla A.A., Phillips A.H., Mina A.N., and Ahmed R.R. Photon-assisted transport in carbon nanotube mesoscopic device. Accepted for publication in *International Journal of Nanoscience*, 2010.
21. Shafranjuk S. Probing the intrinsic state of a one-dimensional quantum well with photon-assisted tunneling. *Physical Review B*, 2008, v.78, 235115.
22. Abergel D.S.L. and Chakraborty T. Generation of valley polarized current in bilayer graphene. *Applied Physics Letters*, 2009, v.95, 062107.
23. Rocha C.G., Foa Terres L.E. F., and Cuniberti G. AC-transport in graphene-base Fabry-Perot devices. *Physical Review B*, 2010, v.81, 115435.
24. Bonaccorso F., Sun Z., Hasan T., and Ferrari A.C. Graphene photonics and optoelectronics. *Nature Photonics*, 2010, v.4, 611.

Progress in Physics is an American scientific journal on advanced studies in physics, registered with the Library of Congress (DC, USA): ISSN 1555-5534 (print version) and ISSN 1555-5615 (online version). The journal is peer reviewed and listed in the abstracting and indexing coverage of: Mathematical Reviews of the AMS (USA), DOAJ of Lund University (Sweden), Zentralblatt MATH (Germany), Scientific Commons of the University of St.Gallen (Switzerland), Open-J-Gate (India), Referential Journal of VINITI (Russia), etc. Progress in Physics is an open-access journal published and distributed in accordance with the Budapest Open Initiative: this means that the electronic copies of both full-size version of the journal and the individual papers published therein will always be acessed for reading, download, and copying for any user free of charge. The journal is issued quarterly (four volumes per year).

Electronic version of this journal: http://www.ptep-online.com

Postal address:
Department of Mathematics and Science,
University of New Mexico, 200 College Road, Gallup, NM 87301, USA

Printed in the United States of America